TECHNISCHE UNIVERSITÄT MÜNCHEN

Wissenschaftszentrum Weihenstephan für Ernährung, Landnutzung und Umwelt

Lehrstuhl für Phytopathologie

Regulation of the cell surface receptor kinase LORE in the *Pseudomonas syringae-Arabidopsis thaliana* interaction

Milena Pia Schäffer

Vollständiger Abdruck der von der Fakultät Wissenschaftszentrum Weihenstephan für Ernährung, Landnutzung und Umwelt der Technischen Universität München zur Erlangung des akademischen Grades einer

Doktorin der Naturwissenschaften (Dr. rer. nat.)

genehmigten Dissertation.

Vorsitzende:	Prof. Dr. Brigitte Poppenberger-Sieberer
Prüfer der Dissertation:	1. TUM Junior Fellow Dr. Stefanie Ranf
	2. Prof. Dr. Kay H. Schneitz

Die Dissertation wurde am 13.03.2019 bei der Technischen Universität München eingereicht und durch die Fakultät Wissenschaftszentrum Weihenstephan für Ernährung, Landnutzung und Umwelt am 18.10.2019 angenommen.

1 Contents

2 Abbreviations

A	Golden Gate fusion site TATA
ABA	abscisic acid
AHA	H^+-ATPases
AhalLORE	*At*LORE ortholog from *Arabidopsis halleri*
AlyrLORE	*At*LORE ortholog from *Arabidopsis lyrata*
AprA	ALKALINE PROTEASE A
Arabidopsis	*Arabidopsis thaliana*
ARC1	ARM-REPEAT CONTAINING PROTEIN 1
At	*Arabidopsis thaliana*
***At*LORE**	LIPOOLIGOSACCHARIDE -SPECIFIC REDUCED ELICITATION
ATP	adenosine-5'-triphosphate
ATS	Arabidopsis thaliana solution
Avr	avirulence factor
AWFs	apoplastic wash fluids
BAK1	BRI1-ASSOCIATED RECEPTOR KINASE 1
BiFC	bimolecular fluorescence complementation
BIK1	BOTRYTIS INDUCED KINASE 1
BIR2	BAK1-INTERACTING RECEPTOR-LIKE KINASE 2
BRI1	BRASSINOSTEROID INSENSITIVE 1
C	Golden Gate fusion site TTGG
$[Ca^{2+}]_{cyt}$	cytosolic calcium concentration
CC	coiled-coil domain
cDNA	complementary DNA
CD14	CLUSTER OF DIFFERENTIATION 14
CDPK	CALCIUM-DEPENDENT PROTEIN KINASE
CEBiP	CHITIN OLIGOSACCHARIDE ELICITOR BINDING PROTEIN
CERK1	CHITIN ELICITOR RECEPTOR KINASE 1
cfu	colony forming unit
CL line	complementation line
COI1	CORONATINE INSENSITIVE 1
CoIP	co-immunoprecipitation
COR	coronatine
CPK 4/5/6/11/28	CALCIUM DEPENDENT PROTEIN KINASE 4/5/6/11/28
CrubLORE	*At*LORE ortholog from *Capsella rubella*
DAMP	damage-associated molecular pattern
DMSO	dimethyl sulfoxide
DNA	deoxyribonucleic acid
dNTPs	deoxynucleotides (dATP, dTTP, dCTP, dGTP)
DTT	dithiothreitol
DUF3403	domain of unknown function 3403

eAlyrLORE	ectodomain of AlyrLORE
eATP	extracellular ATP
***Ec* B4**	LPS of *E. coli* B4
EDTA	ethylenediaminetetraacetic acid
EFR	EF-TU RECEPTOR
EF-Tu	elongation factor thermo unstable
EGF-like	epidermal growth factor-like domain
eLORE	ectodomain of LORE
eSD123i	ectodomain of SD123i
eSD128i	ectodomain of SD128i
ET	ethylene
ETI	effector-triggered immunity
ETS	effector-triggered susceptibility
flg22	peptide flagellin 22
FLS2	FLAGELLIN-SENSING 2
FLS3	FLAGELLIN-SENSING 3
FRK1	FLAGELLIN-RESPONSIVE KINASE 1
GFP	green fluorescent protein
GlcNAc	β-1,4-linked *N*-acetyl-glucosamine
GNA-type RLK	*Galanthus nivalis* agglutinin-type RLK
GPR84	G protein-coupled receptor 84
h	hours
HA	hemagglutinin
3-HDA	3-hydroxydecanoic acid
HR	hypersensitive response
hv	hyper-variable region
iLORE	intracellular plus transmembrane domain of LORE
IP	immunoprecipitation
IPK	Leibniz-Institut für Pflanzengenetik und Kulturpflanzenforschung
JA	jasmonate
JA-Ile	jasmonate-isoleucine
JAZ	JASMONATE ZIM DOMAIN
L	liter
L_{max}	total luminescence remaining
kLORE	intracellular domain of LORE
LBP	LPS-binding protein
LecRK-I.9	L-type lectin receptor kinase-I.9
LecRK-V.2	L-type lectin receptor kinase-V.2
LecRK-VII.1	L-type lectin receptor kinase-VII.1
LLD1/2	lectin-like domain 1/2
LORE	coding sequence of *At*LORE
LPS	lipopolysaccharide
LRR	leucine-rich repeat
LSK1	LARGE SPIKE S-DOMAIN RECEPTOR-LIKE KINASE 1
LYK4/5	LYSM CONTAINING RECEPTOR KINASE 4/5
LysM	lysin motif
MAMP	microbe-associated molecular pattern

MAPK/MPK	mitogen-activated protein kinases
MAP3K	mitogen-activated protein kinase kinase kinase
mCherry	red fluorescent protein
MD2	MYELOID DIFFERENTIATION FACTOR 2
MeOH	methanol
MES	2-(*N*-morpholino) ethanesulfonic acid
MLPK	M-LOCUS PROTEIN KINASE
N	Golden Gate fusion site TTCA
NAC	NAM-ATAF-CUC2
NADPH	Nicotinamide adenine dinucleotide phosphate
NASC	Nottingham Arabidopsis Stock Centre
NHL10	NDR1/HIN1-LIKE 10
NLP1	NECROSIS AND ETHYLENE-INDUCING PEPTIDE 1
NLR	NUCLEOTIDE-BINDING SITE LEUCINE-RICH REPEAT
NT	no tag
OE line	overexpression line
OE-GFP	overexpression of LORE-GFP
OE-HA	overexpression of LORE-HA
OE-NT	overexpression of LORE-NT
OPS	O-polysaccharide chain
Os	*Oryzae sativa*, rice
OST1	OPEN STOMATA 1
P	Golden Gate fusion site CACC
***Pa* H4**	LPS of *P. aeruginosa* H4
PAN/APPLE	plasminogen nematode/apple
PBL	AvrPphB SUSCEPTIBLE LIKE PROTEIN
PBS1	AvrPphB SUSCEPTIBLE1
PCR	polymerase chain reaction
pGGEntL	Golden Gate entry vector
pGGIn	Golden Gate intermediate vector
PGN	peptidoglycan
pGGPlantXL /pGGPXB	Golden Gate binary vector
PROM	Golden Gate fusion site CGAG
PRR	pattern recognition receptor
PR1	PATHOGENESIS-RELATED 1
***Pst* DC3000**	LPS of *Pto* DC3000
PTI	pattern-triggered immunity
***Pto* DC3000**	*Pseudomonas syringae* pv. *tomato* DC3000
***Pto* DC3000 COR⁻**	*Pseudomonas syringae* pv. *tomato* DC3000 coronatine⁻
PUB	plant U-box protein
PVPP	polyvinylpyrrolidon
qRT-PCR	quantitative real time PCR
RBOHD	RESPIRATORY BURST OXIDASE HOMOLOG D
RIN4	RPM1-INTERACTING PROTEIN 4
RLU	relative light units

RLCK	receptor-like cytoplasmic kinase
RLK	receptor-like kinase
RLP	receptor-like protein
RNA	ribonucleic acid
ROI	region of interest
ROS	reactive oxygen species
rpm	rotation per minute
RPM1	RESISTANCE TO *Pseudomonas syringae* pv. *maculicola* 1
R protein	resistance protein
RPS2/5	RESISTANCE TO *P. syringae* 2/5
RT	room temperature
SA	salicylic acid
SAR	systemic acquired resistance
SCR	S-LOCUS CYSTEINE-RICH PROTEIN
SD	standard deviation
SD-RLK	S-domain receptor-like kinase
SDS	sodium dodecyl sulfate
SDS2	SPL11 CELL-DEATH SUPPRESSOR 2
SEM	standard error of the mean
SERK	SOMATIC EMBRYOGENESIS RECEPTOR KINASES
SI	self-incompatibility
SIK2	STRESS-INDUCED PROTEIN KINASE 2
SLAC1	SLOW ANION CHANNEL 1
SLG	S-locus glycoprotein
SOBIR/EVR	SUPPRESSOR OF BAK1-INTERACTING RECEPTOR-LIKE KINASE1-1/EVERSHED
SOD	superoxide dismutase
SP	signal peptide
SPL11	SPOTTED-LEAF 11
SPYCE	carboxy-terminal part of YFP
SPYNE	amino-terminal part of YFP
sqPCR	semi-quantitative PCR
SRK	S-LOCUS RECEPTOR KINASE
START	Golden Gate fusion site AATG
STOP	Golden Gate fusion site TAGT
STP13	SUGAR TRANSPORTER PROTEIN 13
T-DNA	transfer DNA
TEMED	*N*, *N*, *N´*, *N´* tetramethylethylenediamine
TERM	Golden Gate fusion site CCGC
TIR	Toll-interleukin 1-like receptor
tLORE	ectodomain plus transmembrane domain of LORE
TLR	TOLL-LIKE RECEPTOR
TM	transmembrane domain
U	unit
UBQ5	UBIQUITIN 5
WRKY33	WRKY DNA BINDING PROTEIN 33

XA21	LRR-RLK mediating resistance against *X. oryzae* pv. *oryzae* in rice
***Xcm*#2**	LPS of *X. campestris* pv. *malvacearum*
***Xcm*#4**	LPS of *X. campestris* pv. *malvacearum*
YFP	yellow fluorescent protein
YLS9	YELLOW-LEAF-SPECIFIC GENE 9

3 Introduction

Abiotic and biotic stresses such as extreme temperature, insufficient water and nutrient supply, weeds, or pathogens such as fungi, oomycetes, and bacteria, cause yield losses of important crop plants and can reduce the product quality and marketability. Abiotic and biotic stresses are a threat to the food security of the society (Seck *et al.*, 2012, Oerke, 2006). Facing a growing world population, production of important crops for adequate nutrition needs to increase about 2.4% per year (Ray *et al.*, 2013). However, suitable farmland is restricted which points out the great importance of the prevention of crop losses due to pathogen infection and the need to increase the yield by breeding more resistant plant varieties (Ray *et al.*, 2013, Seck *et al.*, 2012, Mansfield *et al.*, 2012). Almost half of the world's population relies on the nutrition with rice (*Oryza sativa*) (Seck *et al.*, 2012). *Xanthomonas oryzae* pv. *oryzae* is the causal agent of bacterial leaf blight on rice in Asia and disease outbreaks can decrease the yield by up to 50% (Mew *et al.*, 1993). Other foliar diseases like bacterial blight or spot disease caused by *Pseudomonas* spp., but also *Xanthomonas* spp., on crops such as tomato, bean, or soybean are considered as major hazards for the agricultural industry and food security (Ray *et al.*, 2013, Mansfield *et al.*, 2012, Leben *et al.*, 1971). Disease symptoms occur on the fruit, but mainly on leaves as water-soaked spots, wilting, or necrotic lesions. Economically relevant *Brassica* species like cabbages or radishes are infected by *Xanthomonas campestris* pv. *campestris* causing black rot. Infection symptoms are yellow lesions on leaves and blackening of veins (Mansfield *et al.*, 2012, Williams, 1980). In favorable environmental conditions for the pathogen such as high humidity, aggressive microbial multiplication can reduce yield and product quality (Xin *et al.*, 2016, Hirano *et al.*, 2000, Leben *et al.*, 1971). To date, disease outbreaks are mainly controlled by the application of plant-protective chemicals such as insecticides, bactericides, and fungicides (Jaggard *et al.*, 2010). Bacterial pathogens are controlled by the application of copper and chemicals or avirulent bacterial strains to induce the plant's own immune system (Yuliar *et al.*, 2015, Mansfield *et al.*, 2012). Permanent application of chemicals in the field risks the emergence of resistances to plant-protective substances in pathogens (Bardin *et al.*, 2015, Jaggard *et al.*, 2010). The climate change will lead to an increased temperature which potentially favors disease outbreaks and disease progression even more. For this reason, novel approaches to increase crop yields are needed. Durable resistance of crops might also be achieved by genetic engineering of the plant and its immune system to reduce yield losses due to infection (Jaggard *et al.*, 2010, Oerke, 2006, section 3.11). Therefore, it is of great importance to understand plant-microbe interaction in more detail to meet the challenges of a growing world population and the climate change.

3.1 Plant immunity

Plants are constantly at risk of infection by pathogenic microbes. Plants are not defenseless, but have evolved various mechanisms to ward off possible threats (Boller *et al.*, 2009, Jones *et al.*, 2006). Plant resistance is multi-tiered and comprises pre-formed structural and chemical barriers as well as inducible plant immunity (Jones *et al.*, 2006). Pre-formed barriers are structural obstacles formed by the plant such as the cuticle or the cell wall (Schreiber, 2010). If pathogens overcome the pre-formed barriers, plants are able to detect microbes by the perception of microbe-associated molecular patterns (MAMP). MAMPs are molecular signatures that are conserved and essential for microbial survival, but are absent from the host for instance bacterial flagellin (Boller *et al.*, 2009). MAMP-sensing is mediated by specific cell surface pattern recognition receptors (PRR) that initiate a common set of cellular signaling and defense responses, typically, referred to as pattern-triggered immunity (PTI) (Jones *et al.*, 2006). PTI is also triggered upon sensing of damage-associated molecular patterns (DAMP), defined as host-derived substances occurring upon infection or wounding. The induction of PTI leads to immune responses including the production of reactive oxygen species (ROS), ion fluxes, stomatal closure, and transcriptional reprogramming which help the plant to confine bacterial invasion into the leaf interior (Boller *et al.*, 2009, Jones *et al.*, 2006). Pathogens secrete various effectors to impede defense responses of the plant to promote disease progression, resulting in effector-triggered susceptibility (ETS). However, plants survey their cellular space using specialized resistance proteins (R proteins) which recognize these effectors. Successful perception leads to effector-triggered immunity (ETI) which can result in local cell death known as hypersensitive response (HR) (Yu *et al.*, 2017). Conceptually, ETI represents the second layer of defense in plants. Effectors are also termed avirulence factors when they are perceived by R proteins as they reveal the presence of the pathogen (Jones *et al.*, 2006). This relation was summarized by Jones *et al.* (2006) in the zigzag model (Figure 1). Both, hosts and pathogens, are under constant evolutionary pressure which can lead to the development of new effectors and R proteins. The zigzag model decomplicates the correlation of PTI, ETS, and ETI. However, it neglects the complexity of immune responses and does not take the manifold interactions between PTI and ETI into account. An increasing body of evidence shows that PTI and ETI share the same signaling machinery, but differences are found in the signature and duration of single responses (Peng *et al.*, 2017). In general, ETI induces prolonged and enhanced responses compared to PTI (Tsuda *et al.*, 2010). Another layer of complexity of immune responses is added by SAR (systemic acquired resistance) (Ross, 1961). Local infection induces broad-spectrum and long-lasting resistance in distant tissues which is associated with the accumulation of the phytohormone salicylic acid (SA) and pathogenesis-related proteins (Spoel *et al.*, 2012).

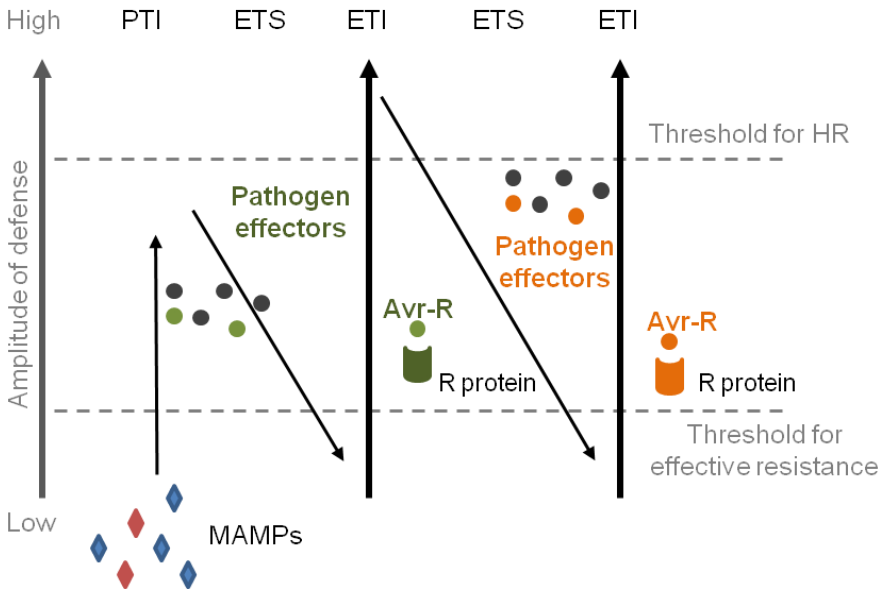

Figure 1 The zigzag model describes the interplay of pathogenic microorganisms and plant immune responses. Plants detect invading pathogens *via* microbe-associated molecular patterns (MAMP) with the help of cell surface receptors. Immune responses are then initiated leading to pattern-triggered immunity (PTI). Pathogens secrete effector proteins to suppress plant immunity and promote disease development resulting in effector-triggered susceptibility (ETS). Surveillance by the plant of the cellular space is mediated by so-called R proteins (resistance proteins) recognizing specific effectors (avirulence factors (Avr-R)) resulting in effector-triggered immunity (ETI). In infected tissues, plants induce the hypersensitive response (HR) causing local cell death (modified from Jones *et al.*, 2006).

3.2 Pre-formed immunity

Pre-formed defense is mediated by morphological structures which are constantly present in the plant. Aim of these defenses is to prevent pathogens from entry into the plant interior (Freeman *et al.*, 2008). The cuticle is the very first pre-formed mechanical barrier for microbes arriving on the leaf surface (Schreiber, 2010). It prevents microbial contact to the epidermis and due to its hydrophobic nature also the accumulation of water. Wet spots might be beneficial for bacterial motility, fungal spore germination, or degrading enzymes of the plant cell wall which is a matrix formed of cellulose fibers cross-linked to branched polysaccharide chains such as hemicelluloses and pectin (Schreiber, 2010). Lignification of the plant cell wall confers further rigidity and impermeability (Passardi *et al.*, 2004). Plants respond with deposition of β-1,3 glucan polymers (callose deposition) at the penetration site of fungal pathogens to hinder invasion (Freeman *et al.*, 2008, Hückelhoven, 2007). Plants also produce a great number of secondary metabolites including alkaloids, terpenoids, and phenolic compounds with a repellent effect on insects, but also protective characteristics against bacteria and fungi (Freeman *et al.*, 2008, Glazebrook *et al.*, 1994). Synthesis can be induced upon pathogen detection,

but some are constitutively produced by plants as a measure to reduce infection (Halkier *et al.*, 2006). Another important immune response at the pre-invasive level is the regulation of the stomatal aperture described in more detail in section 3.4 (Sawinski *et al.*, 2013).

3.3 Induced immunity

Defense responses, helping to establish PTI, are induced upon perception of MAMPs by PRRs *via* the activation of downstream signaling cascades (Jones *et al.*, 2006). Immune regulatory processes and plant–pathogen interactions take place in the apoplast which is an important space for the establishment of immunity (Doehlemann *et al.*, 2013).

3.3.1 Pattern-triggered immunity

Plants do not solely rely on the hindrance of pathogens to enter the leaf interior by mechanical and chemical barriers, but evolved sophisticated molecular mechanisms to counteract infection (Jones *et al.*, 2006). Recognition of MAMPs by PRRs results in die initiation of PTI, the first layer of defense. MAMPs are often motifs of conserved structures important for microbial survival and are perceived by a wide range of plants such as *Arabidopsis thaliana* (hereafter referred to as Arabidopsis). The perception of MAMPs can also be described as a non-self detection (Boller *et al.*, 2009). Such molecules are for example flagellin, part of the bacterial flagellum, elongation-factor Tu, involved in prokaryotic protein biosynthesis, constituents of the bacterial cell wall such as peptidoglycan (PGN) or lipopolysaccharide (LPS), as well as fungal cell wall components like chitin (Ranf *et al.*, 2015, Gust *et al.*, 2007, Kunze *et al.*, 2004, Felix *et al.*, 1999). Plants also sense DAMPs which can be described as self or altered-self detection. DAMPs are molecules released upon infection or wounding by the plant. Extracellular adenosine-5'-triphosphate (eATP) was shown to act as a DAMP and is potentially released by damaged plant cells (Tanaka *et al.*, 2014). Moreover, plant cell wall fragments such as oligogalacturonides derived from mechanical forces or enzymatic degradation are perceived as a DAMP in Arabidopsis (Brutus *et al.*, 2010). PTI comprises various biochemical changes. These can be divided into early responses emerging seconds to minutes after pathogen detection or late responses appearing hours later. Temporally, the influx of calcium into the cytosol is induced resulting in an elevated cytosolic calcium concentration ($[Ca^{2+}]_{cyt}$). The rapid increase of cytosolic calcium is depending on passive fluxes *via* calcium channels into the cytoplasm (Ranf *et al.*, 2015, Seybold *et al.*, 2014, Ranf *et al.*, 2011). Another typical rapid response is the production of apoplastic reactive oxygen species (ROS) (Torres, 2010). The ROS burst, also termed oxidative burst, is induced a few minutes after elicitation, the maximum is reached after around 15 to 20 min and declines around 30 min. Plasma membrane-localized NADPH oxidases such as *At*RBOHD and *At*RBOHF (RESPIRATORY BURST OXYGENASE HOMOLOG D/F) transfer electrons from NADPH

(Nicotinamide adenine dinucleotide phosphate) to apoplastic oxygen molecules forming superoxide anions. Dismutases convert superoxide to hydrogen peroxide, but this conversion can also happen spontaneously (Lamb *et al.*, 1997). ROS is thought to strengthen the cell wall by cross-linkage of cell wall polymers as well as forming a toxic border to pathogens (Kimura *et al.*, 2017, Torres, 2010). Calcium fluxes have a positive effect on ROS production. *At*RBOHD contains two EF hand motifs which undergo conformational changes due to calcium binding (Ogasawara *et al.*, 2008). Additionally, phytohormones play an eminent role in plant immunity. The phytohormones SA, jasmonate (JA), and ethylene (ET) are associated with immune responses. JA, ET, and SA show an antagonistic character which fine-tunes defense responses specific to the type of invading pathogen. SA is mainly connected to resistance against hemibiotrophs such as *Pseudomonas syringae* pv. *tomato* DC3000 (*Pto* DC3000) (Glazebrook, 2005). JA, but also ET are connected to resistance against necrotrophs such as *Alternaria brassicicola* (Glazebrook, 2005). This classification is generally applicable, but SA, JA, and ET can have an effect also on defense responses to necrotrophs or hemibiotrophs, respectively (Glazebrook, 2005). JA signaling is described in more detail in section 3.4. Pathogen challenges cause the rise of SA in plants which is achieved by differential gene expression of SA catabolizing enzymes (Wildermuth *et al.*, 2001). The SA level increases in the phloem, but also in distant tissues upon the induction of SAR (Spoel *et al.*, 2012). Production of the phytohormone ET can be observed within the first 6 h upon infection (Felix *et al.*, 1999). ET deploys a positive effect on defense gene expression by ET-responsive transcription factors (Boutrot *et al.*, 2010). Transcriptional reprogramming is a hallmark of plant immune responses and genes upregulated in response to MAMP treatment involve genes of transcription factors, genes involved in hormone signaling, regulatory genes, and genes coding for PRRs (Gust *et al.*, 2007, Navarro *et al.*, 2004, Zipfel *et al.*, 2004).

3.3.2 Receptor complex formation in plant immunity

Defense signaling is mediated by multi-protein complexes with PRRs, co-receptors, and other regulatory proteins allowing rapid signal transduction as well as dynamic regulation of immune responses after pattern recognition. Oligomerization and dimerization of proteins play a crucial role in receptor complex activation of PRRs (Couto *et al.*, 2016). PRRs belong to the class of receptor-like kinases (RLK) or receptor-like proteins (RLP) forming large protein families in Arabidopsis (Fritz-Laylin *et al.*, 2005, Shiu *et al.*, 2004). Cell surface-localized RLKs and RLPs orchestrate a wide range of physiological processes from hormone perception to development to immunity (Shiu *et al.*, 2001b). Genes encoding RLKs are expanding in the genome of plants which emphasizes their importance for plants (Shiu *et al.*, 2004). RLKs consist of an intracellular serine/threonine kinase domain, a single-pass transmembrane domain, and differ in their extracellular domains. RLPs are structurally similar, but lack the intracellular kinase domain. Extracellular domains are likely to determine ligand-specificity and ligand-binding. RLKs can be classified into 44 subfamilies by the architecture of their extracellular domain which can be leucine-rich repeats (LRR), lectins, or Lysin motifs (LysM) (Shiu

et al., 2001a). The best-studied PRR-ligand pair is *At*FLS2 (FLAGELLIN-SENSING 2) and bacterial flagellin (Gomez-Gomez *et al.*, 2000, Chinchilla *et al.*, 2006). A 22 amino acid fragment of the N terminus of flagellin (flg22) has immunogenic activity in Arabidopsis (Gomez-Gomez *et al.*, 2000). *At*FLS2 belongs to the class of LRR-RLKs, the largest group of RLKs with 200 members in Arabidopsis (Shiu *et al.*, 2003). *At*FLS2 has 28 LRRs and repeat 3 to 16 are involved in ligand binding. *At*FLS2 forms a ligand- and receptor-induced heteromeric complex with the extracellular domain of the co-receptor *At*BAK1 (BRASSINOSTEROID INSENSITIVE1-ASSOCIATED RECEPTOR KINASE 1) (Sun *et al.*, 2013b, Chinchilla *et al.*, 2007, Heese *et al.*, 2007) (Figure 2). The extracellular domains of *At*FLS2 and *At*BAK1 interact with each other, and the C-terminal part of flg22 additionally functions as a bridge between the ectodomains (Sun *et al.*, 2013b). Upon heterodimerization, transphosphorylation events of *At*FLS2 and *At*BAK1 intracellular domains occur, leading to the activation of *At*FLS2 and *At*BAK1 and initiating plant immune outputs (Schwessinger *et al.*, 2011, Schulze *et al.*, 2010, Chinchilla *et al.*, 2007). Current understanding of *At*FLS2/*At*BAK1 heterodimerization was recently complemented by a study of Somssich *et al.*, 2015. Upon flg22 perception, *At*FLS2 and *At*BAK1 form higher complexes consisting of two *At*BAK1 proteins flanked by two *At*FLS2 proteins (Somssich *et al.*, 2015). *At*BIR2 (BAK1-INTERACTING RECEPTOR-LIKE KINASE 2) constitutively interacts with *At*BAK1 in the absence of flg22 and negatively regulates *At*BAK1 function (Halter *et al.*, 2014). Upon ligand binding to *At*FLS2, the complex of *At*BIR2 and *At*BAK1 dissociates, and *At*BAK1 enters a complex with *At*FLS2 to induce immune responses (Halter *et al.*, 2014). Mutants lacking a functional *At*FLS2 are more susceptible to spray infection with the bacterial plant pathogen *Pto* DC3000, but not to direct infection of the leaf apoplast (Zipfel *et al.*, 2004). *At*BAK1 is part of the SERK (SOMATIC EMBRYOGENESIS RECEPTOR KINASES/*At*SERK3) protein family and functions as a versatile co-receptor for several LRR-RLKs such as *At*EFR (EF-Tu RECEPTOR) or *At*BRI1 (BRASSINOSTEROID INSENSITIVE 1) (Schulze *et al.*, 2010, Li *et al.*, 2002). *At*BRI1 perceives the plant-specific hormone brassinosteroid and orchestrates plant growth and developmental processes (Santiago *et al.*, 2013). Receptor complex formation of *At*BAK1 and *At*BRI1 is similar to the one described for *At*FLS2. Brassinosteroid binding induces heterodimerization of the LRR domains of *At*BAK1 and *At*BRI1 (Sun *et al.*, 2013a). Intriguingly, the function of *At*BAK1 in development is independent of its function in immunity of plants relying on phosphorylation-dependent regulation (Perraki *et al.*, 2018, Schwessinger *et al.*, 2011). The PRR *At*EFR recognizes the immunogenic 18 amino acid-long peptide (elf18) from the abundant prokaryotic protein elongation factor Tu in Arabidopsis (Kunze *et al.*, 2004). In rice, the LRR-RLK *Os*XA21 mediates resistance against *X. oryzae* pv. *oryzae*, and constitutively associates with the *At*BAK1 ortholog *Os*SERK2 in a ligand-independent manner (Chen *et al.*, 2014, Song *et al.*, 1995). Another important class of PRRs represent the LysM-containing RLKs. LysM-RLKs mediate sensing of major cell wall structures such as chitin of fungi or PGN of bacteria (Gust *et al.*, 2007). Chitin is sensed by a multi-protein complex consisting of LysM-RLKs *At*LYK4, *At*LYK5 (LysM-

CONTAINING RECEPTOR KINASE 4/5), and *At*CERK1 (CHITIN ELICITOR RECEPTOR KINASE 1) in Arabidopsis (Cao *et al.*, 2014, Wan *et al.*, 2012 Wan *et al.*, 2008, Miya *et al.*, 2007). The extracellular domain of *At*CERK1 comprises three LysM domains where domain two binds to chitin oligomers consisting of seven to eight *β*-1,4-linked *N*-acetyl-glucosamine (GlcNAc) units (Liu *et al.*, 2012, Petutschnig *et al.*, 2010). Chitin fragments (*N*-acetylchitooligosaccharides), in particular chitin octamers, bind to the extracellular domain of two *At*CERK1 monomers inducing *At*CERK1 homodimerization and signal transduction (Wan *et al.*, 2008, Miya *et al.*, 2007) (Figure 2). *At*LYK5 possesses an even higher binding affinity to chitin compared to *At*CERK1 itself indicating that *At*LYK5 is the actual receptor for chitin oligomers (Cao *et al.*, 2014). *At*LYK5 interacts with *At*CERK1 and promotes chitin-induced homodimerization of *At*CERK1. Interestingly, *At*LYK5 kinase activity is dispensable for chitin signaling, but the kinase domain is required for *At*CERK1 and *At*LYK5 oligomerization (Cao *et al.*, 2014). Strikingly, chitin perception in *O. sativa* evolved differently and is described as a 'sandwich-type dimerization' (Hayafune *et al.*, 2014). The RLP, *Os*CEBIP (CHITIN OLIGOSACCHARIDE ELICITOR BINDING PROTEIN) forms chitin-mediated homodimers and recruits *Os*CERK1 to the complex. *Os*CERK1 has only a single LysM domain which does not bind chitin, but has an active kinase domain required for signaling (Hayafune *et al.*, 2014, Shimizu *et al.*, 2010). The perception of the bacterial cell wall component PGN in Arabidopsis is reminiscent of chitin perception in rice. The RLPs *At*LYM1 and *At*LYM3 (LysM DOMAIN PROTEIN 1/3) bind to PGN, but as they lack the cytoplasmic kinase domain a co-receptor for the induction of intracellular signaling is required. Signal transduction upon PGN perception relies on *At*CERK1. Upon PGN binding, *At*LYM1 and *At*LYM3 oligomerize with *At*CERK1 and induce downstream signaling (Willmann *et al.*, 2011). This example illustrates multiple roles of *At*CERK1 in PTI in Arabidopsis (Willmann *et al.*, 2011). The LRR-RLK SOBIR1/EVR (SUPPRESSOR OF BAK1 INTERACTING RECEPTOR-LIKE KINASE 1-1/EVERSHED) was identified as an adaptor kinase in tomato to associate with RLPs (Liebrand *et al.*, 2014, Liebrand *et al.*, 2013, Gao *et al.*, 2009). SOBIR1/EVR associates with the RLP Cf-4 of tomato to mediate resistance against the fungal pathogen *Cladosporium fulvum* (Liebrand *et al.*, 2013). Ligand-independent interaction of *At*SOBIR1/EVR with RLPs was shown in Arabidopsis (Albert *et al.*, 2015). Lectin receptor-like kinases (LecRLKs) form a class of RLKs characterized by the N-terminal lectin motifs which accordingly divides into the three subgroups GNA- (G), legume-like- (L), and calcium-dependent- (C)-type lectin RLKs (Bellande *et al.*, 2017, Vaid *et al.*, 2012). GNA-type (*Galanthus nivalis* agglutinin) or G-type lectin resembles an α-D-mannose binding motif (Van Damme *et al.*, 2007). Legume-like or L-type lectin resembles soluble legume lectins and C-type lectin domains are similar to mammalian calcium-dependent lectin motifs (Vaid *et al.*, 2012). L-type and G-type RLKs are expanded in plants and C-type RLKs in animals (Bellande *et al.*, 2017). G-type LecRLKs, also termed bulb-type (B) lectin RLK and best known as S-domain-RLKs, are described in section 3.9 (Vaid *et al.*, 2012, Bouwmeester *et al.*, 2009). The L-type LecRLKs protein family has 45

members in Arabidopsis further divided into nine clades LecRK-I to LecRK-IX and various members are associated with plant immunity (Bouwmeester *et al.*, 2009).

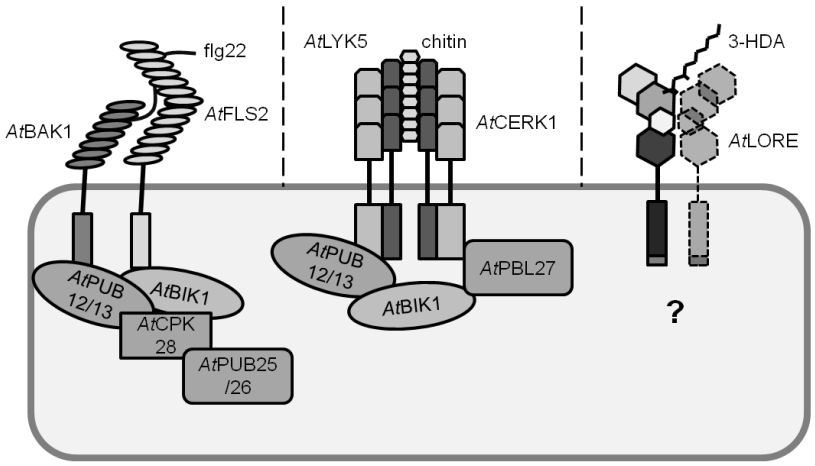

Figure 2 Schematic illustration of receptor complex formation in plant immunity. Microbe-associated molecular patterns (MAMPs) are perceived by specific pattern recognition receptors (PRRs). *At*FLS2 (FLAGELLIN-SENSING 2) perceives flg22 (22 amino acid peptide of bacterial flagellin) and forms a ligand-induced complex with *At*BAK1 (BRI1-ASSOICIATED KINASE 1). *At*FLS2 recruits the receptor-like cytoplasmic kinase *At*BIK1 (BOTRYTIS INDUCED KINASE 1) which is regulated by *At*CPK28 (CALCIUM-DEPENDENT PROTEIN KINASE 28) and *At*PUB25/26 (PLANT U-BOX 25/26). Regulation of *At*FLS2 is mediated by *At*PUB12/13 (PLANT U-BOX 12/13). *At*CERK1 (CHITIN ELICITOR RECEPTOR KINASE 1) associates with homodimers of *At*LYK5 (LYSM CONTAINING RECEPTOR KINASE 5) which bind oligomers of the fungal cell wall component chitin. Signal transduction requires *At*BIK1 as well as *At*PBL27 (PBS1-LIKE PROTEIN 27). The receptor complex activation of *At*LORE (LIPOOLIGOSACCHARIDE-SPECIFIC REDUCED ELICITATION) and binding of 3-HDA (3-hydroxydecanoic acid) is not completely elucidated yet and is therefore marked with a question mark.

Multiple roles in immunity are described for the RLK *At*LecRK-I.9. Mutant plants lacking a functional *At*LecRK-I.9 produce less callose in response to *Phytophthora brassicae* indicating a role in cell wall-associated immunity (Bouwmeester *et al.*, 2011). Interestingly, *At*LecRK-I.9 is also involved in resistance to *Pto* DC3000. *At*LecRK-I.9 most likely regulates JA signaling components (Balagué *et al.*, 2017). Additionally, another study identified *At*LecRK-I.9 as the receptor for the DAMP eATP and named the receptor *At*DORN1 (DOES NOT RESPOND TO NUCLEOTIDES 1) (Choi *et al.*, 2014).

3.3.3 Signaling components involved in plant immune responses

Detection of pathogens *via* PRRs induces a common set of physiological responses in plants. This requires not only the activation of membrane bound receptor proteins, but activation of a multilayered network of signaling components (Couto *et al.*, 2016). Receptor-like cytoplasmic kinases (RLCK), calcium-dependent protein kinases (CDPK), and mitogen-activated protein kinases (MAPK) take over crucial roles in signal transduction in response to a variety of MAMPs (Couto *et al.*, 2016). RLCKs belong to the class of RLKs, but lack a transmembrane domain and an extracellular domain for ligand-binding (Shiu *et al.*, 2004). In Arabidopsis, 149 RLCKs are present which can be divided into 17 subgroups (RLCK-II; RLCK-IV to RLCK-XIX) (Shiu *et al.*, 2004). The membrane-tethered RLCK *At*BIK1 (BOTRYTIS INDUCED KINASE 1) belongs to the RLCK-VII subgroup and was identified by transcript analysis of Arabidopsis treated with *Botrytis cinerea* which induced the expression of *AtBIK1*. *At*BIK1 is part of the *At*FLS2 receptor complex and is directly phosphorylated by *At*BAK1 upon flg22 recognition (Lu *et al.*, 2010, Zhang *et al.*, 2010). This initiates further phosphorylation events. *At*BIK1 phosphorylates *At*FLS2 and *At*BAK1 before dissociation from the receptor complex. Dissociated *At*BIK1 relays the immune response by phosphorylation of the N terminus of *At*RBOHD, and thus positively regulates the oxidative burst independent of calcium signaling (Kadota *et al.*, 2014, Li *et al.*, 2014). *At*RBOHD itself is part of the *At*FLS2 receptor complex. In addition to the ROS burst, which is reduced in *bik1*, mutant plants are also disturbed in calcium influx to the cytosol, ET signaling, and plant growth (Ranf *et al.*, 2014, Laluk *et al.*, 2011, Lu *et al.*, 2010, Zhang *et al.*, 2010). *At*BIK1 acts also downstream of *At*CERK1to induce immune responses (Zhang *et al.*, 2010). This illustrates that *At*BIK1 is a convergent RLCK addressed by multiple PRRs (Lu *et al.*, 2010, Zhang *et al.*, 2010). However, PRRs can maintain signal specificity by recruitment of particular components controlling PTI. *At*PBL27 (AvrPphB SUSCEPTIBLE 1-LIKE PROTEIN 27) is preferentially acting downstream of *At*CERK1 (Shinya *et al.*, 2014). Immune responses such as the activation of MAPKs in response to flg22 are not strongly changed in *pbl27*, but when treated with chitin (Shinya *et al.*, 2014). Interestingly, RLCKs can also function as negative regulators of PTI. One example is *At*PBL13 (AvrPphB SUSCEPTIBLE 1-LIKE PROTEIN 13) which associates with *At*RBOHD in a flg22-independent manner to prevent immune signaling (Lin *et al.*, 2015).

CDPKs act as Ca^{2+} sensors and modulate PTI responses both in a positive as well as in a negative way, and form a structurally conserved protein family with 34 members in Arabidopsis (Cheng *et al.*, 2002). CDPKs contain a conserved serine/threonine kinase domain, four Ca^{2+}-binding EF hand motifs at the C terminus and a variable N-terminal domain (Liese *et al.*, 2013). *At*CPK4, *At*CPK5, *At*CPK6, and *At*CPK11 (CALCIUM-DEPENDENT PROTEIN KINASE 4/5/6/11) act redundantly upon flg22 treatment and are important regulators of the ROS burst as well as the expression of defense genes such as *AtNHL10* (*NDR1/HIN1-LIKE 10* also known as *AtYLS9* (*YELLOW-LEAF-SPECIFIC GENE 9*)) (Boudsocq *et al.*, 2010, Dörmann *et al.*, 2000). Detection of MAMPs is associated with an elevated $[Ca^{2+}]_{cyt}$ level. Binding of Ca^{2+} to the EF hand motifs of CDPKs leads to conformational changes and

subsequently kinase activation (Dubiella *et al.*, 2013). Activated CDPKs positively regulate the ROS burst by phosphorylation of N-terminal serine residues of *At*RBOHD (Dubiella *et al.*, 2013). On the other hand, *At*CPK28 (CALCIUM-DEPENDENT PROTEIN KINASE 28) dampens the immune response. *At*CPK28 phosphorylates *At*BIK1 which is in turn degraded *via* the 26S proteasome pathway (Monaghan *et al.*, 2014). This example for signal attenuation is described in more detail in section 3.5. MAPKs regulate a wide variety of cellular responses involved in immunity, development, and growth in plants (Meng *et al.*, 2013). Generally, phosphorylation and activation of MAPKs is composed of a tripartite mechanism. The MAPK kinase kinase (MEKK/MAP3K) phosphorylates and thus activates MAPK kinase (MKK/MAP2K) which phosphorylates MAPK at the conserved Thr-Glu-Tyr/Thr-Asp-Tyr motif (Meng *et al.*, 2013). Activated MAPKs phosphorylate different target proteins and in this way, activate or inactive gene expression and metabolic processes (Meng *et al.*, 2013). The MAPK cascade composed of *At*MEKK1, *At*MKK4/5, and *At*MPK3/6 (MITOGEN-ACTIVATED PROTEIN KINASE 3/6) positively regulates PTI signaling (Asai *et al.*, 2002). Defense expression of the flg22-responsive gene *AtFRK1* (*FLG22-INDUCED RECEPTOR-LIKE KINASE 1*) is highly dependent on MAPK signaling, but does not require CDPK signaling (Boudsocq *et al.*, 2010, Asai *et al.*, 2002). The activation of the transcription factor *At*WRKY33 (WRKY DNA BINDING PROTEIN 33) relies also on phosphorylation by *At*MPK3 and *At*MPK6 (Guan *et al.*, 2015). *At*WRKY33 induces the transcription of key regulatory enzymes in the ET production pathway (Guan *et al.*, 2015). Additionally, *At*MPK6 directly phosphorylates *At*ACS6 (1-AMINOCYCLOPROPANE-1-CARBOXYLIC ACID SYNTHASE 6). Phosphorylated *At*ACS6 accumulates and promotes ET production (Liu *et al.*, 2004). Also, other MAP3Ks such as *At*MAP3K5 have an impact on immunity. *At*MAP3K5 preferentially acts in response to chitin downstream of *At*CERK1. The RLCK *At*PBL27 binds both *At*CERK1 and *At*MAP3K5 and thus might be the missing link connecting receptor activation and MAPK signaling (Yamada *et al.*, 2016b).

3.4 Stomatal movement and stomatal immunity

Stomata play a critical role in the pre-invasive immunity of plants (section 3.2). The stomatal pore is encompassed by a pair of guard cells in the epidermis regulating uptake of carbon dioxide (CO_2) and transpiration by the adjustment of the stomatal aperture through turgor changes (Zoulias *et al.*, 2018). The stomatal aperture is influenced by temperature, concentration of carbon dioxide, light, and relative humidity (Zoulias *et al.*, 2018). Moreover, the movement of stomata is important in the regulation of drought stress mainly regulated by the phytohormone abscisic acid (ABA) (Zoulias *et al.*, 2018). Pathogenic bacteria rely on natural leaf openings such as stomata or wounds to gain access to host tissue (Melotto *et al.*, 2006). Upon detection of invading pathogens, plants induce stomatal closure and inhibit stomatal opening to prevent bacterial invasion, a process named stomatal immunity or defense which counts to the pre-invasive immune responses (Sawinski *et al.*, 2013, Melotto *et al.*,

2006). As a countermeasure, *Pto* DC3000 has evolved mechanisms to reopen stomata upon infection which is described in section 3.7.2 and 3.8 (Melotto *et al.*, 2006). It was shown that plants react with stomatal closure to the treatment with MAMPs such as flg22, LPS, chitin, and elf18, but also DAMPs like eATP (Chen *et al.*, 2017, Zeng *et al.*, 2010, Desikan *et al.*, 2008, Melotto *et al.*, 2006, Lee *et al.*, 1999). The unrevealing of guard cell signaling upon perception of MAMPs is a matter of current research, but shows similarities to ABA-mediated stomatal movement (Ye *et al.*, 2016). Similar to the drought stress response, the guard cell-specific SnRK2.6 (SUCROSE NON FERMENTING 1-related protein kinase) *At*OST1 (OPEN STOMATA 1) is central for flg22- and LPS-induced stomatal closure (Guzel Deger *et al.*, 2015, Melotto *et al.*, 2006, Mustilli *et al.*, 2002). *At*OST1 activates S-type anion channels such as *At*SLAC1 (SLOW ANION CHANNEL 1) leading to anion efflux and plasma membrane depolarization in response to flg22 and ABA (Guzel Deger *et al.*, 2015, Merlot *et al.*, 2007, Mustilli *et al.*, 2002). A prerequisite for flg22-triggered stomatal closure is ROS produced by *At*RBOHD (Li *et al.*, 2014). ABA signaling relies on *At*RBOHD and *At*RBOHF which are phosphorylated by *At*OST1 (Sirichandra *et al.*, 2009, Kwak *et al.*, 2003). The CDPK *At*CPK6 positively regulates *At*SLAC1 activity by phosphorylation resulting in stomatal closure (Li *et al.*, 2014, Scherzer *et al.*, 2012). CDPKs such as *At*CPK6 are addressed by ABA as well as MAMP-signaling and hence represent a shared point of signaling (Ye *et al.*, 2016). MAMP-mediated *At*CPK6 activation depends on the elevation of $[Ca^{2+}]_{cyt}$ (Dubiella *et al.*, 2013, Boudsocq *et al.*, 2010). Also *At*AHA1/2 (H^+-ATPases 1/2), modulate the stomatal aperture by the transport of H^+ into the apoplast. Changes in the plasma membrane potential and subsequent uptake of charged substances and water lead to stomatal opening (Liu *et al.*, 2009). Sensing of MAMPs might lead to the suppression of H^+-ATPase activity and inhibition of stomatal opening (Liu *et al.*, 2009). *At*DORN1 is involved in regulation of the stomatal aperture upon recognition of the DAMP eATP (Chen *et al.*, 2017). The exact downstream signaling pathway of *At*FLS2 and *At*DORN1 to close stomata is not resolved yet. ABA- and MAMP-mediated stomatal closure differ upstream of *At*OST1, but show similarities downstream of *At*OST1 (Ye *et al.*, 2016). Moreover, stomatal immunity is a cell-autonomous response, not all stomata of a challenged leaf close their stomata and the relative humidity has an influence on stomatal defense (Panchal *et al.*, 2016, Melotto *et al.*, 2006).

3.5 Immune response attenuation

Desensitization and attenuation of signaling responses is a crucial regulatory step in plant immunity. Otherwise, activated receptor complexes might signal permanently or become insensitive to reactivation upon pathogen attack. Therefore, it is of great importance to maintain signaling competence. Moreover, constant activation of defense signaling can be detrimental for the growth and yield of plants (Huot *et al.*, 2014). Long-term exposure of plants to MAMPs such as flg22 or elf18 results in seedling growth inhibition which can be explained by a rebalancing of the energy

consumption and reallocation of resources from growth to defense (Huot *et al.*, 2014, Zipfel *et al.*, 2006, Gómez-Gómez *et al.*, 1999). Autoactivation of immune components such as *At*BAK1 can be accompanied by spontaneous cell death phenotypes which is described as autoimmunity (Domínguez-Ferreras *et al.*, 2015). Plants maintain signaling competence by the tight regulation of activated receptor complexes. One possibility to attenuate immune responses is the regulation of the subcellular compartmentalization of PRRs. *At*FLS2 is internalized into intracellular vesicles in a ligand- and time-dependent manner followed by protein degradation (Smith *et al.*, 2014, Beck *et al.*, 2012, Robatzek *et al.*, 2006). *At*FLS2 is present in endosomes 30 min upon treatment with flg22, and degradation is observed after 60 min (Beck *et al.*, 2012, Robatzek *et al.*, 2006). At this point no reelicitation with flg22 is possible, resensitization of cells reemerges after 2 h which goes in line with novel *At*FLS2 protein production (Smith *et al.*, 2014). Proteasomal degradation relies on a multi-enzymatic process of ubiquitylation of proteins. E1 is a ubiquitin-activating enzyme. E3 ligases mediate the substrate specificity and interact *via* their U-box domain with the ubiquitin-conjugating E2 enzymes (Trujillo, 2017). Target proteins can be mono- or polyubiquitinated and degraded *via* the 26S proteasome (Trujillo, 2017). Various members of the plant U-box protein family (PUBs) were shown to be involved in the attenuation of immune responses *via* ubiquitylation (Trujillo, 2017). *At*PUB12 and *At*PUB13 (PLANT U-BOX 12/13) are recruited to the activated *At*FLS2/*At*BAK1 receptor complex and phosphorylated by *At*BAK1. *At*PUB12/13 in turn ubiquitinate *At*FLS2 (Lu *et al.*, 2011). Lately, it was published that the heteromeric receptor for chitin, *At*CERK1/*At*LYK5 is also controlled by *At*PUB12/13 (Zhou *et al.*, 2018, Yamaguchi *et al.*, 2017, Liao *et al.*, 2017). Intriguingly, *At*PUB12 preferentially ubiquitinates *At*CERK1 whereas *At*PUB13 ubiquitinates *At*LYK5. Ectopic expression of *At*CERK1 in *N. benthamiana* leads to strong cell death which is suppressed by the co-expression with *At*PUB12 (Yamaguchi *et al.*, 2017). Interestingly, *At*PUB13 controls *At*LYK5 turnover in the absence of an elicitor, showing different mechanisms by which PUBs regulate receptor protein levels (Liao *et al.*, 2017). Nonetheless, signaling is not only controlled at the receptor level. The triplet *At*PUB22/23/24 negatively regulates cellular responses (Trujillo *et al.*, 2008). Mutant *pub22/23/24* plants are impaired in the attenuation of immune responses such as the ROS burst and are therefore more resistant to infection with pathogens. In a pre-activation state, *At*PUB22 is present as a homodimer conducting autoubiquitination leading to self-degradation. Upon activation, *At*PUB22 is stabilized *via* phosphorylation by *At*MPK3 leading to monomeric *At*PUB22 which is thought to mark downstream substrates for degradation (Furlan *et al.*, 2017). A subunit of the exocyst complex *At*Exo70B2 is discussed as a substrate for *At*PUB22 to accomplish immune response depletion (Stegmann *et al.*, 2012). Conclusively, *At*PUBs can act in different ways dependent on the associated RLK. This might be due to other, yet unidentified, interacting components regulating PUB activity. Wang *et al.* (2018) published an integrative model for the regulation of *At*BIK1 including positive and negative feedback loops (section 3.3.3). In 2014, *At*CPK28 was identified as a negative regulator of *At*BIK1 protein turnover as *At*BIK1 protein abundance is higher in *cpk28* (Monaghan *et al.*, 2014).

This aspect was further studied by Wang *et al.* (2018) resulting in the identification of *At*PUB25 and *At*PUB26 (PLANT U-BOX 25/26) as the E3 ligases involved in *At*BIK1 degradation. *At*CPK28 positively regulates *At*PUB25/26 by phosphorylation upon pattern recognition, and activated *At*PUB25/26 ubiquitinate *At*BIK1 which is then degraded to achieve signal attenuation (Wang *et al.*, 2018).

3.6 Substantial qualities of *Pseudomonas* bacteria for plant pathogenicity

Pseudomonads are rod-shaped, Gram-negative bacteria and can be beneficial as well as pathogenic to plants. *Pseudomonas syringae* is a plant pathogen with a great variety of host plants and comprises 50 pathovars with a narrow host range (Hirano *et al.*, 2000). *Pseudomonas syringae* pv. *tomato* DC3000 (*Pto* DC3000) was isolated from tomato plants, but was shown to also infect the model plant Arabidopsis under laboratory conditions (Whalen *et al.*, 1991). Oku (1994) defined three substantial qualities for fungal plant pathogenicity. Accordingly, a pathogen needs to be able to invade plant tissue, overcome host resistance, and promote disease development. These three features apply likewise to bacterial pathogens such as *Pto* DC3000 (Taguchi *et al.*, 2006). Tissue invasion of bacteria, unlike fungal pathogens, occurs exclusively *via* wounds or natural plant openings like hydathodes and stomata (Melotto *et al.*, 2006, Hugouvieux *et al.*, 1998, Mansvelt *et al.*, 1989). Investigation of bacteria infected leaf imprints suggests a patchy, but not random distribution of bacterial communities specifically at sites with nutrient and water supply such as veins, trichomes, and stomata (Monier *et al.*, 2004, Mansvelt *et al.*, 1989). *Pseudomonas* mutants lacking functional flagella are less virulent. *P. syringae* pv. *tabaci* flagellin glycosylation-defective mutants have a reduced flagellar motility, and these mutants are less virulent when sprayed onto the leaf as compared to infiltration into the leaf interior (Taguchi *et al.*, 2006). Also flagellar-defective *ΔfliC* mutants of *Pseudomonas* and *Ralstonia solanacearum* are less virulent when sprayed, but show wild type-like virulence when directly infiltrated (Ichinose *et al.*, 2003, Tans-Kersten *et al.*, 2001). Consequently, motility is beneficial for the pathogen in entering the plant as it helps to reach leaf openings. Moreover, chemotaxis was shown to be essential for successful tissue invasion. *R. solanaceum* strains lacking CheA or CheW, key components of chemotaxis, are less virulent than wild type (Yao *et al.*, 2006). Nontactic mutants are reduced in their virulence comparable to motility mutant strains when not directly inoculated in the plant indicating that directed movement is important for colonization. GFP-labeled *Pto* DC3000 was shown to accumulate around open rather than closed stomata, but whether this is due to the attraction by nutrients or other substances remains elusive (Melotto *et al.*, 2006). Altogether, these findings reinforce the role of stomata in pre-invasive immunity. *Pto* DC3000 is a hemibiotrophic pathogen with two distinct life styles. It grows epiphytically on the leaf surface or endophytically in the intercellular space (Hirano *et al.*, 2000, Beattie *et al.*, 1995). Both lifestyles occur simultaneously whereas the epiphytic growth on the healthy plant predominates upon inoculation, the endophytic life style

emerges with the disease initiation at later time points. Disease symptoms like water-soaking spots or necrosis correlate with massive colonization of the inner leaf space which shows the ability of *Pto* DC3000 to promote disease development. Infection and disease progression are promoted by high humidity, rain, and mild temperatures (Panchal *et al.*, 2016, Xin *et al.*, 2016, Hirano *et al.*, 2000). A switch from epi- to endophytic growth is associated with differential gene expression as both habitats require adaptation to different environmental conditions and stresses (Yu *et al.*, 2013). Bacteria in their resident phase on the leaf surface are exposed to changes in humidity, temperature changes, light irradiation, and nutrient limitation (Lindow *et al.*, 2003, Wilson *et al.*, 1999). Genes expressed in this phase are mainly related to motility and chemotaxis (Yu *et al.*, 2013). Bacteria in their invasive phase are exposed to an acidified pH of the apoplast, oxidative stress, and plant defense responses (Beattie *et al.*, 1995). Genes expressed in the endophytic phase are, for instance, virulence factors which help the pathogen to suppress plant immune responses and promote disease development (Yu *et al.*, 2013).

3.7 Effector-triggered susceptibility

Plant-induced immune responses, described in section 3.1, attempt to harm bacteria, limit their invasion, and growth. In contrast, pathogens evolved molecular strategies to mitigate host responses, a substantial quality for pathogens as described in section 3.6. Successful pathogens secrete a range of phytotoxins and effector proteins to promote pathogenicity by suppression of plant immunity. A multitude of effectors with enzymatic activity are identified and they interfere with nearly all layers of immunity, beginning with direct inhibition of a PRR or co-receptor to downstream signaling components such as RLCK, CDPKs, or MAPKs (Wei *et al.*, 2017, Lozano-Duran *et al.*, 2014, Liu *et al.*, 2009, Göhre *et al.*, 2008, Zhang *et al.*, 2007). Also the interference with plant hormone signaling, metabolism, and the plant cytoskeleton is described (Guo *et al.*, 2016, Brooks *et al.*, 2005). The type III secretion system (T3SS) is an important weapon for pathogenic bacteria to deliver effector proteins. T3SS is conserved in pathogenic *P. syringae* strains. Mutants lacking a functional T3SS become non-virulent also if directly infiltrated into the apoplastic space showing the importance of effector proteins for the disease progression (Cunnac *et al.*, 2011, Roine *et al.*, 1997).

3.7.1 Effector proteins interfere with plant immune responses

Pathogens evolved various mechanisms to mitigate plant immune responses and one strategy is to avoid recognition by PRRs. *Pto* DC3000 releases the alkaline protease AprA which degrades flagellin monomers resulting in the circumvention of *At*FLS2-mediated defense responses (Pel *et al.*, 2014, Bardoel *et al.*, 2011). The direct interference with PRR activity is described for the bacterial effector AvrPtoB. AvrPtoB encodes an E3 ubiquitin ligase that ubiquitinates PRRs such as *At*FLS2 and *At*CERK1, and suppresses the activation of PTI responses by the degradation of PRRs (Gimenez-

Ibanez *et al.*, 2009, Göhre *et al.*, 2008). A growing body of evidence indicates that effector proteins often possess multiple modes of actions. The effector HopM1 from *Pto* DC3000 interferes with plant immunity by various means. HopM1 impairs stomatal immunity and the MAMP-induced ROS burst most likely by mimicking 14-3-3 regulatory function (Lozano-Duran *et al.*, 2014). 14-3-3 proteins are regulatory factors which can through binding to their client proteins prevent the interaction with other proteins, impair degradation, or alter the subcellular localization (Lozano-Durán *et al.*, 2015). Xin *et al.* (2016) discovered that *Pto* DC3000 actively manipulates the conditions of the apoplastic space which are of vital importance for successful disease progression. The effector HopM1 induces water-soaking of the apoplast (Xin *et al.*, 2016). Presumably an aqueous apoplastic space is beneficial for bacterial growth and disease progression because of the improved supply with water and nutrients.

3.7.2 Phytotoxins counteract host defense responses

Pathogens produce phytotoxins to interfere with plant immune responses such as syringolin, syringomycin, or coronatine (Bender *et al.*, 1999). Coronatine (COR) is a well-characterized phytotoxin from *Pto* DC3000 which is also produced by other pathovars such as *P. syringae* pv. *maculicola*. The virulence factor COR induces stomatal opening, supports the development of disease symptoms, and promotes bacterial growth in the apoplastic space (Melotto *et al.*, 2006, Brooks *et al.*, 2004, Bender, 1999). Infection with COR-deficient *Pto* DC3000 strains results in less symptom development as compared to *Pto* DC3000 wild type (Brooks *et al.*, 2005, Brooks *et al.*, 2004). The COR-deficient *Pto* DC3000 mutant (*Pto* DC3000 COR^{-}) has weak virulence compared to wild type when dip-inoculated on tomato or Arabidopsis leaves and multiplicates less than wild type when directly infiltrated into the leaf apoplast (Brooks *et al.*, 2004, Mittal *et al.*, 1995). However, Melotto *et al.* (2006) show a comparable virulence of *Pto* DC3000 COR^{-} and *Pto* DC3000 upon infiltration into the leaf interior. Nonetheless, these studies suggest that COR is important in the early phase of infection and critical for overcoming stomatal immunity which is part of the pre-invasive immune response (Melotto *et al.*, 2006, Brooks *et al.*, 2004). *Pto* DC3000 is thought to employ COR to mimic JA signaling and induce stomatal opening by interference with SA-mediated defense responses because COR functionally mimics the active version of the phytohormone JA, JA-Ile (jasmonate-isoleucine) (Melotto *et al.*, 2006, Brooks *et al.*, 2005). How COR-mediated signaling induces stomatal closure is under investigation. Arabidopsis plants insensitive to COR and JA application, but more resistant to infection with *Pto* DC3000, were identified in a mutant screening and named *coi1* (*coronatine insensitive1*) (Feys *et al.*, 1994). *At*COI1, the JA receptor, is an F-box protein and part of the multi-protein ubiquitin ligase complex SCF^{COI1} (SKP CULLIN F-BOX containing complex) which is involved in protein degradation *via* the 26S proteasome (Yan *et al.*, 2009). JA-Ile, but also COR function as molecular glues between the SCF^{COI1}complex and the transcriptional repressor *At*JAZ (JASMONATE ZIM DOMAIN) (Thines *et al.*, 2007). Consequently, *At*JAZ is degraded and

transcription of JA-responsive genes is induced *via* the master regulator *At*MYC2 such as the *At*NAC transcription factors (NAM-ATAF-CUC2) which induce gene expression of SA catabolizing enzymes and repress genes involved in SA production to interfere with plant immunity (Cui *et al.*, 2018, Zheng *et al.*, 2012, Thines *et al.*, 2007).

3.8 Effector-triggered immunity

Pathogens actively suppress PTI to promote disease progression as described in section 3.7. Plants do not solely rely on cell surface PRRs, but evolved proteins surveying the cellular space for non-self or damaged-self molecules. This second layer of plant immunity is named ETI. So-called resistance proteins (R proteins), which are often NLRs (NUCLEOTIDE-BINDING SITE LEUCINE-RICH REPEAT PROTEIN), perceive the interference of effectors with plant immune responses (Jones *et al.*, 2006). Two distinct groups of NLRs are defined according to their N-terminal domain, a coiled-coil (CC) or TIR (Toll-interleukin 1-like receptor) domain. Flor (1971) summarizes the interaction of one NLR with a specific effector to induce ETI in the gene-for-gene hypothesis. ETI can be initiated in different ways. First, NLRs monitor host proteins for modifications caused by effector proteins also known as guard hypothesis. Second, NLRs function as a decoy to trap effector proteins (Cui *et al.*, 2015). Sensing of effector interference in either way leads to strong immune response often resulting in local cell death, also called HR (Jones *et al.*, 2006). Typical immune responses include the production of ROS, the activation of MAPKs, and changes in gene expression. In general, ETI responses appear to be enhanced compared to PTI (Tsuda *et al.*, 2010). *P. syringae* strains developed several effectors targeting *At*RIN4 (RPM1 (RESISTANCE TO *Pseudomonas syringe* pv. *maculicola* 1)-INTERACTING PROTEIN 4). *At*RIN4 phosphorylation is enhanced by the effector AvrB through the exploitation of a host RLCK. This is sensed by the host guard *At*RPM1 (RESISTANCE TO *Pseudomonas syringae* pv. *maculicola* 1) which induces ETI (Chung *et al.*, 2011, Mackey *et al.*, 2002). Furthermore, phosphorylated *At*RIN4 associates with *At*AHA1/2 to modulate the stomatal aperture (Liu *et al.*, 2009, section 3.4). AvrB release results in pathogen-induced stomata reopening (Lee *et al.*, 2015). The RLCK *At*PBS1 (AvrPphB SUSCEPTIBLE 1) functions as a decoy for the effector AvrPphB. *At*PBS1 is bound by inactive *At*RPS5 (RESISTANT TO *P. syringae* 5) (Ade *et al.*, 2007). Cleavage of *At*PBS1 by the protease AvrPphB leads to activated *At*RPS5 which in turn induces ETI. AvrPphB targets also other RLCKs such as *At*BIK1 indicating that *At*PBS1 acts as a decoy for AvrPphB (Zhang *et al.*, 2010). Bacteria use the sugar content, which is of particular importance of bacterial growth, in their surrounding as a measure to modulate the release of virulence factors. This makes the control of the metabolite flux to the apoplast important for the plant (Yamada *et al.*, 2016a). The *At*STP13 (SUGAR TRANSPORTER PROTEIN 13) is activated during PTI, pumping monosaccharides out of the apoplastic space, limiting the energy supply for bacterial growth, but as a consequence also influences the amount of effectors released by bacteria (Yamada *et al.*, 2016a).

3.9 Lipopolysaccharide and its role in immunity

3.9.1 Lipopolysaccharide perception in plants

The cell wall of Gram-negative bacteria consists of the outer membrane, followed by a layer of peptidoglycan which is surrounded by the periplasmic space. LPS is the main component of the outer leaflet of the outer membrane of most Gram-negative bacteria. LPS confers stability to the bacterial cell and protects the cell interior against unfavorable environmental conditions (Whitfield *et al.*, 2014). LPS is an amphiphilic molecule and can be separated in three parts (Alexander *et al.*, 2001). It consists of a lipophilic part, lipid A, a di-glucosamine equipped with acyl chains of varying lengths which anchors the LPS molecule into the outer membrane (Figure 3A). The hydrophilic part, termed core region, is an oligosaccharide. The third part is an O-polysaccharide chain (OPS) which is linked to the core oligosaccharide. This chain is highly variable in length and composition (Figure 3A) (Alexander *et al.*, 2001). Besides variation in the sugar residues of the OPS, also acyl chain patterns of the lipid A or the phosphorylation status can differ among bacterial strains and even within an individual bacterial cell. Non-stoichiometric addition of sugars such as 4-amino-4-deoxyarabinose are also possible (Figure 3A) (Alexander *et al.*, 2001). LPS is known to act as a MAMP and elicit defense responses in plants. Treatment of *Capsicum anuum* (pepper) or *Brassica campestris* with LPS from *X. campestris* pv. *campestris* induces the production of defense-related genes (Newman *et al.*, 1995, Newman *et al.*, 2000). Another example, LPS from *Burkholderia cepacia* triggers an oxidative burst and elevation of $[Ca^{2+}]_{cyt}$ in suspension-cultured *N. tabacum* cells (Gerber *et al.*, 2004). Even though examples for the effect of LPS on plant immunity are plentiful in literature, the respective PRR remained unidentified. Previously, the RLK *At*LORE/SD1-29 (LIPOOLIGOSACCHARIDE-SPECIFIC REDUCED ELICITATION/S-DOMAIN-1 KINASE 29) was identified in a forward genetic screen for mutants insensitive to LPS as a key component of LPS signaling in Arabidopsis (Ranf *et al.*, 2015). Mutants of *At*LORE are strongly impaired in PTI responses to LPS such as the oxidative burst, $[Ca^{2+}]_{cyt}$ elevation, MAPK activation, callose deposition, and defense gene expression (Ranf *et al.*, 2015). Consequently, *lore*-1 plants are more susceptible to infection with pathogenic *Pseudomonas* bacteria. Gain-of LPS-responsiveness upon transient expression of *At*LORE in naturally LPS-insensitive *N. benthamiana* illustrates a pivotal role of *At*LORE in LPS perception. *Pseudomonas aeruginosa* H4 (*Pa* H4) LPS was used for the high-throughput mutant screening (Ranf *et al.*, 2015).

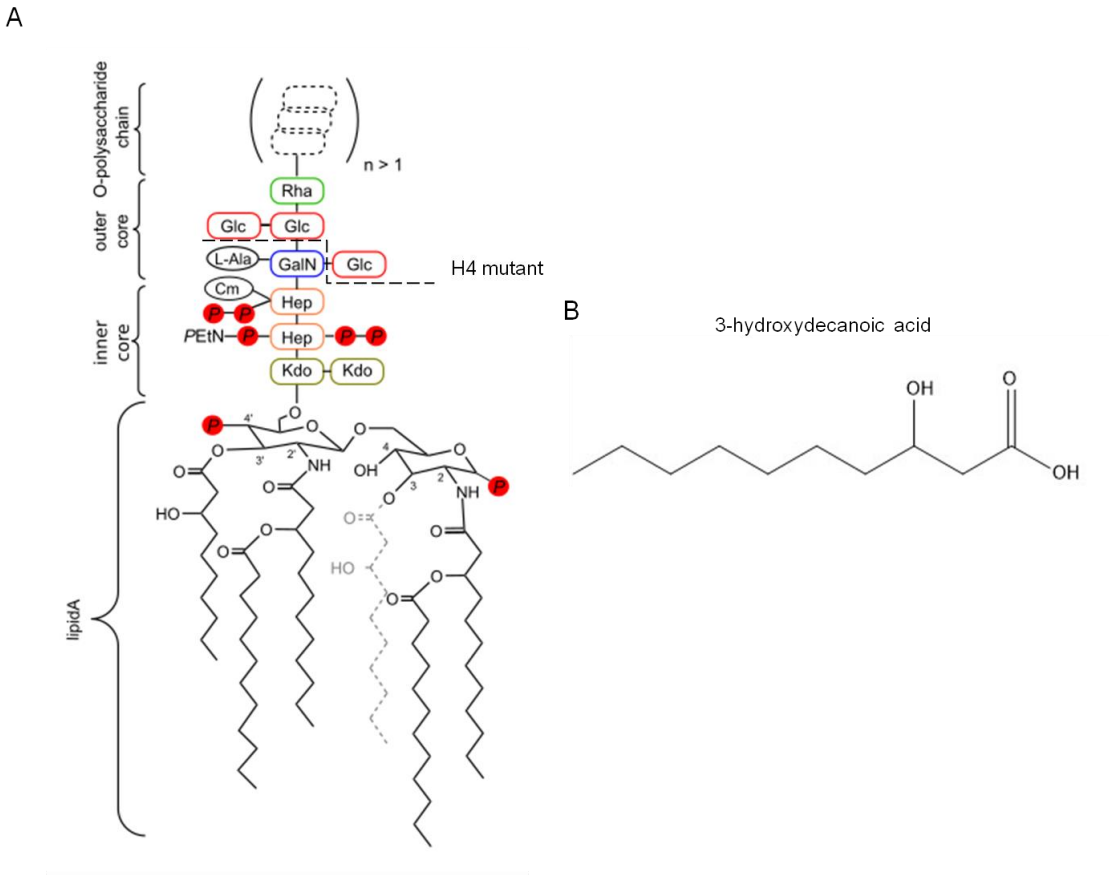

Figure 3 Structure of LPS from *P. aeruginosa* and 3-HDA. A) Lipopolysaccharide (LPS) consists of a lipophilic lipid A part anchored into the bacterial outer cell membrane. LPS from *P. aeruginosa* is mostly penta-acetylated and carries a 3-OH C10:0 at positions 3' and 3 of the di-glucosamine and 3-OH C12:0 at position 2' and 2. The acyl chain at position 3 is depicted in grey as LPS is often deacylated at position 3 after synthesis. The core region is divided into an inner and outer core oligosaccharide. The core region contains monosaccharides like Kdo (3-deoxy-D-*manno*-oct-2-ulsonic acid), Hep (L-*glycero*-D-*manno*-heptose), GalN (galactosamine), Glc (glucose), and Rha (L-rhamnose). The core region can be phosphorylated (*P*) and is further decorated with ethanolamine (Etn), carbamoyl (Cm), or an L-alanyl group (L-Ala). The dashed line indicates the LPS produced by the LPS biosynthesis mutant *P. aeruginosa* H4. B) Structure of 3-hydroxydecanoic acid (3-HDA).

Pseudomonas syringae pv. *tomato* LPS and *Xanthomonas campestris* LPS are also perceived in an *At*LORE-dependent manner. Interestingly, LPS from enterobacteria like *Escherichia coli* or *Salmonella enterica* is not sensed in Arabidopsis (Ranf *et al.*, 2015). In contrast, other studies show that LPS from *E. coli* induce defense responses in Arabidopsis, rice cells, and *B. campestris* (Desaki *et al.*, 2006, Newman *et al.*, 1995). *P. aeruginosa* H4 is an LPS biosynthesis mutant which produces LPS containing the lipid A and the major part of the core oligosaccharide, but lacks parts of the outer core and an OPS (indicated by a dashed line in Figure 3A). *Pa* H4 LPS is sufficient to induce *At*LORE-dependent responses in Arabidopsis. Therefore, it was thought that the immunogenic epitope of LPS

lies within the lipid A and core oligosaccharide (Ranf *et al.*, 2015). While the study at hand was conducted, it was shown that the bacterial metabolite 3-hydroxydecanoic acid (3-HDA) (Figure 3B) co-purifies while isolating LPS from bacterial cultures (Kutschera *et al.*, 2019, unpublished). Repurified LPS preparations lacking free 3-HDA do not induce *At*LORE-dependent immune responses in Arabidopsis. Synthetic 3-HDA, on the other hand, triggers immune responses in Arabidopsis (Kutschera *et al.*, 2019, unpublished). 3-HDA is incorporated as an acyl chain in the lipid A at the 3' and 3 position of *Pseudomonas* LPS (Figure 3A). However, only local application of 3-HDA, but not repurified LPS lacking free 3-HDA, induces systemic resistance to pathogen infection in Arabidopsis indicating that 3-HDA is not released from LPS during infection (Kutschera *et al.*, 2019, unpublished). This finding shows that *At*LORE-dependent immunity is mediated by sensing 3-HDA, a low complexity bacterial metabolite (Kutschera *et al.*, 2019, unpublished). Consequently, LPS preparations used within this study were contaminated with the *At*LORE-sensed 3-HDA. Treatment with LPS is indicated in the respective figure legends and described as LPS/3-HDA sensitivity in the text. *At*LORE is part of the plant-specific class of B-type lectin or S-domain-1 kinases (SD-RLKs) with 32 members in Arabidopsis (Xing *et al.*, 2013, Vaid *et al.*, 2012, Shiu *et al.*, 2003). Gene expression data shows co-regulation of *AtLORE* with the PRRs *AtFLS2* and *AtEFR* upon pathogen stimuli *in planta* supporting a key role of *At*LORE in plant immunity (Vaid *et al.*, 2012). However, the signaling pathways downstream of *At*LORE and the mechanism of receptor activation are elusive. Known PRRs and their signaling components were analyzed in respect of their involvement in *At*LORE-dependent LPS/3-HDA responses. The LRR-RLKs *At*FLS2, *At*EFR, and the co-receptor *At*BAK1 are dispensable for downstream responses (Ranf *et al.*, 2015). Also *At*CERK1 and *At*LYK4 are not required for LPS/3-HDA-sensing in Arabidopsis, but ROS production upon elicitation with LPS/3-HDA is dependent on *At*RBOHD (Ranf *et al.*, 2015). Recently, it was shown that 3-HDA has only a low binding affinity to the *At*LORE ectodomain produced in insect cells which indicates the necessity of a co-receptor (Kutschera *et al.*, 2019, unpublished). A recent study addressed the molecular perception mechanism of LPS in rice in more detail (Desaki *et al.*, 2018). Interestingly, LPS recognition in rice relies on *Os*CERK1 which is, besides *Os*CEBiP, essential for chitin perception (Desaki *et al.*, 2018, Hayafune *et al.*, 2014, section 3.3.2). *At*CERK1 is also involved in chitin perception, but not required for LPS/3-HDA-sensing in Arabidopsis (Ranf *et al.*, 2015). Desaki *et al.* (2018) showed that ROS production in *oscerk1* upon LPS elicitation is diminished (Desaki *et al.*, 2018). The three closest related SD1-RLKs from rice to *At*LORE are not involved in LPS perception in rice which suggests that rice and Arabidopsis evolved different perception systems for LPS/3-HDA and demonstrates the versatility of *At*CERK1 (Desaki *et al.*, 2018, section 3.3.2).

3.9.2 Lipopolysaccharide perception in mammals

In distinction from plants, LPS perception in mammals is studied extensively. TLRs (TOLL-LIKE RECEPTOR) function as PRRs in mammals (Miller *et al.*, 2005). Various receptor complexes are able

to sense Lipid A, among them is the TLR4-MD2-CD14 (MYELOID DIFFERENTIATION FACTOR 2; CLUSTER OF DIFFERENTIATION 14) receptor complex (Poltorak *et al.*, 1998). To make LPS available for recognition, LPS is dissociated from the bacterial membrane or outer membrane vesicles into single molecules by LBP (LPS-BINDING PROTEIN). CD14 concentrates LPS and facilitates receptor binding (Wright *et al.*, 1990). TLR4-MD2 form a heteromeric dimer which oligomerizes upon lipid A binding and induces an inflammatory response (Miller *et al.*, 2005, Shimazu *et al.*, 1999).

3.10 Roles of S-domain receptor-like kinases in plants

SD-RLKs are widespread among land plants, but in general, not much is known about SD-RLKs and their biological functions, receptor complexes, or signaling pathways (Xing *et al.*, 2013). The exception is the well-studied SD-RLK, SRK (S-LOCUS RECEPTOR KINASE) from *Brassica*. The receptor kinase is involved in the self-incompatibility response (SI), and discriminates between self- and non-self pollen (Stein *et al.*, 1991, Takasaki *et al.*, 2000). The ligand of SRK, SCR (S-LOCUS CYSTEINE-RICH PROTEIN) is the pollen-determinant of SI (Schopfer *et al.*, 1999). So-called hyper-variable regions (hv regions) of the receptor extracellular domain were identified to be involved in the specificity of ligand-binding (Ma *et al.*, 2016, Boggs *et al.*, 2009). The SI response favors cross-pollination by the prevention of self-pollination (Ivanov *et al.*, 2010). Plant immunity and the SI response have mechanistic similarities. Both processes distinguish between self and non-self structures, and rely on similar signaling components, but result in different final signal outputs. In case of SI, self-pollen is rejected to prevent inbreeding, whereas PRRs recognize non-self structures to prevent infection (Sanabria *et al.*, 2008, Hodgkin *et al.*, 1988). SRK as the female determinant is expressed in stigma epidermal cells. In terms of pollination, SCR diffuses or is actively transported to epidermal stigma cells. Self-SCR binds to the extracellular domain of SRK and induces signaling and prevents pollen germination and pollen tube development (Kachroo *et al.*, 2001, Kemp *et al.*, 2007). In case of cross-pollination, non-self SCR does not bind to and activate SRK. The exact signaling cascade to achieve SI remains mainly unknown. However, some SRK interacting proteins have been identified. A RLCK, MLPK (M-LOCUS PROTEIN KINASE) was identified as a positive regulator of the SI response, and SRK complex formation implicates binding of MLPK (Murase *et al.*, 2004). Another positive regulator is ARC1 (ARM-REPEAT CONTAINING PROTEIN 1) a ubiquitin E3 ligase. ARC1 associates with the SRK/MLPK complex (Gu *et al.*, 1998) (Figure 4). ARC1 is phosphorylated and relocates to the 26S proteasome in presence of activated SRK, most likely guiding other proteins for degradation (Stone *et al.*, 2003). The Exo70A1 (EXOCYST COMPLEX 70 A1) was identified as a putative target of ARC1 (Samuel *et al.*, 2009). Degradation of Exo70A1 prevents exocytosis, and conceivably, prevents the release of substances needed for germination or hydration of pollen (Samuel *et al.*, 2009). THL1 and THL2 (THIOREDOXIN-H-LIKE PROTEIN 1/2) were identified as negative regulators (Bower *et al.*, 1996). THL1/2 prevent SRK autophosphorylation, thus

activation in the absence of the ligand SCR (Cabrillac *et al.*, 2001). SRK mediated signaling includes changes in Ca^{2+} fluxes similar to the plant defense response. The elevation of $[Ca^{2+}]_{cyt}$ in stigma cells is observed upon SCR-binding to SRK, but in which way Ca^{2+} fluxes modulate signal transduction and control self-pollination remains elusive (Iwano *et al.*, 2015).

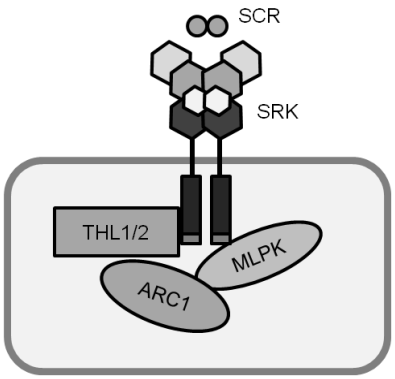

Figure 4 Schematic illustration of receptor complex formation of the S-locus receptor kinase. SRK (S-LOCUS RECEPTOR KINASE) from *Brassica* discriminates self- and non-self pollen in the self-incompatibility response. SRK forms most likely pre-formed dimers and recognizes the pollen expressed peptide SCR (S-LOCUS CYSTEINE RICH PROTEIN). Signal transduction relies on the receptor-like cytoplasmic kinase MPLK (M-LOCUS PROTEIN KINASE) and the E3 ubiquitin ligase ARC1 (ARM-REPEAT CONTAINING PROTEIN 1). THL1 and THL2 (THIOREDOXIN-H-LIKE PROTEIN 1/2) are negative regulators of SRK activity.

Other SD-RLKs with a designated role can be found in rice. SD-RLKs in rice form a subgroup of 100 RLKs (Shiu *et al.*, 2004). *Os*SIK2 (STRESS-INDUCED PROTEIN KINASE 2) was described as a SD-RLK involved in abiotic stress tolerance (Chen *et al.*, 2013). *OsSIK2* expression is increased upon drought-, cold-, and salt stress as well as ABA treatment. Overexpression of *Os*SIK2 full-length protein and a truncated version encompassing the intracellular domain influences leaf development and confers enhanced resistance to stress stimuli (Chen *et al.*, 2013). Another characterized SD-RLK is *Os*LSK1 (LARGE SPIKE S-DOMAIN RECEPTOR-LIKE KINASE 1) (Zou *et al.*, 2015). *Os*LSK1 participates in abiotic stress responses, and is involved in growth processes. Zou *et al.* (2015) found that overexpression of the ectodomain leads to improved traits in respect of plant height and grain yield. Heterodimerization of *Os*LSK1 with closely related SD-RLKs of rice was investigated to unravel the underlying molecular mechanisms and was found to be a common mode of action of SD-RLKs. The authors propose that the overexpression of the ectodomain results in a dominant-negative effect on the activation of receptor complex formation (homo- as well as heteromeric receptor complexes) and that this has a positive impact on yield components (Zou *et al.*, 2015). Recently, *Os*SDS2 (SPL11 CELL-DEATH SUPPRESSOR 2) was identified in a suppressor screening of *Os*SPL11-mediated (SPOTTED LEAF 11) cell death in rice (Fan *et al.*, 2018, Shirsekar *et al.*, 2014).

*Os*SPL11 is an E3 ubiquitin ligase and negative regulator of plant immunity and mutation results in enhanced resistance to infection with *X. oryzae* pv. *oryzae* (Zeng *et al.*, 2004). *Os*SPL11 is homologues to *At*PUB13 of Arabidopsis involved in PRR regulation (Shirsekar *et al.*, 2014, section 3.5). *Os*SDS2 phosphorylates *Os*SPL11 which in turn ubiquitinates the SD-RLK demonstrating a similar mode of action as proposed for Arabidopsis RLK regulation (Shirsekar *et al.*, 2014, section 3.5). Also, the recruitment of downstream signaling components of *Os*SDS2 is similar to what is known from Arabidopsis. *Os*SDS2 signaling relies on the activation of *Os*RLCK118 which in turn phosphorylates *Os*RBOHB to generate ROS and finally regulate cell death and immunity. The overexpression of *Os*SDS2 leads to increased immune responses and elevated ROS accumulation in the absence of a pathogen (Fan *et al.*, 2018). Another PUB of rice was identified to interact with a SD-RLK. *Os*PUB15 from rice interacts with the rice blast resistance protein *Os*PID2 which belongs to the SD-RLKs. Overexpression lines of *Os*PUB15 show increased ROS accumulation and expression of immune-related genes resulting in enhanced resistance against fungal rice blast infection caused by *Magnaporthe oryzae*. The interaction of *Os*PUB15 and *Os*PID2 is mediated *via* the ARM domain and requires an active *Os*PID2 kinase (Wang *et al.*, 2015, Chen *et al.*, 2006). Samuel *et al.* (2008) hypothesized a conserved regulatory pathway of SD-RLKs and PUBs. This study found that various kinase domains of SD-RLKs from Arabidopsis (among them *At*LORE) were able to interact with a wide range of ARM domains of PUBs (*At*PUB13, 14, 45, 9, 29, 38, 44). This hypothesis is supported by examples in literature such as *Os*SDS2/*Os*SPL11, *Os*PID2/*Os*PUB15, and SRK/ARC1 interaction (Fan *et al.*, 2018, Wang *et al.*, 2015, Gu *et al.*, 1998).

3.10.1 Domain structure of S-domain receptor-like kinases

Domain predictions based on sequence similarity divide the extracellular domain of SD-RLKs in a bulb-type lectin (B-lectin) domain, SLG (S-locus glycoprotein) domain overlapping with an EGF-like domain, and a PAN/APPLE (Xing *et al.*, 2013, Naithani *et al.*, 2007). The predicted structure of *At*LORE is illustrated in Figure 5A. Highlighted are conserved cysteines and the ATP binding site of the kinase domain. *At*LORE has a serine/threonine kinase domain followed by a domain of unknown function 3403 (DUF3403). Naithani *et al.* (2007) suggested a different domain segmentation based on structural modelling of the ectodomains of SRK6 and SRK13 from *Brassica* (Naithani *et al.*, 2007). Accordingly, the ectodomain of SRK is defined by two adjacent lectin-like domains (LLD1, LLD2), and a region with twelve cysteines. Six cysteines lie within an EGF-like domain and the other six cysteines within a domain similar to a PAN/APPLE domain (Figure 5C).

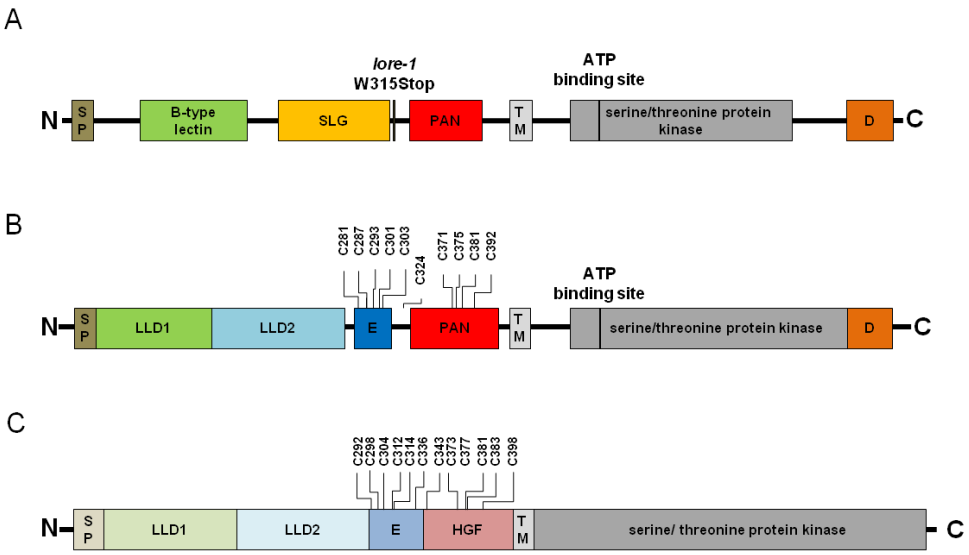

Figure 5 Schematic illustration of SRK9 and *At*LORE domain segmentation. A) *At*LORE domain segmentation according to sequence similarities (The UniProt Consortium, 2017, accessed November 19, 2018). The ectodomain is divided into the signal peptide (SP), a B-type lectin domain, a SLG domain (S-locus glycoprotein), a PAN/APPLE domain (PAN), and the transmembrane domain (TM). The intracellular domain consists of a serine/threonine kinase domain, followed by a domain of unknown function DUF3403 (D). The ATP binding site at position 516 is highlighted. The mutant *lore*-1 carries a mutation at position 315 leading to a premature stop codon (Ranf *et al.*, 2015). B) *At*LORE domain segmentation according to Naithani *et al.* (2007) which was taken as a basis for this study. Accordingly, the ectodomain consists of the signal peptide (SP), two contiguous lectin-like domains (LLD1, LLD2), an EGF-like domain (E), and a PAN/APPLE domain (PAN). Conserved cysteines characteristic for these domains are highlighted (C281, C287, C293, C301, C303, C321, C371, C375, C381, and C392). The transmembrane domain (TM) is followed by a serine/threonine kinase domain and by the DUF3403 (D). C) The domain segmentation of SRK9 according to Ma *et al.* (2016). The ectodomain consists of the signal peptide (SP), two contiguous lectin-like domains (LLD1, LLD2), an EGF-like domain (E), and a hepatocyte growth factor-like domain (HGF). Conserved cysteines characteristic for these domains are highlighted (C292, C298, C304, C312, C314, C336, C343, C373, C383, and C398). The transmembrane domain (TM) is followed by a serine/threonine kinase domain. C) is modified from Ma *et al.* (2016).

The overall domain structure is supported by the crystal structure of the ectodomain of SRK9 published in 2016 (Ma *et al.*, 2016). Notably, both studies use slight variations for the domain borders which are discussed in section 4.4. The PAN/APPLE domain was renamed by Ma *et al.* (2016) to HGF-like domain (hepatocyte growth factor-like domain) because of its high structural similarity. The HGF domain belongs to the PAN/APPLE protein family and is involved in heparin-binding (Ma *et al.*, 2016). Multiple sequence alignments of SD-RLKs of Arabidopsis and SRKs indicate a comparable

domain architecture for *At*LORE. The study at hand based the domain segmentation of *At*LORE on the study from Naithani *et al.* (2007) and remains with the nomenclature PAN/APPLE (Figure 5B).

3.10.2 Receptor complex formation in the self-incompatibility response

Receptor complex formation including homo- and heterooligomerization is often dependent on the initiation by ligand-binding to the extracellular domain as described for *At*FLS2 and flg22 or *At*CERK1 and chitin (section 3.3.2). For SRK, however, homodimerization in a ligand-independent manner was reported (Giranton *et al.*, 2000, Figure 4). Preformed dimers might aid rapid signal transduction upon ligand recognition. Interaction studies in yeast propose the PAN/APPLE and EGF-like domain to be involved in ligand-independent receptor dimerization (Naithani *et al.*, 2007). Structural information revealed by the crystal structure of the ectodomain of SRK9 (eSRK9) of *Brassica rapa* suggests a different mode of receptor complex formation contradicting the earlier results (Ma *et al.*, 2016). Accordingly, the ligand SCR is involved in receptor dimerization and various residues of subdomains of the ectodomain participate in dimerization and ligand binding (Ma *et al.*, 2016). An *At*LORE ectodomain model compared to the crystal structure of eSRK9 will be discussed in section 4.4.

3.11 Strategies to generate broad-spectrum disease resistance in plants

The growing world population is accompanied by a feeding problematic as described in the first section of the introduction. To date, breeding of resistant plant species focused mainly on the intrafamily transfer of *R* genes, often identified in wild species, to reduce yield losses caused by plant diseases (Dangl *et al.*, 2013). However, R protein mediated resistance is race-specific and therefore often non-durable on the field as pathogens rapidly adapt to the presence of new R proteins (Dangl *et al.*, 2013). The intrafamily transfer of PRRs promises to confer durable resistance because PRRs recognize conserved and widespread microbial structures essential for microbial fitness (Boutrot *et al.*, 2017). The expression of the SD-RLK *Os*PID2 in susceptible rice species confers durable resistance against fungal rice blast *M. oryzae* in otherwise susceptible rice varieties (Chen *et al.*, 2006). In addition, biotechnological approaches enabled the interfamily transfer of immune receptor proteins to enhance and confer durable broad-spectrum resistance to otherwise susceptible plant species which is of particular interest for food security. Transfer of PRRs to distantly related plant species was shown to be possible by the heterologous expression of *At*EFR in solanaceous species (Lacombe *et al.*, 2010). Expression of *At*EFR in *S. lycopersicum* variety Moneymaker and *N. benthamiana*. confers resistance to a wide range of phytopathogens from *Pseudomonas, Xanthomonas, Ralstonia,* and *Agrobacteria* (Lacombe *et al.*, 2010). The PRR *At*EFR was also transferred to the economically important monocotyledonous crop rice which is then able to perceive elf18 derived from *E. coli* and *X. oryzae*

pv. *oryzae* (Lu *et al.*, 2015, Schwessinger *et al.*, 2015). These studies show that downstream signaling components required for resistance establishment are conserved among plant species. Interfamily transfer of receptor proteins to widen the recognition spectrum of plants has been repeatedly performed. The genetic engineering of chimeric receptor variants is another strategy to improve disease resistance in plants. Expression of chimeras of the ectodomain of *At*EFR fused to the kinase domain of *At*FLS2 yielded fully functional elf18 receptor (Albert *et al.*, 2010). The generation of a chimeric receptor between the ectodomain of XA21 from rice fused to the intracellular domain of *At*EFR is also functional when expressed in Arabidopsis and confers resistance towards *Pto* DC3000 (Holton *et al.*, 2015). Another example is the expression of the chimeric RLK between the RLP *Os*CEBiP and the kinase domain of the SD-RLK *Os*PID2 which confers enhanced resistance to *M. oryzae* and enhanced immune outputs in response to chitin treatment in otherwise susceptible rice species (Kouzai *et al.*, 2013, section 3.3.2 and 3.10). An increasing body of evidence shows the possibilities of biotechnological approaches, besides classical breeding, to improve plant immunity.

3.12 Objectives

*At*LORE was identified as a key component of LPS/3-HDA-induced immunity in Arabidopsis and belongs to the SD-RLKs (Ranf *et al.*, 2015, section 3.9). Typical PTI responses such as production of ROS, MAPK activation, or defense gene expression are impaired in *lore*-1 in response to LPS/3-HDA (Ranf *et al.*, 2015). Nonetheless, the molecular mechanisms of how *At*LORE orchestrates LPS/3-HDA-induced immune responses and establishes resistance to *Pto* DC3000 remain largely unknown. Hence, the aim of this work is to broaden the knowledge of *At*LORE regulation and to elucidate the function of *At*LORE in pre- and post-invasive defense responses to *Pseudomonas* bacteria. This will improve the conceptual understanding of *At*LORE-mediated immunity in mechanistic detail.

This work focused on the investigation of *At*LORE homodimerization and the ability to form heterodimers with other SD-RLKs. Furthermore, important domains of *At*LORE involved in complex formation and activation were investigated by the generation of truncated variants of the extracellular and the intracellular domain of *At*LORE. Receptor activation was tested using chimeric receptor variants of *At*LORE with close para- and orthologs of LPS insensitive plant species in transient gain-of-function experiments in *N. benthamiana*. The identification of LPS/3-HDA insensitive species was performed by a ROS screening of various Brassicaceae in response to LPS application. The role of *At*LORE in plant immunity was further addressed with the generation of stable Arabidopsis lines expressing *At*LORE with or without an epitope tag under the control of the endogenous pLORE or the constitutive 35S promoter. Comprehensive characterizations of these lines, focusing on typical PTI responses, were carried out and bacterial infections assays performed. These experiments should help

to define the role of *At*LORE in pre- and post-invasive defense responses and complement understanding of 3-HDA signaling in Arabidopsis.

4 Results

4.1 Investigation of LPS/3-HDA perception in Brassicaceae

SD-RLKs are ubiquitous in land plants and presumably, SD-RLKs originated from one gene fusion event and developed from there (Xing *et al.*, 2013). Phylogenetic analysis of *At*LORE revealed that closely related *At*LORE homologs are exclusively found within other Brassicaceae (Ranf *et al.*, 2015, Xing *et al.*, 2013). This finding corresponds to a previous study which showed that the clade *At*LORE belongs to is expanded in Arabidopsis compared to rice (Vaid *et al.*, 2012). A protein blast using the *At*LORE amino acid sequence as query identified closely related SD-RLKs particularly in other Brassicaceae (Ranf *et al.*, 2015). This raised the question if these plant species are able to sense LPS/3-HDA to induce immune responses comparable to Arabidopsis, and if other plant species with more distantly related SD-RLKs such as *N. benthamiana* or *O. sativa* are insensitive to the treatment with LPS/3-HDA. The ability of plant species to perceive LPS/3-HDA was functionally analyzed by screening of ROS production upon treatment with LPS isolated from different bacteria, synthetic 3-HDA, and flg22 (section 8.1.18 and 8.1.19). *At*LORE is able to mediate the perception of LPS/3-HDA purified from bacterial species such as *Pseudomonas* and *Xanthomonas*. More precisely, LPS/3-HDA from *Pseudomonas aeruginosa* (*Pa* H4 LPS), *Pseudomonas syringae* pv. *tomato* (*Pst* DC3000 LPS), and *Xanthomonas campestris* pv. *malvacearum* (*Xcm* #2, *Xcm* #4 LPS) is sensed (Ranf *et al.*, 2015). In contrast, *E. coli* LPS (*Ec* B4 LPS) is not sensed in an *At*LORE-dependent manner (Ranf *et al.*, 2015, section 3.9). Besides Brassicaceae, also plants of Solanaceae, Fabaceae, and Poaceae including important crop plants were tested. The functional assessment supported the phylogenetic analysis (Figure 6). Plant species, which possess distantly related SD-RLKs, like *Hordeum vulgare* (barley), *O. sativa*, *Glycine max* (soybean), and *Solanum lycopersicum* (tomato) were insensitive to all tested LPS preparations as well as synthetic 3-HDA, but were sensitive to flg22 (Figure 6A). An exception is *Populus trichocarpa* (poplar) which was additionally insensitive to flg22 (Figure 6A). LPS/3-HDA-sensitive species were found within the Brassicaceae such as *Arabidopsis shokei*, *Arabidopsis suecica*, *Sinapis arvensis*, and *Eruca sativa* (Figure 6A). The ROS response to LPS/3-HDA by *Capsella rubella*, *Brassica nigra*, and *Brassica juncea* are exemplarily depicted (Figure 6B). All three species generated ROS upon treatment with LPS and 3-HDA. The oxidative burst, however, was weaker in comparison to the oxidative burst in response to flg22. To emphasize the response to the LPS preparations, the response to flg22 is not shown except for *A. lyrata*. *A. lyrata* did not induce an oxidative burst in response to LPS application, but in response to flg22. All LPS/3-HDA-sensitive species displayed a similar recognition pattern as compared to Arabidopsis. *Pseudomonas* and *Xanthomonas* LPS as well as 3-HDA were sensed, but not LPS from enteric bacteria such as *E. coli* (Figure 6A and B).

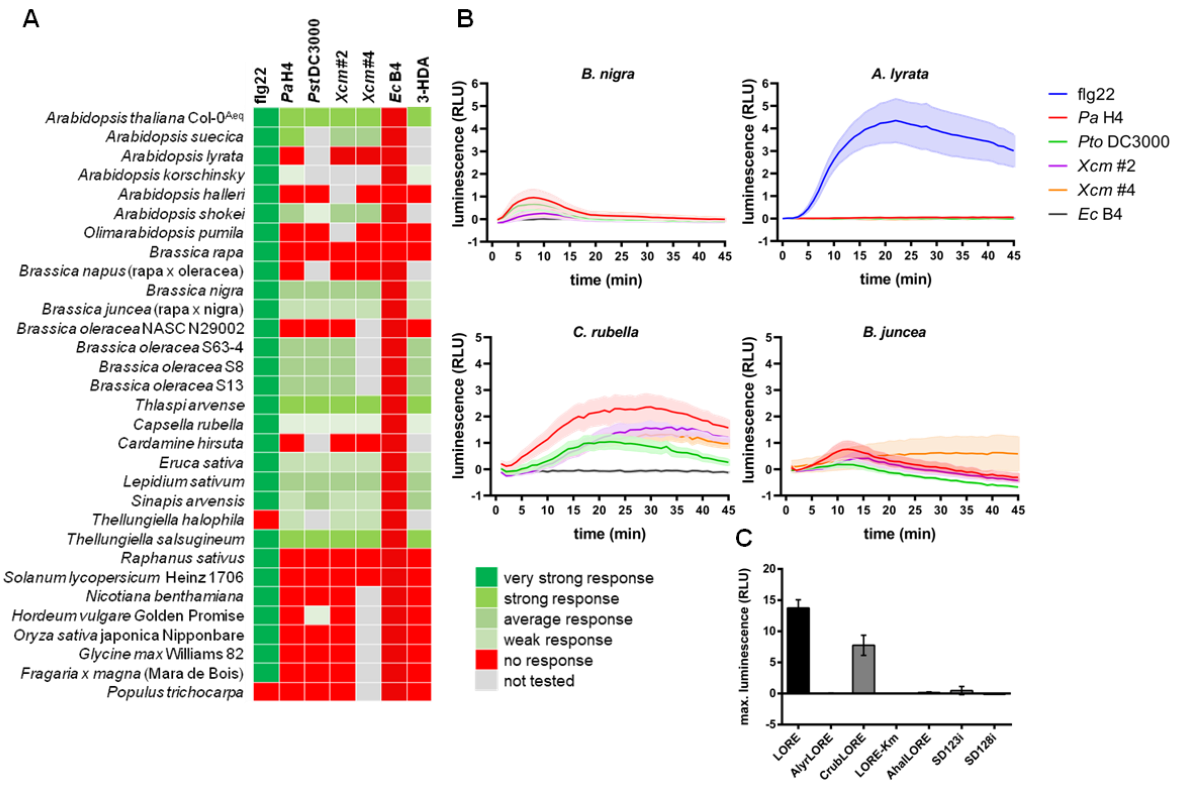

Figure 6 Sensing of LPS and 3-HDA among members of the Brassicaceae. A) Heat map of the LPS and 3-HDA sensitivity screening of different plant species. ROS accumulation in response to 500 nM flg22, 20 µg/mL LPS from *Pseudomonas Pa* H4, *Pst* DC3000, *Xanthomonas Xcm* #2, *Xcm* #4, *Escherichia coli Ec* B4, or 1 µM 3-HDA was measured in leaf discs of 10-weeks-old plants. Various shades of green indicate very strong to weak response, red indicates insensitivity and grey represents not tested. B) Examples of ROS accumulation of the LPS sensitivity screening of leaf discs from *Brassica nigra*, *Arabidopsis lyrata*, *Capsella rubella*, and *Brassica juncea*. The response to flg22 of *B. nigra*, *C. rubella*, and *B. juncea* is not depicted to emphasize the responses to the different LPS preparations. Data represent the mean ± SEM (n = 8) depicted as relative light units (RLU). Each plant line was tested three times. Depicted is one representative experiment. C) ROS accumulation in transient gain-of-function experiments of LORE-GFP, LORE-Km-GFP, AlyrLORE-GFP, CrubLORE-GFP, AhalLORE-GFP, SD123i-GFP, and SD128i-GFP in response to 5 µM 3-HDA in *N. benthamiana*. Data represent the mean ± SEM of n = 8 leaf discs per treatment depicted as the maximal luminescence in RLU.

Intriguingly, perception of LPS/3-HDA was not congruent with the percentage of amino acid identity between *At*LORE and its putative orthologs. AlyrLORE, the *At*LORE ortholog of *A. lyrata*, shares 94% identical amino acids with *At*LORE, but *A. lyrata* was insensitive to LPS as well as 3-HDA (Figure 6B, Supplementary Figure 1). CrubLORE, the *At*LORE ortholog of *C. rubella*, on the other hand, shares 92% identical amino acids. *C. rubella* was sensitive to LPS and 3-HDA (Figure 6B, Supplementary Figure 1). *B. oleracea* shares only 80% identical amino acids, but was able to perceive

LPS and 3-HDA (Figure 6A). *B. rapa*, on the other hand, shares also 80% identical amino acids, but was insensitive to the LPS treatment (Figure 6A). To rule out the possibility that the LPS/3-HDA insensitivity phenotype was an effect of a low expression level of the putative *At*LORE orthologs, the coding sequences of AlyrLORE, AhalLORE, and CrubLORE were cloned under the control of the constitutive 35S promoter and functionally tested. Also *At*LORE paralogs *At*SD1-23 (79% identical amino acids) and *At*SD1-28 (68% identical amino acids) from Arabidopsis were cloned. *At*SD1-23 is the closest *At*LORE paralog in Arabidopsis and was therefore chosen for detailed analysis. Mutant plants *sd1-23* exhibited a wild type-like ROS burst in response to the treatment with LPS, indicating that *At*SD1-23 is not required for LPS/3-HDA-sensing in Arabidopsis (Ranf *et al.*, 2015). *At*SD1-28 falls within the same subclade of SD-RLKs in Arabidopsis, but is more distantly related to *At*LORE than *At*SD1-23 (Supplementary Figure 1). The ortho- and paralogs were analyzed in transient gain-of-function experiments in *N. benthamiana* (section 8.1.17). The abbreviation LORE is used afterwards and refers to clones of *At*LORE encompassing only the coding sequence missing the introns of *AtLORE* (section 8.1.9). The same applies to *At*SD1-23 (SD123) and *At*SD1-28 (SD128), but no difference is made for AlyrLORE, CrubLORE, and AhalLORE (section 8.1.9). Expression of SD-RLKs other than LORE and AlyrLORE was lethal for *E. coli* (personal communication Dr. Ranf, TU München). Therefore, the first intron of LORE was introduced into the coding sequence of SD1-23 and SD1-28, and is indicated by the letter i (SD1-23i; SD1-28i, section 8.1.9). *N. benthamiana* itself is insensitive to LPS treatment (Figure 6A), but heterologous expression of LORE-GFP confers LPS/3-HDA sensitivity (Ranf *et al.*, 2015). *N. benthamiana* leaves transformed with CrubLORE-GFP and LORE-GFP reacted with the accumulation of ROS in response to LPS treatment (Figure 6C). All other *N. benthamiana* leaves transformed with the RLKs AlyrLORE-GFP, AhalLORE-GFP; SD123i-GFP, and SD128i-GFP were not sensitive to the LPS application. Also *N. benthamiana* leaves transformed with LORE-Km (LORE-Kinase mutated), carrying an ATP-binding site mutation in the kinase domain (lysine at position 516 is substituted with alanine), did not induce an oxidative burst (Ranf *et al.*, 2015, Figure 6C). The orthologs can possess non-functional kinases which would also lead to non-responsive *N. benthamiana* to LPS/3-HDA treatment upon transient expression. However, the kinase domains of AlyrLORE, SD123i, and SD128i were active (section 4.3.1, Figure 13). Unfortunately, the molecular cloning of the putative *At*LORE orthologs from *B. rapa*, *B. oleracea*, *B. juncea*, *B. napus*, and *B. nigra* was not successful, and therefore, the ROS screening results could not be confirmed by heterologous expression. As mentioned above, LPS/3-HDA sensitivity of the tested plant species did not correspond to the amino acid sequence similarity of the putative orthologs. The protein blast was performed using the complete amino acid sequence of *At*LORE as query. The ectodomain of receptor proteins is essential for ligand recognition and receptor complex activation (Couto *et al.*, 2016, section 3.3.2). For this reason, amino acid sequences of the extracellular domains of *At*LORE and its ortho- and paralogs were compared. The ectodomains of AlyrLORE and *At*LORE share 94% identical amino acids. The ectodomains of CrubLORE, *At*SD1-23, and *At*SD1-28 share

93%, 81%, and 65% identical amino acids, respectively with *At*LORE. In numbers, 22 amino acids of the ectodomain of AlyrLORE and 28 amino acids of CrubLORE are different to *At*LORE, but *At*SD1-28 has already over 80 amino acids that differ from *At*LORE (Supplementary Figure 11). The 22 distinct residues of AlyrLORE and *At*LORE seem to make the difference between the ability to sense LPS/3-HDA or not. 20 of them lie within conserved protein domains. More precisely, 5 different amino acids are located within LLD1, another 5 amino acids within LLD2, 3 in the EGF-like domain and 7 in the PAN/APPLE domain (Supplementary Figure 11). Whether ligand binding or receptor complex formation is disturbed, remains unknown. But these insensitive ortho- and paralogs were a good tool to analyze receptor functionality in more detail (section 4.2).

In summary, LPS/3-HDA-sensitive plant species are found among Brassicaceae. More distantly related species seem to be insensitive to LPS/3-HDA treatment. All species identified as LPS/3-HDA-sensitive have a similar recognition pattern as compared to Arabidopsis. The transient expression in *N. benthamiana* of putative orthologs from *At*LORE, CrubLORE, AlyrLORE, and AhalLORE confirm the initial LPS/3-HDA screening results. Expression of CrubLORE, but not expression of AlyrLORE, AhalLORE, or the paralogs SD123i, and SD128i confer LPS/3-HDA sensitivity to *N. benthamiana*.

4.2 Receptor complex formation of LORE

Receptor complex formation including homo- and heterooligomerization to form higher order complexes is central for receptor activation in defense responses (Couto *et al.*, 2016, section 3.3.2). *At*LORE-dependent immune responses do not require the co-receptor *At*BAK1 or the PRRs *At*FLS2, *At*EFR, or *At*CERK1 (Ranf *et al.*, 2015, section 3.9). This, and the fact that *At*LORE is an SD-RLK, suggested the assumption that *At*LORE receptor complex formation differs to what is known for the well-studied PRRs *At*FLS2 and *At*CERK1. Giranton *et al.* (2000) found that SRK from *Brassica* is present as homodimers in the stigma plasma membrane in the absence of the ligand (section 3.10.2). The EGF-like and PAN/APPLE domain of the ectodomain were identified in experiments in yeast as crucial for receptor dimerization (Naithani *et al.*, 2007). For this reason, LORE receptor complex formation focusing on homodimerization was investigated, and two approaches were chosen. The ability of LORE to dimerize was analyzed by the use of co-immunoprecipitation experiments (CoIP) as well as bimolecular fluorescence complementation (BiFC) assays (section 8.1.28 and 8.1.33). The experiments were conducted with full-length, kinase-inactive, and truncated receptor variants of LORE. Parts of the here presented experiments were initially performed by Tina Illig and Sonja Eibel within their master theses. Previous work on LORE demonstrated that kinase activity is required for LORE-dependent signal transduction. Also, LORE-Km does not induce ROS production in response to LPS/3-HDA treatment (Ranf *et al.*, 2015, section 4.1). Seemingly, an active kinase domain of LORE is needed to activate the receptor complex. If the kinase activity is also critical for the initial formation

of the receptor complex, was analyzed in the study at hand. Truncated proteins comprising only the ectodomain (eLORE), the ectodomain plus transmembrane domain (tLORE), only the intracellular domain (kLORE) as well as the intracellular domain plus transmembrane domain (iLORE) were generated (Figure 7A and B). The truncated variants were used to identify the domains essential for the formation of *At*LORE receptor complexes. Localization of the truncated protein variants was evaluated upon transient expression in *N. benthamiana* leaves (Figure 7C).

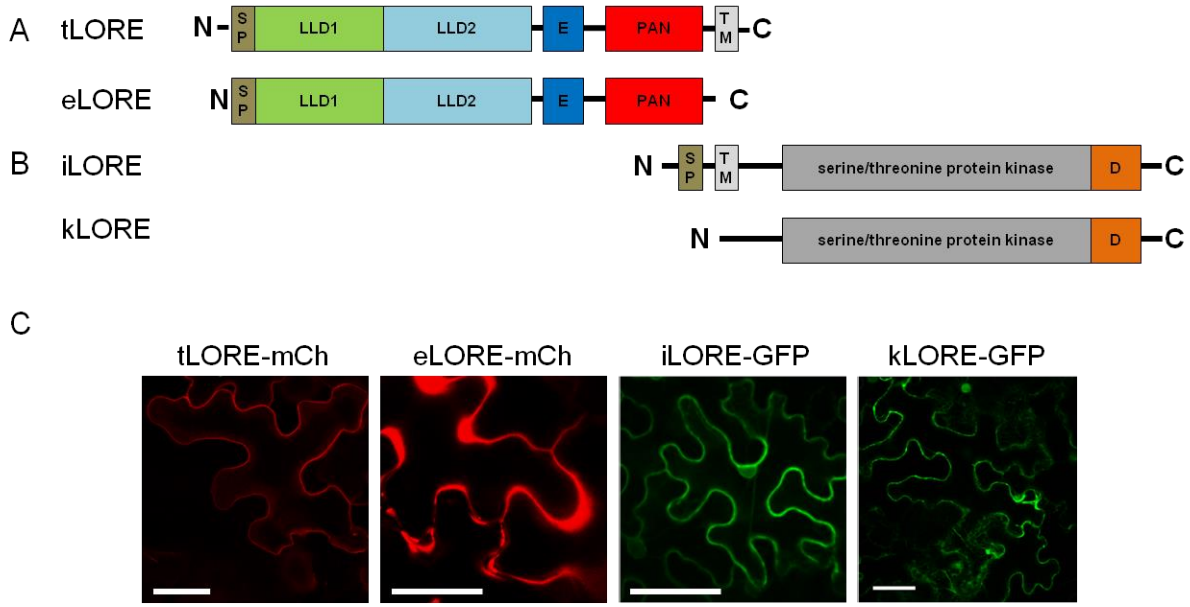

Figure 7 Schematic illustration and localization of LORE truncations. A) Truncated variant of LORE comprising the signal peptide (SP), lectin-like domain 1 and 2 (LLD1/LLD2), the EGF-like domain (E), the PAN/APPLE domain (PAN) with transmembrane domain (TM; tLORE), or without TM (eLORE). B) Truncated variant of LORE comprising the SP, the complete kinase domain, the domain of unknown function 3403 (D) with TM (iLORE), or without TM and SP (kLORE). C) Microscopic evaluation of GFP- and mCherry fluorescence of LORE truncation proteins (tLORE-mCherry, eLORE-mCherry, iLORE-GFP, kLORE-GFP) transiently expressed in *N. benthamiana*. Scale bar 50 µm. Pictures of tLORE-mCherry and eLORE-mCherry were taken by Tina Illig within her master thesis.

tLORE-mCherry was detected in the plasma membrane. Fluorescence was sometimes also detected around the nucleus which indicates localization to the endoplasmic reticulum (not shown). Fluorescence signal of eLORE-mCherry was detected in the apoplastic space. kLORE-GFP localized to the cytoplasm. Localization around the nucleus and in cytoplasmic strains was observed (Figure 7C). The localization of iLORE-GFP, a truncated receptor variant still possessing the transmembrane domain, was not that clear. Fluorescent signal was detected at the plasma membrane, but also in the cytoplasm around the nucleus, indicating partial mis-localization possibly due to strong overexpression.

4.2.1 Investigation of LORE homodimerization

CoIP experiments were performed to evaluate LORE homodimerization using transient co-transformation of *N. benthamiana* leaves. LORE-GFP was transiently co-transformed with LORE-mCherry or cytosolic mCherry, respectively. After 48 h total protein was extracted, and CoIP, using a GFP trap binding to LORE-GFP, was performed (section 8.1.28). Immunoblot analysis showed that LORE-GFP as well as LORE-mCherry were not detected in the input sample (total protein extract), but in the immunoprecipitated fraction, indicating interaction of LORE-GFP with LORE-mCherry (Figure 8). Cytosolic mCherry was present in the input, but not in the immunoprecipitated fraction, indicating that cytosolic mCherry itself was not interacting with LORE nor binding unspecifically to the GFP trap.

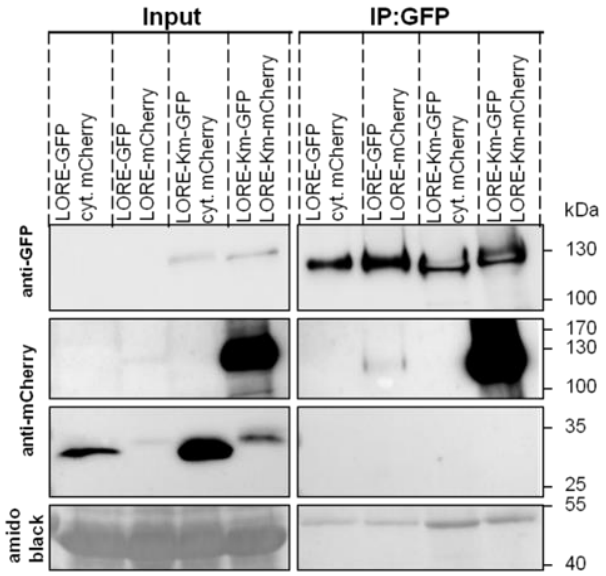

Figure 8 LORE forms homodimers upon transient transformation of *N. benthamiana*. Immunoblot analysis of co-immunoprecipitation experiments of LORE after transient expression in *N. benthamiana*. LORE-GFP (~130 kDa) or LORE-Km-GFP (~130 kDa) were co-transformed with LORE-mCherry (~130 kDa), LORE-Km-mCherry (~130 kDa), or cytosolic mCherry (~30 kDa), respectively, and precipitated from total protein extracts using a GFP trap (IP: GFP). The experiment was repeated three times. Amido black staining shows equal protein loading. SuperSignal® West Femto Maximum Sensitivity Substrate (Pierce, Rockford, USA) was used for detection. This immunoblot was generated by Tina Illig within her master thesis.

However, the amido black staining showed residual levels of other proteins in the immunoprecipitated fraction suggesting unspecific binding of proteins of the total protein extract from *N. benthamiana* to the GFP trap. Expression of the kinase-active LORE caused cell death in *N. benthamiana* (Supplementary Figure 2A). The cell death might be an explanation for the low abundance of active LORE protein in the input sample and indicates high protein turn over. The same experiment was

conducted with the kinase-inactive variants LORE-Km-GFP and LORE-Km-mCherry. Here, both proteins were detectable in the input as well as in the immunoprecipitated fraction (Figure 8). Cytosolic mCherry was detected in the input fraction, but was not co-immunoprecipitated together with LORE-Km-GFP. LORE-Km did not cause cell death in *N. benthamiana*, and the protein accumulated to a higher degree (Figure 8, Supplementary Figure 2A). Interestingly, in the input sample from LORE-mCherry as well as from LORE-Km-mCherry, a band slightly above the size of cytosolic mCherry was detected. Most likely, these were degradation products of LORE-mCherry or LORE-Km-mCherry. Notably, these experiments were performed with heterologous expressed proteins and no LPS/3-HDA was applied, indicating that LORE interacted without the presence of the putative ligand.

BiFC in transiently transformed *N. benthamiana* leaves was performed as an independent experiment to investigate LORE homodimerization (Figure 9, section 8.1.33). The method BiFC has the advantage that protein-protein interaction can be observed *in vivo* in cellular compartments such as the plasma membrane (Kudla *et al.*, 2016). Moreover, fluorescence reconstitution occurs exclusively when the proteins of interest are in close proximity to each other (Waadt *et al.*, 2008). Besides the general ability of LORE to dimerize, also the domains involved in homomeric interactions were investigated. For this reason, truncated receptor variants were generated. iLORE is lacking the extracellular domain, and tLORE is missing the intracellular kinase domain (Figure 7A and B). LORE-Km fused to the N-terminal part of YFP (LORE-Km-N) was co-transformed with LORE-Km-C, iLORE-C, tLORE-C fused to the C-terminal part of YFP (C), or the negative control, a cytosolically expressed C-terminal part of YFP (cyt. C). Fluorescence reconstitution of all combinations was assessed *via* fluorescence intensity measurements and confocal microscopy 36 h post infiltration of *N. benthamiana*. Immunoblot analysis confirmed protein expression. LORE-Km-N and LORE-Km-C co-expression led to the complementation of the YFP signal (Figure 9A and B). The fluorescence intensity was significantly higher than for LORE-Km-N co-expressed with cyt. C. LORE-Km-N and LORE-Km-C fusion proteins were detected by immunoblot analysis (Figure 9C). The cytosolic C-terminal part of YFP is only 10 kDa in size and was not detected on the immunoblot (Figure 9C). The protein ladder indicated that proteins of this size migrated out of the gel. Low molecular weight proteins are best resolved in high percentage SDS gels. On the other hand, high molecular weight proteins are best resolved in low percentage SDS gels. LORE-Km-N and LORE-Km-C (~110 kDa) were not detected when higher percentage SDS gels were used. Background fluorescence of LORE-Km-N co-expressed with cyt. C indicated expression of the C-terminal part of YFP (Figure 9A). The detection of LORE-Km-N and LORE-Km-C expression was considered to be more important, therefore, low percentage SDS gels were used (section 8.1.31).

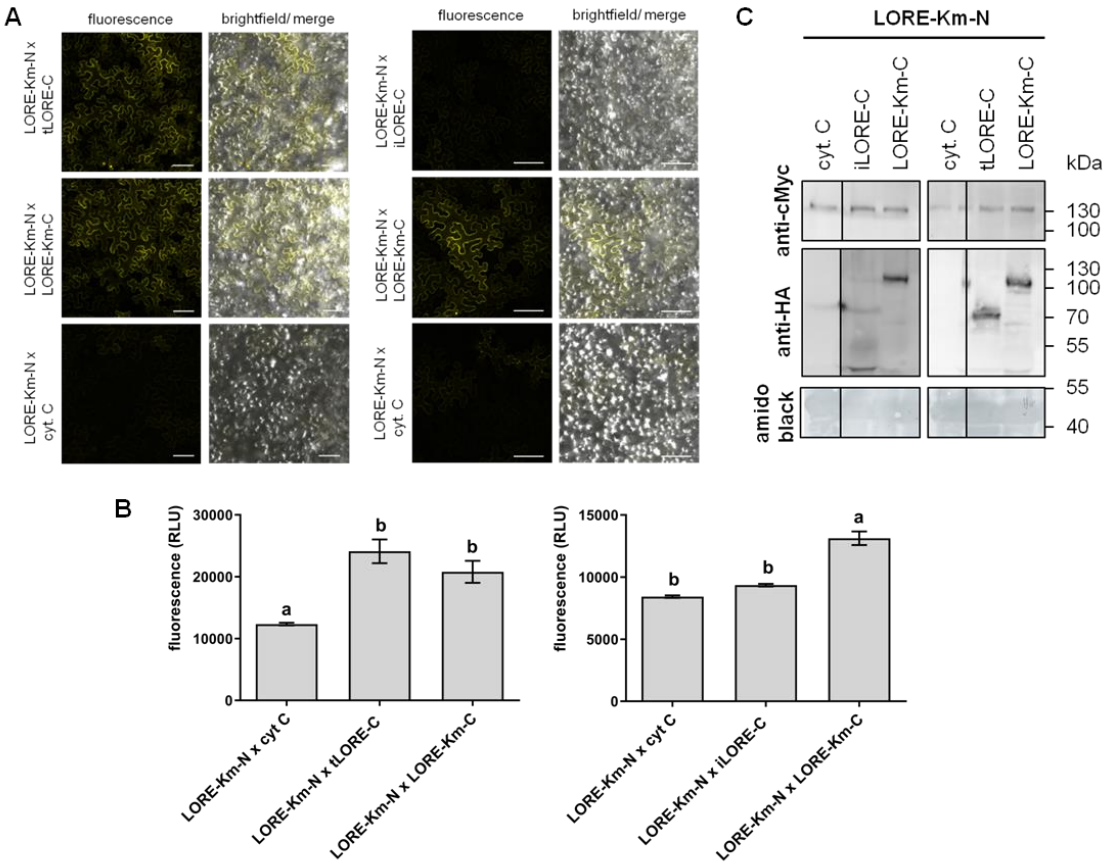

Figure 9 Co-expression of LORE-Km-N with LORE-Km-N and tLORE-C leads to YFP reconstitution. BiFC assay of *N. benthamiana* leaves transiently co-transformed with LORE-N (LORE fused to N-terminal YFP) with LORE-C (LORE fused to C-terminal YFP), iLORE-C, tLORE-C, or cytosolic C-terminal YFP. A) Microscopic evaluation of YFP signal from transiently transformed leaf discs of *N. benthamiana*. All combinations were imaged with the same microscope settings. Scale bar 100 µm. B) The fluorescence intensity was measured in leaf discs (24 per combination) excited with 485 nm and the emission was measured at 518 nm. Data represent mean ± SEM (n = 24) depicted as RLU. Data were analyzed with a one-way ANOVA and Tukey's multiple comparison post test. Different letters indicate significant differences ($P < 0.05$). C) Immunoblot analysis of the protein expression of the BiFC assay. N-terminal YFP epitope-tagged proteins were detected with anti-cMyc antibody (LORE-Km-N 110 kDa), C-terminal YFP epitope-tagged proteins with anti-HA antibody (LORE-Km-C 110 kDa, iLORE-Km-C 50 kDa, tLORE-C 60 kDa). Amido black staining shows equal protein loading. SuperSignal® West Femto Maximum Sensitivity Substrate (Pierce, Rockford, USA) was used for detection. These data were generated by Sonja Eibel within her master thesis.

The fluorescence complementation of LORE-Km-N co-expressed with iLORE-C was comparable to the fluorescence complementation of the negative control and was significantly lower than for LORE-Km-N with LORE-Km-C (Figure 9A and B). On the contrary, LORE-Km-N co-transformed with tLORE-C resulted in a similar fluorescence intensity as the positive control (LORE-Km-N/LORE-

Km-C) and was significantly higher compared to the negative control (Figure 9A and B). Both truncated receptor variants were expressed (Figure 9C). Notably, iLORE-C was expressed rather weakly compared to tLORE-C. Microscopic evaluation was performed 36 h after transformation. At later time points strong fluorescence signal was also detected for the negative control. The YFP reconstitution is irreversible and fluorescence signal accumulates over time which potentially leads to false positive results (Kudla *et al.*, 2016). All genes in this experiment were expressed under the strong constitutive 35S promoter possibly resulting in high protein accumulation over time which limited the period of time to obtain reliable results. Unfortunately, the heterologous protein expression in *N. benthamiana* required the use of a constitutive promoter as the endogenous pLORE promoter did not result in sufficient LORE-GFP fluorescence signal to use it for experiments (personal communication Dr. S. Ranf, TU München). Promising preliminary data of BiFC assays in Arabidopsis protoplasts confirmed the obtained results on LORE dimerization (Supplementary Figure 2D). Here, the constructs were also under the control of the 35S promoter, but the native genetic background might have the advantage to use pLORE or kinase-active LORE to investigate receptor dimerization in future.

Taken together, the results indicate that LORE full-length proteins are able to form homodimers *in planta*. The dimerization is independent of ligand-binding and kinase activity, and consequently, LORE might form pre-formed dimers in the plasma membrane to allow rapid signal transduction. The extracellular domain of LORE, but not the intracellular domain is crucial for dimerization with LORE full-length according to the results obtained with truncated LORE variants. Further research is required to underpin the conclusions because of limitations of the applied methods such as strong overexpression of the genes, problems with the negative controls, and performance of the experiments in a heterologous system. Furthermore, both methods do not provide evidence for direct protein-protein interaction (Kudla *et al.*, 2016).

4.2.2 Analysis of homodimerization of the soluble ectodomain of LORE

A detailed mechanistic study of the receptor complex formation of SRK dimerization was published while the study at hand was conducted (Ma *et al.*, 2016). The study showed that the extracellular domain of SRK9 (eSRK9) from *B. rapa* is sufficient for ligand-dependent homodimerization contradicting earlier results showing ligand-independent dimerization (Giranton *et al.*, 2000). According to the new study, the kinase domain of SRK9 as well as plasma membrane localization of the protein seem not to be critical for receptor complex formation (Ma *et al.*, 2016, section 3.10.2 and 4.4). Obtained results on LORE homodimerization suggested likewise that the kinase domain is not required (section 4.2). To confirm if the LORE ectodomain is sufficient to form homodimers, truncations of LORE lacking the intracellular domain and the transmembrane domain (eLORE) were generated (Figure 7A). As eLORE is not integrated into the plasma membrane, apoplastic wash fluid

of *N. benthamiana* were harvested and used for experiments (Figure 7C, Figure 10, section 8.1.26). eLORE-HA, eLORE-mCherry, and cytosolic mCherry were expressed in separate leaves, proteins were extracted and pull-down experiments were conducted (section 8.1.30). Apoplastic wash fluid containing eLORE-HA was mixed with equal amounts of the apoplastic wash fluid containing eLORE-mCherry and from cytosolic mCherry expressing leaves. eLORE-HA and eLORE-mCherry were detected in the input sample as well as enriched in the immunoprecipitated fraction (Figure 10A). Cytosolic mCherry was not detected in the apoplastic wash fluid showing that the harvesting process did not extract proteins located in the cytosol. The used anti-rabbit antibody potentially cross reacted with the HA trap which would explain the two lower bands detected in the immunoprecipitated samples (Figure 10A, indicated by arrows). This experiment was also repeated with apoplastic mCherry as a negative control (Figure 15). Here, eLORE-HA and eLORE-mCherry were detected in the input as well as in the immunoprecipitated fraction. Multiple bands were detected for eLORE-HA and eLORE-mCherry. The detection of multiple bands correlated with the time of expression in *N. benthamiana*. The apoplastic wash fluids used for the experiment shown in Figure 10A were harvested after 3 days of heterologous expression. The apoplastic wash fluids used for the experiment shown in Figure 15 were harvested after 5 days of heterologous expression. Possibly, the multiple bands were protein degradation products. Other possible reasons are discussed in section 4.3.4. A longer time of expression was chosen to obtain a higher protein concentration in the apoplastic wash fluids. After 3 days of expression, the amido black staining of proteins was too faint for photography and is therefore not depicted. A higher protein concentration was aimed for, to determine the protein concentration and use eLORE for further experiments such as binding studies. Apoplastic mCherry was detected in the input sample and residual levels were also detected in the immunoprecipitated sample with eLORE-HA (Figure 15). This indicated that apoplastic mCherry binds unspecifically to eLORE-HA or the HA trap. The amido black staining showed a strong band approximately at the size of apoplastic mCherry in the input fraction which was with a lower intensity also detected in the immunoprecipitated fraction (~30 kDa, Figure 15). Possibly, the high protein concentration of apoplastic mCherry led to the co-immunoprecipitation of apoplastic mCherry with eLORE-HA, although it is not directly interacting with eLORE-HA.

In summary, the pull-down experiment suggests that the soluble extracellular domain is sufficient for LORE homodimerization. This finding further signifies that receptor complex formation of LORE is similar to what is known for SRK. However, LORE dimerization seems to be ligand-independent as the presented experiments were conducted without elicitation with 3-HDA.

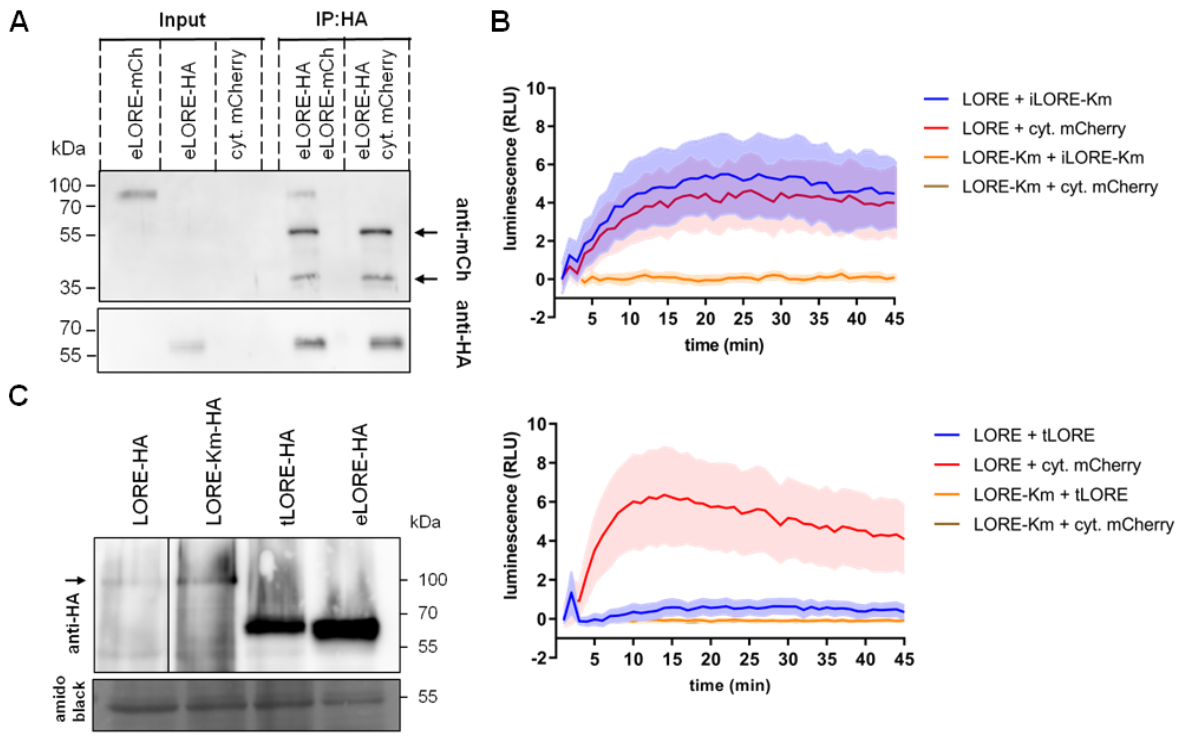

Figure 10 The ectodomain of LORE forms homodimers and exerts a dominant-negative effect on the function of LORE. A) Immunoblot analysis of eLORE-HA (70 kDa) and eLORE-mCherry (~100 kDa, eLORE-mCh) pull-down experiments. Proteins were individually expressed in *N. benthamiana* leaves. eLORE-HA containing apoplastic wash fluid was mixed with equal amounts of the eLORE-mCherry or cytosolic mCherry containing apoplastic wash fluid. Cytosolic mCherry cannot be detected in the apoplastic wash fluid. The anti-rabbit antibody used to detect anti-mCherry possibly cross detects parts of the HA-trap (two bands ~50 kDa and ~40 kDa, indicated by arrows). Amido black staining is not shown as the stained protein bands were too faint to be visible on a photograph. SuperSignal® West Femto Maximum Sensitivity Substrate (Pierce, Rockford, USA) was used for detection. The experiment was repeated three times with similar results. B) Competitive ROS accumulation in transiently co-transformed *N. benthamiana* leaves transformed with LORE-GFP or LORE-Km-GFP and tLORE-HA, iLORE-Km-HA, or cytosolic mCherry, respectively, upon treatment with 5 µM 3-HDA. Values represent the mean ± SEM (n = 8). This experiment was repeated three times with similar results. Depicted is a representative experiment. C) Detection of LORE-HA (~100 kDa), LORE-Km-HA (~100 kDa), tLORE-HA (~70 kDa), or eLORE-HA (~65 kDa). 80 leaf discs were harvested and total protein was extracted. 20 µL total protein extract was loaded, and the protein abundance was analyzed with anti-HA antibody. For LORE-HA a longer developed immunoblot is shown, the protein band is indicated by an arrow. Amido black shows equal protein loading. SuperSignal® West Dura Extended Duration Substrate (Pierce, Rockford, USA) was used for detection.

4.2.3 Investigation of a dominant-negative influence of tLORE

Based on the findings presented in sections 4.2.1 and 4.2.3, LORE dimerization seems to be ligand-independent. This raises the question if dimerization is required for receptor complex activation. To investigate this, competitive gain-of-function experiments were conducted (Figure 10B, section 8.1.17). LORE-GFP was co-expressed with tLORE-HA, iLORE-Km-HA, or cytosolic mCherry as a negative control in *N. benthamiana*. Agrobacteria carrying the plasmid encoding LORE-GFP were mixed in a ratio of 1:3 with Agrobacteria carrying the plasmid encoding tLORE-HA, iLORE-Km-HA, or cytosolic mCherry before infiltration into *N. benthamiana* leaves (section 8.1.17). ROS production in response to 3-HDA treatment was analyzed after 48 h. Theoretically, tLORE-HA binds to LORE-GFP forming an inactive receptor complex. Inactive, because only one kinase domain of LORE-GFP is present in the heterocomplex and binding of the ligand to the extracellular domain will not result in transphosphorylation of the kinase domain and subsequent signal transduction to trigger the production of apoplastic ROS. If the majority of receptor complexes are inactive, a dominant-negative effect on the generation of ROS should be detectable. Co-expression of LORE-GFP with the negative control cytosolic mCherry rendered *N. benthamiana* sensitive to the application of 3-HDA which induced the accumulation of ROS. Co-expression of LORE-GFP and tLORE-HA resulted in a strongly reduced response compared to LORE-GFP co-expressed with cytosolic mCherry (Figure 10B). In comparison, co-expression of LORE-GFP with iLORE-Km-HA resulted in an equal ROS generation upon 3-HDA treatment as co-expression of LORE-GFP and cytosolic mCherry. The expression of LORE-Km-GFP did not render *N. benthamiana* sensitive to 3-HDA independent of the co-expression of iLORE-Km-HA, tLORE-HA, or cytosolic mCherry (Figure 10B). This experiment was also performed using the soluble ectodomain of LORE (eLORE-HA) as well as the soluble ectodomain of LORE with an N-terminal HA epitope tag (eLORE-nHA, section 4.2.4) which both showed no dominant-negative effect on the ROS production (Supplementary Figure 3A and B). In contrast, tLORE-nHA exerts a dominant-negative effect on the ROS production stimulated by LORE-GFP similar as tLORE-HA (Supplementary Figure 3A). These are preliminary results, but indicate that only truncations located at the plasma membrane interact with full-length LORE-GFP. It is possible that the low ROS response results from elicitor depletion by tLORE. However, no difference in the accumulation of ROS was detected by the co-expression of LORE-GFP with eLORE-HA compared to LORE-GFP co-expressed with apoplastic mCherry (Supplementary Figure 3B). But depletion of the elicitor and thus a low ROS response should also be mediated by eLORE which also forms homodimers (section 4.2.1, Figure 10A). Since this is not the case, the reduced ROS response is rather caused by non-productive heterocomplexes of LORE-GFP with tLORE-HA or tLORE-nHA. The protein abundance of LORE-HA, LORE-Km-HA, and the truncated variants tLORE-HA and eLORE-HA upon transient transformation of *N. benthamiana* was examined. The immunoblot illustrates higher protein accumulation for truncated protein variants compared to LORE-Km and active LORE (Figure 10C). This indicated that the actual protein abundance of full-length LORE is lower than for

the truncated protein and thus the ratio of the two proteins will be higher than the aimed 1:3 (Figure 10C). Interestingly, preliminary CoIP experiments of the combinations used in the gain-of-function experiments supported interaction of LORE-Km-GFP with tLORE-HA, but suggested also interaction of LORE-Km-GFP with iLORE-Km-HA (Supplementary Figure 3D). The fact that CoIP experiments give no evidence for direct interaction should be taken into consideration. False positive results could be obtained, because LORE-Km-GFP and iLORE-Km-HA localize close to each other or the interaction could be bridged by other proteins.

In summary, tLORE-HA, but not iLORE-Km-HA or eLORE-HA exerts a dominant-negative effect on the activity of LORE-GFP in *N. benthamiana*. These findings indicate that LORE homodimerization is required for receptor complex activation.

4.2.4 Co-immunoprecipitation experiments of truncated and full-length LORE variants

Competition gain-of-function experiments of LORE-GFP and eLORE-HA indicated that the soluble ectodomain of LORE did not exert a dominant-negative effect on LORE and thus did not interact with LORE full-length proteins (section 4.2.3). To analyze the interaction of LORE truncations and LORE full-length protein, CoIP experiments were performed upon transient expression in *N. benthamiana* (Figure 11). LORE-Km-HA was co-transformed with LORE-GFP, tLORE-GFP, eLORE-GFP as well as with kLORE-GFP, iLORE-GFP (Figure 7), or cytosolic GFP as a negative control. tLORE-GFP, eLORE-GFP, cytosolic GFP, and LORE-Km-HA were detected in the input fraction (Figure 11). LORE-Km-HA was also detected in the immunoprecipitated sample, indicating interaction with LORE-Km-GFP. Interestingly, LORE-Km-HA was immunoprecipitated with tLORE-GFP and iLORE-GFP, but not with the soluble extra- or intracellular domain of LORE, indicating that the transmembrane domain was required for interaction with full-length LORE (Figure 11). This finding contradicted the BiFC assay results where no fluorescence reconstitution was seen for the interaction of LORE-Km and iLORE (Figure 9A-C). The input fractions of tLORE-GFP, eLORE-GFP, kLORE-GFP, iLORE-GFP, and cytosolic GFP showed multiple bands around the size of 30 kDa. Potentially, these were degradation products of the truncated variants. However, the fact that the input sample of cytosolic GFP showed the same additional band did not support this hypothesis (Figure 11). The input samples consist of the total protein extracts plus a variety of buffer ingredients (section 8.1.28). Therefore, the used antibody for detection of GFP-labeled proteins might have cross-reacted with components or proteins present in the input sample. The additional band was not detected in the co-immunoprecipitated fractions (Figure 11). Moreover, this additional band was also detected in total protein samples extracted from Arabidopsis (section 4.5.2, Figure 20B and D).

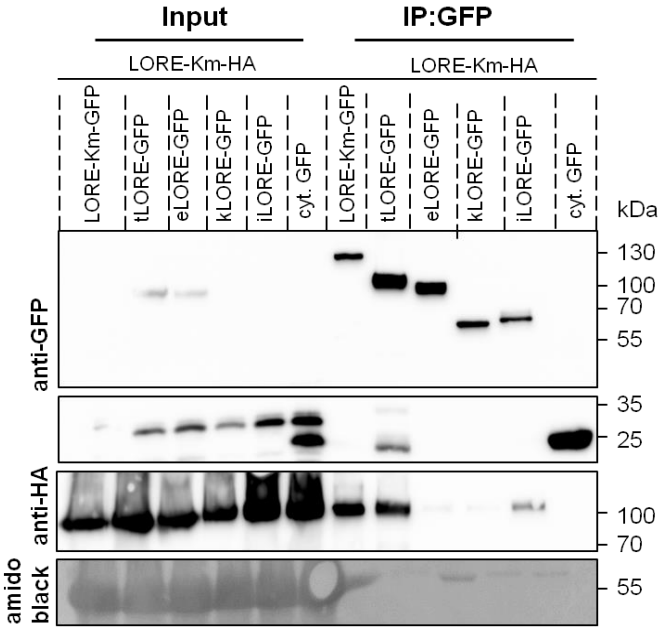

Figure 11 Influence of the presence of the transmembrane domain or C-terminal epitope tag on LORE homodimerization with truncated LORE variants. Immunoblot analysis of CoIP experiments of transiently transformed *N. benthamiana*. LORE-Km-HA (~100 kDa) was co-transformed with LORE-Km-GFP (~130 kDa), tLORE-GFP (~100 kDa), eLORE-GFP (~90 kDa), iLORE-GFP (~70 kDa), kLORE-GFP (~65 kDa), or cytosolic GFP (~30 kDa, cyt. GFP). Interacting proteins were immunoprecipitated with a GFP trap. The experiment was repeated two times. Amido black staining shows equal loading in the input samples. SuperSignal®West Dura Extended Duration Substrate (Pierce, Rockford, USA) was used for detection.

The obtained CoIP results implied that eLORE-GFP was not able to bind to the full-length protein of LORE. Potentially, the C-terminal GFP epitope tag (30 kDa) hindered the interaction of eLORE with LORE which is integrated into the plasma membrane. Thus, truncations of LORE N-terminally fused to HA were generated (tLORE-nHA, eLORE-nHA). The N-terminal HA epitope tag is located between the signal peptide and start of the ectodomain of LORE (LORE-nHA). LORE-nHA was shown to be active in transient gain-of-function experiments in *N. benthamiana* (personal communication Dr. S. Ranf, TU München). LORE-Km-GFP was co-transformed with tLORE-nHA, eLORE-nHA, tLORE-HA, and eLORE-HA to elucidate the effect of a C-terminal epitope tag on the interaction with LORE full-length protein (Supplementary Figure 2B). Interaction was assessed *via* CoIP experiments upon transient transformation in *N. benthamiana*. LORE-Km-GFP was immunoprecipitated with the membrane-bound, but not with the soluble ectodomain of LORE regardless of an N- or C-terminal HA fusion protein. This finding indicated that an epitope tag does not prevent interaction between eLORE and LORE-Km, and was in accordance with the findings of competitive gain-of-function experiments described in section 4.2.3. The CoIP experiment using LORE truncations fused to an N- and C-terminal HA epitope tag was repeated once, and therefore

represents a preliminary result. Additionally, for all truncated LORE variants only a weak signal was detected in the immunoprecipitated fraction (Supplementary Figure 2B).

4.2.5 Investigation of the influence of 3-HDA on LORE homodimerization

eSRK9 homodimerization requires the presence of the ligand SCR as previously published (Ma *et al.*, 2016). The influence of the addition of 3-HDA on complex formation of eLORE was analyzed in pull-down experiments. 0.5 µM, 1 µM, 5 µM 3-HDA, or methanol (MeOH) as a control were added to the apoplastic wash fluid of eLORE-HA mixed with equal amounts of the wash fluid of eLORE-mCherry (Supplementary Figure 3E). The impact of the presence of the ligand on dimerization was inconclusive. The experiment was repeated two times with varying outcomes. Although equal amounts of extracts were used for the experiments, different protein concentrations cannot be excluded as the protein concentration of extracts used for pull-down experiments could not be determined. Pull-down of different samples might be of variable efficiency, and therefore, comparison of signal intensity is not possible. However, the inconclusiveness points out that the application of 3-HDA had no strong positive effect on dimerization.

Taken together, soluble extracellular domains of LORE can interact with each other, but interaction with the LORE full-length protein requires a transmembrane domain. This assumption is based on the finding that eLORE-nHA and eLORE-HA do not bind to LORE-Km-GFP, but eLORE-HA can interact with eLORE-mCherry. Moreover, tLORE-HA is able to interact with LORE-Km-GFP. This raises the question why tLORE, but not eLORE is able to interact with LORE. This could be caused by the abundance and availability of interacting partners. LORE and tLORE are integrated into the membrane and eLORE is located in the apoplast (section 4.2, Figure 7). The chance of eLORE to meet LORE to form a complex might be less likely than for tLORE. However, eLORE might interact with LORE-Km in *planta*, but the interaction could be rather weak and more prone to disruption during the process of protein extraction than the interaction of tLORE and LORE-Km both integrated into the plasma membrane. CoIP experiments do not provide evidence for direct interactions of proteins. RLKs localize to nanodomains in the plasma membrane and membrane patches can be immunoprecipitated leading to potential false positive results (Bücherl *et al.*, 2017, Jarsch *et al.*, 2014).

4.3 Influence of LORE extracellular domains on receptor activation

The experiments presented in the preceding sections focused on the identification of domains involved in LORE homodimerization (section 4.2, section 4.2.2). In addition to it, domains involved in receptor complex activation were investigated. As described in section 4.4, the extracellular domain is composed of LLD1, LLD2, an EGF-like, and a PAN/APPLE domain. Investigation of domain

functionality was approached by the generation of domain swap receptor variants with *At*LORE orthologs from previously identified LPS/3-HDA-insensitive plant species and close paralogs not involved in 3-HDA-sensing in Arabidopsis (section 4.1). AlyrLORE as an ortholog as well as SD1-23i and SD1-28i as paralogs were chosen as they do not confer 3-HDA sensitivity to *N. benthamiana* (section 4.1, Figure 6C). First, chimeric receptors with domain swaps (DS) of the whole extracellular domain (LLD1, LLD2 (LL), EGF-like (E), PAN/APPLE (P)) plus transmembrane domain (T) (DSAlyr-LLEPT, DS123-LLEPTi, DS128-LLEPTi) or the intracellular domain including the kinase domain (JK) and domain of unknown function 3403 (D) (DSAlyr-JKD, DS123-JKD, DS128-JKD) were generated and functionally tested in transient gain-of-function experiments in *N. benthamiana* (Figure 12). The exact domain swap sites on an amino acid level are depicted in Supplementary Figure 11, listed in Table 2, and are based on the domain border prediction according to Naithani *et al.* (2007) (section 3.10.1).

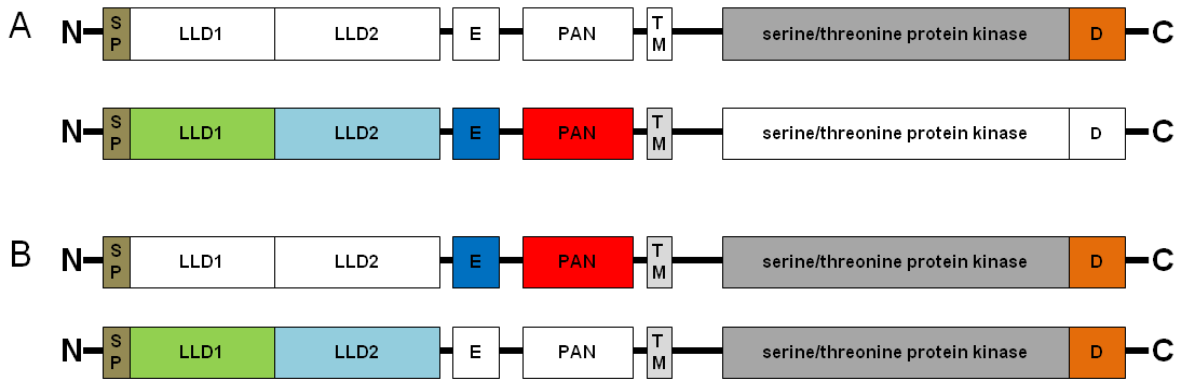

Figure 12 Schematic illustration of generated chimeric receptor variants of LORE with AlyrLORE, SD1-23i, and SD1-28i. Domains depicted in white originate from AlyrLORE, SD1-23i, or SD1-28i, and colored domains originate from LORE. A) Domain swaps (DS) of the complete extracellular domain. The transmembrane domain (TM), PAN/APPLE (PAN), EGF-like domain (E), and lectin-like domain 1 and 2 (LLD1/LLD2) were swapped. For the domain swap of the complete intracellular domain, the serine threonine kinase domain (JK) and the domain of unknown function (D) were swapped (DSAlyr-LLEPT, DSAlyr-JKD, DS123-LLEPTi, DS123-JKD, DS128-LLEPTi, DS128-JKD). B) Domain swaps of the extracellular domain. Domains were swapped in pairs e.g. LLD1 and LLD2 or E and PAN (DSAlyr-LL, DSAlyr-EP, DS123-LLi, DS123-EP, DS128-LLi, DS128-EP).

4.3.1 Functional analysis of chimeras with complete extra- or intracellular domain swaps

The domain swap variants were functionally tested in transiently transformed *N. benthamiana* for their ability to activate ROS production in response to 3-HDA. The chimeric receptor variants with the exchanged intracellular domain (DSAlyr-JKD, DS123-JKD, DS128-JKD; Figure 12A) were still

functional and induced ROS accumulation when triggered with 3-HDA (Figure 13A, B, and C). Apparently, the kinase domain of LORE was exchangeable with the kinase domains of AlyrLORE, SD1-23i, and SD1-28i. Hence, the kinase domain of LORE was not obligatory for 3-HDA recognition.

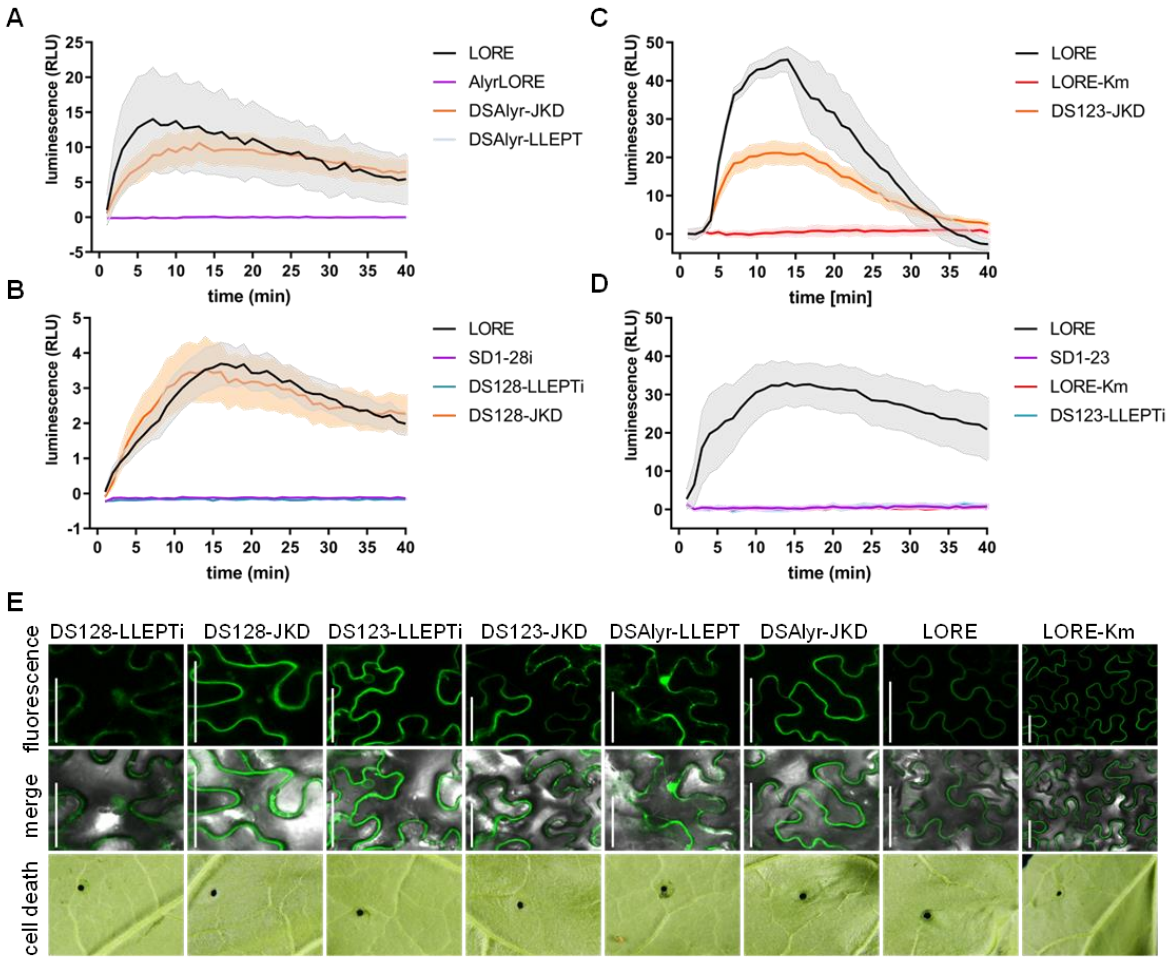

Figure 13 ROS measurements, localization, and induction of cell death of chimeric receptor variants with complete extra- or intracellular domain swaps upon transient transformation in *N. benthamiana*. Measurement of ROS accumulation in leaf discs of transiently transformed *N. benthamiana* leaves in response to 5 µM 3-HDA (A, B, D) or 25 µg/mL LPS *Pst* DC3000 (C). Data represent the mean ± SEM (n = 8) depicted in RLU. Experiments were repeated three times with similar results (A, B, C, D). A) Transient expression of LORE-GFP, AlyrLORE-GFP, DSAlyr-JKD-GFP, and DSAlyr-LLEPT-GFP. B) Transient expression of LORE-GFP, SD128i-mCherry, DS128-JKD-GFP, and DS128-LLEPTi-GFP. C) Transient expression of LORE-GFP, LORE-Km-GFP, and DS123-JKD-GFP. D) Transient expression of LORE-Km-GFP, SD123i-GFP, and DS123-LLEPTi-GFP. E) Microscopic evaluation of GFP fluorescence and photographs of the induction of cell death of domain swap proteins transiently expressed in *N. benthamiana* after 36 h from A, B, C, and D. Scale bar 50 µm. The experiment depicted in C) was performed by Tina Illig within her master thesis.

Furthermore, this experiment provided evidence that all tested ortho- and paralogs possess active kinase domains which are essential for signal transduction. Intriguingly, expression of chimeric receptor variants with an exchanged extracellular domain (DSAlyr-LLEPT, DS123-LLEPTi, DS128-LLEPTi) did not render *N. benthamiana* sensitive to the application of 3-HDA (Figure 13A, B, and D). Evidently, the extracellular domain of LORE was critical for receptor activation. From these experiments, it cannot be judged, if the ligand was still able to bind to the chimeric receptors or if receptor activation or signal transduction were hindered due to incompatibility of the chimeric proteins. In line with the induction of an oxidative burst in response to 3-HDA was the presence of cell death in transiently transformed *N. benthamiana* (Figure 13E). Cell death was observed for the chimeric receptor variants DSAlyr-JKD, DS123-JKD, and SD128-JKD, but not DSAlyr-LLEPT, DS123-LLEPTi, and DS128-LLEPTi. Due to the low protein accumulation of active LORE and other active SD-RLKs, protein abundance could not be confirmed by immunoblot analysis upon transient transformation of *N. benthamiana* (section 4.2, Supplementary Figure 2A). The expression of the chimeric receptors as well as AlyrLORE-GFP, SD123i-GFP, SD128i-GFP, LORE-GFP, or LORE-Km-GFP was evaluated by a screening of fluorescent signal and the presence of the cell death phenotype before ROS measurements (Figure 13C). All tested chimeric receptor variants of one set (corresponding to one graph in Figure 13; AlyrLORE-GFP, DSAlyr-JKD-GFP, DSAlyr-LLEPT-GFP) were infiltrated on the same leaf as the positive control LORE-GFP assuming a comparable expression level of the proteins on one leaf.

4.3.2 Functional analysis of chimeras with partial extracellular domain swaps

The extracellular, but not the intracellular domain of LORE seems to be critical for 3-HDA-sensing (section 4.3.1). To narrow down the involvement of specific domains, further domain swaps of LORE and the para- and orthologs (AlyrLORE, SD123i, SD128i) of the extracellular domains were generated. The extracellular domains were swapped in pairs. Either, both lectin-like domains from the para- and orthologs (DSAlyr-LL, DS123-LLi, DS128-LLi) or EGF-like and PAN/APPLE from the para- and orthologs (DSAlyr-EP, DS123-EP, DS128-EP) were swapped with LORE (Figure 12B). The exact domain swap sites are depicted in Supplementary Figure 11 and listed in Table 2. The domain swaps were functionally tested in transient gain-of-function experiments in *N. benthamiana* (Figure 14A-C). The transient transformation of partial domain swaps of the extracellular domains of AlyrLORE with LORE (DSAlyr-LL and DSAlyr-EP) rendered *N. benthamiana* sensitive to 3-HDA (Figure 14A). Similarly, the transient transformation with the domain swaps of *At*SD1-23 with LORE (DS123-LLi and DS123-EP) rendered *N. benthamiana* likewise responsive to 3-HDA (Figure 14C). Apparently, the level of ROS accumulation by the chimeric receptors (DS123-LLi, DS123-EP, DSAlyr-LL, DSAlyr-EP) was lower compared to LORE-mediated ROS accumulation. In independent experiments the level of ROS accumulation varied and was sometimes as strong as the ROS response mediated by LORE, but representative ROS burst kinetics are depicted.

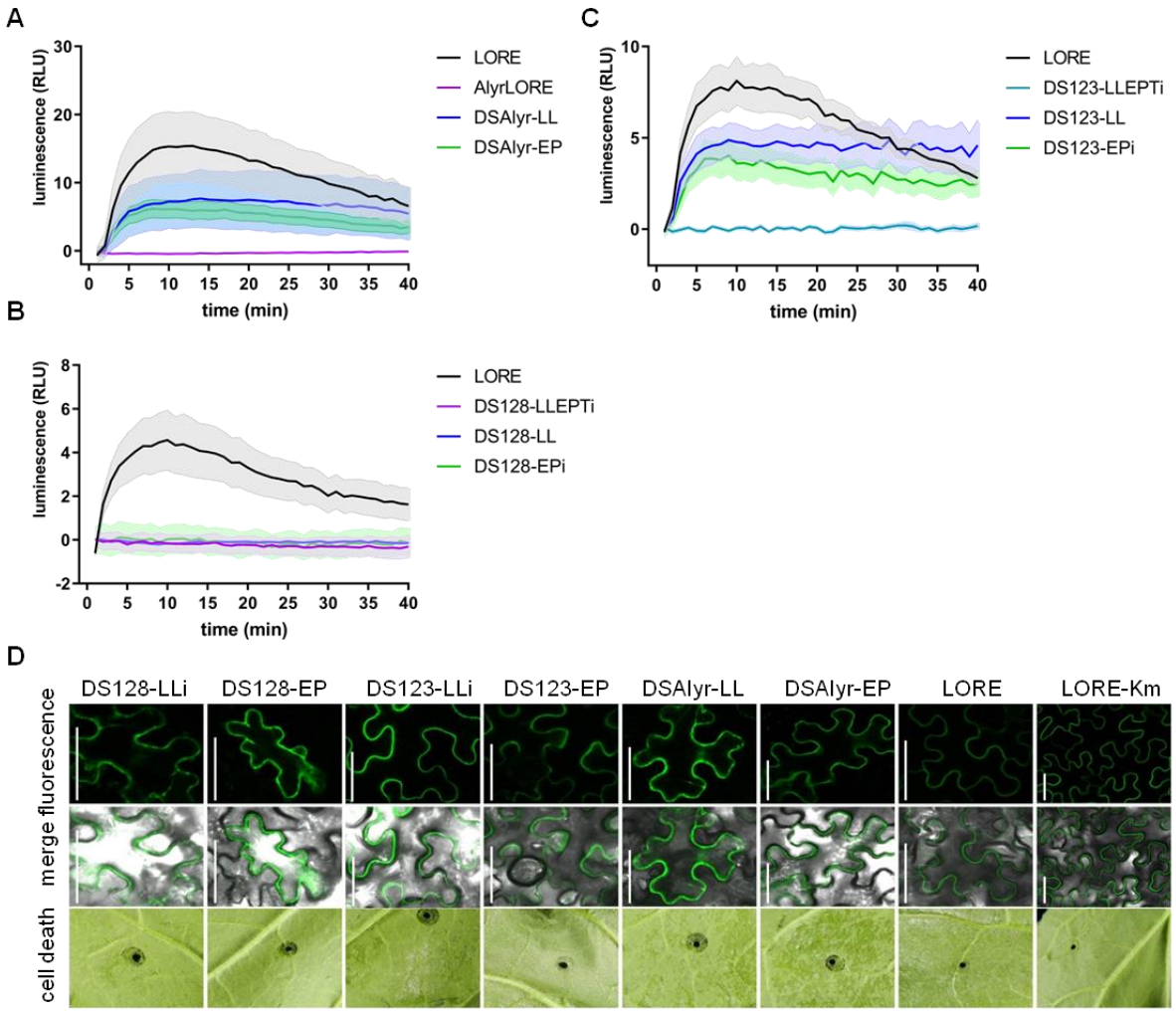

Figure 14 ROS measurements, localization, and cell death induction of chimeric receptor variants with partial extracellular domain swaps upon transient transformation in *N. benthamiana*. Measurement of ROS accumulation in leaf discs of transiently transformed *N. benthamiana* leaves in response to 5 µM 3-HDA (A, B, C). Data represent the mean ± SEM (n = 8) depicted in RLU. Experiments were repeated three times with similar results (A, B, C). A) Transient expression of LORE-GFP, AlyrLORE-GFP, DSAlyr-LL-GFP, and DSAlyr-EP-GFP. B) Transient expression of LORE-GFP, DS128-LLEPTi, DS128-LL-GFP, and DS128-EPi-GFP. C) Transient expression of LORE-GFP, DS123-LLEPTi-GFP, DS123-LL-GFP, and DS123-EPi-GFP. D) Microscopic evaluation of GFP fluorescence and photographs of the induction of cell death of domain swap proteins transiently expressed in *N. benthamiana* after 36 h from A, B, and C. Scale bar 50 µm.

Interestingly, expression of the chimeric receptor variants with the most distantly related SD-RLK used for the domain swaps *At*SD1-28, DS128-LLi, and DS128-EP did not confer sensitivity to 3-HDA to *N. benthamiana* (Figure 14B). The tested activity was in line with the presence of the cell death phenotype observed for active LORE (Figure 14D). The expression of the domain swaps DSAlyr-LL,

DSAlyr-EP, DS123-LLi, and DS123-EP resulted in cell death of *N. benthamiana*. The expression of the domain swaps DS128-LLi and DS128-EP did not lead to cell death (Figure 14D).

4.3.3 Localization and expression analysis with confocal microscopy

Expression and localization of the chimeric receptor variants was imaged with confocal laser scanning microscopy (Figure 13E, Figure 14D). LORE-GFP and LORE-Km-GFP were shown to localize to the plasma membrane (Ranf *et al.*, 2015). All chimeric receptor proteins carry the signal peptide from LORE to ensure successful protein secretion (section 8.1.10). Fluorescent signal of DSAlyr-JKD-GFP and DS128-JKD-GFP was detected at the plasma membrane (Figure 13E). The localization of DS123-JKD-GFP, however, was not as clear. Transient expression of DS123-JKD-GFP rendered *N. benthamiana* sensitive to LPS/3-HDA treatment. Additional to the plasma membrane localization of DS123-JKD-GFP, intracellular fluorescent signal can be detected which might indicate only partial secretion of the recombinant protein (Figure 13C). The chimera DS123-LLEPTi-GFP was localized to the plasma membrane and fluorescent signal seems to be detected intracellularly, possibly in the endoplasmic reticulum (Figure 13D). Fluorescent signal of DSAlyr-LLEPT-GFP and DS128-LLEPTi-GFP can be detected at the plasma membrane. DS128-LLEPTi-GFP seems to localize also intracellularly, possibly to the endoplasmic reticulum indicating only partial secretion. DS128-LLi-GFP and DS128-EP-GFP showed likewise intracellular localization (Figure 14D). DS123-LLi-GFP and DS123-EP-GFP as well as DSAlyr-EP-GFP were localized to the plasma membrane (Figure 14D). DSAlyr-LL-GFP, in contrast, showed additional intracellular localization, but confers 3-HDA responsiveness to *N. benthamiana* supporting localization to the plasma membrane (Figure 14D). All kinase domains of the chimeric receptors are active and cell death accompanies the expression of some chimeras (Figure 13E, Figure 14D). Mis-localization due to cell death cannot be completely excluded. Active LORE-GFP, on the other hand, showed no localization around the nucleus indicating rather a mis-localization of the domain swap proteins independent of the occurrence of cell death. The transient transformation of DS128-LLi-GFP and DS128-EP-GFP did not confer 3-HDA sensitivity to *N. benthamiana* and did not lead to any cell death symptoms which might be explained by the sole intracellular localization. Interestingly, fluorescence signal intensity varied among the chimeric receptor proteins, and therefore, differences in the intensity of the ROS response should be interpreted with caution. The first intron of *AtLORE* was introduced to SD1-28i and SD1-23i as expression of *At*SD1-23 during molecular cloning was lethal for *E. coli*. The correct splicing of the mRNA in *N. benthamiana* was analyzed for SD1-23i and SD1-28i (personal communication Dr. S. Ranf, TU München). However, problems with the expression are possible, since especially for the domain swaps with SD1-28i rather low fluorescence intensity as well as transformation rate compared to LORE-Km and the domains swaps with AlyrLORE was observed. In case of chimeras derived from SD1-28i and LORE, intracellular localization upon transient transformation correlated with insensitivity of *N. benthamiana* to 3-HDA. Correlation between localization and induction of ROS production was also

true for the domain swaps of AlyrLORE and SD1-23i with LORE (Figure 13B and E, Figure 14A and D).

In summary, the exchange of the whole intracellular domain of LORE generates receptor variants which render *N. benthamiana* sensitive to 3-HDA whereas the exchange of the whole extracellular domain generates receptor variants which do not mediate 3-HDA-sensing. Chimeric receptors with just partial domain swaps with SD1-23 and AlyrLORE render *N. benthamiana* 3-HDA-sensitive. Hence, LLD1/LLD2 as well as the EGF-like/PAN/APPLE domains are involved in receptor activation and possibly in ligand binding. A prerequisite for the receptor complex activation of the chimeric receptor variants with closely related SD-RLKs seems to be that parts of the extracellular domain originate from LORE as complete swaps of the extracellular domain do not confer 3-HDA sensitivity. This is not the case for the partial domain swaps with the SD1-28 extracellular domain which are insensitive, but seem to only localize intracellularly. All chimeric receptor variants which render *N. benthamiana* sensitive induce also cell death. The localization, however, is not in all cases clearly only at the plasma membrane which could result from incomplete secretion.

4.3.4 Investigation of LORE heterodimerization

The functional analysis of domain swaps of LORE with close para- and orthologs suggested that the substitution of the whole ectodomain of LORE produces inactive receptor variants (section 4.3.1). Inactive receptor variants can either not bind the ligand or are not activated upon ligand-binding. Dimerization is critical for receptor complex activation of LORE, and thus dimerization might be impaired in the chimeric receptor variants (section 4.2.3, section 4.3). LORE dimerization is likely mediated by the extracellular domain (section 4.2). To further investigate if dimerization is abolished, soluble ectodomains of AlyrLORE, SD1-23i, and SD1-28i (eAlyrLORE, eSD123i, eSD128i) were generated, and tested for their ability to heterodimerize with eLORE-HA. Apoplastic wash fluids were harvested and pull-down experiments were conducted and analyzed *via* immunoblots (section 8.1.26 and 8.1.30). eLORE-mCherry, eAlyrLORE-mCherry, and apoplastic mCherry were detected in the input fraction. eSD123i-mCherry, eSD128i-mCherry as well as eLORE-HA were expressed to a lower extent and not detected in the input fraction. All truncated variants were immunoprecipitated with eLORE-HA. However, the detected band in the immunoprecipitated fraction of eSD128i-mCherry was rather weak (Figure 15). The lower expression level could explain the lower enrichment in the immunoprecipitated fraction. On the other hand, eSD123i-mCherry showed stronger enrichment in the immunoprecipitated sample compared to eSD128i-mCherry, but was likewise not detectable in the input fraction. Apoplastic mCherry was detected in the input sample. Residual levels of apoplastic mCherry were also detected in the immunoprecipitated fraction of eLORE-HA and apoplastic mCherry. It is possible that apoplastic mCherry binds unspecifically to eLORE-HA or the HA trap (Figure 15). Intriguingly, a strong band in the size of apoplastic mCherry (~30 kDa) was detected in

the amido black staining in the input sample which was strongly reduced in the immunoprecipitated sample. Potentially, the high concentration of apoplastic mCherry in the apoplastic wash fluid led to false positive results (Figure 15). The detected band of eSD128i-mCherry in the immunoprecipitated faction was in its intensity comparable to the band of apoplastic mCherry. Therefore, it is likely that the co-immunoprecipitation of eSD128i-mCherry with eLORE-HA represented likewise a false positive result. This experiment was repeated three times and there were always residual levels of apoplastic mCherry detected in the immunoprecipitated fraction. The apoplastic wash fluid was harvested after 5 days incubation to gain higher protein abundance. Multiple bands are detected on the immunoblot for all tested soluble ectodomains. Unfortunately, the longer period of expression goes in line with more degradation products which were not present after 3 days of protein production (Figure 10A). For eLORE-HA, three bands of a similar size were detected which could point to differential or only partial glycosylation of the ectodomain. Seven glycosylation sites are predicted for LORE in the ectodomain (The UniProt Consortium, 2017, accessed November 19, 2018).

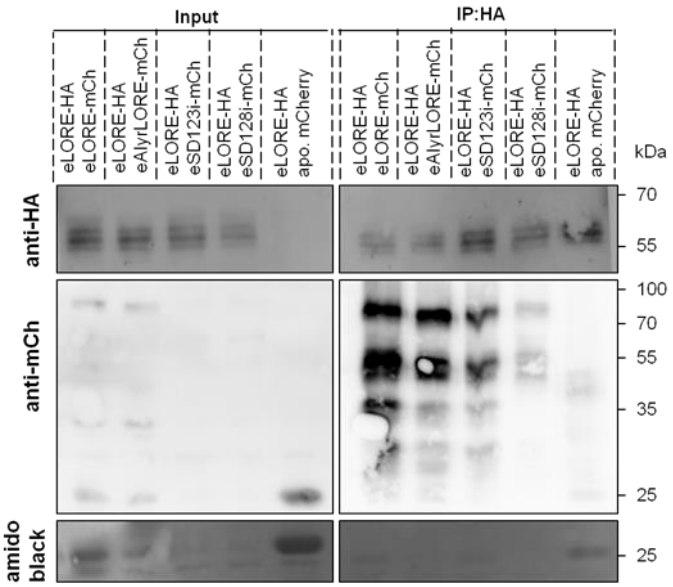

Figure 15 Heterodimerization of LORE. Immunoblot analysis of pull-down experiments from eLORE-HA (~65 kDa) with eLORE-mCherry (~100 kDa, eLORE-mCh), eAlyrLORE-mCherry (~100 kDa, eAlyrLORE-mCh), eSD123i-mCherry (~100 kDa, eSD123i-mCh), eSD128i-mCherry (~100 kDa, eSD128i-mCh), or apoplastic mCherry (~30 kDa, apo. mCherry). Proteins were expressed in individual *N. benthamiana* leaves for five days. eLORE-HA apoplastic wash fluid was mixed with equal amounts of the other soluble ectodomains or apoplastic mCherry wash fluid. Multiple bands detected on the immunoblot can be degradation products or differential or partial glycosylated ectodomains. Amido black staining shows protein abundance in the input and immunoprecipitated samples. The experiment was repeated three times with similar results. SuperSignal® West Femto Maximum Sensitivity Substrate (Pierce, Rockford, USA) was used for detection.

Preliminary data of CoIP experiments of full-length proteins support heterodimerization of SD1-23 and AlyrLORE with LORE (Supplementary Figure 3D). Interaction of full-length proteins from SD1-28 and LORE was not investigated yet. Also interaction of eSD128i-mCherry with eLORE-HA was not convincingly proofed by the performed pull-down assays. If eSD128i does not interact with eLORE-HA then tSD128i (extracellular domain plus transmembrane domain of SD128i) should also not have a dominant-negative effect on the generation of ROS in a competition assay as described in section 4.2.3 for tLORE-HA and LORE-GFP. Indeed, preliminary data suggests that tSD128i-HA co-expressed with LORE-GFP full-length protein had no dominant-negative effect on the generation of ROS and thus the formation of active receptor complexes (Supplementary Figure 3C). Notably, it is not possible to exclude lower protein expression for tSD128i in the transient assay as observed for the accumulation of eSD128i-mCherry in the pull-down assay. Nonetheless, all obtained data on SD1-28 suggested that SD1-28 was not able to sense 3-HDA and that complex formation in the form of dimerization with LORE was impaired.

To summarize all results presented on LORE receptor complex formation, the intracellular domain is dispensable for LORE dimerization which seems to be mediated by the extracellular domain. Also soluble variants of the ectodomain of LORE interact with each other after expression in individual leaves. Interestingly, tLORE, but not iLORE, eLORE, nor tSD128i have a dominant-negative effect on the generation of ROS mediated by LORE upon 3-HDA treatment in *N. benthamiana*. 3-HDA recognition specificity lies also within the extracellular domain. The kinase domain of LORE can be swapped with kinase domains of other SD-RLKs. Partial domain swaps of the extracellular domain with closely related SD-RLKs remain active, partial domain swaps with SD1-28 are inactive. This is supported by the ability of eLORE to heterodimerize with eAlyrLORE and eSD123i, but most likely not with eSD128i.

4.4 *In-silico* analysis of the ectodomain of LORE

In 2016, the crystal structure of the ectodomain of SRK9 from *B. rapa* produced in insect cells and bound to its ligand SCR9 was published. This gave new insights into receptor complex formation of the SRK (Ma *et al.*, 2016, section 3.10). The crystal structure revealed a tetrameric complex of two SCR9 ligand peptides and of two eSRK9 monomers leading to a ‘V’-shape (Figure 16A). The homodimerization is ligand-, but also receptor-mediated. The ligand SCR9 mediates homodimerization *via* the interaction with the hyper-variable region II (hvII) of one monomer of eSRK9 and with hvII of the other monomer. Interestingly, the hv regions of SRK were shown before to play a role in the self-recognition of the SI response (Sato *et al.*, 2002, Nasrallah, 1997).

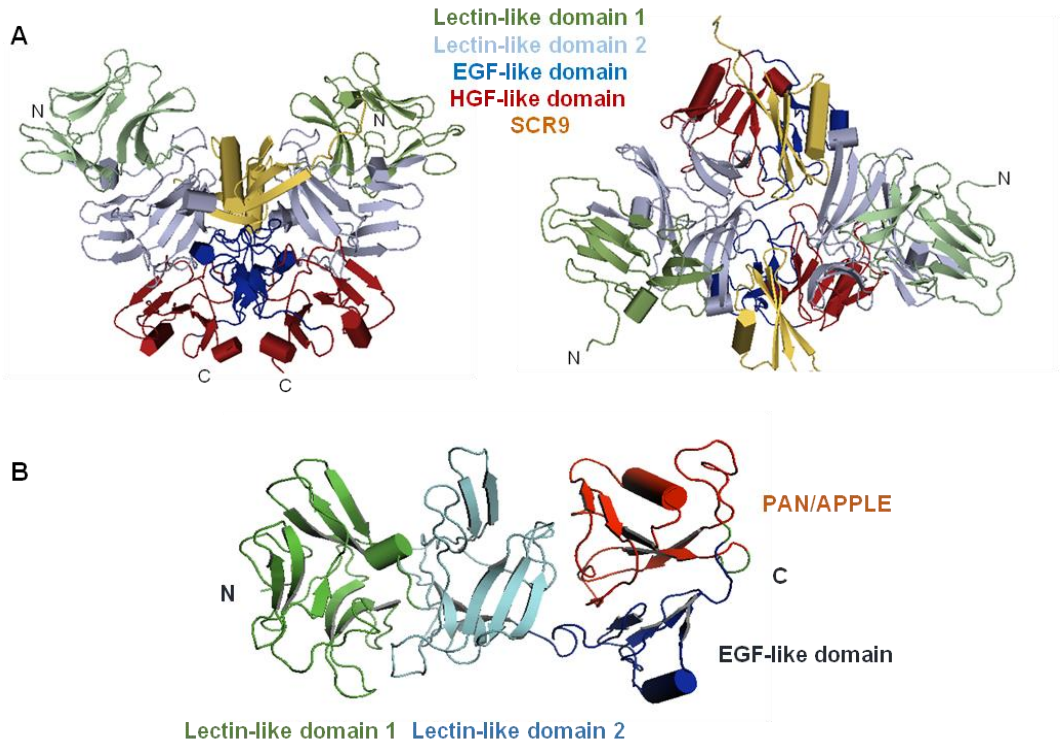

Figure 16 Overall structure of the receptor complex of eSRK9 with SCR9 and the ectodomain of LORE. A) Two eSRK9 monomers form a tetrameric complex in the shape of a 'V' with two SCR9 (beige) ligand peptides. Depicted are the lateral view (left) and the top view (right) of the receptor complex. N represents the N terminus and C the C terminus. Homodimerization is ligand- and receptor-mediated. One SCR9 ligand is interacting with both eSRK9 monomers and SCR9 is located between LLD2 of both monomers in a hydrophobic pocket created by the interaction of LLD2 with the EGF-like domain. B) Overall structural model of one monomer of the ectodomain of LORE (eLORE) based on an eSRK9 model. eLORE is defined by two adjacent lectin-like domains (LLD1 (green), LLD2 (turquoise)), followed by an EGF-like domain (blue) and a PAN/APPLE domain (red). The model for eSRK9 and eLORE were kindly provided by Dr. Rui Ma (Tsinghua University). A) is adapted from Ma *et al.* (2016). The figure was created using PyMOL (Delano Scientific LLC., 2006).

The looped-out helix of the EGF-like domain of one monomer of eSRK9 interacts with LLD2 of the other monomer and *vice versa* (Figure 16A, Ma *et al.*, 2016). The interaction of LLD2 with the EGF-like domain forms a hydrophobic pocket for SCR9 which is located between the LLD2s of both monomers (Figure 16A, Ma *et al.*, 2016). The crystal structure of eSRK9 further supports the domain structure defined by Naithani *et al.* (2007) but applies different domain borders (section 3.10.1). Structural modeling of eLORE, kindly provided by Dr. Rui Ma (Tsinghua University), predicts a similar domain architecture and folding of eLORE (Figure 16B, Figure 17). This is supported by multiple sequence alignments of SD-RLKs from Arabidopsis, *C. rubella*, *A. halleri*, and *A. lyrata* as well as SRK9 from *B. rapa* (Figure 18). Important residues involved in the folding of the LLDs from eSRK9 are highly conserved among SD-RLKs (Figure 17A, residues marked with red boxes). The

residues are mainly hydrophobic pointing into the protein core as shown by Ma *et al.* (2016). Trp178/Trp280 are key residues in the intramolecular folding of LLD1 and LLD2 of one eSRK9 monomer (Figure 17B). Trp169/Trp270 of eLORE are homologues to Trp178/Trp280 of eSRK9, located at the outer surface of LLD2 and are highly conserved among SD-RLKs indicating a similar mode of folding. A multiple sequence alignment of SD-RLKs shows that LLD1 is more conserved than LLD2 (Figure 18). Intriguingly, the hv regions involved in SCR9 binding lie within LLD2 of eSRK9 (Ma *et al.*, 2016). LLD2 is also crucial for homodimerization of eSRK9. Interaction of an antiparrallel β-sheet of the LLD2 of one monomer with the looped-out helix of the EGF-like domain of the other monomer forms a homodimerization interface with mainly hydrophobic interactions (Figure 16A, Ma *et al.*, 2016). Following the LLDs, the predicted EGF-like domain forms a large hydrophobic pocket and is defined by six cysteines (Figure 16A, Figure 17A). Disulfide bridges play an important role in the formation of protein structures. The disulfide bridges Cys298-Cys312, Cys314-Cys335, and Cys292-Cys304 can be found in eSRK9. Trp326 located in hvIII packs against the disulfide bond Cys298-Cys312 and Cys314-Cys335, and supports protein folding. Multiple sequence alignments of the EGF-like and PAN/APPLE domain of SD-RLKs confirm conservation of the twelve cysteine residues and the tryptophane indicating a similar mode of folding in other SD-RLKs (Figure 17A, Figure 18). According to the Uniprot database, the disulfide bonds Cys287-Cys301 and Cys303-Cys324 located in the EGF-like domain are predicted for LORE by similarity, which are homologues to the disulfide bonds Cys298-Cys312 and Cys314-Cys335 of eSRK9 (The UniProt Consortium, 2017, accessed October 10, 2018). A disulfide bridge between the residues Cys281-Cys293 of eLORE, homologues to Cys292-Cys304 of eSRK9, is not possible according to the residue orientation in the model of eLORE (Figure 17C, Cys292-Cys304 of eSRK9 are highlighted in orange). Trp315 (W315) of eLORE (equivalent to Trp326 of eSRK9) packs against the disulfide bonds Cys287-Cys301 and Cys303-Cys324, supporting a similar structure from eLORE as shown for eSRK9 (Figure 17C). The PAN/APPLE domain is characterized by a five-stranded anti-parallel β-sheet, two long loops, and an α-helix (Figure 16A and B). The loops play an important role in the formation of the monomer fold as they bind to the EGF-like domain and LLD2.

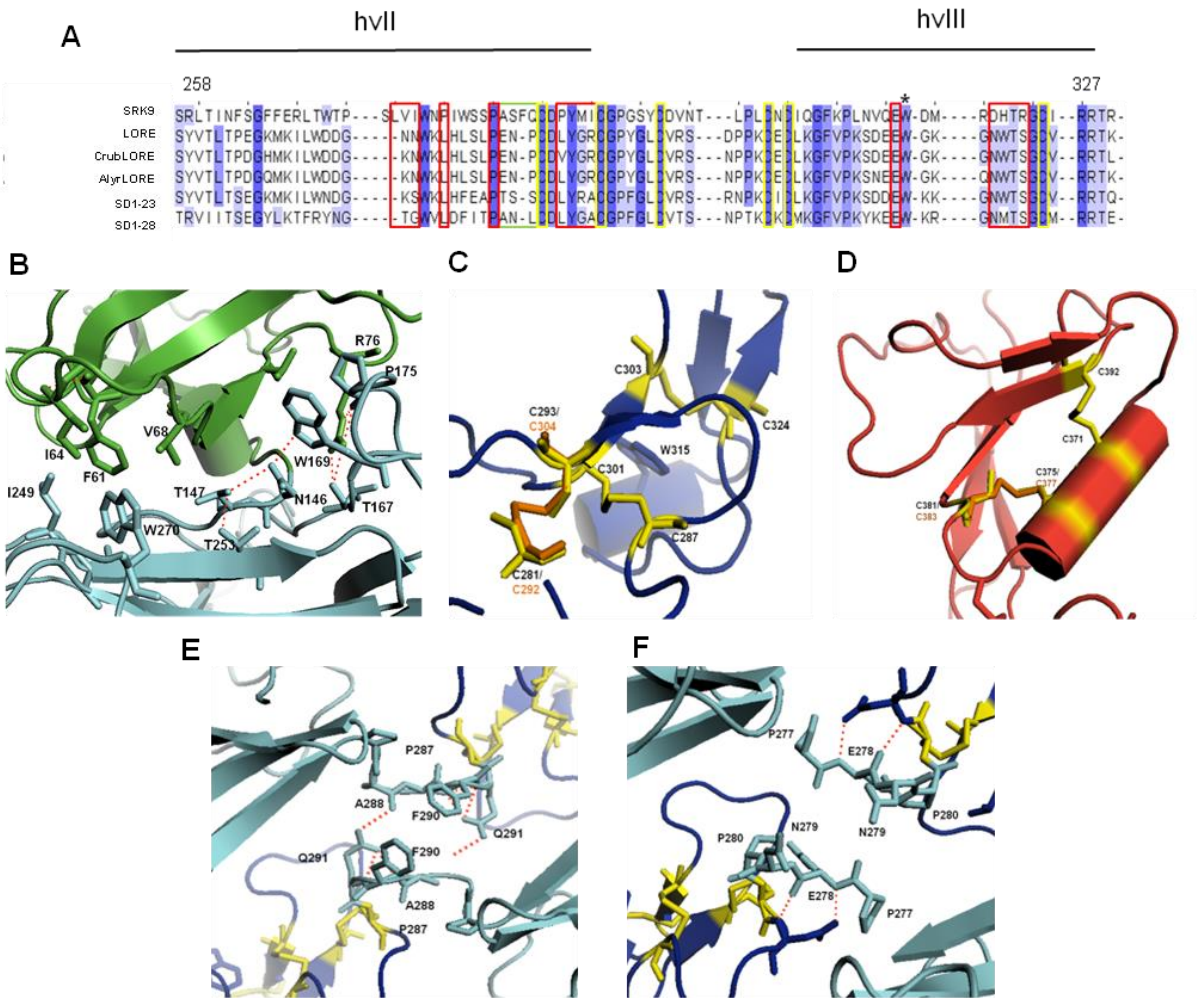

Figure 17 *In-silico* analysis of the eLORE structural model. A) Multiple sequence alignments of the hyper-variable regions hvII and hvIII of SRK9, LORE, CrubLORE, AlyrLORE, SD1-23, and SD1-28. Residues of eSRK9 involved in ligand binding are highlighted with red boxes. The dimerization interface is highlighted with a green box, and conserved cysteines are indicated by yellow boxes. Trp326 is marked with a black star. Percentage identity of the amino acids is color-coded in blue. B) Detail of residues mediating intramolecular folding of LLD1 (green) and LLD2 (turquoise) in eLORE. W169/W270 of eLORE are key residues of LLD2 interacting with LLD1. C) Disulfide bonds formed by conserved cysteines (Cys287-Cys301, Cys303-Cys324) of the EGF-like domain in eLORE are indicated in yellow. The residues Cys281 and Cys293 of eLORE are homologues to Cys292 and Cys304 of eSRK9 (shown in orange), but do not form a disulfide bond in eLORE. D) The disulfide bond Cys371-Cys392 characterizes the PAN/APPLE domain. The residues Cys375 and Cys381 do not form a disulfide bond in eLORE. Depicted in orange is the disulfide bond Cys377-Cys393 of eSRK9. E) Dimerization interface formed by LLD2 of eSRK9. F290 of both monomers stack to each other. A288 of one monomer and Q291 of the other monomer form a hydrogen bond. F) Putative dimerization interface of LLD2 of eLORE according to sequence alignments with eSRK9 and structural modelling (see also A). Hydrogen bonds are indicated by dashed lines in red (B, C, D).

eSRK9 forms three disulfide bridges in the PAN/APPLE domain. For LORE only two disulfide bridges are predicted and only one, Cys371-Cys392, is sterically possible (Figure 17D). LLD2 of SRK9 forms a dimerization interface with residues located at the surface (Figure 17D). The residues Phe290 (F290) of both eSRK9 monomers stack against each other. Gln291 (Q291) and Ala288 (A288) of the respective opposite monomer form hydrogen bonds (Figure 17E). Interestingly, the dimerization interface shown for eSRK9 is not conserved in eLORE (Figure 17A, dimerization interface sequence highlighted by a green box). The respective residues are replaced by Pro280 (P280), Glu278 (E278), and Asn277 (N277) forming a different surface (Figure 17F). Glu278 forms hydrogen bonds with Asp282 (D282). Proline is a bulky amino acid introducing a loop break, thus initiating the interface (Figure 17F). The putative dimerization interface of eLORE is highly conserved among close LORE orthologs (e.g. AlyrLORE), but not among the Arabidopsis SD-RLK family in general (Figure 17A). The domain border prediction of Naithani *et al.* (2007) locates the dimerization interface at the beginning of the EGF-like domain and not at the end of LLD2 (Supplementary Figure 11). This means that the DS-EP chimeric receptor variants generated within this study carry the respective dimerization interface of the ortho- and paralog used for the domain swaps (section 4.3). A closer look at the dimerization interfaces shows that AlyrLORE and *At*LORE possess the same amino acid sequence (Pro-Glu-Asn; Figure 17B). The dimerization interface of SD1-23 has substitutions (Pro-Thr-Ser; Figure 17B). Threonine substitutes Glu278 and serine substitutes Asn277 of LORE. Both amino acids might also participate in hydrogen bonds as formed by Glu278 and Asn277 of LORE. In the dimerization interface of SD1-28 (Pro-Ala-Asn; Figure 17A) alanine, a hydrophobic amino acid, substitutes Glu278. Alanine confers different structural characteristics to the dimerization interface as alanine is often buried inside the protein core and does not participate in hydrogen bonds. These differential structural characteristics might help to explain the results obtained with the chimeric receptor variants with SD1-28 (section 4.3, section 5).

Overall, a similar protein structure of eLORE compared to eSRK9 is very likely. However, the proposed structure of eLORE differs in the number of formed disulfide bonds and the dimerization interface sequence. Differences in the biological function of the RLKs LORE and SRK9 are resembled in the different biochemical properties of the (putative) ligands. SCR9 belongs to the group of cysteine rich peptides, and the small molecule 3-HDA is the motif for LORE immune sensing in Arabidopsis (section 3.9). SCR9 interaction with eSRK9 is mainly mediated by residues of the hv regions (hvI, hvII, and hvIII) whereas hvII carries most interaction sites (Figure 17A). These residues differ among SD-RLKs and could explain the recognition of a variety of ligands (Boggs *et al.*, 2009). Direct binding of 3-HDA to *At*LORE was investigated. 3-HDA showed only low binding affinity towards the ectodomain of LORE produced in insect cells (Kutschera *et al.*, 2019, unpublished). It is not known if other accessory proteins are required for 3-HDA-sensing mediated by *At*LORE. For this reason, possible binding sites were not investigated in the study at hand.

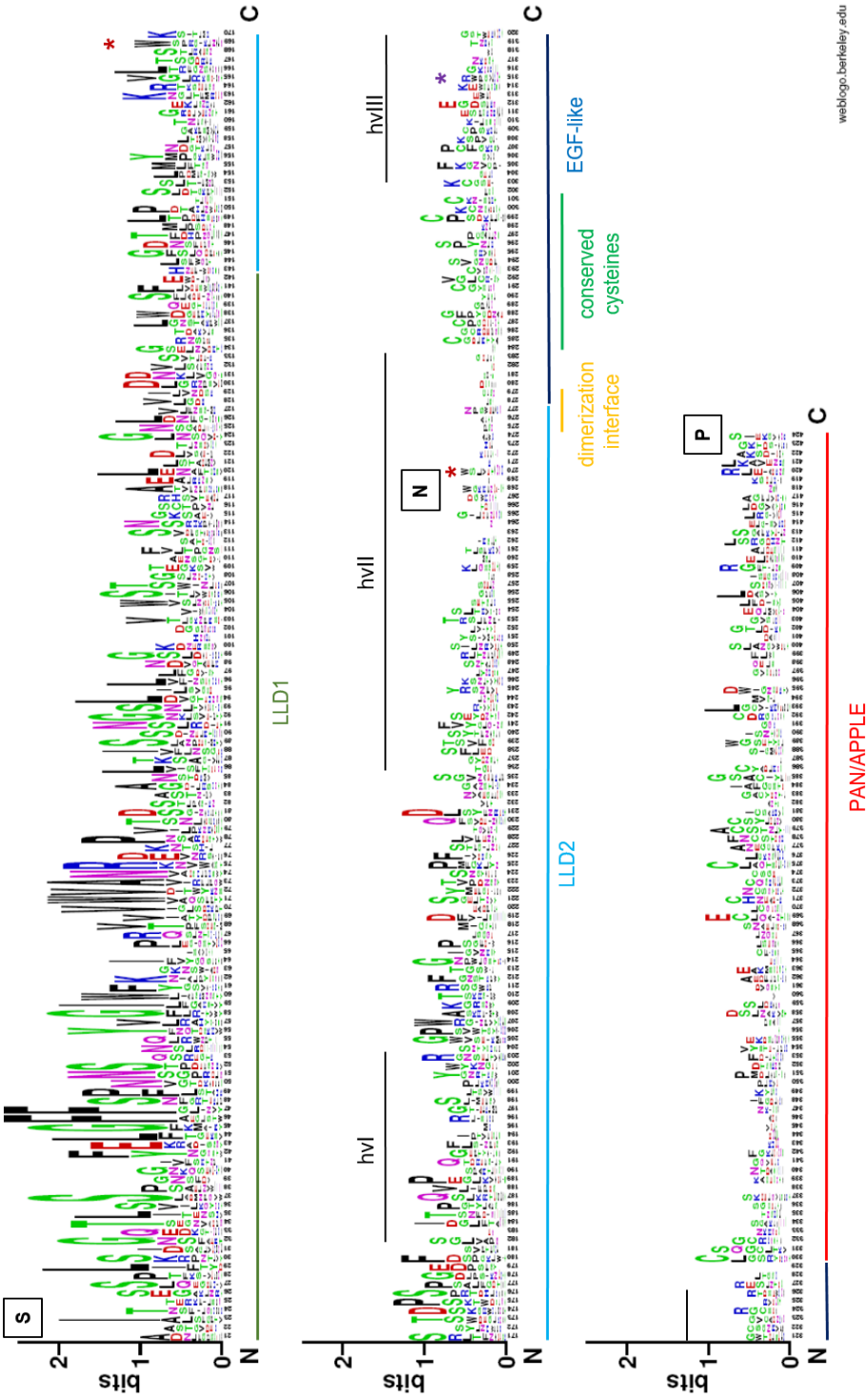

Figure 18 WebLogo of a multiple sequence alignment of the ectodomains of the SD-RLK family from Arabidopsis, CrubLORE, AlyrLORE, AhalLORE, and SRK9 from *B. rapa*. The predicted LORE domains according to Ma *et al.* (2016) are highlighted as followed lectin-like domain 1 (LLD1) in green, lectin-like domain 2 (LLD2) in turquoise, EGF-like domain in blue, and PAN/APPLE domain in red. The signal peptide sequence was left out for reasons of clarity and space. Trp169/Trp270 are marked with red asterisks, Trp315 with a purple asterisk. The hyper-variable regions hvI, hvII, and hvIII are indicated above the sequence. Residues of the dimerization interface are underlined in yellow. The region containing the conserved cysteines involved in disulfide bridges are underlined with light green. The domain swaps sites are indicated above the sequence with S, N, and P in bold (see also Supplementary Figure 11). The sequence logo was produced with the WebLogo software (Crooks *et al.*, 2004).

4.5 Investigation of phenotypes from LORE overexpression lines

Overexpression and complementation lines of LORE (OE and CL lines) were generated to gain further insights into the localization, signaling, and regulation of LORE *in planta* as well as to evaluate its role in different aspects of plant immunity in more detail.

4.5.1 Generation and phenotypic analysis of LORE overexpression lines

Stable OE and CL lines of LORE were generated by agrobacterium-mediated transformation of *lore*-1 *via* floral-dip inoculation (section 8.1.16). The coding sequence of *AtLORE* fused to the epitope tags GFP, HA, or the complete open reading frame of *AtLORE* without an epitope tag under the control of the constitutive 35S promoter as well as a pLORE, a 2 kb promoter fragment upstream of *AtLORE*, were transformed (Ranf *et al.*, 2015, section 8.1.9). The offspring was functionally analyzed with measurements of the $[Ca^{2+}]_{cyt}$ elevation in seedlings upon LPS treatment. Promising candidates with an enhanced $[Ca^{2+}]_{cyt}$ elevation compared to wild type were propagated. Stable homozygous plant lines were verified by functional analysis in the T3 generation where no insensitive seedlings were detected. OE lines for LORE without an epitope tag were established (OE lines no tag (OE-NT) OE-NT1, OE-NT2, and OE-NT3) and CL lines of LORE fused to GFP (CL-GFP1 and CL-GFP2). During the screening process it became obvious that seedlings with two distinct growth phenotypes were present in heterozygous populations of plants transformed with a LORE variant fused to one of the epitope tags GFP or HA under the control of the 35S promoter. Bigger and smaller seedlings were present in liquid MS medium (Figure 19B). When analyzed with $[Ca^{2+}]_{cyt}$ elevation measurements after LPS treatment, small seedlings showed a higher $[Ca^{2+}]_{cyt}$ elevation peak compared to bigger seedlings of the same parental line indicating that smaller seedlings reacted stronger to the application of LPS. In parallel, these plant lines were grown on soil and characterized according to their ability to accumulate ROS upon LPS elicitation. All tested plants from the OE lines showed less ROS accumulation compared to the Col-0^{Aeq} wild type. Presumably, smaller seedlings were sorted out and not chosen for further testing on soil. To circumvent this bias, seedlings were grown in liquid MS medium and tested in $[Ca^{2+}]_{cyt}$ elevation assays. Seedlings with increased LPS/3-HDA responsiveness compared to wild type were rescued. In this way, putative homozygous OE-HA lines (OE-HA1 and OE-HA2) were identified. The rescued promising and putatively homozygous OE-GFP plants were grown to induce seed production. However, these plants showed a dwarfed growth phenotype and did not produce any seeds (Figure 19A and D). Stereomicroscopic examination of flower characteristics of OE-GFP lines revealed that the stigma-anther separation was enhanced (Figure 19C). This phenomenon is described as a flower morphology to avoid self-pollination, also known as stigma exsertion (Tantikanjana *et al.*, 2009, Barrett, 2002). In comparison, flowers of OE-HA2, OE-NT3, and the wild type Col-0^{Aeq} grown under the same conditions and sown at the same time were able to pollinate the stigma. Differences in the stigma exsertion were also observed for the other OE lines (Figure 19C).

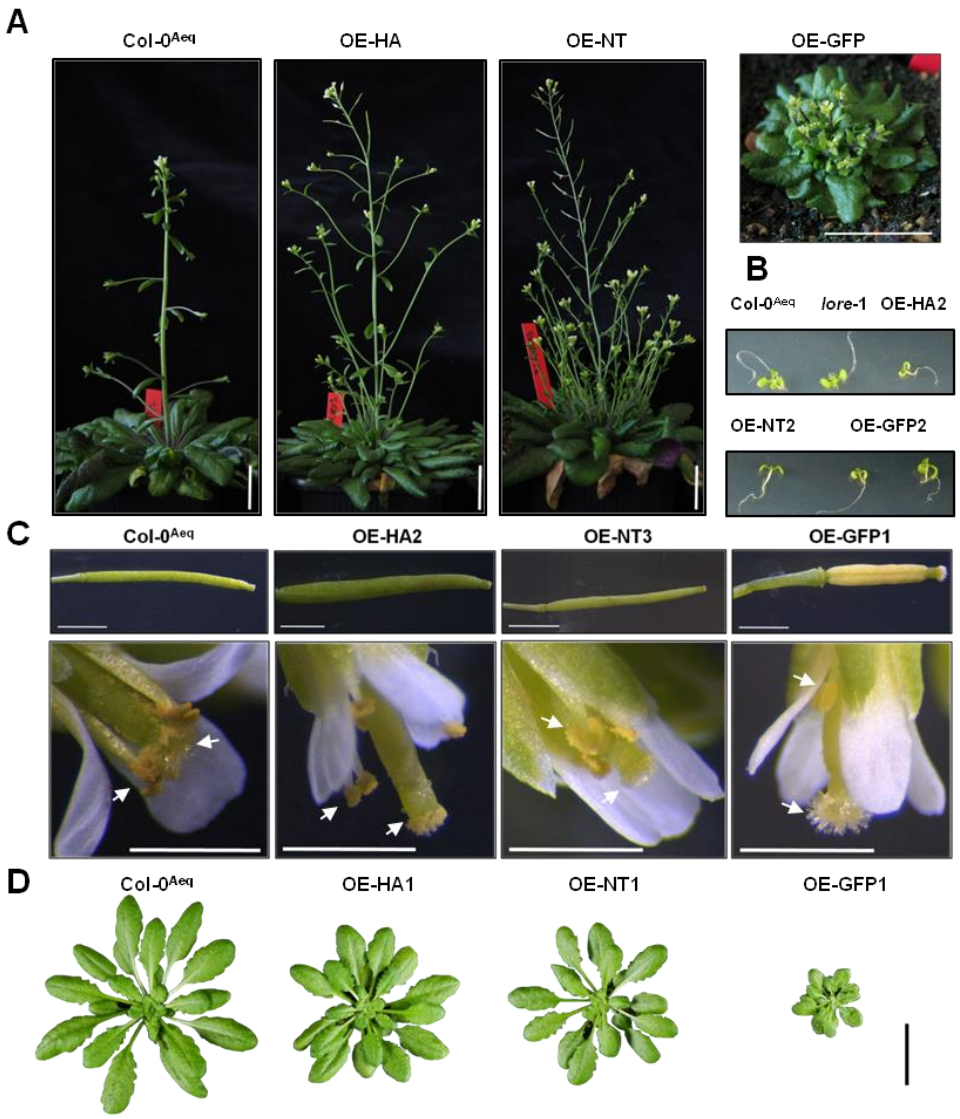

Figure 19 Growth phenotypes of LORE overexpression lines. A) Growth phenotype of 16-weeks-old OE-HA, OE-NT, and OE-GFP lines. OE lines have more floral stems. All plant lines were sown at the same time and grown under the same conditions. Scale bar 2 cm. B) Growth of seedlings (Col-0^{Aeq}, *lore*-1, OE-HA2, OE-NT2, and OE-GFP2) in liquid MS medium after 10 days. OE line seedlings are smaller compared to *lore*-1 and Col-0^{Aeq}. For OE-GFP2, heterogenous seedling growth phenotypes are observed. C) Comparison of flower characteristics and siliques of 16-weeks-old OE lines (OE-HA2, OE-NT3, and OE-GFP1) and wild type. Col-0^{Aeq} anthers pollinate the stigma (indicated by arrows). OE-HA2 anthers carry pollen. The pollen can be detected at the stigma, but anthers and stigma differ in height (indicated by arrows). Pollen is present at the pistil of OE-NT3 (indicated by arrows). Anthers carry no pollen in OE-GFP1, and the height separation of anthers and stigma is increased compared to wild type. The siliques of OE-GFP1 are shorter and do not contain seeds in comparison to the other lines. Pictures were taken with a stereomicroscope. Scale bar 2 mm. D) Growth phenotype of 8-weeks-old Col-0^{Aeq}, OE-HA1, OE-NT1, and OE-GFP1 rosettes. Rosette morphology is similar, but OE lines grow slower. Putative homozygous OE-GFP lines show a dwarfed growth phenotype. Scale bar 2 cm.

Possibly, these minor differences permitted enough pollination for sufficient propagation. The siliques produced by OE-GFP lines did not carry any seeds and were shorter compared to wild type siliques (Figure 19C). OE-HA and OE-NT lines had a delayed growth compared to wild type plants on soil. The plant growth of OE-HA and OE-NT became more similar compared to wild type over the period of growth (Figure 19A). Further, the overexpression of LORE had an enhancing effect on the quantity of floral stems in OE-HA, OE-NT, and OE-GFP lines (Figure 19A).

4.5.2 LORE-GFP expression and localization *in planta*

The OE-GFP lines were characterized in respect to LORE-GFP localization *in planta* and LORE-GFP expression. LORE-GFP localization was previously analyzed in transiently transformed *N. benthamiana* leaves showing plasma membrane localization (Ranf *et al.*, 2015). LORE-GFP under the control of the constitutive 35S promoter, as expected, was detected in the plasma membrane and in guard cells in Arabidopsis (Figure 20A, upper and middle panel). Strong GFP signal was only detected in dwarfed OE-GFP lines (Figure 20C). Interestingly, the development of stomata in OE-GFP lines seemed to be disturbed (Figure 20A, middle panel). Stomata develop by means of asymmetric cell division and are equally distributed at the leaf surface manifested by the one-cell spacing rule (Sachs, 1991). Hence, stomata are separated by at least one pavement cell. Stomatal patterning in OE-GFP followed this rule, but frequently, the cells destined to develop into a stoma were arrested in their development (Figure 20A). This was observed for two independent OE-GFP lines. Correctly developed stomata were counted once to rule out that all OE lines are disrupted in the development of stomata. All other OE lines had a comparable number of stomata per leaf surface area as *lore*-1 and the wild type Col-0^{Aeq}. Only, OE-GFP1 had approximately 50% normal developed stomata and 50% growth arrested cells (Supplementary Figure 4A). Next to OE lines, also CL lines with the coding sequence of *AtLORE* under the control of the pLORE promoter fragment were established (CL-GFP1, CL-GFP2). Here, a signal was detected at the plasma membrane of stomata. A lambda scan (490 nm–780 nm) did not provide clear evidence that the detected signal is derived from a fluorophore. The lambda scan detected an atypical GFP emission spectrum for one detected signal (Supplementary Figure 4B). Another detected signal of CL-GFP1 shows a similar emission spectrum as detected for fluorescence derived from stomata of OE-GFP1 with a clear emission maxima around 510 nm which indicates fluorescence derived from GFP (Supplementary Figure 4B). Moreover, signal bleaching in CL-GFP1 was observed while microscoping pointing into direction of GFP fluorescence. Only a weak signal was detected at the plasma membrane in CL lines. Immunoblot analysis of CL-GFP and OE-GFP lines revealed that LORE-GFP cannot be detected in total protein extracts of Arabidopsis leaves (Figure 20B and D, section 8.1.29). However, LORE-GFP was detected upon enrichment using a GFP trap. As described above, heterozygous OE-GFP lines had two different growth phenotypes. An immunoprecipitation (IP) was performed with a wild type-like and a dwarfed plant (Figure 20C and D).

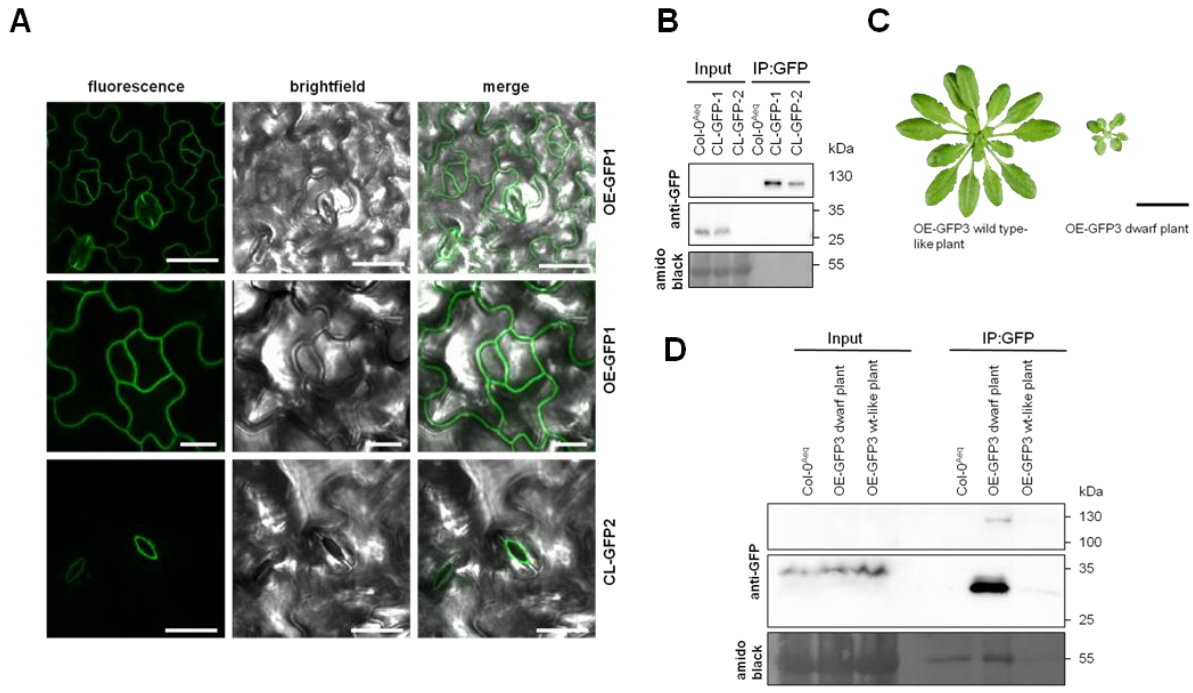

Figure 20 Localization and expression of LORE-GFP in Arabidopsis. A) LORE-GFP under the control of the 35S promoter (upper/middle panel) or the endogenous pLORE promoter (lower panel). LORE-GFP signal can be detected at the plasma membrane and stomata in OE-GFP1. OE-GFP lines display a stomata development arrest phenotype (middle panel). In CL-GFP1, the signal can be detected mainly in the plasma membrane of guard cells. Leaf discs of stable transgenic lines were imaged with confocal laser scanning microscopy. Scale bar 15 µm. B) Immunoprecipitation (IP) of LORE-GFP from 3-weeks-old seedlings from stable transgenic CL-GFP1 and CL-GFP2 grown on soil. LORE-GFP (~130 kDa) signal cannot be detected in the input, but in the immunoprecipitated fraction (IP: GFP). Unspecific bands are detected in the input fraction around the size of 30 kDa. Amido black staining shows equal protein loading. C) Picture of the two distinct growth morphologies (wild type-like and dwarfed) of 8-weeks-old OE-GFP3 plants used for IP experiments in D. Scale bar 2 cm. D) IP of LORE-GFP of the two distinct growth morphologies of the stable overexpression line OE-GFP3 (see C). LORE-GFP can be detected in the IP of the dwarfed plant. Free GFP is detected at around 30 kDa in the immunoprecipitated fraction. Unspecific bands are detected in the input samples. Amido black staining shows equal protein loading. SuperSignal® West Femto Maximum Sensitivity Substrate (Pierce, Rockford, USA) was used for detection (B, D).

LORE-GFP was detected in the immunoprecipitated fraction of the dwarfed, but not the wild type-like plant. One dwarfed plant grown on soil and an equal amount of plant material from the wild type-like plant were used for the IP. Interestingly, also free GFP (~30 kDa) was detected on the immunoblot indicating cleavage of the GFP epitope tag from LORE (Figure 20D). Free GFP was not detected in the IP of the CL-GFP lines. Nevertheless, unspecific bands approximately the size of GFP were detected in the input fractions of CL-GFP, OE-GFP, but also Col-0^{Aeq} plants. Potentially, the used

GFP antibody bound unspecifically to components of the total protein extracts which was also seen for total protein extracts from *N. benthamiana* (section 4.2.4, Figure 11).

4.5.3 LORE-HA expression and regulation

As a consequence of the problems occurring with the GFP epitope tag, only OE-HA and OE-NT lines were characterized in more detail. Different from LORE-GFP, LORE-HA was detected in total protein extracts from leaves of OE-HA1, OE-HA2, and OE-HA3 (Figure 21A). OE-HA3 is a heterozygous descendant. The intensity of the detected signal using the anti-HA-HRP antibody corresponds to the protein expression level of LORE-HA in the stable plant lines. No signal was detected in wild type or *lore*-1 protein extracts. All experiments presented from here on were performed with two independent LORE-HA OE lines, OE-HA1 and OE-HA2, as well as two independent LORE-NT OE lines, OE-NT1 and OE-NT2. For reasons of clarity, only the results of OE-HA1 and OE-NT1 are shown in this section. The results of OE-HA2 and OE-NT2 had always the same tendency, and are depicted in the supplements.

Col-0^{Aeq} (black), *lore*-1 (red), OE-HA1 (blue), and OE-NT1(green) seedlings were analyzed regarding the expression level of *AtLORE* after treatment with MeOH or 3-HDA for 4 h (Figure 21B, Supplementary Figure 5A). The expression level of *AtLORE* was greatly increased in OE lines treated with MeOH compared to wild type treated with MeOH. When treated with 3-HDA the transcript level in OE lines did not change, showing the strong constitutive *AtLORE* expression under the control of the 35S promoter. In Col-0^{Aeq}, induction of *AtLORE* increased upon treatment with 3-HDA, and in *lore*-1 no changes of the *AtLORE* level were detected due to the treatment. The influence of 3-HDA application on the LORE-HA protein level was also examined (Figure 21C, Supplementary Figure 5B). As described in section 3.5, immune signaling attenuation can be achieved by the internalization of PRRs followed by protein degradation (Robatzek *et al.*, 2006). *At*FLS2 degradation in response to flg22 can be detected on immunoblots in a time-dependent manner (Smith *et al.*, 2014). Seedlings of OE-HA1 were treated with MeOH or 3-HDA for 0, 2, 5, 10, 20, and 60 min. Total protein was extracted, and LORE-HA abundance was analyzed by immunoblot. Treatment of 3-HDA had no obvious influence on the LORE-HA level as LORE-HA was detected in all samples to a comparable level. The constitutive high LORE-HA level possibly disguised putative degradation of LORE-HA which did not become evident on immunoblots. Degradation of LORE upon 3-HDA treatment due to internalization might be detectable if the endogenous *At*LORE abundance in wild type or CL lines will be assessed.

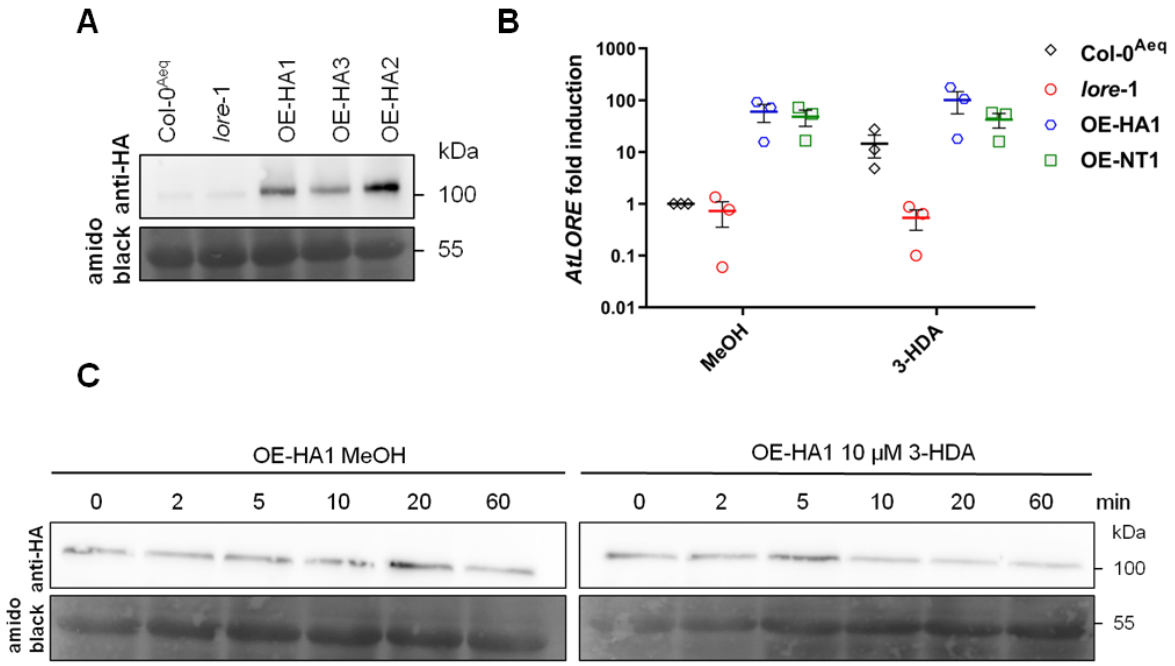

Figure 21 LORE-HA expression and *AtLORE* regulation in response to 3-HDA. A) Immunoblot analysis of LORE-HA expression in OE-HA lines. LORE-HA can be detected around 100 kDa in 50 µg of total protein extracts isolated from 30 leaf discs of mature leaves of OE-HA1, OE-HA2, and OE-HA3. Amido black staining shows equal protein loading. B) Relative quantitative expression analysis of *AtLORE* in Col-0^{Aeq}, *lore*-1, OE-HA1, and OE-NT1 seedlings treated for 4 h with MeOH or 5 µM 3-HDA. Expression levels of *AtLORE* were normalized to *AtUBQ5*. Fold change induction was calculated relatively to Col-0^{Aeq} treated with MeOH. Single data are presented in a dot blot with the mean ± SEM of three biological replicates. C) Immunoblot analysis of OE-HA1 10-days-old seedlings treated with MeOH or 10 µM 3-HDA for 0, 2, 5, 10, 20, or 60 min. 50 µg of total protein extracts were loaded. LORE-HA can be detected around 100 kDa. Amido black staining shows equal protein loading. SuperSignal® West Femto Maximum Sensitivity Substrate (Pierce, Rockford, USA) was used for detection (A, C).

In summary, LORE overexpression has an influence on the growth of Arabidopsis. This effect is most evident in the severe dwarfed growth phenotype of putative homozygous OE-GFP plants. Here, no pollen is produced and the anther-stigma separation is increased resulting in sterile plants. Moreover, stomatal patterning seems to be disrupted in OE-GFP lines. Interestingly, this is not observed for OE-HA or OE-NT lines. However, also OE-HA and OE-NT lines are delayed in their growth. OE lines show a high *AtLORE* expression which is not induced upon 3-HDA treatment. This is in line with the use of the strong and constitutive 35S promoter. *AtLORE* expression, on the other hand, is inducible by 3-HDA treatment in wild type plants. The overexpression of LORE-GFP and LORE-HA was also analyzed on the protein level. Intriguingly, LORE-GFP cannot be detected in total protein extracts whereas LORE-HA can be detected. However, free GFP as well as LORE-GFP are detected in putative

homozygous OE-GFP plants upon enrichment. The effect of 3-HDA on LORE-HA degradation was also analyzed. LORE-HA degradation was not detected which could be due to the high overexpression of LORE.

4.6 Influence of an elevated LORE dosage on immune responses in Arabidopsis

The general influence of elevated LORE levels on immunity in Arabidopsis was investigated by analysis of typical PTI responses presented in section 3.3.1 upon treatment with 3-HDA. These immune outputs help Arabidopsis to ward off invading pathogens. The aim of these experiments was to characterize and define the role of LORE in pre- and post-invasive immunity and gain knowledge about the regulation of LORE. Moreover, the effect of elevated LORE levels onto resistance towards infection with *Pto* DC3000 was investigated.

4.6.1 Analysis of the influence of 3-HDA on signaling and growth in overexpression lines

As described in section 3.3.1, changes in the cytosolic Ca^{2+} level are an essential defense response. Therefore, $[Ca^{2+}]_{cyt}$ elevation in response to treatment with 3-HDA was measured in seedlings of the OE lines, *lore*-1, and Col-0^{Aeq} to investigate the effect of elevated LORE levels (Figure 22A, Supplementary Figure 6A). All OE lines (OE-HA1 (blue), OE-NT1 (green), and OE-GFP1 (orange)) showed rapid on-set and stronger $[Ca^{2+}]_{cyt}$ elevation compared to wild type (black). *lore*-1 (red) did not induce $[Ca^{2+}]_{cyt}$ elevation in response to 3-HDA (Figure 22A). Interestingly, differences can also be observed in the kinetic of the response. The maximal response intensity was reached earlier by OE lines than by the wild type (Figure 22B). OE-NT1 reacted strongest to elicitation with 3-HDA. In contrast, OE-HA1 and OE-GFP1 clustered together and reacted stronger than Col-0^{Aeq}, but less than OE-NT1. It should be noted that only small, putative homozygous OE-GFP1 seedlings were used for the measurement. Furthermore, the residual $[Ca^{2+}]_{cyt}$ level remained higher in OE lines after the initial decline of the response as highlighted in the second detail section (Figure 22C). Apparently, the $[Ca^{2+}]_{cyt}$ level of OE-HA1 and OE-GFP1 did not decline completely. The cytosolic $[Ca^{2+}]_{cyt}$ level of OE-NT1, on the other hand, showed reduction after approximately 40 min, but leveled out later than the cytosolic calcium level of Col-0^{Aeq} which reduces after 30 min. In addition, $[Ca^{2+}]_{cyt}$ elevation in response to the treatment with *Pa* H4 LPS of CL-GFP1 (brown) and CL-GFP2 (turquoise) was investigated (Figure 22D). CL-GFP1 and CL-GFP2 did not fully complement the $[Ca^{2+}]_{cyt}$ elevation to the wild type level (black). Here, the response was analyzed over a period of 30 min. Therefore, differences in the signal attenuation are not detected.

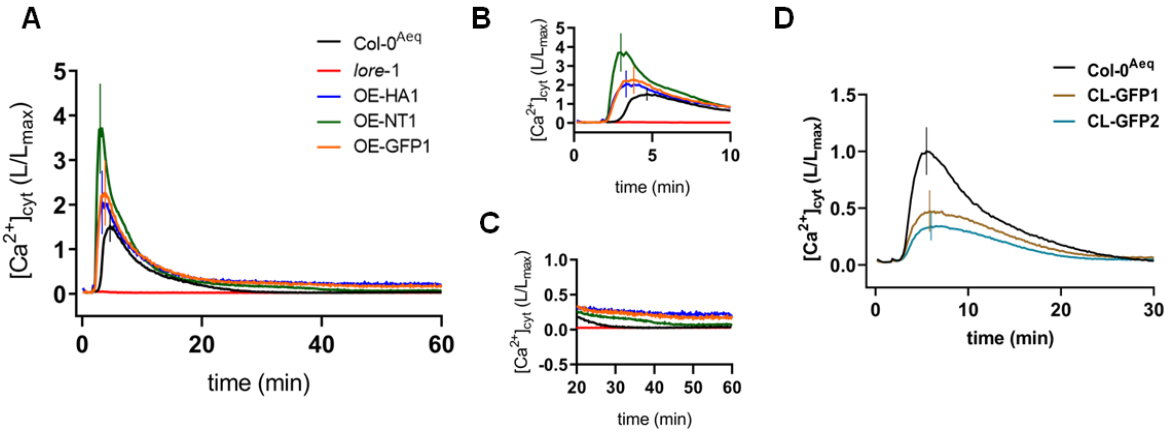

Figure 22 LORE overexpression lines show an enhanced $[Ca^{2+}]_{cyt}$ elevation in response to 3-HDA compared to wild type. A) $[Ca^{2+}]_{cyt}$ elevation level of Col-0^{Aeq} (n = 12), *lore*-1 (n = 12), OE-HA1 (n = 24), OE-GFP1 (n = 24), and OE-NT1 (n = 24) in response to 1 µM 3-HDA measured in 10-days-old seedlings for 60 min. B) The image section of A depicts the first 10 min in detail. C) The image section of A depicts the last 40 min in detail. Depicted is the mean ± SD at the maximum of one experiment (A, B). Measurements were repeated four times with similar results (A, B, C). D) $[Ca^{2+}]_{cyt}$ elevation level of Col-0^{Aeq}, CL-GFP1, and CL-GFP2 in response to 10 µg/mL *Pa* H4 LPS measured in 10-days-old seedlings for 30 min. Depicted is the mean ± SD (each n = 24) at the maximum of one experiment. Measurements were repeated two times with similar results.

Immune responses consume energy and therefore, plants react with growth arrest to the constant presence of a MAMP (section 3.5). Seedling growth inhibition of Col-0^{Aeq} was not observed after long-term exposure to LPS (personal communication Dr. Ranf, TU München). However, already during the screening process growth phenotypes of the OE lines were observed in a state lacking a pathogen challenge (section 4.5.1). Therefore, the influence of 3-HDA on plant growth was analyzed. Surface-sterilized seeds of OE lines, Col-0^{Aeq}, and *lore*-1 were transferred to ATS medium supplemented with MeOH or 3-HDA (section 8.1.15, section 8.1.25). After 8 days, pictures were taken and the primary root length of the seedlings was measured (Figure 23A and B, Supplementary Figure 6B and C).

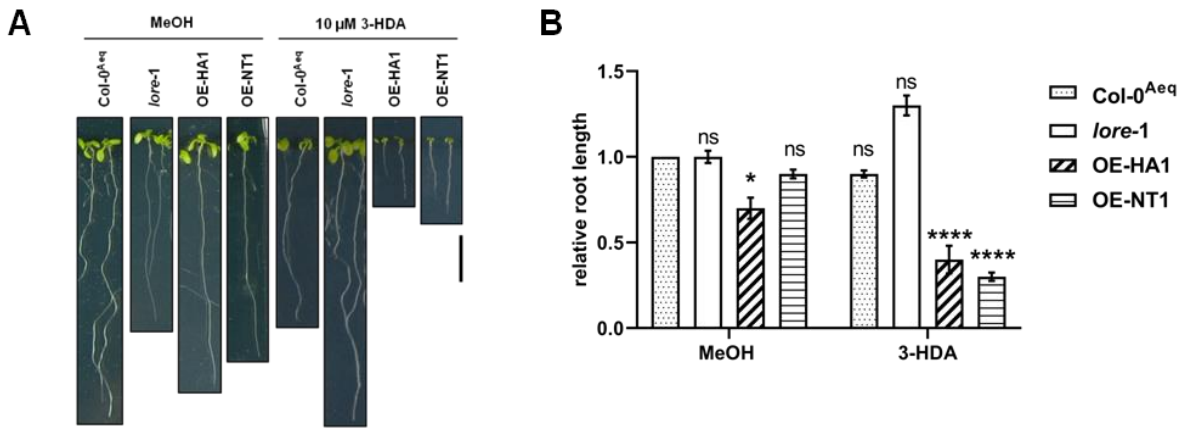

Figure 23 LORE overexpression lines react with growth inhibition in response to 3-HDA. Col-0^{Aeq}, *lore*-1, OE-HA1, and OE-NT1 seedlings grown on ATS medium supplemented with 10 µM 3-HDA or MeOH and grown for 8 days under long day conditions in a vertical position. A) Picture of single representative seedlings. Scale bar 2 cm. B) Analysis of root growth inhibition. Depicted is the relative root length compared to Col-0^{Aeq} treated with MeOH (mean ± SEM, pooled data of two independent experiments with each n ≥ 22 seedlings of each genotype per treatment). Data were analyzed with a two-way ANOVA and Dunnett's multiple comparison post test in comparison to Col-0^{Aeq} treated with MeOH. Asterisks indicate significant differences (* $P < 0.05$, **** $P < 0.0001$).

When grown on ATS medium supplemented with MeOH, OE-HA1 had shorter roots compared to wild type. A significant difference between OE-NT1 and *lore*-1 compared to wild type was not detected. When the OE lines OE-HA1 and OE-NT1 grew on 3-HDA containing ATS medium, both OE lines showed a significant reduction in root length compared to wild type grown on ATS medium supplemented with MeOH. The OE lines reacted with an obvious growth arrest to the presence of 3-HDA and the fresh weight was too light to be scaled. After 10 days, 3-HDA presence was lethal for overexpression plants. The cotyledons of OE line seedlings turned yellow to brown and withered (pictures not shown). This shows an increased sensitivity of the OE lines to treatment with 3-HDA. A growth arrest of Col-0^{Aeq} or *lore*-1 in response to 3-HDA was not observed.

To sum up, seedlings of OE-HA, OE-GFP, and OE-NT react with elevated $[Ca^{2+}]_{cyt}$ levels in response to 3-HDA treatment compared to wild type. Differences are observed in the initiation as well as in the attenuation of the signal. The decline of the response in OE lines is slower. The $[Ca^{2+}]_{cyt}$ elevation signature of the OE lines with a C-terminal epitope tag differs to OE-NT. OE-HA and OE-GFP possess a lower $[Ca^{2+}]_{cyt}$ elevation compared to OE-NT. CL-GFP have reduced $[Ca^{2+}]_{cyt}$ elevation compared to wild type. This data suggests that a C-terminal epitope tag hinders the full signal activation, but also complete signal attenuation. The growth of Col-0^{Aeq} on media supplemented with LPS did not result in seedling growth inhibition. However, growth of OE lines on media supplemented with 3-HDA lead to a severe growth arrest phenotype which was not observed in wild type and *lore*-1.

4.6.2 Investigation of the accumulation of ROS in response to 3-HDA in LORE overexpression lines

The generation of ROS is another early PTI response and was investigated with respect to the effect of an elevated LORE dosage (section 3.3.1). ROS production of Col-0^{Aeq}, *lore*-1, OE-HA, OE-NT, and OE-GFP in response to 3-HDA was analyzed in leaf discs of 6-weeks-old plants (Figure 24A and B, Supplementary Figure 7A). *lore*-1 (red) did not react with the accumulation of ROS in response to 3-HDA. OE-NT1 (green) generated more ROS compared to wild type (black), but also to OE-HA1 (blue) and OE-GFP1 (orange). The signature of the ROS accumulation from OE-NT1 was similar to the wild type reaction which is characterized by a peak around 30 min after treatment with 3-HDA. OE-HA1 showed also increased ROS production compared to wild type. Interestingly, the ROS kinetic of OE-HA1 differs compared to OE-NT1 and wild type. The ROS peak of OE-HA1 around 30 min upon elicitation was elongated compared to Col-0^{Aeq}. Intriguingly, OE-HA1 had a strong and prolonged second ROS burst lasting up to 6 h. The second burst was also present in wild type and OE-NT1, but not as prominent as in OE-HA1. OE-GFP1 displayed a biphasic ROS burst as OE-HA1, but only if leaf discs of putative homozygous OE-GFP plants were used for the ROS measurements (Figure 24B). Apparently, the second ROS burst is enhanced in OE lines of LORE with a C-terminal epitope tag. To rule out that this phenotype is caused by a combination of effects from the C-terminal epitope tag and the strong overexpression of LORE, also CL lines with a C-terminal epitope tag were tested in ROS measurements. Therefore, the accumulation of ROS in CL-GFP (CL-GFP1; brown) and CL-NT (CL-F12; purple, section 8.1.14) in comparison with Col-0^{Aeq} (black), *lore*-1 (red), OE-HA1 (blue), and OE-NT1 (green) upon treatment with 3-HDA were investigated (Figure 24C). In general, CL-GFP1 did not fully complement *lore*-1 to a wild type-like level in ROS which was already observed in $[Ca^{2+}]_{cyt}$ elevation measurements (Figure 24D, Figure 22D). However, also CL-GFP1 lines displayed the biphasic ROS consisting of an elongated first and stronger second burst, but not as strong as OE-HA1. The second ROS burst in Col-0^{Aeq} and CL-F12 emerged later compared to OE-HA1 and CL-GFP1.

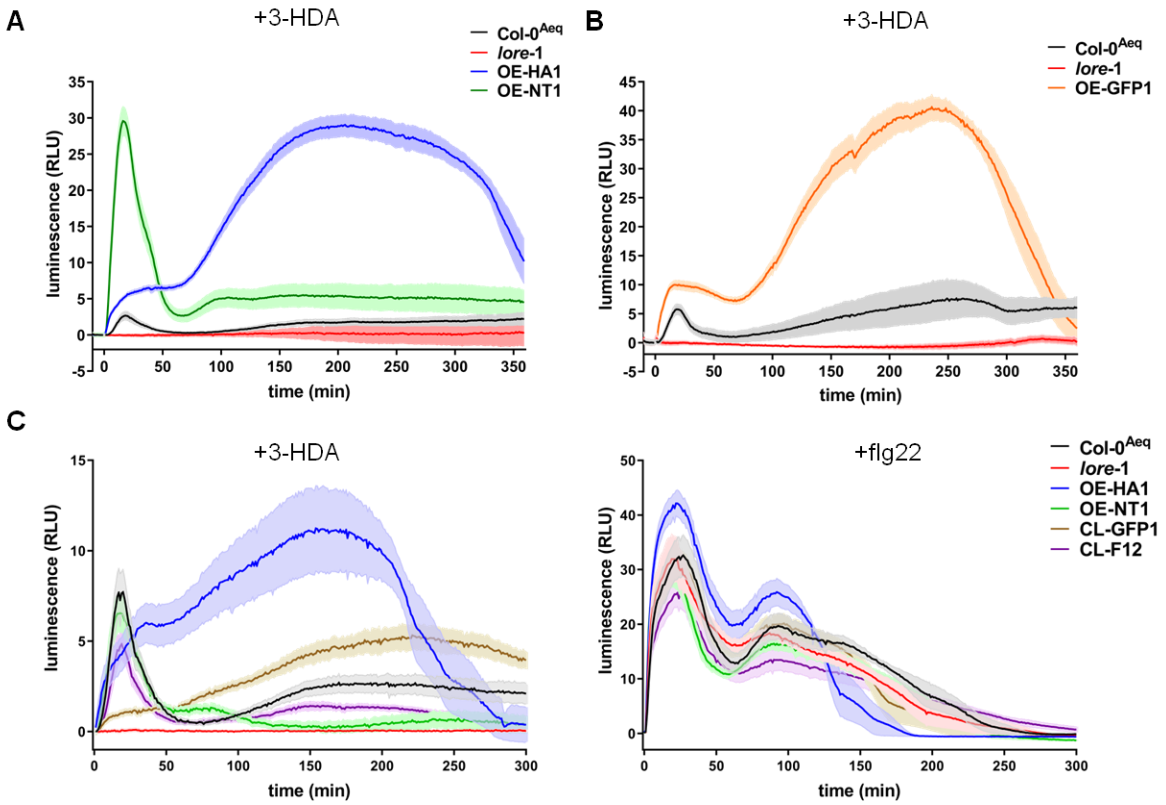

Figure 24 LORE overexpression lines show enhanced ROS accumulation in response to 3-HDA compared to wild type. The accumulation of ROS was measured in leaf discs of 6-weeks-old plants in response to 1 µM 3-HDA. Data represent the mean ± SEM in RLU. All measurements were repeated at least three times with similar results. A) ROS accumulation of Col-0^{Aeq}, *lore*-1, OE-HA1, and OE-NT1 (each n = 16). B) ROS accumulation of Col-0^{Aeq}, *lore*-1, and OE-GFP1 (dwarf growth phenotype) (each n = 16). C) ROS accumulation of Col-0^{Aeq}, *lore*-1, OE-HA1, OE-NT1, CL-GFP1, and the CL line without tag CL-F12 (each n = 8) in response to 1 µM 3-HDA (left) or 100 nM flg22 (right).

Similar to the higher residual cytosolic calcium level described in section 4.6.1, also the occurrence of the second ROS burst seems to correlate with the presence of a C-terminal epitope tag. This raises the question if the second ROS burst is specific to the activation of LORE and thus elicitation with 3-HDA or if also other immunogenic molecules such as flg22 or chitin cause a second oxidative burst. Therefore, measurements of the ROS accumulation in response to chitin and flg22 were performed (Figure 24C, Figure 26A and B). The second ROS burst in OE-HA1 (blue) was specific to the treatment with 3-HDA. Application of flg22 or chitin did not result in a similar ROS signature which was supported by measurements of the generation of ROS of CL-GFP1 upon flg22 treatment (Figure 24C). However, the ROS burst upon treatment with flg22 showed a second peak in all tested lines which differed in its kinetic to the one observed in OE-HA upon 3-HDA treatment. The first peak was comparable in its intensity to the wild type response in all tested lines.

4.6.3 Investigation of the origin of the produced ROS in overexpression lines in response to 3-HDA

The measurements of the accumulation of ROS in response to 3-HDA were repeated various times. Interestingly, the second ROS burst was always measurable and stronger compared to the first burst of OE-HA, but the duration varied from 3 to 6 h (Figure 24A, Figure 26A). Therefore, concerns whether the second burst is actually accumulation of ROS or due to other modifications in the leaf disc affecting the experimental setup (e.g. pH-changes) arose.

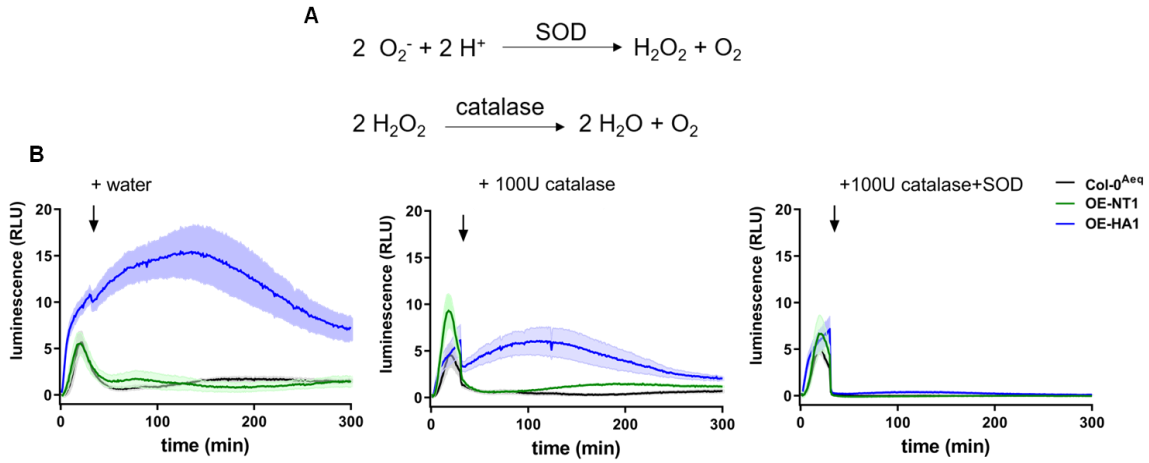

Figure 25 The application of superoxide dismutase and catalase diminish the ROS burst in overexpression lines and wild type. A) Chemical equation of the superoxide conversion. *At*RBOHD produces superoxide anions. Superoxide dismutase (SOD) converts superoxide anions to hydrogen peroxide which is more stable. Catalase functions as a scavenging enzyme and converts hydrogen peroxide to water and oxygen (Lamb *et al.*, 1997). B) ROS accumulation was measured in leaf discs of 8-weeks-old plants of Col-0^{Aeq}, OE-HA1, and OE-NT1 in response to 1 µM 3-HDA. After 30 min 100 U catalase, 100 U catalase with 100 U superoxide dismutase (SOD), or water as control were added. Data represent the mean ± SEM (each n = 8) in RLU. The experiment was repeated three times with similar results.

ROS accumulation is measured in a luminol-based system. Oxidized luminol emits chemiluminescence and the oxidation is catalyzed by the horseradish peroxidase by consumption of ROS (Zielonka *et al.*, 2013). To proof that the second burst is caused by ROS, catalase or catalase in combination with superoxide dismutase (SOD) were added to the reaction. SOD catalyzes the reaction of superoxide to hydrogen peroxide. Catalase in turn catalyzes the reaction of hydrogen peroxide to water and oxygen (Figure 25A, Lamb *et al.*, 1997). That is why the second luminescence elevation should be diminished upon treatment with SOD and catalase if hydrogen peroxide and superoxide are the causing reagents. The accumulation of ROS was induced in OE-HA1 (blue), OE-NT1 (green), and Col-0^{Aeq} (black) by the application of 3-HDA. 30 min later, water, catalase or catalase in combination

with SOD were added to the measurement (Figure 25B, Supplementary Figure 7B). Addition of catalase led to a strong reduction of the ROS burst. However, only the combined application of catalase and SOD fully eliminated the second burst. This finding showed that the second burst is caused by ROS. Another conclusion can be drawn from this experiment. Catalase and SOD were exogenously applied resulting in the diminished ROS burst. Therefore, the produced ROS upon 3-HDA treatment was apoplastic.

4.6.4 Identification of mutant plants with a biphasic ROS burst in response to 3-HDA

Enhanced accumulation of ROS in response to a MAMP such as flg22 was reported previously. The mutant *pub22/23/24* was shown to generate more ROS in response to flg22 as compared to wild type plants (Trujillo *et al.*, 2008). The treatment of *pub22/23/24* with *Pa* H4 LPS resulted also in an increased ROS accumulation (unpublished). Additionally, the ROS kinetic of *pub22/23/24* was elongated compared to wild type plants (Trujillo *et al.*, 2008). *At*PUB22/23/24 are ubiquitin E3 ligases and involved in immune signal attenuation (section 3.5). Typically, ROS is measured for 60 min, a time frame which is not long enough to detect the biphasic burst in OE-HA lines in response to 3-HDA. For this reason, the generation of ROS by *pub22/23/24* (orange) in comparison to OE-HA (blue), OE-NT (green), *lore*-1 (red), and wild type (black and brown) was tested upon treatment with 3-HDA, flg22, and chitin for a longer period of time (Figure 26). Col-0 is the appropriate wild type control for *pub22/23/24* and was therefore tested additionally to Col-0^{Aeq} (section 8.1.14). The *pub22/23/24* mutant showed rapid and enhanced ROS accumulation in response to all three tested elicitors (Figure 26A and B). In case of 3-HDA, the first ROS burst was clearly stronger compared to Col-0 as well as Col-0^{Aeq}, but comparable to OE-NT1. Intriguingly, the second ROS burst was present in *pub22/23/24* when treated with 3-HDA, but not when treated with other elicitors such as flg22 and chitin (Figure 26A and B). The signature of the biphasic ROS burst of *pub22/23/24* in response to 3-HDA was different compared to OE-HA1. The mutant *pub22/23/24* exhibited an overall shorter ROS burst and the first and second ROS burst were comparable in their amplitude. In contrast, the second ROS burst of OE-HA1 was always stronger than the first ROS burst. Interestingly, the ROS kinetic of *pub22/23/24* in response to 3-HDA, but also flg22 was different in the amplitude and duration in independent experiments. In some measurements, the ROS kinetic of *pub22/23/24* was highly similar to the ROS kinetic seen for OE-HA plants (Supplementary Figure 7B). In other measurements, the ROS signature differed more compared to OE-HA (Figure 26A and B). The observed variations might be caused by differences in the plant age or minimal changes of the growth conditions. The *pub22/23/24* mutant reacts sensitive to watering, and hyperhydration can result in the loss of the ROS phenotype in response to flg22 (personal communication Dr. M. Trujillo, University of Freiburg). The

source of the biphasic ROS burst was also examined for *pub22/23/24* by the addition of catalase and SOD. The second ROS burst was shown to be caused by apoplastic ROS (Supplementary Figure 7B).

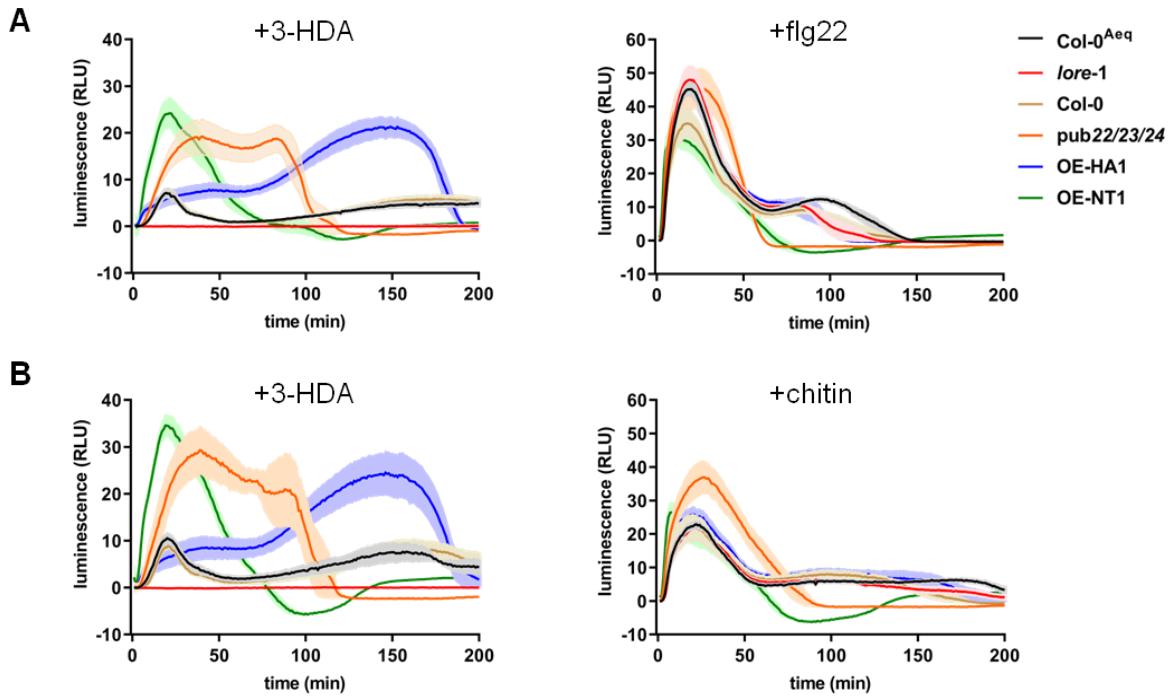

Figure 26 The mutant *pub22/23/24* has an enhanced second ROS burst in response to 3-HDA. Measurement of the ROS accumulation in leaf discs from 8-weeks-old plants of Col-0^{Aeq}, *lore*-1, OE-HA1, OE-NT1, Col-0, and *pub22/23/24*. Depicted is the mean ± SEM in RLU. All measurements were repeated at least three times. A) ROS accumulation in response to 1 µM 3-HDA (n = 8; left) or 100 nM flg22 (n = 8; right). B) ROS accumulation in response to 1 µM 3-HDA (n = 8; left) or 50 µg/mL chitin (n = 8; right).

Preliminary data identified a second mutant having a similar ROS kinetic as OE-HA and *pub22/23/24*. *At*PUB22 is phosphorylated by *At*MPK3, in this way stabilized and able to ubiquitinate other signaling components (Furlan *et al.*, 2017, section 3.5). ROS measurements of *mpk3-1* were performed, and the first and second ROS burst were detected, but again with a modified signature compared to OE-HA1 and *pub22/23/24* (Supplementary Figure 7C). The first ROS burst of *mpk3-1* was similar to the ROS burst generated by OE-NT1. It was not elongated as observed for the first peak from OE-HA. The first ROS burst of *mpk3-1* declined and then a second ROS burst comparable to the second burst of OE-HA emerged (Supplementary Figure 7C).

Altogether, the presented results show that the C-terminal epitope tag has an influence on the ROS kinetic of OE lines compared to wild type and OE-NT. Moreover, the second oxidative burst is specific to the treatment with 3-HDA. It is not a phenotype observed only in LORE OE lines, but also in CL lines carrying a C-terminal GFP epitope tag. The produced ROS is apoplastic and can be diminished by the application of SOD and catalase. The identification of two other Arabidopsis mutant plants,

with a similar ROS phenotype as OE-HA lines upon 3-HDA treatment, supports the biological relevance of this finding. As described in section 3.5, *At*PUB22/23/24 are involved in the immune signal attenuation. Hence, the C-terminal epitope tag might interfere with LORE regulation and retard signal attenuation.

4.6.5 Analysis of further immune outputs in overexpression lines

Another early response in plant immunity is the activation of MAPK cascades which regulate other downstream processes. Recognition of bacterial MAMPs converges in the activation of the partially redundant *At*MPK3 and *At*MPK6 (Asai *et al.*, 2002, section 3.3). LPS treatment was also shown to activate *At*MPK3 and *At*MPK6 in Arabidopsis (Ranf *et al.*, 2015). Col-0^{Aeq}, *lore*-1, OE-HA1, and OE-NT1 seedlings were treated with 3-HDA for 0, 2, 3, 10, 20, and 60 min to investigate the activation of MAPKs (Figure 27A, Supplementary Figure 8A). 3-HDA activated *At*MPK3 and *At*MPK6 in wild type, but not *lore*-1. In OE-NT1 MAPKs showed a rapid on-set after 2 min whereas in wild type and OE-HA1, MAPKs showed activation after 4 min. In wild type signal attenuation was observed around 20 min. In OE-NT1 and OE-HA1, on the other hand, MAPKs were still activated after 20 min and showed weak activation after 60 min. The MAPK activation was also elucidated in Col-0 and *pub22/23/24* in response to flg22 and *Pa* H4 LPS/3-HDA treatment (Figure 27B). In Col-0 strong activation of *At*MPK3 and *At*MPK6 was detected up to 30 min and weaker activation was detected up to 120 min upon flg22 treatment. The *pub22/23/24* mutant showed activation of *At*MPK3 and *At*MPK6 up to 60 min after flg22 treatment which was weakened and detected up to 120 min upon flg22 treatment. In response to *Pa* H4 LPS/3-HDA, *At*MPK3 and *At*MPK6 were activated after 10 min and showed weak activation after 30 min in wild type. In *pub22/23/24*, *At*MPK3 and *At*MPK6 were longer activated in response to *Pa* H4 LPS/3-HDA as compared to Col-0.

*At*MPK3 and *At*MPK6 play an important role in the manifestation of immune responses in Arabidopsis as they take over crucial regulatory tasks (Asai *et al.*, 2002). The production of the phytohormone ET is modulated by *At*MPK3 and *At*MPK6 downstream actions (section 3.3.1). ET production was measured in response to 3-HDA, nlp20, or MeOH after 4 h incubation. The 20 amino acid containing peptide nlp20 from NLP1 (NECROSIS AND ETHYLENE-INDUCING PEPTIDE 1), a protein produced by bacteria and fungi, was identified as an immunogenic epitope inducing stronger ET production in *Brassica* compared to flg22 (Böhm *et al.*, 2014). Thus, *Fo*nlp20, a peptide derived from *Fusarium oxysporum*, was used as a positive control for the ET production measurements. *Fo*nlp20 strongly induced ET formation in all tested plant lines (Col-0^{Aeq}, *lore*-1, OE-HA, OE-NT) (Figure 27C, Supplementary Figure 8B). However, the ET response showed high variability in individual leaf discs of one experiment. The measured ET contents varied between 15 and 22 pmol/mL of leaf discs in one experiment. The variation increased within independent experiments using individual plants. 3-HDA activated ET production in wild type only on a low level and hardly distinguishable from the background (5 pmol/mL, background level 2 pmol/mL). However, OE-HA1 and OE-NT1 reacted

with a stronger ET response (8 to 7 pmol/mL) compared to wild type. The response to 3-HDA was weaker than the ET formation in response to *Fo*nlp20 in OE lines. The investigation of ET production in response to 3-HDA show that OE lines help to characterize the role of LORE in immunity as weak effects of the wild type become more pronounced in OE lines.

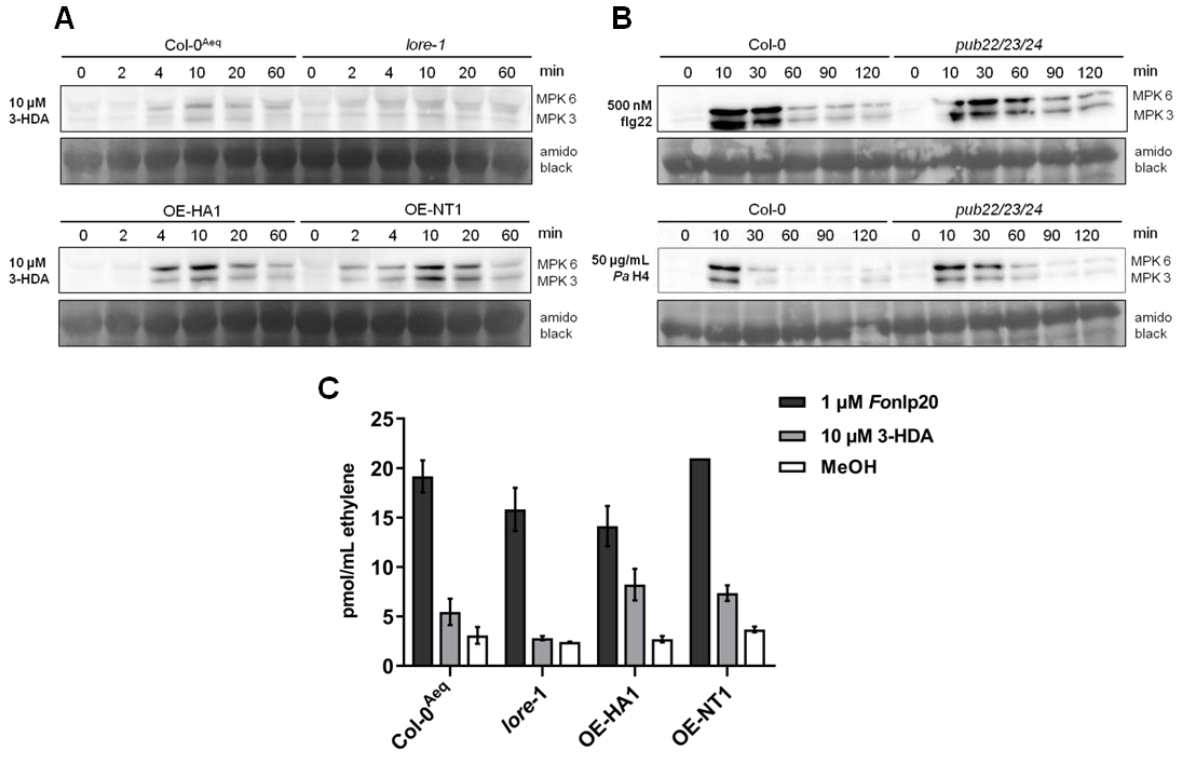

Figure 27 LORE overexpression lines show enhanced MAPK activation and ethylene production in response to 3-HDA. A) Immunoblot analysis of *At*MPK3 and *At*MPK6 activation. Col-0^{Aeq}, *lore*-1, OE-HA1, and OE-NT1 10-days-old seedlings were treated with 10 µM 3-HDA for 0, 2, 3, 10, 20, or 60 min. This experiment was repeated three times with similar results. B) Immunoblot analysis of *At*MPK3 and *At*MPK6 activation. Col-0 and *pub22/23/24* 10-days-old seedlings were treated with 50 µg/mL *Pa* H4 LPS or 500 nM flg22 for 0, 10, 30, 60, 90, or 120 min. This experiment was repeated two times with similar results. Amido black staining shows equal protein loading (A, B). SuperSignal® West Femto Maximum Sensitivity Substrate (Pierce, Rockford, USA) was used for detection (A, B). C) Analysis of ethylene production in Col-0^{Aeq}, *lore*-1, OE-HA1, and OE-NT1 leaf discs of 8-weeks-old plants in response to 1 µM *Fo*nlp20, 10 µM 3-HDA, or MeOH as control after 4 h. Depicted is the amount of ethylene as the mean ± SEM (n = 3) in pmol/mL. This experiment was repeated twice with similar results.

Transcriptional reprogramming is a typical feature of immunity in Arabidopsis. The expression of PTI marker genes *AtFRK1* (At2g19190) and *AtNHL10* (At2g35980) was analyzed in seedlings treated with MeOH or 3-HDA for 4 h (Figure 28A and B, Supplementary Figure 8C). In *lore*-1 (red) no induction

of *AtFRK1* or *AtNHL10* upon 3-HDA treatment was detectable. In Col-0^{Aeq} (black), elicitor treatment induced the gene expression of *AtNHL10* and *AtFRK1* as compared to the treatment with MeOH as previously shown by Kutschera *et al.* (2019). Also OE lines showed enhanced expression levels of *AtNHL10* and *AtFRK1* upon 3-HDA treatment compared to the wild type treated with MeOH. *AtFRK1* and *AtNHL10* were also strongly expressed in a state lacking elicitation with 3-HDA in OE-HA1 (blue) and OE-NT1 (green). This indicated constitutive defense signaling in these lines.

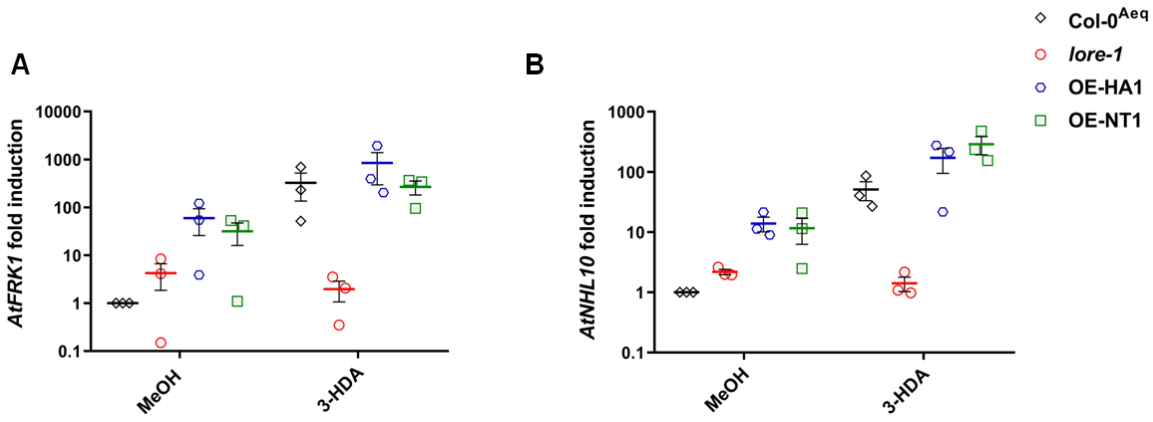

Figure 28 Typical PTI marker genes are constitutively expressed in overexpression lines. Relative quantitative expression of PTI marker genes *AtFRK1* (A) and *AtNHL10* (B) in seedlings of Col-0^{Aeq}, *lore*-1, OE-HA1, and OE-NT1 treated for 4 h with MeOH or 5 µM 3-HDA. Expression levels were normalized to the expression of *AtUBQ5*. Fold change induction was calculated relatively to Col-0^{Aeq} treated with MeOH. Single data are presented in a dot blot with the mean ± SEM of three biological replicates.

In summary, elevated and prolonged *At*MPK3 and *At*MPK6 activation is observed in OE-HA, OE-NT, and *pub22/23/24* in response to treatment with 3-HDA or *Pa* H4 LPS treatment compared to wild type, respectively. Also, the ET production in response to 3-HDA is enhanced in OE-HA and OE-NT compared to Col-0^{Aeq}. Col-0^{Aeq}, but not *lore*-1, reacts with defense gene expression upon 3-HDA treatment. Defense gene expression is constitutive in OE lines and is strongly induced by the treatment with 3-HDA. All tested PTI responses such as $[Ca^{2+}]_{cyt}$ elevation level, ROS generation, MAPK activation, ET production, and defense gene expression are increased upon treatment with 3-HDA in OE lines compared to wild type. Remarkably, differences in OE lines with a C-terminal epitope tag such as GFP or HA and in OE lines without an epitope tag are detected. Differences are detected in the decline and the kinetic of signal outputs such as the ROS burst and $[Ca^{2+}]_{cyt}$ elevation levels. MAPK activation, ET production, and defense gene expression seem not to differ between OE-HA and OE-NT. Two other mutant plants (*pub22/23/24* and *mpk3-1*) were identified with a similar ROS phenotype in response to 3-HDA. The occurrence of the second ROS burst is specific to the treatment with 3-HDA and does not occur upon flg22 or chitin treatment. This finding supports that the

regulation of LORE signaling is disturbed with a comparable effect as the addition of a C-terminal epitope tag to LORE.

4.7 Effects of LORE overexpression on the plant-bacteria interaction

The results presented in the preceding section 4.6 show that overexpression of LORE leads to enhanced and prolonged PTI responses in Arabidopsis. This raises the question if these changes in PTI also positively impact the resistance of Arabidopsis against infection with phytopathogenic bacteria.

4.7.1 Investigation of bacterial infection of overexpression lines

The influence of the enhanced PTI onto resistance of OE lines to infection with pathogens was evaluated on the basis of *Pto* DC3000 infection experiments (section 8.1.27). *Pto* DC3000 was directly infiltrated into the leaf apoplast of Col-0^{Aeq}, *lore*-1, OE-HA, and OE-NT (Figure 29A, Supplementary Figure 9A). The bacterial titers of the apoplastic space were evaluated on day 0 (4 h) and day 3 post infection. Equal bacterial titers were found on day 0 in all genotypes, indicating an even infiltration of the bacterial suspension into the leaf interior (Figure 29A). On day 3 no significant difference of the bacterial titers was observed among Col-0^{Aeq} and *lore*-1 or OE-HA1 or OE-NT1. *Pto* DC3000 multiplicated to comparable levels in the apoplastic space of wild type and OE lines. The direct infiltration of bacteria into the leaf apoplast enables bacterial populations to establish directly in the apoplastic space and omits the necessity of bacterial entry *via* wounds or stomata (section 3.4 and 3.6). Spray inoculation is therefore considered as the more natural pathogen infection as bacteria need to actively enter the plant interior (section 3.4, section 8.1.27). Leaves of Col-0^{Aeq}, *lore*-1, OE-HA, and OE-NT were surface-inoculated with *Pto* DC3000 (Figure 29B, Supplementary Figure 9B). Bacterial populations, which entered the leaf interior and established in the apoplast, were analyzed 4 h after inoculation on day 0 and 3 days later. In Col-0^{Aeq} and *lore*-1 equal levels of bacterial titers were detected on day 0 (Figure 29B). No significant difference was observed for bacterial populations established in the apoplast of OE-NT1 compared to wild type on day 0. Interestingly, a significant difference of the bacterial titer was observed in OE-HA1 compared to wild type on day 0. This difference was manifested 3 days post infection in OE-HA1 resulting in a significant lower bacterial titer in the apoplastic space than in the wild type (Figure 29B). OE-NT1, however, showed bacterial titers comparable to wild type plants 3 days post infection. The same was observed for bacterial populations established in the apoplastic space from *lore*-1 plants (Figure 29B).

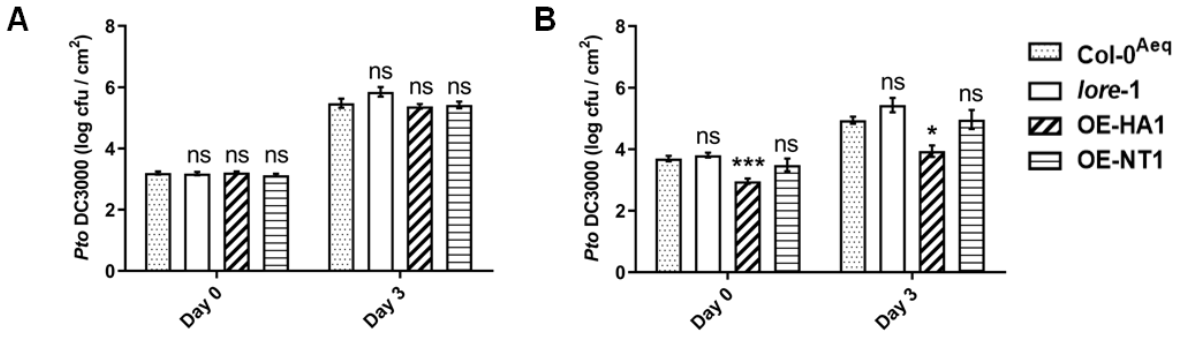

Figure 29 Bacterial infection assays reveal that OE-HA is more resistant to spray inoculation. Bacterial titers were assessed on day 0 (4 h) and on day 3 post infection of Col-0^{Aeq}, *lore*-1, OE-HA1, and OE-NT1. Data represent the colony forming units (cfu) per cm^2 leaf area, and are depicted as the mean ± SEM. A) *Pto* DC3000 was syringe-infiltrated into the leaf apoplastic space (n = 12; pooled data of four independent experiments). B) Leaf surface-inoculation with *Pto* DC3000 (n = 9, pooled data of three independent experiments). Data were analyzed with a one-way ANOVA and Dunnett's multiple comparison post test comparing each genotype to Col-0^{Aeq} (A, B). Day 0 and day 3 were analyzed separately (* $P < 0.05$, *** $P < 0.001$, ns = not significant) (A, B).

In summary, elevated resistance of OE lines is not detected upon direct inoculation of the apoplastic space with *Pto* DC3000 compared to wild type. Upon spray infection, only OE-HA shows enhanced resistance towards *Pto* DC3000, but not OE-NT. This shows that the C-terminal epitope tag fused to LORE has an influence on the bacterial resistance, likely at the pre-invasion stage.

4.7.2 Analysis of causes of the reduced bacterial titers in the apoplast of OE-HA

The *Pto* DC3000 infection experiments described in section 4.7.1 revealed that only OE-HA shows enhanced resistance towards bacterial spray infection but not upon direct infiltration. The observed differences of bacterial titers in the apoplast can be caused by less efficient colonization of the leaf interior of OE-HA or by a reduced survival of bacteria on the leaf surface or in the apoplastic space of OE-HA. To test both possibilities, two other experiments were conducted. First, bacterial infection assays using the *Pseudomonas* strain *Pto* DC3000 COR^- were used to analyze the differential regulation of stomata opening in OE-HA. Second, bacterial survival on the leaf surface and in the leaf apoplast was investigated. As described in section 3.7.2, the phytotoxin COR released by *Pto* DC3000 is important for the induction of stomatal reopening in the plant-pathogen interaction. *Pto* DC3000 COR^- was therefore sprayed on the leaf surface of Col-0^{Aeq}, *lore*-1, OE-HA, and OE-NT (Figure 30A, Supplementary Figure 9C). Bacterial titers of the leaf apoplast were analyzed on day 0 and day 3 post infection. In wild type and *lore*-1 comparable bacterial titers were observed on day 0 and day 3 post

infection. Significantly less bacterial titers were detected in the OE-HA1, but also in the OE-NT1 apoplast compared to Col-0^{Aeq} on day 0. Interestingly, the bacterial titer pattern of *Pto* DC3000 COR^{-} at day 3 was comparable to the spray infection with *Pto* DC3000, although bacterial titers of *Pto* DC3000 COR^{-} where much lower than *Pto* DC3000 wild type (Figure 29B and Figure 30A). The OE-HA1 apoplastic space showed significantly reduced bacterial colonization as compared to Col-0^{Aeq}. By contrast, the apoplastic space of OE-NT1 showed a similar colonization as wild type on day 3. Seemingly, *Pto* DC3000 COR^{-} is still able to multiplicate in the apoplastic space of OE lines as well as wild type and *lore*-1.

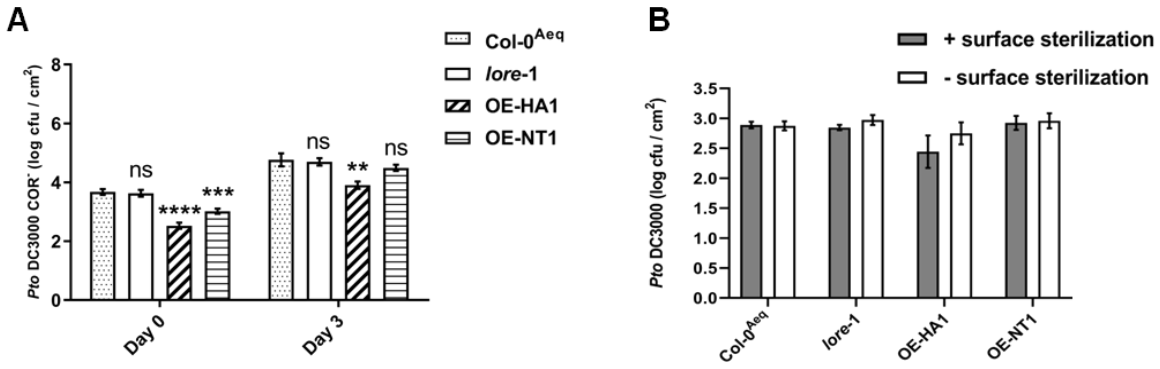

Figure 30 Reduced bacterial titers in the apoplast upon spray inoculation are caused by reduced bacterial entry. A) Surface-inoculation of Col-0^{Aeq}, *lore-1*, OE-HA1, and OE-NT1 with *Pto* DC3000 COR^{-} (n = 12, pooled data of four independent experiments). Bacterial titers were assessed on day 0 (4 h) and on day 3 post infection. Data represent colony forming units (cfu) per cm^2 leaf area and are depicted as the mean ± SEM. Data were analyzed with a one-way ANOVA and Dunnett's multiple comparison post test comparing each genotype to Col-0^{Aeq}. Samples of day 0 and day 3 were analyzed separately (** $P < 0.01$, *** $P < 0.001$, **** $P < 0.0001$, ns = not significant). B) Differences of bacterial titers of leaves with (+ sterilization) and without surface sterilization (- sterilization) of Col-0^{Aeq}, *lore*-1, OE-HA1, and OE-NT1 spray-inoculated with *Pto* DC3000 3 h post infection. Data represent cfu per cm^2 leaf area and are depicted as the mean ± SEM (n = 5, pooled data of two independent experiments). No significant difference was detected.

Usually, leaf material is surface-sterilized for assessment of apoplastic bacterial titers in bacterial infection assays (section 8.1.27). To differentiate between bacterial titers found in the apoplastic space and the apoplastic space plus leaf surface, bacterial titers of leaves with and without surface sterilization were investigated (Figure 30B). Bacterial colonization in wild type, OE-NT1, and *lore*-1 was similar, irrespective of surface sterilization. The bacterial titers of the leaf surface plus apoplastic space seemed to be equivalent among all lines. No significant reduction of the bacterial titer was

detected for the apoplastic space of OE-HA with surface sterilization compared to the bacterial titer of OE-HA without surface sterilization. A tendency towards a lower bacterial titer is noticeable in the apoplastic space of OE-HA as compared to wild type. The bacterial infection assays using spray inoculation of *Pto* DC3000 and *Pto* DC3000 COR^{-} indicated that the colonization is changed and therefore, stomatal immunity seems to be differently regulated in OE-HA lines compared to the other plant lines.

4.7.3 Investigation of the stomatal aperture in overexpression lines

The observed different bacterial titers in the apoplastic space of OE-HA compared to the wild type seem to be based on the differential regulation of stomatal opening. Stomata are not only point of entry for pathogens, but control also loss of water due to transpiration by the adjustment of the stomatal aperture. With water, heat energy is released. That is why plants with open stomata have a lower temperature than plants with closed stomata (section 3.4). Accordingly, leaf temperature is an indicator for the status of the stomatal aperture. To analyze the regulation of the stomatal aperture upon 3-HDA treatment, thermal imaging of plant leaves was performed (section 8.1.35). Therefore, Col-0^{Aeq}, *lore*-1, OE-HA, and OE-NT were sprayed with 3-HDA or MeOH as control treatment (Figure 31A, B and D, Supplementary Figure 9D and E). The leaf temperature measured for Col-0^{Aeq} without treatment was 22.6°C, the leaf temperature of *lore*-1 was also 22.6°C. OE-HA1 had a leaf temperature of 23.0°C and OE-NT1 of 22.9°C. The Δ leaf temperature of the OE lines compared to wild type of untreated plants was 0.4°C for OE-HA1 and 0.3°C for OE-NT1, showing a constitutive elevated leaf temperature of the OE lines and a significant difference (Figure 31A, Supplementary Figure 9D). Treatment with MeOH did not induce significant changes in the leaf temperature of wild type, *lore*-1, OE-HA1, or OE-NT1 (Figure 31A). The stomatal response to 3-HDA application was calculated differently as a consequence of the general elevated leaf temperature of OE lines. The Δ leaf temperature of each genotype upon treatment with 3-HDA was calculated by the subtraction of the temperature of the respective MeOH-treated genotype (Figure 31B, Supplementary Figure 9B, section 8.1.35, Table 11). Wild type treated with 3-HDA was compared to wild type treated with MeOH, OE-HA treated with 3-HDA was compared to OE-HA treated with MeOH and so forth. In this way, the sole effect of the elicitor treatment is highlighted and the constitutive difference in stomatal aperture of the OE lines is omitted.

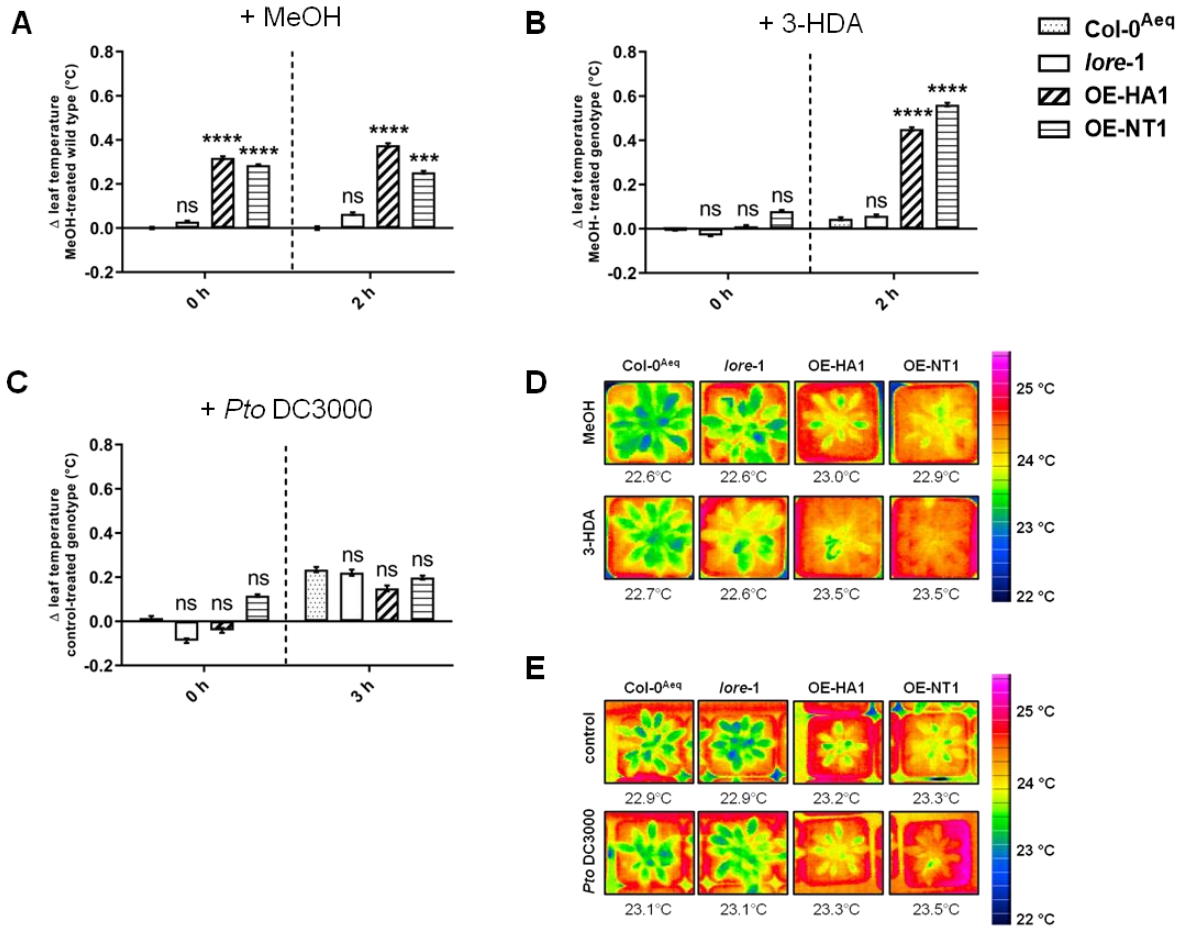

Figure 31 LORE overexpression lines respond with enhanced stomatal closure to 3-HDA. 7-weeks-old plants grown under 60% relative humidity were used for the experiments. A) Calculation of the leaf temperature change (Δ leaf temperature) of OE-HA1, OE-NT1, and *lore*-1 compared to Col-0^{Aeq} treated with MeOH. B) Calculation of the Δ leaf temperature in response to 3-HDA of Col-0^{Aeq}, *lore*-1, OE-HA1, and OE-NT1 compared to the leaf temperature of the respective MeOH-treated genotype. C) Calculation of the Δ leaf temperature in response to *Pto* DC3000 (OD 0.2) spray inoculation of Col-0^{Aeq}, *lore*-1, OE-HA1, and OE-NT1 compared to the leaf temperature of the respective control-treated genotype. Data represent the mean ± SEM of two independent experiments (n ≥ 49 leaves per genotype, treatment, and time point) (A. B, C). Data of each time point were analyzed with a one-way ANOVA and Tukey's multiple comparison post test in relation to the wild-type control (A, B, and C at 0 h) or to the control-treated genotype (A and B at 2 h, C at 3 h). Asterisks indicate significant differences (*** $P < 0.001$, **** $P < 0.0001$, ns = not significant) (A, B, C). A third experiment with similar results was performed. Because of minor changes in the experimental setup, data were not included into the calculation. D and E) Thermograms of Col-0^{Aeq}, *lore*-1, OE-HA1, and OE-NT1 in response to MeOH and 10 µM 3-HDA (D) or control treatment and *Pto* DC3000 (E) (OD 0.2) 2 h and 3 h post spray-inoculation. The leaf temperature is indicated in absolute values (E, D).

No significant difference of the leaf temperature change was found for wild type and *lore*-1 upon treatment with 3-HDA. The Δ leaf temperature in OE-HA1 was about 0.4°C and in OE-NT1 about 0.6°C 2 h after treatment with 3-HDA. This was a significant increase in temperature compared to the leaf temperature change in wild type. Considering also the constitutive differences in leaf temperature, a total Δ leaf temperature of about 0.8°C for OE-HA1 and 0.9°C for OE-NT1 were observed. This difference was obvious already by a visual assessment of thermograms and stressed differences of the stomatal response in OE lines compared to the wild type (Figure 31D). The underlying assumption that OE-HA lines ward off bacteria more efficiently by the differential regulation of the stomatal aperture was tested by spraying *Pto* DC3000 or the control treatment on OE-HA1, OE-NT1, *lore*-1, and Col-0^{Aeq} (Figure 31C, Supplementary Figure 9F). Col-0^{Aeq}, *lore*-1, and OE-NT1 reacted with an elevation in leaf temperature of about 0.2°C upon treatment with *Pto* DC3000. The leaf temperature of OE-HA1 elevated only about 0.1°C 3 h upon spray inoculation. This indicated a general stomatal responsiveness to the application of *Pto* DC3000 in all genotypes. However, no differences of the stomatal aperture of OE lines were observed compared to wild type. The increase of the leaf temperature in response to *Pto* DC3000 was not obvious by visual assessment (Figure 31D).

4.7.4 Effect of 3-HDA pre-treatment on the bacterial growth phenotype in LORE overexpression lines

Based on the previously described observations that 3-HDA induces stomatal closure, bacterial infection assays with a 3-HDA pre-treatment were performed to investigate if a pre-treatment reduces bacterial populations entering the leaf apoplast. Therefore, Col-0^{Aeq}, *lore*-1, OE-HA1, and OE-NT1 were pre-sprayed with MeOH or 3-HDA. After 2 h *Pto* DC3000 was sprayed and bacterial colonization was analyzed after additional 4 h (Figure 32, section 8.1.27). The pre-treatment with 3-HDA had an effect on the bacterial titers of the leaf apoplast in OE-HA, OE-NT, and Col-0^{Aeq}. The colonization of the apoplast of Col-0^{Aeq}, OE-HA1, and OE-NT1 was significantly reduced in comparison to the pre-treatment with MeOH. No significant difference was detected in the colonization of the apoplast of *lore*-1, irrespective of the pre-treatment. This showed that the stomatal closure in OE lines, but also in wild type in response to 3-HDA treatment hinders the bacterial entry into the apoplastic space.

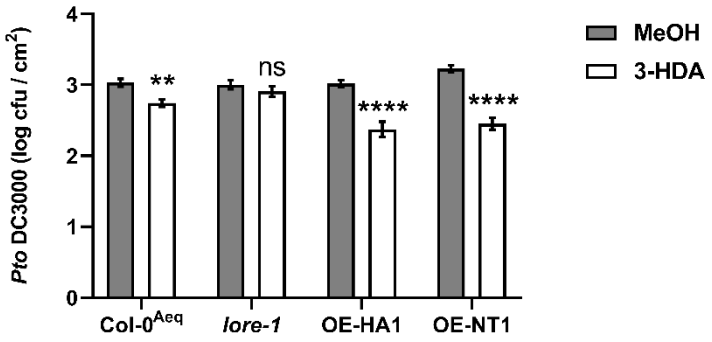

Figure 32 Pre-treatment with 3-HDA reduces the bacterial entry into the apoplast in overexpression lines and wild type. 10 µM 3-HDA or MeOH was sprayed on Col-0^{Aeq}, *lore*-1, OE-HA1, and OE-NT1. *Pto* DC3000 was spray-inoculated 2 h later, and bacterial titers were assessed after 6 h. Data represent colony forming units (cfu) per cm^2 leaf area, values represent the mean ± SEM (n = 9, pooled data of three independent experiments). Data were analyzed with an unpaired t-test comparing 3-HDA treated samples with the respective MeOH treatment of each genotype. Asterisks indicate significant differences (** $P < 0.001$, **** $P < 0.0001$, ns = not significant).

In summary, no differences in *Pto* DC3000 titers can be observed after direct infiltration of the bacterial suspension into the apoplast of OE lines, wild type, and *lore*-1. Spray inoculation of *Pto* DC3000 gives a different result. Here, the apoplastic space of OE-HA is less colonized than the apoplastic space of wild type, *lore*-1, and OE-NT. Spray inoculation of *Pto* DC3000 COR^- confirms this finding and shows that the apoplast of OE-NT is less colonized using the COR-deficient *Pseudomonas* strain. Differences of bacterial survival on the leaf surface or in the apoplastic space were not detected. A constitutive elevated leaf temperature of OE lines compared to wild type was found. 3-HDA treatment increases the leaf temperature of OE lines which is not detected for wild type or *lore*-1. No significant difference in the leaf temperature of OE lines, *lore*-1, and wild type was observed upon spray-inoculation with *Pto* DC3000. The pre-treatment with 3-HDA reduces the colonization of the apoplastic space in OE lines and wild type, but not *lore*-1, indicating a higher responsiveness of the OE lines to 3-HDA. Altogether, the data of the infection assays enforce the obtained results on the difference of LORE with a C-terminal epitope tag and without an epitope tag. Moreover, it proposes an important role of LORE in pre-invasive immunity which can be stimulated by the addition of 3-HDA.

5 Discussion

5.1 LPS/3-HDA perception in plants

5.1.1 Natural variation of the responsiveness to LPS/3-HDA

Plants evolved a multi-tiered immune system to ward off pathogenic microbes. PRRs located at the cell-surface contribute substantially to the restriction of pathogenic growth *via* the induction of immune responses establishing PTI. Many evolutionarily conserved microbial structures are known to elicit immunity in plants (section 3.1). However, the cognate PRR remains often unidentified. Efforts to identify the respective PRR are made using the model organism Arabidopsis (Ranf *et al.*, 2015, Gust *et al.*, 2007, Zipfel *et al.*, 2006, Zipfel *et al.*, 2004). In this way, *At*LORE was identified as a key signaling component in response to the MAMP LPS/3-HDA (Ranf *et al.*, 2015). Phylogenetic analysis of *At*LORE revealed that LORE is taxonomically restricted to Brassicaceae (Ranf *et al.*, 2015). The natural variation of responsiveness to LPS/3-HDA was evaluated in a ROS screening with different plant species. In general, the functional assessment supports the phylogenetic approach. LPS/3-HDA-sensitive species are exclusively identified within the Brassicaceae (Ranf *et al.*, 2015, section 4.1, Figure 6). Taxonomic restriction is also described for other signaling components involved in immunity. The PRRs *At*EFR and *Os*XA21 are restricted in their distribution and not present in most plant genomes (Schwessinger *et al.*, 2015, Kunze *et al.*, 2004). Insensitive to the treatment with EF-Tu are species outside of the Brassicaceae for instance *G. max, S. tuberosum, S. lycopersicum*, and *N. tabacum* (Kunze *et al.*, 2004). The sensing of flg22 and nlp20 shows also variation among different plant species (Böhm *et al.*, 2014, Takai *et al.*, 2008, Robatzek *et al.*, 2007, Zipfel *et al.*, 2004). Tomato is for example insensitive to the treatment with nlp20, elf26, and LPS, but responds with the formation of ethylene in response to the treatment with flg22, indicating that the genome of tomato encodes FLS2, but no PRRs for nlp20, elf26, or LPS (Böhm *et al.*, 2014, Robatzek *et al.*, 2007, Kunze *et al.*, 2004, section 4.1). The here conducted ROS screening revealed that the crops barley, soybean, and rice are insensitive to the treatment with LPS/3-HDA under the used conditions (section 4.1, Figure 6). *Os*CERK1 was recently described to be involved in immunity in response to LPS in rice which contradicts the findings of the study at hand (Desaki *et al.*, 2018). Desaki *et al.* (2018) use suspension-cultured rice cells to measure the generation of ROS in response to LPS whereas here, leaf discs of rice were used. This might explain the different obtained results. *At*CERK1 was shown to not be required for *At*LORE-dependent immune responses (Ranf *et al.*, 2015). This indicates that LPS/3-HDA-sensing is not exclusively mediated by *At*LORE and its orthologs, but that other recognition systems evolved (Desaki *et al.*, 2018, Shang-Guan *et al.*, 2018). Also *Brassica* species such as *B. rapa*, *B. napus*, and *B. oleracea* obtained from NASC (Nottingham Arabidopsis Stock Centre) were insensitive although a putative ortholog of *At*LORE is present in the genome (section 4.1, Figure 6A). SD-RLKs are a rapid expanding subfamily of RLKs, but *At*LORE-dependent LPS/3-HDA-sensing

seems not to be widely distributed (Xing *et al.*, 2013, Vaid *et al.*, 2012). Therefore, it will be interesting to investigate the natural variation of plant species responsive to 3-HDA. The fact that low-complexity metabolites such as 3-HDA are constantly released by bacteria, but LORE is not widely distributed, underpin the potential of *At*LORE as a tool for breeding to generate more resistant plant species (Kutschera *et al.*, 2019, unpublished, Rapicavoli *et al.*, 2018, Xin *et al.*, 2013, Mansfield *et al.*, 2012).

5.1.2 Genetic engineering of PRRs for broad-spectrum disease resistance

The PRR arsenal present in plant species is highly variable, and of potential use to develop broad-spectrum disease resistance *via* inter- and intraspecies transfer of PRRs with the aim to enlarge the MAMP recognition spectrum in economically important crop species (Boutrot *et al.*, 2017, section 3.11 and 5.1.1). The introduction of multiple PRRs to species lacking the orthologous receptor promises long-lasting resistance in the field, and would be an environmentally friendly crop protection alternative to the application of chemical plant-protective substances (Boutrot *et al.*, 2017, Holton *et al.*, 2015, Schwessinger *et al.*, 2015, Dangl *et al.*, 2013, section 3.11). Currently, single *R* genes mediating resistance are identified in wild species and introduced into economically used crop varieties (Bouwmeester *et al.*, 2014, Dangl *et al.*, 2013). However, the race-specific *R* gene mediated resistance is often quickly overcome in the field as single effector proteins contribute only partial to the full virulence of a pathogen and loss of one effector from the repertoire has no significant effect on the overall infection success (Boutrot *et al.*, 2017, Bouwmeester *et al.*, 2014, Dangl *et al.*, 2013). The introgression of *R* genes from wild species into otherwise susceptible varieties was successfully performed in monocots such as rice (Liu *et al.*, 2014, Chen *et al.*, 2006). The interspecies transfer of *R* genes or PRRs using biotechnological methods, which improved over the past years, is an additional option to extend the recognition repertoire. Lacombe and colleagues rendered *S. lycopersicum* Moneymaker and *N. benthamiana* sensitive to a range of phytopathogenic bacteria by the heterologous expression of *At*EFR, and demonstrated that intraspecies transfer of PRRs is applicable (Lacombe *et al.*, 2010). There are more examples of successful PRR transfer showing that PTI downstream signaling converges at some point and required signaling components are conserved between plant families (Holton *et al.*, 2015, Schwessinger *et al.*, 2015, Bouwmeester *et al.*, 2014, Lacombe *et al.*, 2010). Heterologous expression of *At*LORE in *N. benthamiana* renders it sensitive to LPS/3-HDA application, showing that also downstream signaling components of *At*LORE are conserved and supporting the potential of *At*LORE as a tool to increase the number of ligands perceived in economically important plant species (Ranf *et al.*, 2015). The ROS screening revealed that *B. rapa*, *B. napus*, and *B. oleracea* were insensitive to 3-HDA (section 4.1). Some *Brassica* species are economically important vegetables for instance varieties of the cole crop *B. oleracea*, and are therefore, interesting targets for breeding resistant species (Warwick, 2011). *Brassica* species are infected by *Xanthomonas campestris* pv. *campestris* and the introduction of *At*LORE to plants lacking a functional *At*LORE ortholog might improve diseases resistance against *Xanthomonas* infections as

*At*LORE is able to sense LPS/3-HDA from *Xanthomonas* (Ranf *et al.*, 2015, section 4.1). Another strategy to improve recognition or to enlarge the recognition spectrum of plants is the genetic engineering of PRRs (De Lorenzo *et al.*, 2011, Albert *et al.*, 2010, Brutus *et al.*, 2010). Genetic engineering can be used to produce chimeric receptor variants with RLKs from different plant species (Holton *et al.*, 2015, Schwessinger *et al.*, 2015). Immune responses, downstream signaling components, and activation of receptors are conserved among plants allowing the transfer of proteins from monocotyledons to dicotyledons and allowing the combination of protein modules to functional chimeras (Holton *et al.*, 2015, Schwessinger *et al.*, 2015, Lacombe *et al.*, 2010). Chimeras of the PRRs *At*FLS2 and *At*EFR were shown to be functional in Arabidopsis (Albert *et al.*, 2010). Other studies using fusions of the RLP *Os*CEBiP and the kinase domain of *Os*PID2 or the intracellular domain of *Os*XA21 and the extracellular domain of *At*BRI1 confirm these findings and expand the possible targets to RLPs and RLKs involved in other biological processes than immunity (Kouzai *et al.*, 2013, He *et al.*, 2000). Kouzai *et al.* (2013) artificially fused a kinase domain to an RLP naturally lacking an intracellular domain which results in a functional receptor. The chimera of *Os*CEBiP and *Os*PID2 induced even stronger immune responses compared to wild type rice (Kouzai *et al.*, 2013). Chimeras derived from *At*LORE and other SD-RLKs were initially generated to map domains involved in receptor complex formation (section 4.3). Additionally, these experiments show that SD-RLKs can be generally used to produce chimeras and engineer PRRs. The here provided data of OE lines of *At*LORE fused to an epitope tag support the possibility that genetic manipulation of PRRs can result in enhanced immune responses and subsequently in enhanced bacterial resistance (section 4.6, section 4.7). The effect of the addition of a C-terminal epitope tag on LORE is discussed in section 5.3.1. To date, all identified PRRs belong to the class of RLKs or RLPs (Couto *et al.*, 2016). The majority of the *RLK*s and *RLP*s encoded in the genome of Arabidopsis are orphan receptors showing that there are still plethora of RLKs and RLPs to discover (Shiu *et al.*, 2001b). Exploiting the natural variation of PRR characteristics to assemble receptors in a modular way to generate receptor proteins with improved features such as a stronger kinase domain, other binding abilities, or longer signal transduction might be of interest for future research and bases on the great mechanistic similarity of receptor activation and signal transduction beyond receptor classes (Boutrot *et al.*, 2017, Helft *et al.*, 2016, Kouzai *et al.*, 2013). Combination of multiple PRRs, genetically engineered PRRs sensing a wide range of MAMPs, or enhanced signaling capacity as well as R proteins recognizing core effectors present in various pathogens might improve the development of durable broad-spectrum disease resistance, avoid yield losses, and combat plant diseases (Boutrot *et al.*, 2017, Lacombe *et al.*, 2010, section 3.11).

5.2 LORE receptor complex formation

5.2.1 LORE forms ligand-independent homodimers

Ligand-induced receptor activation and complex formation are required for the induction of a wide range of biological processes in plants such as the perception of hormones, the regulation of growth, and disease resistance (Couto *et al.*, 2016, Shiu *et al.*, 2001b). PRRs rely on the association with other RLKs or RLPs for the establishment of defense responses as described in section 3.3.2 and section 3.3.3. The majority of structural information, currently available, is derived from LRR-RLKs. Therefore, the apparently predominant and best understood mechanism for complex formation of receptors and activation in plants is the ligand-induced heterodimerization (Song *et al.*, 2017). Other concepts, reported for receptor kinases from mammalians but so far only debated for a few RLKs from plants, are the ligand-induced homodimerization and ligand-independent homodimerization (Song *et al.*, 2017, Lemmon *et al.*, 2010). The complex formation of the PRR *At*FLS2 categorizes to the ligand-induced heterodimerization. *At*FLS2 forms a heterodimer with the co-receptor *At*BAK1 upon binding of flg22 to the extracellular domains of both interacting partners (Sun *et al.*, 2013b, Chinchilla *et al.*, 2007, Heese *et al.*, 2007). *At*BAK1 is promiscuous in its choice of interacting partner and associates with other LRR-RLKs such as *At*EFR or *At*BRI1, but is not necessary for *At*CERK1- and *At*LORE-dependent immune responses (Ranf *et al.*, 2015, Cao *et al.*, 2014, Liu *et al.*, 2012, Schulze *et al.*, 2010, Li *et al.*, 2002). A recent study from Smakowska-Luzan *et al.* (2018) investigated the cell surface interaction network of LRR-RLKs shedding new light on the general organization of signaling networks. Interestingly, LRR-RLKs with a short LRR-domain (less than 12 LRR repeats) such as *At*BAK1 were found at internodes of the network and were highly interconnected. They further found that LRR-RLKs with a short LRR domain preferentially interacted with LRR-RLKs with a long domain (more than 12 repeats). Short LRR-RLKs do not only serve as co-receptors, but take over crucial roles as network scaffold proteins (Smakowska-Luzan *et al.*, 2018). Ligand-induced heterodimerization of LRR-RLKs with versatile short LRR-domain RLKs seems to be a common mode of action to control the transduction of external stimuli and suggests a similar mode of receptor complex formation for all LRR-RLKs namely heterodimerization. It was suggested that the super helical structure of the LRR-domains might even prohibit receptor homodimerization (Hothorn *et al.*, 2011, She *et al.*, 2011). Receptor homodimerization, on the other hand, is essential according to the prevailing hypothesis for SRK receptor formation in the SI response. It was thought that dimerization occurs spontaneously at the plasma membrane. The ligand SCR would only be able to bind to SRK dimers, but not to monomers (Shimosato *et al.*, 2007, Giranton *et al.*, 2000, section 3.10.2). The mechanisms underlying *At*LORE receptor complex formation and activation were investigated in comparison to the so far best-studied SD-RLK, SRK (section 4.2). The receptor complex formation of *At*LORE was analyzed using LORE and LORE-Km full-length proteins in BiFC and CoIP experiments. Here, LORE forms homodimers in the absence of 3-HDA and kinase activity is not

required for homodimerization, but for signal transduction (Ranf *et al.*, 2015, section 4.2.1, Figure 8). The complex formation of LORE shows analogies to the mechanism described for SRK, but differs to the complex formation described for *At*FLS2 (Ma *et al.*, 2016, Naithani *et al.*, 2007, Sun *et al.*, 2013b, Shimosato *et al.*, 2007, Giranton *et al.*, 2000). The above described concepts of receptor complex formation (ligand-induced heterodimerization, ligand-induced homodimerization, and ligand-independent homodimerization) seem to correlate with the architecture of the extracellular domain which seems to determine the mode of dimerization emphasizing the importance of the extracellular domain for receptor complex formation and activation. In 2016, Ma and colleagues added new information to the understanding of SRK complex formation of the extracellular domain (Ma *et al.*, 2016). Ma *et al.* (2016) demonstrated that the complex association is dependent on the receptor itself and the presence of the ligand SCR. As a consequence, receptor formation of SRK needs to be reclassified as ligand-dependent homodimerization. The crystal structure encompasses only the extracellular domain of SRK indicating that the intracellular domain is not critical for ligand-dependent homodimerization. Here, experiments with truncated variants of *At*LORE show that homodimerization is mediated by the extracellular domain, but not the intracellular domain (section 4.2.1, Figure 8 and Figure 9). As observed for SRK, also the soluble extracellular domain, eLORE, is sufficient to homodimerize (Ma *et al.*, 2016, section 4.2.2, Figure 10). eLORE does not interact with the full-length *At*LORE protein. Only tLORE, a truncation variant still anchored into the plasma membrane, interacts with *At*LORE (section 4.2.3 and 4.2.4, Figure 10 and Figure 11). One possible explanation could be that eLORE and *At*LORE interaction is rather weak and disrupted by the here chosen methods. Interaction could also be impeded by the localization of eLORE in the apoplastic space and *At*LORE in the plasma membrane. An influence of the C-terminal epitope tag on the interaction capability of eLORE and *At*LORE was excluded (Supplementary Figure 2). eLORE homodimerization is not dependent on the addition of 3-HDA, which contradicts the observations made with eSRK9, and underpins the idea of a ligand-independent receptor formation (Supplementary Figure 3). However, all *in planta* experiments include the possibility that additional proteins bind to eLORE or 3-HDA which could promote dimerization. Binding studies of eLORE produced in insect cells with 3-HDA indicate a rather low binding affinity which might support the involvement of additional proteins bridging 3-HDA/eLORE binding (Kutschera *et al.*, 2019, unpublished). The crystal structure of eSRK9 is in contrast with previous findings which showed that SRK associates into pre-formed dimers (Shimosato *et al.*, 2007, Giranton *et al.*, 2000). It is conceivable that the lack of the transmembrane domain and the intracellular domain reason the contradicting results to the hypothesis of ligand-independent homodimerization *in planta* (Ma *et al.*, 2016). The transmembrane domain plays a crucial role in dimerization of various RLKs and RLPs as well as for receptor kinases of mammals. The motif GxxxG is conserved in the transmembrane domain of the adaptor kinase SOBIR1/EVR and essential for the interaction with LRR-RLPs (Bi *et al.*, 2016). This motif is neither present in *At*LORE nor SRK9 from *B. rapa* (Supplementary Figure 11). The transmembrane region,

including the juxtamembrane, is further important for receptor activity (discussed below in section 5.2.2). The relevance of the extracellular domain in dimerization of *At*LORE is also supported by the finding that tLORE, but not iLORE or eLORE, form dysfunctional heterodimers with LORE, keeping LORE in an inactive state (section 4.2.3, Figure 10). tLORE exerts a dominant-negative effect on the 3-HDA-induced ROS generation in *N. benthamiana*. A dominant-negative influence by the overexpression of the extracellular domains forming non-functional receptor complexes and preventing the induction of downstream signaling is reported for other RLKs (Domínguez-Ferreras *et al.*, 2015, Zou *et al.*, 2015, Liu *et al.*, 2012). The overexpression of the ectodomain anchored into the plasma membrane of *At*BAK1 results in a dose-dependent signaling blockade of flg22-induced responses (Domínguez-Ferreras *et al.*, 2015). A soluble variant of the *At*BAK1 extracellular domain possesses no dominant-negative effect which is in line with the observations made for eLORE (Domínguez-Ferreras *et al.*, 2015). Receptor truncations of the extracellular domain located at the plasma membrane of the SD-RLK *Os*LSK1 likewise form non-productive dimers with *Os*LSK1 (Zou *et al.*, 2015). In case of *At*CERK1, a soluble truncation encompassing the three LysM domains comprises chitin-dependent signal outputs of *At*CERK1 (Liu *et al.*, 2012). Alternatively, the intracellular domain can also have a dominant-negative effect on receptor activity as reported for *At*FLS2 and *Os*SIK2 (Chen *et al.*, 2013, Sun *et al.*, 2012). The intracellular domain of *At*FLS2 mediates a dose-dependent effect on downstream signal transduction of the MAMP with no discrimination between a transmembrane bound or soluble intracellular domain (Sun *et al.*, 2012). Overexpression of the intracellular domain of *Os*SIK2, on the other hand, transfers enhanced resistance to stress stimuli in rice by the differential gene expression compared to full-length *Os*SIK2 (Chen *et al.*, 2013). In this context, the ectodomains of *At*LORE, *At*BAK1, *Os*LSK1, and *At*CERK1 exert a dominant-negative effect on the activation of their receptor complexes. All associate *via* their extracellular domains to form higher complexes. Also, the intracellular domain of *At*FLS2 exerts a dominant-negative effect, presumably, *via* the interaction of the intracellular domain with *At*FLS2 full-length protein, outcompeting binding of *At*BAK1, forming non-productive receptor complexes (Sun *et al.*, 2012). In contrast, the intracellular domain of *At*LORE, iLORE, does not exert a dominant-negative effect, and BiFC experiments indicate no interaction with full-length *At*LORE, but iLORE was shown to interact in CoIP assays with full-length *At*LORE (section 4.2.1, Figure 8 and Figure 9, section 4.2.4, Figure 11). Sun *et al.* (2012) show ligand-independent association from *At*FLS2 to homodimers which was analyzed with CoIP experiments. Another study using BiFC and FRET (Fluorescence resonance energy transfer) failed to find *At*FLS2 homomeric interactions (Ali *et al.*, 2007). Another example from literature facing the same discrepancy of results obtained from CoIP and BiFC assays is the interaction of *At*LecRLK with *At*BAK1 and *At*FLS2 by Yekondi *et al.* (2017). Constant interaction of *At*LecRLK with *At*BAK1 and *At*FLS2 irrespective of the addition of the ligand was observed using CoIP analysis. In contrast, BiFC experiments refined the results and showed interaction of *At*LecRLK with *At*FLS2 only upon elicitation with flg22 (Yekondi *et al.*, 2017). Here,

interaction between *At*LORE and iLORE was detected in CoIP experiments, but not in BiFC assays (section 4.2.1 and 4.2.4, Figure 8 and Figure 11). Both methods, CoIP and BiFC, do not show direct protein-protein interaction (Kudla *et al.*, 2016). Receptor complexes are multi protein complexes consisting of proteins directly interacting with the ligand (e.g. *At*FLS2 and *At*BAK1), but also proteins important for the execution of downstream signaling (e.g. *At*BIK1 and *At*RBOHD). A model, where additional proteins bridge the association of *AtL*ORE and iLORE or of *At*FLS2 and the intracellular domain of *At*FLS2 is possible. Which signal components execute *At*LORE-mediated signaling remains largely unknown. Further research will shed light on other proteins associated to the receptor complex. Other studies provide evidence that RLKs are decentralized into microdomains at the plasma membrane according to their function in immunity or growth, respectively (Bücherl *et al.*, 2017, Jarsch *et al.*, 2014). Hence, it is possible that iLORE, but also tLORE are integrated into the same microdomain as *At*LORE and as a result, are co-immunoprecipitated even though no physical interaction is involved. With BiFC assays spatial proximity of two proteins is analyzed and close localization of two proteins indicates joint participation in signaling (Kudla *et al.*, 2016). Pull-down experiments of the soluble eLORE expressed individually in separate leaves further shows a dynamic interaction of the extracellular domains. Accumulating evidence support the theory of *At*LORE ligand-independent homodimerization. This raises the question why *At*LORE would form pre-formed dimers whereas all other characterized complexes rely on the induction by ligand-binding. Pre-formed dimers have the advantage that responses are induced in the presence of a low amount of the activating-ligand ensuring fast signaling, but examples of pre-formed dimers in literature are rare (Song *et al.*, 2017). The mature CLV3 (CLAVATA3) peptide regulates stem cell homeostasis in the shoot and floral meristem by binding to the LRR-RLKs *At*CLV1 and *At*CLV2 (CLAVATA 1/2) (Bleckmann *et al.*, 2010, Ogawa *et al.*, 2008). *At*CLV1 associates into pre-formed homodimers in the plasma membrane and *At*CLV1 homodimers oligomerize upon ligand-binding (Somssich *et al.*, 2015, Bleckmann *et al.*, 2010). Somssich *et al.* (2015) speculate that differences in the mechanism of receptor activation of *At*CLV1 and *At*FLS2 are based on their different biological role. *At*CLV1 regulates stem cell homeostasis, a continuous process. In contrast, *At*FLS2 is exclusively activated in the presence of flg22, meaning only if plants are actually threatened by infection with pathogens. Constant activation of immune responses is detrimental for plants and has a negative effect on growth and development (Somssich *et al.*, 2015, Gomez-Gomez *et al.*, 2000). An effect also observed in the OE-GFP lines of LORE which further support the idea of ligand-independent complex formation. Signaling in OE-GFP seems to be triggered in the absence of the ligand (section 4.6.1, Figure 23). Apparently, homodimerization and thus receptor activation are reinforced by the C-terminal GFP epitope tag (discussed below in section 5.3.1). The data obtained from OE-GFP lines also highlight the importance of strict control mechanisms to regulate PRR activity and prevent negative effects of constant defense signaling. *At*LORE and *At*FLS2 belong to two distinct classes of RLKs in respect to their extracellular domain (Ranf *et al.*, 2015, Chinchilla *et al.*, 2007). RLKs can be further categorized in respect of the

presence of the RD motif in their kinase subdomain VIa. The RD motif describes the presence of a conserved arginine (R, Arg) followed by the key catalytic aspartate (D, Asp) in the catalytic domain of the kinase domain (Nolen *et al.*, 2004, Johnson *et al.*, 1996). Phosphorylation of the kinase activation loop, which is in spatial proximity to the RD motif, contributes to kinase activation (Krupa *et al.*, 2004). RD kinases are often activated *via* autophosphorylation of the activation segment which is not true for non-RD kinases (Dardick *et al.*, 2012, Johnson *et al.*, 1996). This mechanistic difference might be one aspect of differential receptor complex formation. *At*FLS2 and *At*EFR belong to the class of non-RD kinases undergoing heterodimerization with the RD kinase *At*BAK1 (Roux *et al.*, 2011, Chinchilla *et al.*, 2007, Heese *et al.*, 2007). *At*FLS2 possesses only a weak kinase activity and relies on the co-receptor *At*BAK1 for signal transduction to downstream signaling components by phosphorylation (Perraki *et al.*, 2018, Sun *et al.*, 2013b, Schwessinger *et al.*, 2011, Roux *et al.*, 2011). In contrast, *At*LORE and *At*CERK1 belong to the class of RD kinases forming at least partially homodimers. Chitin-induced signaling requires the activity of the CERK1 kinase in Arabidopsis and rice (Cao *et al.*, 2014, Hayafune *et al.*, 2014, Shimizu *et al.*, 2010). It was reported that autophosphorylation of Thr479 located in the activation segment of the kinase domain of *At*CERK1 is essential for chitin-triggered defense responses (Suzuki *et al.*, 2016). Structural modeling showed that Thr479 potentially forms a hydrogen bond with Asp441 of the RD motif (Suzuki *et al.*, 2016). The corresponding Thr502 of *At*BAK1 is also target of autophosphorylation and important for downstream signal transduction (Yan *et al.*, 2012). This residue is conserved among SD-RLKs (Thr653 in *At*LORE, Supplementary Figure 11). Another conserved tyrosine residue crucial for receptor activation is conserved among RD and non-RD kinases. Autophosphorylation of the residue Tyr428 of *At*CERK1 corresponding to Tyr836 of *At*EFR is essential for receptor activation (Suzuki *et al.*, 2018, Macho *et al.*, 2014). Both PRRs are targets of a phosphatase released by bacteria specifically dephosphorylating this tyrosine residue to inactive PTI signaling (Liu *et al.*, 2018, Macho *et al.*, 2014). This tyrosine is also conserved in *At*LORE and corresponds to Tyr600 (Supplementary Figure 11). Although *At*CERK1, *At*EFR, and *At*LORE belong to three distinct classes of RLKs, all share common activation mechanisms, but differ in others. Transient overexpression of kinase-active *At*LORE induces cell death in *N. benthamiana* (Supplementary Figure 2A). This phenomenon is also described for the overexpression of *At*CERK1 in *N. benthamiana* (Shinya *et al.*, 2014). It is conceivable that if *At*LORE forms pre-formed dimers, strong overexpression leads to autoactivation which would induce immune responses and cell death in a comparable way as described for *At*CERK1 (Shinya *et al.*, 2014, Pietraszewska-Bogiel *et al.*, 2013). This hypothesis is further supported by the finding that typical PTI marker genes are constitutively expressed in OE lines indicating constant defense signaling and thus receptor activation (section 4.6, Figure 28). All the above presented findings show that phosphorylation is of eminent importance for the activity of kinases and therefore, precise control mechanisms of autophosphorylation are crucial to prevent constant signaling. Various examples can be found in literature. *At*BAK1, for example, is only released from the complex with the negative

regulator *At*BIR2 when flg22 is present ensuring signaling only in the presence of the *At*FLS2-activating ligand (Halter *et al.*, 2014). *At*CERK1 homodimerization is only induced upon ligand-binding to *At*LYK5, and SRK activation is inhibited by binding of THL1/2 to the kinase domain in the absence of a ligand (Cao *et al.*, 2014, Cabrillac *et al.*, 2001, Bower *et al.*, 1996). The Arabidopsis genome encodes for *THIOREDOXIN-H-LIKE* and hence, *At*LORE activity could be controlled in a comparable way to the described mechanism of SRK. However, the control of kinase activity with THIOREDOXIN-H-LIKE proteins is not widespread. But again, most knowledge is derived by LRR-RLKs, and therefore, not necessarily simply transferable to other RLK classes. Other possible mechanisms to control *At*LORE activity are discussed in section 5.3.1.

In consideration of the available data, *At*LORE receptor complex formation is mediated by the extracellular domain and potentially by the transmembrane domain. The here provided data support ligand-independent homodimerization of LORE. However, the experiments were performed with heterologous overexpressed LORE fused to C-terminal epitope tags in *N. benthamiana*. Taking account of the results obtained with the OE lines with a C-terminal epitope tag and the effect of the strong overexpression on the growth and development in OE-GFP, ligand-independent homodimerization should be investigated in the native genetic background with lower LORE levels to confirm the here presented findings.

5.2.2 Contribution of single domains from LORE to receptor activation

Limited knowledge of the mode of receptor activation of SD-RLKs was available when the study at hand was initiated. The PAN/APPLE and EGF-like domain were thought to mediate receptor homodimerization (Naithani *et al.*, 2007, section 3.10.2). Within this study, the extracellular domain of *At*LORE was identified to be critical for receptor homodimerization (section 4.2 and 5.2.1). To fine map specific domains involved in receptor complex formation and activation of LORE, domain swaps of LORE with other SD-RLKs not involved in 3-HDA-sensing were generated and functionally tested (section 4.3, Figure 13, Figure 14). Fine mapping of residues crucial for ligand-binding or domains essential for receptor complex formation and activation were successfully performed before by the generation of chimeric receptor variants (Bi *et al.*, 2016, Fradin *et al.*, 2014, Mueller *et al.*, 2012, Albert *et al.*, 2010, Brutus *et al.*, 2010, Boggs *et al.*, 2009, Wulff *et al.*, 2001, He *et al.*, 2000). Albert *et al.* (2010) used chimeras derived from *At*EFR and *At*FLS2 to define the elf18 binding site by the exchange of N-terminal LRR-repeat regions. Chimeras encompassing the ectodomain of *At*LORE and the intracellular domain of AlyrLORE, SD1-23i, and SD1-28i are functional (section 4.3.1, Figure 13). The reciprocal domain swaps where the extracellular domain originates from AlyrLORE, SD1-23i, or SD1-28i and the kinase domain from LORE are not able to induce the generation of ROS upon 3-HDA treatment (section 4.3.1, Figure 13). Apparently, the intracellular domain of LORE does not mediate ligand-specificity. This is in line with other studies reporting that the intracellular domain of

*At*EFR, *At*FLS2, *At*WAK1, and *At*BAK1 can be exchanged. The generated chimeras induce signaling upon treatment with the respective ligand (Albert *et al.*, 2013, Albert *et al.*, 2010, Brutus *et al.*, 2010). In contrast, domain swaps of the extracellular domain of *At*EFR, *At*WAK1, and *At*BAK1, also partial swaps, often result in inactive receptor variants (Fradin *et al.*, 2014, Albert *et al.*, 2010, Brutus *et al.*, 2010). Therefore, signal specificity is mediated by the extracellular domain of *At*LORE, *At*EFR, *At*WAK1, *At*BAK1, and *At*FLS2. Inactivity of chimeric receptor variants of LORE can be explained by a variety of possibilities. First, receptor homodimerization of the chimeras may be abolished as it was shown that homodimerization is essential for the induction of LORE-mediated downstream signaling (section 4.2.3, Figure 10). Opposing to this is the finding that the soluble extracellular domains of AlyrLORE and SD1-23i still heterodimerize with eLORE indicating that the extracellular domains fused to the intracellular domain of LORE do not abolish homodimerization of the generated chimeras. In case of eSD1-28i heterodimerization is questionable and requires further investigation (section 4.3.4, Figure 15). Heterodimerization was also reported for *Os*LSK1 from rice which forms heterodimers with a subset of five related SRKs (Zou *et al.*, 2015). Zou *et al.* (2015) and the study at hand investigated heterodimerization using truncations. Preliminary results of interaction analysis with full-length AlyrLORE, SD1-23i, and LORE confirm heterodimerization with LORE (Supplementary Figure 3A). Ma *et al.* (2016) speculate that SD-RLKs have a common mode of protein folding due to the high conservation of essential structural residues in SD-RLKs. This might indicate a conserved mode of receptor complex formation of SD-RLKs which also allows heteromeric interactions (Ma *et al.*, 2016, section 4.4). A second and very likely possibility is that the extracellular domains of the *At*LORE para- and orthologs do not bind the putative ligand of *At*LORE and therefore do not initiate signaling. This is further supported by the finding that SD1-23 and SD1-28 from Arabidopsis are not involved in 3-HDA-sensing (Ranf *et al.*, 2015, section 4.1, Figure 6C). AlyrLORE shares 94% identical amino acids with *At*LORE, a putative ortholog, but a role in LPS/3-HDA-sensing could not be established in the study at hand (section 4.1, Figure 6A, B and C). A third possibility is that the domain swap borders influence the protein stability and folding (discussed below). More complexity was added by the findings using partial extracellular domain swaps. Here, domain swaps with AlyrLORE and SD1-23i remain active. Chimeras derived from SD1-28i are inactive, but this might be due to localization to the intracellular space and are therefore excluded from the discussion (section 4.3.2, Figure 14D). The presence of parts of the extracellular domain of LORE is sufficient to induce signaling upon 3-HDA treatment in combination with residues from AlyrLORE and SD1-23. All three possibilities presented above apply likewise to the partial extracellular domain swaps. Other studies claim that the origin of the juxtamembrane domain determines the functionality of chimeras (Kouzai *et al.*, 2013, De Lorenzo *et al.*, 2011, Albert *et al.*, 2010, Brutus *et al.*, 2010). The juxtamembrane domains are short regions preceding and following the transmembrane domain and are characterized by a stretch of positively charged amino acids such as lysine and arginine in an individual order for each RLK (De Lorenzo *et al.*, 2011). Chimeric receptor variants of the

extracellular domain of *At*EFR with the kinase domain of *At*FLS2 show that only those retaining the extracellular juxtamembrane domain of *At*EFR are fully functional. Chimeras with the extracellular juxtamembrane domain of *At*FLS2 are strongly reduced in their responses to elf18 (Albert *et al.*, 2010). Kouzai *et al.* (2013) show that only chimeras which retain the transmembrane domain of *Os*PID2 are active and trigger immune responses. Possibly, the juxtamembrane domain is important for maintaining protein stability, correct folding, and thus receptor complex formation. Also, autophosphorylation of residues of non-RD kinases located in the intracellular juxtamembrane domain were identified to be crucial for receptor activation of *At*BRI1 and *Os*XA21 (Oh *et al.*, 2012, Chen *et al.*, 2010, Robatzek *et al.*, 2006). Phosphorylation of the juxtamembrane domains is also critical for the activation of receptors in mammals (Lemmon *et al.*, 2010). Hence, changes in the juxtamembrane region of the chimeras of LORE with other SD-RLKs might influence the activity. The domain swaps of the complete extra- or intracellular domain of *At*LORE generated and characterized within this study carry the domain swap border START and P (Supplementary Figure 11). Hence, the domain swaps of the intracellular domain carry the transmembrane region of LORE and maintain signal competency. The reciprocal domain swaps retain the transmembrane region of the ortho- or paralog and loose signal competency. The partial extracellular domain swaps of the EGF-like and PAN/APPLE domain violate this observation. The domain swap site is located directly before the extracellular juxtamembrane domain and could potentially disrupt this motif (domain swap site N, Supplementary Figure 11). However, the juxtamembrane regions of the SD-RLKs used for the domain swaps with *At*LORE are highly conserved (Supplementary Figure 11). Inactivity cannot be entirely based on the juxtamembrane region as the chimeras with AlyrLORE and SD1-23 remain partially active. Taking the available structural information of eSRK9 into consideration, other important motifs might have an influence on the activation of receptor complexes (Ma *et al.*, 2016, section 4.4). The reported mechanism of eSRK9 receptor complex formation indicates the involvement of residues distributed over the complete extracellular domain. The dimerization interface and the hv regions, in particular hvII located in LLD2, are critical for the complex formation of eSRK9. The chimeric receptors DSAlyr-LL and DS123-LLi carry the dimerization interface of LORE, but hvII region of the respective para- or ortholog. DSAlyr-EP and DS123-EP carry the dimerization interface of the respective para- or ortholog, but the hvII region of LORE (section 4.4, Figure 18). The partial domain swaps with AlyrLORE and SD1-23i remain active independent of the origin of the dimerization interface and hvII. Possibly, the motifs of AlyrLORE, SD1-23, and LORE have similar features which maintain correct receptor complex formation and therefore activation (section 4.4, Figure 18). Notably, Trp270, an important structural residue in hvII, located in close proximity to the dimerization interface of *At*LORE, was chosen as the domain swap site for DS-LL and DS-EP. It is possible that the exchange of amino acids in this area impacts protein folding and activity. SCR9 induced homodimerization of eSRK9 was abolished by the mutation of eSRK9 residues into the equivalent SRK8 residues, Val211Glu and Pro294Met (Ma *et al.*, 2016). These residues are equivalent to Tyr201

and Leu284 in *At*LORE and are in the direct environment of the dimerization interface formed by LLD2 and mutations in this area could potentially destabilize this motif. *At*SD1-28 differs in its dimerization interface compared to LORE. To evaluate the requirement of the dimerization interface of *At*LORE, it will be interesting to address if the full-length chimeras are able to dimerize with LORE. Early work on SRK identified the hv regions to be crucial for SRK activation by the ligand using domain swaps of hvI, hvII, and hvIII from a variety of SRKs which was confirmed recently (Ma *et al.*, 2016. Boggs *et al.*, 2009, section 4.4). Only a subset of the polymorphic amino acid is *de facto* involved in SCR binding. Certainly, this explains the possibility of SRK to discriminate the plethora of SCRs and bind exclusively to the cognate SCR to avoid self-fertilization. The polymorphic residues also support the fact that *At*LORE putatively recognizes 3-HDA which differs in its biochemical characteristic to SCR. A detailed comparison of the eLORE model with the crystal structure of eSRK9 did not focus on the detection of specific residues potentially involved in 3-HDA binding. It is conceivable that also *At*LORE uses the hv regions for ligand-binding, but it is also possible that *At*LORE evolved a different binding site. 3-HDA is a medium chain fatty acid, and in literature receptor proteins for fatty acids are described in mammals (section 3.9, Figure 3B). The pro-inflammatory G protein-coupled receptor 84 (GPR84) is able to bind 3-HDA *via* a positively charged amino acid, Arg172, located at an extracellular loop (Mahmud *et al.*, 2017). Previous studies identified Asp104 buried in the protein core to bind 3-HDA (Nikaido *et al.*, 2015). *At*LORE possesses several arginine or aspartic acid residues located at the surface or buried in the protein core. As suggested for GPR84 also *At*LORE could form multiple binding pockets for 3-HDA. Unfortunately, drawing conclusion from the model of eLORE in regard of ligand-binding is highly speculative as binding studies of 3-HDA and *At*LORE suggest the necessity of a co-receptor (Kutschera *et al.*, 2019, unpublished).

In conclusion, the multiple sequence alignments of SD-RLKs show the conservation of structural important residues identified by the crystal structure of eSRK9. This supports the idea that the protein folding is comparable among SD-RLKs and therefore, it is possible that the mode of receptor complex formation is similar. *At*LORE homodimerization is mediated by the extracellular domain. The partial domain swaps did not result in the identification of single domains involved in receptor activation. However, in consideration of the structural information of eSRK9, it might not be expected to find single domains as residues involved in complex formation are distributed over the complete ectodomain. The accumulated evidence indicates that *At*LORE forms ligand-independent dimers. To proof this hypothesis, the involvement of a potential co-receptor should be investigated or 3-HDA needs to be shown to be the genuine ligand of *At*LORE and homodimerization should be investigated in the native genetic background.

5.3 The role of LORE in pre- and post-invasive immunity

Overexpression lines of *At*BAK1, *Os*SDS2, or cysteine rich receptor-like kinases *At*CRK4, *At*CRK6, and *At*CRK36 provide evidence that enhanced gene dosages can render Arabidopsis and rice more resistant to infection with pathogens (Domínguez-Ferreras *et al.*, 2015, Yeh *et al.*, 2015, Fan *et al.*, 2018). Overexpression of the SD-RLK LORE results in enhanced PTI responses, but does not increase resistance towards infection with *Pto* DC3000 upon direct infiltration into the leaf interior (section 4.7). The here presented data of overexpression lines of LORE fused to a C-terminal epitope tag highlight the role of *At*LORE in pre-invasive immunity. Moreover, the findings show the potential of genetically manipulated RLKs to increase resistance towards phytopathogens (section 5.1.2). At the same time, the findings demonstrate the significance of appropriate controls when working with epitope-tagged proteins (section 4.6).

5.3.1 A C-terminal GFP epitope tag intensifies effects of the overexpression of LORE

As described in section 4.5, stable OE lines of LORE with various fusion proteins were established to use them for the identification of novel interacting partners, to investigate the influence of 3-HDA on protein abundance, localization, or characterization of specific roles of LORE in plant immune responses. However, the generation of stable homozygous OE lines of LORE-GFP was not successful. Two distinct morphologies were present in LORE-GFP lines, a wild type-like plant and a dwarfed plant (section 4.5.2, Figure 20). The severe dwarfism caused by the overexpression of LORE-GFP, but not LORE-HA, can be explained by the stomata development arrest phenotype detected in OE-GFP lines (section 4.5.2, Figure 20). Stomata differentiation is characterized by a series of asymmetric cell division events regulated by the one-cell spacing rule (Sachs, 1991). Meristemoid mother cells divide asymmetrically giving rise to two daughter cells. Eventually, the meristemoid cell differentiates into a guard mother cell which undergoes one symmetrical division resulting in a pair of guard cells (Zoulias *et al.*, 2018). OE-GFP lines seem to arrest in one of the early asymmetrical cell divisions of meristemoid cells. This phenotype is reminiscent of the reported phenotype of *At*MPK3 and *At*MPK6 OE lines which are characterized by rare events of asymmetric cell division and stomata differentiation (Wang *et al.*, 2007). Also, immune responses rely on the activation of the MAPK cascade *At*MEKK1, *At*MKK4/5, and *At*MPK3/6 (section 3.3.3). Constant activation of the MAPK cascade triggered by constitutively active LORE might be responsible for the pleiotropic effects on stomatal patterning or growth. The activation status of *At*MPK3 and *At*MPK6 was not investigated in OE-GFP lines due to the severe growth phenotype. In OE-HA lines, *At*MPK3 and *At*MPK6 show no constitutive activation, but enhanced activation upon treatment with 3-HDA compared to wild type (section 4.6.5, Figure 27). The number of normally developed stomata was counted in all OE lines and exclusively OE-GFP has a phenotype concerning stomata development (Supplementary Figure 4A). A reduced number of

stomata might lead to less gas exchange, less photosynthetic activity, and thus less energy available for growth and development. This raises the question why OE-GFP, but not OE-HA or OE-NT has a severe growth phenotype. All collected data within this work suggests that a C-terminal epitope tag has an influence on LORE receptor activation and signal attenuation. However, only OE-GFP lines have strong pleiotropic effects. This might be explained by the size of the epitope tag. GFP is 30 kDa whereas HA possesses just a few amino acids. Large epitope tags such as GFP might sterically hinder correct protein function (Georgieva *et al.*, 2015). The C-terminal fusion proteins of LORE possibly interfere with potential regulatory residues and the size of the fusion protein might influence the severity of this effect. As it turned out, while the study at hand was conducted, the used GFP in the OE lines is not monomeric and thus possesses an intrinsic ability to associate with other GFP proteins (Zacharias *et al.*, 2002). As discussed in more detail before, receptor homodimerization is crucial for LORE receptor activation (section 5.2). Therefore, the non-monomeric GFP could stabilize LORE ligand-independent homodimers causing constant receptor activation resulting in constant signaling detrimental for Arabidopsis growth and development (section 4.5, Figure 19). The artificial attachment of a C-terminal epitope tag was described to be problematic for other RLKs such as *At*FLS2 and *At*BAK1 (Hurst *et al.*, 2018, Ntoukakis *et al.*, 2011). Comparative analysis of *At*FLS2 fused to a variety of C-terminal epitope tags (GFP, MYC, HA) show a random behavior of the fusion proteins in tests of immune responses such as seedling growth inhibition, defense gene expression, and MAPK activation (Hurst *et al.*, 2018). In general, epitope tags can have an influence on correct localization, correct protein folding, and correct function. A study comparing the localization of proteins fused to GFP with their native forms revealed that 20% of them are mis-localized in mammalian cells (Stadler *et al.*, 2013). LORE fused to GFP or to mCherry co-localize at the plasma membrane in *N. benthamiana* (Ranf *et al.*, 2015). In the study at hand, two different epitope tags had an influence on the severity of the discovered phenotypes in OE lines, but showed always the same tendency and no arbitrary behavior (section 4.6). However, the here provided data emphasizes the effect an epitope tag can have on the biological function of an RLK. An influence on the biological function was also reported for complemented *bak1* mutants with *At*BAK1 fused to any C-terminal epitope tag (GFP, HA). *At*BAK1 with a C-terminal epitope tag is not fully functional in PTI signaling, but retains normal signaling competency in response to brassinosteroid (Ntoukakis *et al.*, 2011). The ligand-induced receptor complex formation with *At*FLS2 is not altered, but the C-terminal fusion protein negatively influences the production of ROS in response to flg22 treatment as well as seedling growth inhibition (Ntoukakis *et al.*, 2011). In contrast, the C-terminal fusion protein of LORE alters the signaling downstream of LORE in a positive way as the responses are not impaired, but increased. Changes in the kinetic of immune responses will be discussed below (section 5.3.2). Fan *et al.* (2018) generated OE lines of the SD-RLK *Os*SDS2-GFP and demonstrate that overexpression of *Os*SDS2-GFP causes a dwarfed growth phenotype in rice which is absent in overexpression lines of *Os*SDS2 without a fusion protein (Fan *et al.*, 2018). These findings match the results obtained for the OE-GFP and OE-

NT lines of LORE. The growth phenotype of OE-GFP plants can also be explained by the trade-off of growth and defense. The benefit-to-cost ratio is discussed in section 5.3.2, but constantly activated defense responses result in reduced growth. Other reports show likewise that the overexpression of RLKs such as *At*BAK1 leads to a severe dwarfed growth, leaf necrosis, and spontaneous cell death phenotype which was not detected in LORE OE lines (Kim *et al.*, 2017, Domínguez-Ferreras *et al.*, 2015). A third possibility for the growth phenotype is the potential of LORE to heterodimerize with other SD-RLKs. LORE under the control of the constitutive 35S promoter leads to expression of *LORE* in tissues where *AtLORE* expression is not common. The suspension of spatio-temporal regulated gene expression might result in receptor complexes which are not formed under wild type conditions. The ability to form heterodimers of SD-RLKs seems to be a general mode of action. Heteromeric interaction of SD-RLKs is found in rice as well as in Arabidopsis albeit only in experimental setups (Zou *et al.*, 2015, section 4.3.4). If heterodimerization is required for signal transduction in any signal pathway in wild type is not elucidated yet. But overexpressed LORE could form heteromeric interactions with other SD-RLKs resulting in activation or inhibtion of signal transduction involved in development processes or growth. This might also explain the other phenotypes of OE-GFP lines such as the abolishment of seed set and the increased stigma exsertion which prevents self-pollination (section 4.5, Figure 19). SRK of *Brassica* is involved in the avoidance of self-fertilization. Possibly also other SD-RLKs overtake regulatory roles in pollination and flower development. Thus it is conceivable that the expression of LORE in flower organs disturbs and influences pollination, flower architecture, and seed production. In contrast, then a more severe phenotype of OE-NT and OE-HA would be expected. Indications that the development and growth of OE-NT and OE-HA is changed compared to wild type are collected as described in section 4.5. However, the fusion of GFP intensifies the observed phenotypes. Domínguez-Ferreras *et al.* (2015) report that about 75% of *At*BAK1 overexpression plants die and that the seed production is reduced compared to wild type. In conclusion, overexpression of LORE, but also other signaling components, do not only improve defense signaling, but indicate that constant activation of defense exerts pleiotropic effects on different aspects of plant biology and impact the fitness of plants.

5.3.2 LORE overexpression enhances PTI outputs in response to 3-HDA, and the C-terminal epitope tag influences the kinetics of some signaling outputs

Typical PTI signaling outputs were investigated in OE lines to determine the influence of elevated LORE protein levels. The *AtLORE* transcript level was investigated upon application of 3-HDA which confirmed a high constitutive gene expression of *AtLORE* in OE lines and is the basis for the increased sensitivity of OE lines towards 3-HDA demonstrated within this study (section 4.5.3, Figure 21B). OE lines of *At*LORE respond with seedling growth inhibition if grown on media supplemented with 3-

HDA (section 4.6.1, Figure 23). Eventually, long-term exposure of OE lines to 3-HDA is lethal, but Col-0^{Aeq} shows no seedling growth inhibition in response to 3-HDA. Recently, inhibition of root growth in response to LPS was reported by Shang-Guan *et al.* (2018). They report a 50% reduction of the primary root length of wild type treated with LPS compared to water-treated wild type. This finding contradicts the here presented data and previous experiments where no inhibition was detected in response to LPS/3-HDA in wild type (personal communication Dr. Ranf, TU München, section 4.6.1, Figure 23). This variation might be reasoned by different LPS concentrations used for the experiments. However, Shang-Guan *et al.* (2018) did not use *lore*-1 as a negative control. Here, OE lines, but not wild type, react with a circa 50% reduction of the root growth in response to 3-HDA. The presented findings for the OE lines upon treatment with 3-HDA are similar to observations of seedling growth inhibition in response to treatment with peptides such as flg22 or elf18 (Zipfel *et al.*, 2006, Gómez-Gómez *et al.*, 1999). Defense responses correlate with high metabolic costs and usage of resources, and nutrients primarily dedicated to other processes need to be allocated to sustain defense responses (Züst *et al.*, 2015, Huot *et al.*, 2014, Tian *et al.*, 2003). The transcription factor *At*BZR1 (BRASSINAZOLE-RESISTANT 1) is involved in the trade-off of growth and defense (Lozano-Durán *et al.*, 2013). *At*BZR1 is a target of brassinosteroid signaling mediated by *At*BRI1 and induces the expression of genes suppressing PTI in response to brassinosteroid (Lozano-Durán *et al.*, 2013). Recently, activation of *At*BZR1 was shown to be dependent on oxidation *via* hydrogen peroxide (Tian *et al.*, 2018). Possibly, constant activation of PTI responses in LORE OE lines, particular in OE-GFP, such as ROS production will result in activation of *At*BZR1 or proteins with a similar function which initiates a shift in the trade-off of growth towards defense. This hypothesis is endorsed by the finding that PTI marker genes such as *AtNHL10* and *AtFRK1* are constitutively expressed in OE lines and expression is further induced by the application of 3-HDA (section 4.6.1, Figure 23). Similarly, overexpression of *At*BAK1 leads to a growth phenotype and is reported to constitutively induce *AtNHL10* and *AtFRK1* expression (Domínguez-Ferreras *et al.*, 2015). Regulation of the protein level of activated RLKs is critical to prevent inappropriate signaling and attenuate signaling to keep the plants responsive to a succeeding pathogen invasion and evade effects on growth and development (Robatzek *et al.*, 2006). However, no clear influence of 3-HDA application was observed on the LORE-HA level (section 4.5.3, Figure 21). In contrast, changes in the protein abundance of *At*FLS2 in response to flg22 treatment are detected in a time-dependent manner (Smith *et al.*, 2014, Beck *et al.*, 2012). Smith *et al.* (2014) report that 60 min upon flg22 treatment reelicitation with flg22 is not possible and this goes along with *At*FLS2 degradation (Robatzek *et al.*, 2006). Resensitization correlates with the *de novo* synthesis of *At*FLS2 (Smith *et al.*, 2014). The constitutive high LORE-HA level potentially covers putative degradation of LORE-HA and an immunoblot might not be sensitive enough to detect subtle changes in the protein level. OE-GFP and CL-GFP lines were not feasible to use as LORE-GFP protein was not detected in total protein extracts, but only in immunoprecipitated samples (section 4.5.2, Figure 20). This finding suggests a high turn-over of LORE-GFP protein.

Surprisingly, also free GFP was detected in immunoprecipitated samples of OE-GFP indicating that the GFP epitope tag is cleaved off resulting in less LORE-GFP detected on the immunoblot. Cleavage of a C-terminal epitope tag is also reported for *At*FLS2-3xMYC (Hurst *et al.*, 2018). However, the biological reason remains elusive. Antibodies specifically recognizing endogenous *At*LORE will enable the detection of intrinsic wild type protein accumulation as it was done for *At*FLS2 (Smith *et al.*, 2014). This will provide better evidence for the *At*LORE regulation in the plant-bacteria interaction. The investigation of other PTI signaling outputs revealed that OE lines respond with enhanced $[Ca^{2+}]_{cyt}$ elevation to the application of 3-HDA in comparison to wild type (section 4.6.1, Figure 22). Differences are detected in the initiation and in the attenuation of signaling. The on-set is more rapid and the maximum is earlier reached, but the decline of the response is slower. The $[Ca^{2+}]_{cyt}$ elevation of OE-NT is higher compared to OE-HA and OE-GFP lines, showing that the C-terminal epitope tag influences also full signal activation. The difference of C-terminal epitope-tagged lines and lines without fusion protein becomes most evident in the altered ROS kinetic (section 4.6.2, Figure 24). OE-NT lines have a greatly elevated first ROS burst compared to wild type, OE-HA, and OE-GFP lines. However, OE-HA and OE-GFP lines possess a strongly enhanced and prolonged second ROS burst which can last up to 6 h. This second ROS burst is also detected in complementation lines of LORE under the control of the endogenous promoter pLORE with a C-terminal epitope tag, but not in complementation lines without a fusion protein. Conclusively, the biphasic ROS burst arises not only from a high *LORE* dosage, but is modulated by the presence of a C-terminal epitope tag. In literature, a biphasic ROS burst is associated with the manifestation of defense responses. The first ROS burst is unspecific in response to various stresses and associated to PTI. The second ROS burst is required for the establishment of the HR (Torres *et al.*, 2005, Grant *et al.*, 2000, Lamb *et al.*, 1997). The establishment of HR was shown to rely on ROS predominantly produced in chloroplasts. Chloroplasts produce, together with mitochondria, the majority of ROS in plants (Zurbriggen *et al.*, 2010, Zurbriggen *et al.*, 2009, Torres *et al.*, 2005). The application of catalase and superoxide dismutase diminishes the second burst of OE-HA suggesting that the source of the ROS in OE lines is apoplastic, most likely produced by *At*RBOHD (section 4.6.3, Figure 25). The first ROS burst is also abolished in *rbohd* in response to LPS/3-HDA as previously published by Ranf *et al.* (2015) supporting the here presented findings. The occurrence of the second ROS burst in *rbohd* in combination with *LORE* overexpression was not investigated. Also, the ROS formation in chloroplasts of OE lines was not addressed in this study at hand. However, a recent report of Shang-Guan *et al.* (2018) demonstrate a partially *At*LORE-dependent ROS burst succeeding the first after several hours originating from chloroplasts in response to treatment with LPS, but not flg22. The second ROS burst is independent from the first ROS burst and conserved among dicots and monocots (Shang-Guan *et al.*, 2018). Both biphasic ROS bursts reported by Shang-Guan *et al.* (2018) and the study at hand differ in the described kinetic, the time of occurrence, the duration, and in the source of ROS production. That is why both biphasic ROS bursts are most likely not linked to each other. Crosses of OE lines

and *rbohd* loss-of-function mutants will conclusively resolve the source of the biphasic oxidative burst in OE lines. Interestingly, direct infiltration of *Pto* DC3000 or 3-HDA in leaves did not result in cell death or HR in OE lines indicating that the second ROS burst does not induce a HR (data not shown), but is rather the result of a changed regulation of LORE. Elevated ROS levels are also described for the OE lines of *Os*SDS2 even in uninfected plants (Fan *et al.*, 2018). Enhanced generation of ROS, but no biphasic kinetics, was detected in OE lines from *Os*SDS2 without a fusion protein in response to chitin and flg22 (Fan *et al.*, 2018). Unfortunately, the ROS production of OE lines from *Os*SDS2-GFP were not examined and no general correlation of SD-RLKs fused to an epitope tag and the occurrence of a biphasic ROS can be drawn. Here, the biphasic ROS burst in OE-HA and OE-GFP from Arabidopsis is specific to the treatment with 3-HDA and not detected upon treatment with chitin or flg22 (section 4.6.2, Figure 24). The overexpression of the PRR *At*EFR-GFP using the ubiquitin promoter of maize in rice results also in a prolonged and enhanced ROS burst in response to elf18 (Schwessinger *et al.*, 2015). This ROS burst lasts 2 h, but is not comparable in its kinetic to the biphasic ROS burst observed in OE-HA and OE-GFP (Schwessinger *et al.*, 2015). It was previously demonstrated that ROS production and $[Ca^{2+}]_{cyt}$ elevation are interconnected (Dubiella *et al.*, 2013, Ranf *et al.*, 2011). The delayed decline of the $[Ca^{2+}]_{cyt}$ elevation in OE-HA and OE-GFP might positively influence the ROS burst. For this reason, it will be interesting to analyze if the inhibition of cytosolic calcium influx has a negative influence on ROS production and especially on the second oxidative burst of OE-HA and OE-GFP. The here provided evidence of the changed kinetics of the oxidative burst and the $[Ca^{2+}]_{cyt}$ elevation in OE-HA indicate that signal attenuation is disturbed by the C-terminal epitope tag of LORE. This raises the question how *At*LORE signaling is regulated and attenuated. As described in section 3.5, RLK activity is controlled by phosphorylation and signal attenuation can be achieved by the ubiquitylation and subsequent protein degradation. In literature, PUBs are discussed to be involved in signal attenuation and mutants of PUBs show also an enhanced ROS burst (Lu *et al.*, 2011, Trujillo *et al.*, 2008). Therefore, the *pub22/23/24* mutant was tested and shown to exhibit a biphasic ROS in response to 3-HDA comparable to OE-HA (section 4.6.4, Figure 26). *At*PUB22 is regulated by *At*MPK3 and targets downstream signaling components such as Exo70B2 to deplete immune signaling (Stegmann *et al.*, 2012). Also, *mpk3-1* exhibits the second ROS burst more strongly compared to wild type when treated with 3-HDA, but not with other elicitors (Supplementary Figure 7C). The attenuation of the ROS burst induced by *At*LORE seems to be mediated by *At*PUB22/23/24 and *At*MPK3. The mutant *pub22/23/24* show elevated ROS level in response to other ligands such as flg22 and chitin, but a biphasic ROS burst is exclusively detected in response to 3-HDA (Trujillo *et al.*, 2008, section 4.6.4, Figure 26). This indicates that *At*LORE signaling is controlled in a different way than *At*FLS2 signaling, but *At*PUB22/23/24 seem to act downstream of both RLKs. Another pair of PUBs, *At*PUB25/26, regulate the activity of *At*BIK1 important for the initiation of the generation of apoplastic ROS (Wang *et al.*, 2018, section 3.3.3). The *At*BIK1 level is increased in *pub25/26*, but also in *pub22/23/24* mutant plants which might be the

reason for the elevated oxidative burst (Wang *et al.*, 2018, Trujillo *et al.*, 2008). The ROS kinetic of *pub25/26* is not shown and was not investigated in response to 3-HDA, but should be analyzed to obtain more evidence on downstream signaling components involved in *At*LORE signaling. Elevated *At*BIK1 protein levels and the occurrence of the second ROS burst triggered by 3-HDA could coincide. Other PUBs such as *At*PUB12 and *At*PUB13 ubiquitinate PRRs to regulate their activity (Liao *et al.*, 2017, Yamaguchi *et al.*, 2017, Lu *et al.*, 2011, section 3.5). In an untargeted yeast two hybrid screening, conducted within the study at hand, *At*PUB14 was found as a putative interacting protein of LORE (unpublished). Interaction of the ARM domain of *At*PUB14 and *At*LORE was also shown by Samuel *et al.* (2008) who demonstrates the association of various *At*SD-RLKs with a range of *At*PUB proteins. They conclude that the interaction of PUBs and SD-RLKs illustrates a conserved signal pathway in Arabidopsis. In fact, also SRK associates with the PUB ARC1 underpinning this hypothesis (Gu *et al.*, 1998). In addition to this, it was shown that *Os*SDS2 is ubiquitinated by *Os*SPL11, an E3 ligase similar to *At*PUB13 (Fan *et al.*, 2018). *At*PUB14 is also related to *At*PUB12/13 and thus might likewise be involved in signal attenuation and direct regulation of *At*LORE (Azevedo *et al.*, 2001). Some PUBs such as *At*PUB12/13 and the homolog of rice *Os*SPL11 directly control activity of PRRs. Other PUBs such as *At*PUB22/23/24 and *At*PUB25/26 control the activity of downstream signaling components. Considering the fact that a C-terminal epitope tag is hindering signal attenuation, it is likely that the epitope tag covers or impedes binding sites of interaction partners at the C-terminus. Within the kinase domain of LORE 11 putative ubiquitylation sites are predicted by similarity by UbPred (Radivojac *et al.*, 2010, accessed January 09, 2019). The domain of unknown function 3403 (DUF3403) is located at the very C-terminus of *At*LORE and contains Lys769, a predicted ubiquitylation site (Supplementary Figure 10). Site-directed mutagenesis of this residue might outline critical regulatory sites and generate phenocopy mutants of OE-HA. Interestingly, DUF3403 possesses another regulatory site, a highly scored putative 14-3-3 protein binding site with the predicted phosphorylated Thr752 (AVDRPN[T]LQVL) (personal communication Dr. Müller, TU München, Supplementary Figure 11). 14-3-3 proteins overtake regulatory roles in the plant immune response and the occupation of 14-3-3 binding sites of *At*FLS2 by the application of a chemical disruptor resulted in diminished ROS burst in response to flg22 in Arabidopsis (Lozano-Durán *et al.*, 2015, Lozano-Duran *et al.*, 2014). 14-3-3 proteins target phosphorylated and thus activated proteins like RLKs and modulate the interaction with other proteins or prevent protein degradation (Lozano-Durán *et al.*, 2015). Conceivably, 14-3-3 proteins bind to LORE, but the C-terminal epitope tag impedes interaction with other proteins and in this way prevents ROS signal attenuation. To determine if the DUF3403 contains important regulatory sites, functional analysis of a truncated variant of LORE lacking DUF3403 (LORE-dD) will be worthwhile. A non-tagged LORE-dD hopefully sheds light on the question if mal-regulation of DUF3403 causes the enhanced second ROS burst. Besides ubiquitination, also phosphorylation is an important regulatory tool. As described and discussed in section 5.2 and section 5.2.2, phosphorylation is a vital mechanism to activate receptor complexes and

to regulate activity in plant immunity. LORE-Km variants mutated in the ATP-binding site are unable to trigger downstream signaling when treated with 3-HDA or LPS showing the importance of phosphorylation events to translate external stimuli into immune outputs in *At*LORE-dependent signaling (Ranf *et al.*, 2015). ROS production in response to flg22 is initiated by a phosphorylation cascade downstream of *At*FLS2 (section 3.3.3). *At*BIK1 requires phosphorylation in the interaction with *At*FLS2 and *At*BAK1 to activate *At*RBOHD by phosphorylation (Kadota *et al.*, 2014, Li *et al.*, 2014, Lu *et al.*, 2010, Zhang *et al.*, 2010). Also *At*CERK1 relies on *At*BIK1, seemingly a commonly shared signaling component maybe also for *At*LORE (Zhang *et al.*, 2010). However, OE-HA induces ROS signaling as fast as OE-NT, and therefore, activation of downstream signaling components such as *At*BIK1 by phosphorylation seems not to be impaired, but experimental proof is missing. With *pub22/23/24* and *mpk3-1*, two independent mutant lines showing a similar phenotype as OE-HA/OE-GFP have been identified. Therefore, the effect seen in OE-HA/OE-GFP is not just an artifact, but has biological relevance. Fortunately, the C-terminal epitope tag specifically changes LORE signaling. The loss-of-function mutants *pub22/23/24* and *mpk3*, on the other hand, have pleiotropic effects as they are disturbed in a variety of processes and function also downstream of other PRR complexes. This makes OE-HA a good tool to analyze specifically the effect of prolonged LORE signaling when activated with 3-HDA. Other immune outputs such as the activation of MAPKs, the production of ethylene, seedling growth inhibition, and the induction of defense gene expression are not obviously differentially regulated between OE lines carrying a C-terminal epitope tag or OE lines without an epitope tag (section 4.6.5). *At*MPK3 and *At*MPK6 activation is enhanced in OE lines in comparison to wild type upon 3-HDA treatment. This is also detected for *pub22/23/24* in response to LPS/3-HDA (section 4.6.5, Figure 27B). MAPKs regulate signal transduction in plant immunity (Meng *et al.*, 2013). The induction of *AtFRK1* is directly dependent on MAPK signaling (Boudsocq *et al.*, 2010, Asai *et al.*, 2002). In OE-HA and OE-NT, *AtFRK1* is constitutively expressed (section 4.6.5, Figure 28). Activation of *At*MPK3 and *At*MPK6 modulates also the production of ET by phosphorylation of *At*ACS resulting in higher ET accumulation (Liu *et al.*, 2004, Figure 27C). The ET production in OE lines is clearly induced, but differences in OE-HA and OE-NT are not evident. This supports the hypothesis that these signal outputs are not influenced by a C-terminal epitope tag indicating the implementation of differential signaling cascades and control mechanisms compared to the generation of ROS or the changes is $[Ca^{2+}]_{cyt}$ level (section 4.6, Figure 22 and Figure 24). It remains largely unknown which specific signaling components are activated to induce and regulate downstream signaling of PRRs (Couto *et al.*, 2016, section 3.3.3). In particular, downstream signaling components of *At*LORE are elusive and more knowledge of these will help to explain the observed phenotypic differences of OE-HA and OE-NT lines.

5.3.3 OE-HA is more resistant to spray infection with *Pto* DC3000

For the investigation of the effect of elevated immune outputs onto the direct interaction with *Pto* DC3000, bacterial growth assays were performed (section 4.7, Figure 29 and Figure 30). The assessment of bacterial growth upon direct infiltration of *Pto* DC3000 into the leaf apoplastic space of OE-HA, OE-NT, *lore*-1, and Col-0^{Aeq} revealed no enhanced resistance of OE lines. Bacterial titers in the apoplastic space of *lore*-1, OE-HA, OE-NT, and wild type are comparable indicating that the elevated PTI outputs do not render Arabidopsis more resistant. Infiltration experiments deliver information about the status of post-invasive immunity. Seemingly, the shown elevated apoplastic defense responses are not sufficient to reduce the bacterial titer in the apoplast of OE lines. Intriguingly, when *Pto* DC3000 is sprayed onto the leaf surface differences among OE-HA, OE-NT, *lore*-1, and Col-0^{Aeq} are observed. Spray inoculation mimics the natural way of infection as leaf-associated bacteria need to invade the leaf apoplast *via* wounds or stomata. Therefore, conclusions about the status of pre-invasive immunity can be drawn from surface-inoculation experiments. On day 0 less bacteria are present in the apoplast of OE-HA, but not of OE-NT, *lore*-1, or wild type 4 h after inoculation. This trend continues on day 3, less bacteria are present in the OE-HA apoplast compared to OE-NT, *lore*-1, and wild type. Different roles in pre- and post-invasive immunity is also described for other PRRs. Zipfel *et al.* (2004) report that *fls2* mutants are as susceptible as wild type upon direct infiltration of *Pto* DC3000 into the apoplast, but are more susceptible than wild type upon spray inoculation. Other studies support this finding attributing a crucial role to *At*FLS2 in the pre-invasive immune response of Arabidopsis (Zeng *et al.*, 2010, Melotto *et al.*, 2006, Zipfel *et al.*, 2004). In contrast, contradicting results are published for mutants of the PRR *At*EFR. Saijo *et al.* (2009) demonstrate that the bacterial titer is higher in the apoplastic space of *efr*-1 compared to wild type 3 days post spray infection. Nekrasov *et al.* (2009), on the other hand, do not observe a susceptibility phenotype of *efr*-1 upon spray inoculation with *Pto* DC3000. Differences might be explained by different experimental conditions (Nekrasov *et al.*, 2009, Saijo *et al.*, 2009). The participation of *At*FLS2 in stomatal immunity is supported by expression analysis showing strong *AtFLS2* expression in guard cells (Beck *et al.*, 2014). For *At*LORE, a role in pre-invasive immunity was published by Ranf *et al.* (2015). *lore*-1 mutants are more susceptible upon spray inoculation of *Pto* DC3000 compared to Col-0^{Aeq}. The expression pattern of LORE-GFP in CL lines was not conclusive, but Genevestigator expression data support the fact that *AtLORE* is strongly expressed in guard cells (Hruz *et al.*, 2008, section 4.5.2, Figure 20, accessed January 07, 2019). The suggested role of *At*LORE in pre-invasive immunity is substantiated by the here provided data. The susceptibility phenotype of *lore*-1, but also the enhanced resistance of OE-HA upon spray inoculation of *Pto* DC3000 reinforce the attributed role of LORE in pre-invasive immunity (Ranf *et al.*, 2015). Ranf *et al.* (2015) demonstrated further that LPS pre-treatment rendered wild type more resistant to subsequent infection with *Pto* DC3000 *via* syringe infiltration compared to *lore*-1. However, OE lines of LORE are not more resistant in the study at hand in infection assays upon direct infiltration of the bacterial suspension.

The successful mitigation of Arabidopsis immune responses by *Pto* DC3000 might be the reason that LORE OE lines, despite the significantly enhanced PTI responses, are not more resistant to the syringe inoculation of *Pto* DC3000 (section 4.7, Figure 29A). *Pto* DC3000 is a full virulent bacterial strain releasing a range of effector proteins and phytotoxins to suppress immune responses of the plant (Wei *et al.*, 2017, Boller *et al.*, 2009, Jones *et al.*, 2006, section 3.7). Göhre *et al.* (2008) report that *Pto* DC3000 lacking the effector proteins AvrPto and AvrPtoB are comprised in their virulence upon infiltration into the apoplast of Arabidopsis (section 3.7.1). A reduced bacterial titer upon direct infiltration of *Pto* ΔAvrPtoΔAvrPtoB indicates efficient apoplastic immunity of Col-0 when it is not down regulated by the pathogen (Göhre *et al.*, 2008, He *et al.*, 2006). Bacteria impaired in the produced number of, or the release of effector proteins become non-virulent (Xin *et al.*, 2016, Cunnac *et al.*, 2011, Roine *et al.*, 1997). Interference of effector proteins with immunity was shown at all levels of PTI. Reports describe the direct inactivation of PRRs, inactivation of MAPKs, interference with RLCK signaling, or disruption of the plant hormone homeostasis (Wei *et al.*, 2017). Although PTI outputs are enhanced and prolonged in LORE OE lines, *Pto* DC3000 may still suppress the induced immune responses showing the powerfulness of a successful pathogen. Therefore, it will be interesting to perform bacterial infection assays using direct infiltration with non-virulent strains such as *Pto* DC3000 hrc$^-$ which is less virulent, but still able to induce stomatal closure, or *Pto* DC3000D28E deficient in 28 effector proteins (Cunnac *et al.*, 2011, Melotto *et al.*, 2006). Then the undisguised effect of an enhanced LORE dosage will become evident and can be used to better understand the versatile roles of *At*LORE in immune responses of Arabidopsis. In spite of that, the reduced bacterial titer in the apoplastic space of OE-HA upon spray-inoculation might be explained on the basis of two hypotheses. First, the invasion success of bacteria is negatively influenced, or second, the bacterial survival on the leaf surface and in the leaf apoplast of OE-HA is changed in comparison to the other plant lines. *Pto* DC3000 survival on the leaf surface is reported to be rather weak and bacterial multiplication occurs preferentially in the apoplastic space (Boureau *et al.*, 2002). Boureau *et al.* (2002) investigated the survival of *Pto* DC3000 populations on the leaf surface of tomato in a time-dependent manner. Already after 24 h most bacterial cells on the leaf surface are dead, but interestingly after 96 h a reappearance of living cells, concomitant with the appearance of symptoms on the leaf, is detected (Boureau *et al.*, 2002). Here, the bacterial titer on the leaf surface in comparison to the leaf apoplast was investigated 3 h upon spray inoculation (section 4.7.2, Figure 30B). The bacteria present on the leaf surface are equal among all plant lines. No significant difference is observed comparing the bacterial titer of OE-HA with and without surface sterilization. This indicates that the survival of *Pto* DC3000 on the leaf surface or the apoplast of OE-HA is not changed. Notably, this experiment was repeated twice and subtle changes in the bacterial titer might not become obvious. Moreover, the chosen time point of 3 h coincides with the induction of stomata reopening induced by *Pto* DC3000. Therefore, differences might first become obvious after 4 h as seen in the spray infection assays (Melotto *et al.*, 2006, section 4.7, Figure 29). Comparison of the bacterial titers present in the apoplast

of OE-HA at day 0 and day 3 in spray infection assays indicates that multiplication of *Pto* DC3000 is not compromised in the apoplast which is in line with the presented results from infiltration assays showing equal bacterial titers in the apoplasts of all plant lines (section 4.7.1, Figure 29). Despite, bacterial titers present in the apoplast of OE-HA at day 0 are reduced compared to the bacterial titers present in the apoplast of wildtype, *lore*-1, and OE-NT upon spray-infection (section 4.7.1, Figure 29). This finding indicates that the bacterial entry into the apoplast of OE-HA is rendered. The limitation of bacterial invasion by the plant is an effective strategy to reduce the bacterial infection success (section 3.2 and section 3.3). Phytopathogenic bacteria invade the plant interior *via* wounds or stomata, plants close their stomata as a countermeasure in response to a pathogen attack (section 3.4). Seemingly, OE-HA prevents the bacterial entry more efficient than OE-NT, wild type, and *lore*-1 as the bacterial survival is not changed. This leads to the assumption that OE-HA differentially regulates the stomatal aperture in response to the detection of *Pto* DC3000. *Pto* DC3000 produces the phytotoxin COR to hijack the JA-Ile signaling pathway to eventually induce reopening of stomata initially closed by the plant (section 3.4). A reopening of stomata induced by the pathogen can be observed about 3 h after spray inoculation. It is known that COR deficient mutants are reduced in their virulence (Brooks *et al.*, 2004, Mittal *et al.*, 1995). Melotto *et al.* (2006) linked the phytotoxin COR to the induction of stomata reopening. Because *At*LORE seems to play a role in an early stage of infection, bacterial spray infection assays with *Pto* DC3000 COR^{-} were performed and revealed that reduced bacterial titers are present at day 0 in the apoplast of OE-HA and, using the less virulent *Pseudomonas* strain, also in OE-NT. The lost ability to reopen stomata discloses an effect of enhanced LORE levels in OE-NT. This finding is in line with the here presented data consistently showing a difference of C-terminal epitope-tagged OE lines to OE-NT lines. Overexpression of LORE in OE-HA and OE-NT, which was shown to have comparable gene dosages, has different effects on the plant–pathogen interaction possibly by the changed LORE activation pattern which is modulated by the presence of a C-terminal epitope tag (section 4.6.1, Figure 21B).

5.3.4 Overexpression lines differentially regulate stomatal closure in response to 3-HDA

A variety of MAMPs is reported to induce stomatal closure as part of the pre-invasive immune response including also LPS (Melotto *et al.*, 2006). Usually, measurements of the stomatal aperture are performed to illustrate changes in stomatal immunity (Yekondi *et al.*, 2017, Guzel Deger *et al.*, 2015, Lozano-Duran *et al.*, 2014, Zeng *et al.*, 2010, Melotto *et al.*, 2006). In the study at hand, a different approach was chosen and thermal imaging was performed to detect differences in the stomatal defense of LORE OE lines compared to wild type and *lore*-1 (section 4.7.3, Figure 31). Changes of the leaf temperature reflect changes in the status of the stomatal aperture. Thermal imaging is a non-invasive method measuring leaf temperature changes of leaves still attached to the plant which

resembles the natural condition. The measurement of stomatal aperture, on the other hand, is performed using microscopic evaluation of epidermal peels or detached leaves treated with MAMPs or bacteria at a specific time point (Guzel Deger *et al.*, 2015, Chitrakar *et al.*, 2010, Melotto *et al.*, 2006). Thermal imaging enables a dynamic observation of the stomatal aperture in a virtually high-throughput screening in response to various stimuli in direct comparison to each other. Another advantage is that a bias is circumvented as stomata are not directly selected by the scientist for the measurement of the width of the stomatal aperture, but the average of a complete leaf is elaborated. Important to note is that not all stomata of one leaf react in the same way e.g. with closure in response to a challenge (Melotto *et al.*, 2006). Therefore, using several leaves of individual plants decreases the risk of being biased in the choice of stomata to measure. The thermal imaging experiments showed that OE-HA and OE-NT have a constitutive elevated temperature compared to wild type and *lore*-1. A higher leaf temperature could also be caused by a reduced number of stomata. The number of stomata per leaf area was counted in OE lines and did not reveal any difference for OE-HA, OE-NT, wild type, and *lore*-1, but for OE-GFP (Supplementary Figure 4A). Reasons are discussed in section 5.3.1. An enhanced temperature based on fewer stomata and as a consequence enhanced resistance can therefore be excluded. Nonetheless, fewer stomata on the leaf surface can also be a strategy to reduce the colonization of pathogens (Ramos *et al.*, 1987). The enhanced leaf temperature of OE lines might be caused by a general reduced stomatal aperture compared to wild type. Morphological differences of stomata in OE lines compared to wild type were not yet investigated. The application of 3-HDA leads to a significantly enhanced temperature elevation of OE-HA and OE-NT compared to wild type indicating that OE-HA and OE-NT induce stomatal closure upon a challenge with 3-HDA. This finding shows that OE lines differentially regulate the stomatal aperture upon sensing of 3-HDA compared to wild type. This is further supported by the finding that pre-treatment of 3-HDA reduces the invasion success of bacteria into the apoplastic space of OE-HA, OE-NT, but also wild type (section 4.7.4, Figure 32). This shows that a specific challenge of LORE with 3-HDA is able to reduce bacterial colonization of the apoplast in OE lines and even wild type, presumably, by the initiation of stomatal closure. Interestingly, changes in the stomatal aperture of wild type upon treatment with 3-HDA do not translate into a detected leaf temperature increase. Nonetheless, these findings together with the results from the infection assays (section 5.3.3) support an important role of *At*LORE in pre-invasive immunity.

5.3.5 How do overexpression lines confine bacterial entry?

An increasing body of evidence supports the hypothesis that OE-HA and OE-NT differentially regulate stomatal aperture and thus limit the amount of bacteria colonizing the leaf interior (section 4.7). Interestingly, OE-NT requires a challenge with 3-HDA to confine bacterial invasion or infection of a less virulent bacterial strain, showing again a biological difference between OE-NT and OE-HA

based on the presence of a C-terminal epitope tag (section 4.7.4, Figure 32). This raises the question how OE lines confine bacterial entry to the leaf interior. ROS generated by *At*RBOHD is a prerequisite for stomatal closure in response to infection, but also drought stress (Li *et al.*, 2014, Sirichandra *et al.*, 2009, Kwak *et al.*, 2003, section 3.4). And as presented in section 4.6.2, OE-HA lines have an outstanding differentially regulated biphasic ROS burst compared to OE-NT and wild type. The importance of ROS in the establishment of stomatal immunity is supported by the finding that COR inhibits guard cell-specific ROS production by NADPH oxidases and in this way prevents stomatal closure (Toum *et al.*, 2016). OE-NT has a greatly elevated ROS burst compared to wild type, but no enhanced resistance upon spray infection with a full virulent *Pseudomonas* strain. OE-HA, on the other hand, has a greatly prolonged ROS burst which leads to enhanced resistance upon spray infection. The prolonged biphasic ROS burst can last up to 6 h in OE-HA (section 4.6.2, Figure 24). This time frame covers the by *Pto* DC3000 induced reopening of stomata which occurs 3 h upon inoculation (Melotto *et al.*, 2006). OE-HA seems to be more persistent against countermeasures of *Pto* DC3000 such as the reopening of stomata as a consequence of the elongated biphasic ROS. Unfortunately, Toum *et al.* (2016) do not show which effect the inhibition of ROS in stomata has on the colonization success of *Pto* DC3000. However, they show that the flg22-induced ROS burst is specifically impaired by COR in guard cells, but not in leaf discs (Toum *et al.*, 2016). In future experiments it will be important to distinguish if a ROS burst in guard cells of OE-HA is also modulated in a way detected for the apoplastic ROS compared to OE-NT and wild type (section 4.6.2, Figure 24). The hypothesis that the strongly prolonged ROS burst endorses stomatal closure in OE-HA is also in accordance with the findings from OE-NT infection assays using the COR-deficient *Pseudomonas* strain (section 4.7.2, Figure 30A). The lack of suppression of stomatal immunity and putatively the lack of suppression of the ROS burst in stomata by COR results in a reduced bacterial titer in the apoplast at day 0 in OE-HA and OE-NT. Also, a challenge with 3-HDA, specifically addressing LORE signaling and inducing ROS signaling, leads to a reduced bacterial titer in the apoplastic space of OE-NT and OE-HA as well as wild type at day 0 (section 4.7.4, Figure 32). This finding indicates that the PTI responses induced during the plant–pathogen interaction are not as strong compared to the specific trigger with 3-HDA. The application of *Pto* DC3000 shows an increase, but no significant elevation of the leaf temperature from OE-NT, OE-HA, wild type, and *lore*-1 (section 4.7.3, Figure 31). In consideration of the leaf temperature changes of OE-HA and OE-NT seen in 3-HDA spray assays a higher change in leaf temperature in OE lines was expected. Nevertheless, the used concentration of 3-HDA used in the thermal imaging spray assay most likely does not resemble the concentration of 3-HDA released by *Pto* DC3000 during the plant-pathogen interaction. It will be crucial to repeat the spray assay with *Pto* DC3000 COR^{-} to determine the real effect of LORE without suppression by the pathogen. Important to note, *At*FLS2 is present in the genetic background of all plant lines used in this study and *At*FLS2 functions in stomatal closure (Zeng *et al.*, 2010, Melotto *et al.*, 2006, Zipfel *et al.*, 2004). Melotto *et al.* (2006) report that LPS-induced stomatal closure is

independent of *At*FLS2 which is in line with the study of Ranf *et al.* (2015) showing that *lore*-1 remains responsive to flg22 (section 4.6.2, Figure 24). However, it is conceivable that no significant temperature change in response to inoculation with *Pto* DC3000 of *lore*-1, wild type, OE-NT, and OE-HA was detected because of the recognition of other MAMPs such as flg22. *At*FLS2 induces, in general, stronger immune responses in comparison to chitin or 3-HDA represented for example in a higher amplitude of the ROS peak or longer activation of MAPKs (Shang-Guan *et al.*, 2018, Figure 24, Figure 27A). Interestingly, the treatment of 3-HDA on Col-0^{Aeq} did not result in a significant leaf temperature increase (section 4.7.3, Figure 31), but pre-treatment with 3-HDA decreased bacterial colonization of the apoplast of wild type (section 4.7.4, Figure 32). Subtle changes in the stomatal aperture might not translate to detectable changes in leaf temperature using thermal imaging. Then, measurements of the stomatal aperture might be beneficial. To evaluate the potential of thermal imaging as a standard method to investigate stomatal immunity, a more comprehensive study defining the limitations of the method is required. Nonetheless, previously published and the here provided data support the critical role of *At*LORE in pre-invasive immunity. The question remains, how the effective closure of stomata results in a reduced amount of bacterial titers in the apoplast of OE lines. Melotto *et al.* (2006) show that *Pto* DC3000 accumulates around open stomata rather than closed stomata. This is complemented by other studies showing aggregation of bacteria around sites with nutrient and water supply (Monier *et al.*, 2004, Mansvelt *et al.*, 1989). Speculatively, a reduced stomatal aperture in OE lines attracts less bacterial cells. But how does *Pto* DC3000 differentiates between open and closed stomata? As described in the introduction section 3.6, bacteria defective in their motility or chemotaxis are less virulent (Taguchi *et al.*, 2006, Yao *et al.*, 2006, Ichinose *et al.*, 2003, Tans-Kersten *et al.*, 2001). One hypothesis is that the reduced stomatal aperture in OE lines results in less leakage of nutrients and therefore less attraction of bacterial cells subsequently leading to a reduced amount of bacteria in the apoplastic space. Bacterial infection assays using *Pseudomonas* strains with impaired motility or chemotaxis will help to verify or falsify this hypothesis.

5.3.6 What is stomatal defense?

As discussed in section 5.3.5, OE lines effectively limit bacterial entry most likely by enhanced stomatal defense characterized by stomatal closure in response to the detection of pathogens. Taking a closer look into literature, a timely gap attracts attention. Stomatal aperture is often measured after 2 to 3 h of treatment with a MAMP or bacteria as this corresponds to the time point of stomata reopening reported by Melotto *et al.* (2006) (Su *et al.*, 2017, Yeh *et al.*, 2015, Montillet *et al.*, 2013, Zeng *et al.*, 2010, Melotto *et al.*, 2006). Bacterial growth, on the other hand, is in most studies presented at 2 or 3 days post spray infection (Yeh *et al.*, 2015, Montillet *et al.*, 2013, Zeng *et al.*, 2010, Melotto *et al.*, 2006, Zipfel *et al.*, 2004). A critical role in stomatal immunity is attributed to *At*FLS2. However, the resistance becomes obvious 3 days post infection whereas the induction of stomatal closure and the reopening triggered by *Pto* DC3000 are executed within the first hours of infection.

This raises the question if the definition of stomatal defense is concise enough. For this reason, it would be critical to determine the bacteria entering at day 0 to draw conclusions if less bacteria can invade or if bacterial multiplication in the apoplast is efficiently prevented over time which would count to post-invasive defense responses (Doehlemann *et al.*, 2013, Sawinski *et al.*, 2013). Zeng *et al.* (2010) performed in-depth characterization of *fls2* mutant plants using infection assays with *Pto* DC3000 and *Pto* DC3000 COR$^-$ and measurements of stomatal aperture. They convincingly show that the stomatal aperture of *fls2* does not change in response to *Pto* DC3000 or *Pto* DC3000 COR$^-$. On the other hand, *efr* still reduces the stomatal aperture similar to wild type in response to both *Pseudomonas* strains. This result is reflected in surface inoculation experiments performed by Zeng *et al.* (2010). *fls2* mutants are more susceptible to infection with both *Pseudomonas* strains in contrast to *efr* and wild type. Unfortunately, only data of day 3 post infection are shown for the surface-inoculation assays making it impossible to judge if the differences in the bacterial titers are caused by efficient apoplastic immunity or the successful prevention of colonization of the apoplastic space. Another example is the OE line of *At*CRK6 which shows a constitutive reduced stomatal aperture (Yeh *et al.*, 2015). However, surface-inoculation data is presented for day 2 post infection which does not allow the differentiation of the invasion and multiplication success of bacteria in the apoplast of these plants (Yeh *et al.*, 2015). In contrast, infection assays of OE-HA show a clear difference already at 4 h post infection. The invasion of bacteria is effectively reduced, but the multiplication in the apoplastic space is not impaired. In other words, OE-HA possesses an enhanced stomatal and thus pre-invasive immune response, but the post-invasive immunity is apparently successfully down regulated by the pathogen allowing bacterial multiplication. Certainly, pre- and post-invasive immune responses are not strictly separated, and therefore, difficult to definitely distinguish. Potentially, a slight reduction of invaded bacterial cells will not become evident using the classical bacterial infection assay and requires more sensitive methods. In case of LORE, only for OE-HA with a strongly enhanced and prolonged biphasic ROS burst which might prevent the reopening of stomata, a phenotype using *Pto* DC3000 was observed. Weaker effects might become evident using stomatal aperture measurements, but not by evaluating bacterial titers. Also environmental conditions such as high humidity can counteract stomatal immunity and influence bacterial virulence and thus modify experimental outcomes (Panchal *et al.*, 2016, Xin *et al.*, 2016). A higher humidity might successfully interfere with stomatal defense responses and can explain contradicting results published for the role of *At*EFR in pre-invasive immunity (Zeng *et al.*, 2010, Nekrasov *et al.*, 2009, Saijo *et al.*, 2009). Contradicting results are also published for the contribution of *At*OST1 in the stomatal movement in response to a challenge with pathogens which might be reasoned by differences in the experimental setup (Guzel Deger *et al.*, 2015, Montillet *et al.*, 2013, Liu *et al.*, 2009, Melotto *et al.*, 2006). More complexity to the role of stomata in the immune response was recently added by a study of Zhang *et al.* (2018) reporting of enhanced resistance to infection with *X. oryzae* pv. *oryzae* of the rice mutant *osaba1* which constitutively opens stomata and does not limit bacterial entry. They hypothesize that

the changes of the water potential in *osaba1* lead to a reduced multiplication of *X. oryzae* pv. *oryzae* (Zhang *et al.*, 2018). These various roles of stomata clearly show that more research is necessary to understand the underlying plant-pathogen interactions, but also detailed understanding of the signaling pathways involved in pre-invasive immunity is lacking to complete current knowledge.

The here provided data sheds new light on *At*LORE regulation, receptor complex formation, and collects data on possible roles of *At*LORE in the plant immune response. Accumulating evidence supports ligand-independent homodimerization mediated by the extracellular domain. The previously reported role of *At*LORE in pre-invasive immunity is supported and the knowledge of *At*LORE signaling is broadened by the findings presented. Future research focusing on the identification of downstream signaling components of *At*LORE and the investigation of 3-HDA binding as well as comprehensive infection studies of OE lines with disarmed *Pseudomonas* strains will complement the here provided evidence and will help to explain the observed phenotypes.

6 Summary

Plants rely on the detection of invading pathogens *via* cell surface-located pattern recognition receptors. These receptor-like kinases and receptor-like proteins induce a common set of immune responses to ward off bacteria and limit bacterial growth known as pattern-triggered immunity (PTI). Conserved and essential molecules of microbes so-called microbe-associated molecular patterns (MAMPs) are sensed. Lipopolysaccharide (LPS) a component of the outer membrane from Gram-negative bacteria as well as its minimal motif 3-hydroxydecanoic acid (3-HDA) serve as MAMPs in *Arabidopsis thaliana*. The S-domain receptor-like kinase *At*LORE (LIPOOLIGOSACCHARIDE-SPECIFIC REDUCED ELICITATION) was identified as a key component of LPS/3-HDA-sensing.

Here, the regulation of *At*LORE in the *A. thaliana-Pseudomonas syringae* interaction was investigated. Receptor complex formation was analyzed using CoIP experiments as well as bimolecular fluorescence complementation assays (BiFC). The results indicate that *At*LORE homodimerizes. Kinase activity and the addition of the putative ligand 3-HDA are not crucial indicating a ligand-independent mode of receptor complex formation. Dimerization is mediated by the ectodomain of *At*LORE anchored into the plasma membrane as outlined by BiFC assays using truncated *At*LORE proteins. Competition gain-of-function assays in *N. benthamiana* demonstrate that dimerization is critical for receptor complex activation. The generation and functional assessment of chimeras derived from *At*LORE and identified *At*LORE para- and orthologs from 3-HDA-insensitive plants failed to identify single extracellular domains important for receptor activation. Stable complementation and overexpression lines (OE lines) of *At*LORE or C-terminal epitope tagged *At*LORE were used to assess the role of *At*LORE in PTI in more detail. Elevated *At*LORE levels increased the intensity of typical cellular immune responses such as the production of reactive oxygen species, protein kinase activation and defense gene expression. Strikingly, the C-terminal tag of LORE rendered signal attenuation. Here, a delayed negative regulation of activated *At*LORE is proposed. Moreover, this led to enhanced resistance towards spray inoculation with *Pseudomonas syringae*. Stomatal immunity was investigated using thermal imaging and illustrates a differential regulation of stomatal aperture in OE lines in response to 3-HDA application.

Taken together, these results indicate an eminent role of *At*LORE in pre-invasive immunity and provide evidence that homodimerization is essential for receptor activation.

7 Zusammenfassung

Pflanzen erkennen eindringende Pathogene mithilfe von Mustererkennungsrezeptoren (*pattern recognition receptor* PRR) welche an der Zelloberfläche lokalisiert sind. Diese Rezeptor-ähnlichen Kinasen (*receptor-like kinase*) und Rezeptor-ähnliche Proteine (*receptor-like protein*) induzieren Immunantworten um Pathogene abzuwehren und deren Ausbreitung zu verhindern. Dies wird als Muster-induzierte Immunität (*pattern-triggered immunity* PTI) bezeichnet. Konservierte und essentielle Bestandteile von Mikroben, genannt Mikroben-assoziierte Molekülmuster (*microbe-associated molecular pattern* MAMP), werden perzipiert. Lipopolysaccharid (LPS), ein Bestandteil der äußeren Zellmembran von Gram-negativen Bakterien, sowie das Zwischenprodukt des bakteriellen Metabolismus 3-Hydroxyldecansäure (3-HDA) werden als MAMP in *Arabidopsis thaliana* erkannt. Die S-domänen Rezeptor-ähnliche Kinase *At*LORE (LIPOOLIGOSACCHARIDE-SPECIFIC REDUCED ELICITATION) wurde als Schlüsselprotein in der Erkennung von LPS/3-HDA identifiziert. In der vorliegenden Arbeit wurde die Regulation von *At*LORE in der Interaktion zwischen *A. thaliana* und *Pseudomonas syringae* untersucht. Die Rezeptorkomplexbildung wurde mittels Ko-immunoprezipitationsexperimenten sowie Bimolekularer Fluoreszenzkomplementation (BiFC) analysiert. Die Ergebnisse weisen daraufhin, dass LORE Homodimere ausbildet. Kinaseaktivität und die Zugabe des Ligandens 3-HDA sind nicht entscheidend für die Dimerisierung, was eine Liganden-unabhängige Rezeptorkomplexbildung vorschlägt. Die Dimerisierung wird durch die membranständige Ektodomäne von *At*LORE vermittelt wie BiFC-Experimente mit verkürzten *At*LORE Proteinen indizieren. Sogenannte *competition gain-of-function* Experimente in *N. benthamiana* zeigen, dass die Dimerisierung essentiell for die Rezeptorkomplexaktivierung ist. Die Herstellung und funktionelle Untersuchung von chimären Rezeptorproteinen bestehend aus *At*LORE und *At*LORE Para- und Orthologen von zuvor identifizierten LPS/3-HDA-insensitiven Pflanzen konnte keine einzelnen extrazellulären Domänen identifizieren welche wichtig für die Rezeptorkomplexbildung sind. Anhand von stabilen Komplementations- und Überexpressionslinien von *At*LORE oder C-terminaler epitopmarkierter *At*LORE wurde die Rolle von *At*LORE in der Muster-induzierten Immunität tiefergehend untersucht. Erhöhte *At*LORE-Level steigern die Intensität von typischen Immunantworten wie z.B. die Produktion von reaktiven Sauerstoffspezies, die Aktivierung von Proteinkinasen sowie die Expression von Abwehrgenen. Bemerkenswerterweise hatte die C-terminale Epitopmarkierung einen Einfluss auf die Signalabschwächung von *At*LORE. In der vorliegenden Arbeit wird deshalb eine verzögerte Signalattenuation als möglicher Grund vorgeschlagen. Dies führt zu einer erhöhten Resistenz gegenüber der Sprühinfektion mit *P. syringae*. Stomatäre Immunität wurde daher mithilfe von Wärmebildaufnahmen untersucht und zeigt eine veränderte Regulation der Stomataöffnung in Überexpressionslinien als Reaktion auf die 3-HDA-Behandlung. Zusammengefasst deuten die Resultate auf eine bedeutende Rolle von LORE in der präinvasiven Immunität hin und zeigen, dass Homodimerisierung essentiell für die Rezeptoraktivierung ist.

8 Material and Methods

8.1 Molecular biology

8.1.1 Transformation of *E. coli* by heat shock

Transformation of chemical competent *Escherichia coli* Dh5α (Clontech, Mountain View, USA) cells was used for the amplification of plasmids. For transformation, competent cells were thawed on ice, the ligation mixture was added and incubated for 10 to 30 min on ice. After 90 s heat shock at 42°C, 1 mL LB medium (section 9.1.1) was added. The cells were incubated for 1 h at 37°C, 250 rpm. Cells were collected by centrifugation at 18000 g, room temperature (RT). The supernatant was removed and the pellet was resuspended in approximately 100 µL LB medium and plated on LB plates containing the appropriate antibiotics (section 9.1.3). Colonies were grown at 37°C over night.

8.1.2 Transformation of *A. tumefaciens* by heat shock

For transformation, chemical competent *Agrobacteria tumefaciens* GV3101 cells were thawed on ice. 5 µL plasmid per 50 µL cells was added and incubated for 10 to 30 min on ice. Tubes were transferred for 1 min to liquid nitrogen, followed by 5 min heat shock at 37°C. 1 mL of LB medium (section 9.1.1) was added and the mixture was incubated at 28°C, 200 rpm. After 2 to 3 h incubation, cells were collected by centrifugation at 18000 g, RT. The supernatant was removed and the pellet was resuspended in approximately 100 µL LB medium and plated on LB plates containing the appropriate antibiotics (section 9.1.3). Colonies were grown at 28°C for at least 48 h.

8.1.3 Plasmid preparation

Isolation of plasmids from *E coli* was achieved *via* alkaline lysis. For isolation of high-copy plasmids, 2 mL TB medium (section 9.1.1) with appropriate antibiotics was inoculated with single bacterial colonies and grown over night at 37°C, 250 rpm. For isolation of low-copy plasmids, 4 mL of over-night culture were inoculated. The bacterial cultures were centrifuged 1 min at 18000 g. The supernatant was removed and the pellet was resuspended in 200 µL P1 buffer (50 mM Tris-HCl, pH 8, 50 mM EDTA (ethylenediaminetetraacetic acid), 15% sucrose, 0.5 mg/mL RNase A). After adding 200 µL P2 buffer (0.2 M NaOH (sodium hydroxide), 1% SDS (sodium dodecyl sulfate)), tubes were inverted and incubated at RT for 5 min. 300 µL of P3 buffer (5 M potassium acetate, 2 M acetic acid, pH 5.2). Two drops of chloroform, for better phase separation, were added. Tubes were inverted and centrifuged for 10 min at 18000 g, RT. The supernatant was transferred into a fresh tube and 500 µL isopropyl was added. The solution was mixed by vortexing and centrifuged for 10 min at 18000 g, RT. The supernatant was discarded. 100 µL 70% ethanol was added to wash the pellet. The mixture

was centrifuged for 10 min at 18000 g, RT. The pellet was dried at 37°C and resuspended in 20 to 30 µL Millipore water.

Plasmids were verified using restriction digestion (section 8.1.7). Positive plasmids were sequenced at Eurofins MWG Operon (Ebersberg, Germany). Clean-up of plasmids for further molecular cloning steps was performed using the Nucleospin Plasmid kit (Macherey-Nagel, Düren, Germany) according to manufacturer's guidelines with minor changes. The washing step was repeated three times. Midi preparations of plasmids were performed with the NucleoBond Xtra Midi Kit according to manufacturers's guidelines (Macherey-Nagel, Düren, Germany).

8.1.4 Polymerase chain reaction

Polymerase chain reaction (PCR) was performed with Phusion High-Fidelity DNA-polymerase (Thermo Fisher Scientific, Waltham, USA) according to manufacturer's guidelines. A standard 50 µL PCR mixture contained 10 to 50 ng template, 1x Phusion HF buffer (Thermo Fisher Scientific, Waltham, USA), 200 µM dNTPs, 0.5 µM forward and reserve primer, and 1 U Phusion High-Fidelity DNA-polymerase. The following programme was used as a standard touch-down PCR programme: initial denaturation at 98°C for 1 min, denaturation at 98°C for 0:20 min, annealing starting e.g. at 72°C for 0:20 min, amplification at 72°C with a template specific time. The annealing temperature was reduced by 1°C during the first 10 cycles. The remaining cycles were performed at the temperature of the last touch-down cycle. Final elongation was performed at 72°C for 10 min. For semi-quantitative PCR (sqPCR), SupraTherm Taq Polymerase (Genecraft, Cologne, Germany), and a standard PCR programme with primer-specific annealing temperature was used (initial denaturation 95°C, 1 min, denaturation 95°C, 0:30 min, primer-specific annealing temperature 0:30 min, amplification 72°C template specific time, termination 72°C, 10 min).

8.1.5 Site-directed mutagenesis

Single nucleotides were mutated to substitute enzyme recognition sites interfering with the Golden Gate cloning approach (section 8.1.8). Therefore, 25 µM dNTPs and 1.5 µL DMSO (dimethyl sulfoxide) in a 50 µL PCR volume were supplemented. The PCR was performed with minor changes as described in section 8.1.4. The amplification cycles were reduced to 10 to 15 cycles. Upon amplification, the PCR reaction was digested with the restriction enzyme DpnI for 2 to 3 h at 37°C and then transformed into *E. coli* (section 8.1.1). DpnI is a methylation-sensitive restriction enzyme which cleaves the template of bacterial origin, but not the generated PCR product carrying the mutagenized nucleotides.

8.1.6 Gel electrophoresis and gel extraction of DNA fragments

PCR products and plasmid restriction digestions were analyzed by agarose gel electrophoresis. Therefore, 1% (m/V) agarose gels supplemented with 0.5 µg/mL ethidium bromide were prepared in 1xTAE buffer (4.84 g/L Tris Ultra, 11.42 mL/L acetic acid, 2 mL/L EDTA pH 8.0, pH 8.5). Gels were run between 100 V and 120 V. In case of preparative PCRs, DNA bands were cut and isolated using a PCR and Gel Clean up Kit (Macherey-Nagel, Düren, Germany). The DNA isolation was performed according to manufacturer's guidelines, with minor changes. The washing step was repeated three times. DNA fragments were resuspended in 30 µL Millipore water.

8.1.7 Restriction digestion

Enzyme restriction digestion was used to verify cloned plasmids. Enzymes were purchased from Thermo Fisher Scientific (Waltham, USA) or New England Biolabs (Ipswich, USA). Restriction digestions were performed according to manufacturer's guidelines. In short, 2 µL of high-copy plasmids or 4 µL of low-copy plasmids were digested in a 20 µL reaction for 1 to 2 h at 37°C or in case of SmaI (New England Biolabs, Ipswich, USA) at 30°C.

8.1.8 Golden Gate cloning

All plasmids used in this study were cloned *via* a Golden Gate-based molecular cloning system constructed by Dr. S. Ranf (Weber *et al.*, 2011, unpublished). The system designed by Dr. S. Ranf is a 3-vector order. The gene of interest is first cloned into an entry vector (pGGEntL) and then subcloned *via* enzyme restriction and ligation into vectors (pGGIn) containing promoter, C- or N–terminal epitope tags, and a terminator. pGGInAE-224C_p35S_CDS_eGFP, for example, puts the gene under control of the constitutive 35S promoter of the cauliflower mosaic virus and fuses the epitope marker eGFP. For expression in agrobacteria, the whole expression cassette from pGGIn can be cloned into the binary vectors pGGPlantXL or pGGPXB. Vector backbones used in this study are listed in Supplementary Table 1. The gene of interest is amplified using primers which add an enzyme recognition site and a determined fusion site START (aATG) or STOP (TAGt) to the DNA fragment which is also site of restriction in the vector (Figure 33). Ligation of the PCR product replaces the LacZ gene of pGGEntL and allows for blue-white screening of colonies. All vectors have an inner and an outer enzyme recognition site indicated by the name pGGEntL-EP21, whereas BpiI (P) is the enzyme used for insertion of the PCR-fragment and Esp3I (E) is used to cut the complete fragment plus fusion sites out to shuffle to the next vector (Figure 34, unpublished). All pGGIn vectors are compatible with the pGGPlantXL vector as they carry additionally fusion sites, promoter PROM (cGAG) and terminator TERM (CCGc).

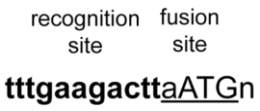

Figure 33 Principal structure of a primer used for gene amplification in this study. The primer adds the enzyme recognition site gaagac (bold) for BpiI plus three nucleotides before and two nucleotides after the recognition site. The determined fusion site added to the PCR template, in this example START (aATG), is underlined.

Figure 34 Principal structure of pGGEntL- and pGGIn-vector backbones. Depicted is

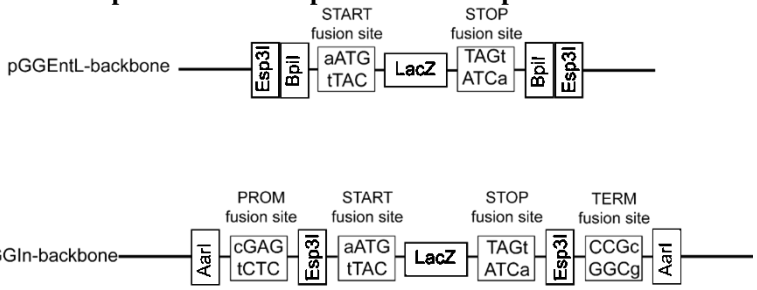

pGGEntL-EP21 which has an inner Bpi and an outer Esp3I recognition site. The inner recognition site is used for cloning the gene of interest into the entry vector. Cutting of the PCR product with the respective enzyme, in this case BpiI, will result in a sticky overhang of the fusion site which will be compatible with the overhang of the digested pGGEntL vector. Ligation of the PCR product in the pGGEntL vector will replace the LacZ-fragment and results in loss-of the enzyme recognition site. The START and STOP fusion sites are compatible between pGGEntL and pGGIn-vectors. PROM and TERM fusion sites are compatible with pGGPlantXL and pGGPXB (not shown).

pGGEntL-cloning

Genes of interest were amplified as described in section 8.1.4. All generated plasmids are listed in Supplementary Table 2. The PCR product was cloned into the pGGEntL vector (50 ng pGGEntL, 50 ng PCR product, 1x appropriate buffer, 0.5U enzyme, 1 mM ATP, 0.05U T4 ligase, final volume 50 µL) by restriction and ligation (2 min 37°C, 5 min 16°C repeated up to 50x, followed by 20 min 80°C).

pGGIn-cloning

The gene cloned into the entry vector pGGEntL was shuffled into pGGIn vectors to add a promoter and epitope tag. To achieve an in-frame addition of a C-terminal epitope tag, the pGGEntL was cut with EciI (New England Biolabs, Ipswich, USA) (500 ng pGGEntL vector, 1xCutSmart, 0.5 µL EciI in a final volume of 20 µL for 1-2 h at 37°C) and treated with T4-DNA polymerase (Thermo Fisher Scientific, Waltham, USA) which removes 3'overhangs of DNA-strands resulting in a blunt end.

Therefore, the mixture was cooled on ice, 2.5 µL 2 mM dNTPs, 2.5 µL 10 mM DTT (dithiothreitol), and 1 µL T4 DNA-polymerase were added and incubated for 10 min at 11°C and 20 min at 80°C. The pGGIn vector was cut with SmaI and dephosphorylated with FastAP thermosensitive Alkaline Phosphatase (both Thermo Fisher Scientific, Waltham, USA) resulting in a blunt end and removed STOP fusion site (500 ng pGGIn-vector, 2 µL 10x Tango buffer, 0.5 µL SmaI, 1 µL FastAP in a final volume of 20 µL, 1 h at 30°C, 30 min at 37°C, 20 min at 80°C). For final shuffling of the gene of interest to the destination pGGIn-vector, Esp3I restriction and ligation was performed. Therefore, 50 ng pretreated pGGEntL and pGGIn were mixed with 1x Tango buffer, 1 µL Esp3I, 5 µL 10 mM ATP, 5 µL 10 mM DTT, and 0.5 µL T4 ligase in a final volume of 50 µL.

pGGPXB

For expression in agrobacteria, the whole expression cassette was shuffled into the binary vector pGGPXB by AarI-mediated restriction and ligation (500 ng pGGIn, 500 ng pGGPXB, 4 µL 10xTango buffer, 2 µL 10 mM ATP, 1 µL AarI, 1 µL T4-ligase). For some clones the pGGPlantXL vector was used which is not compatible with AarI-mediated restriction-ligation as it is carrying an AarI recognition site in the backbone. In this case, pGGIn and pGGPlantXL were digested with AarI separately, heat inactivated and then mixed and ligated.

8.1.9 Cloning of *LORE*, *AtLORE* orthologs, and *AtLORE* paralogs

AtLORE (At1g61380, SD1-29), all *AtLORE* paralogs (*AtSD1-23* (At1g61390), *AtSD1-28* (At1g11280)) and *AtLORE* orthologs (*CrubLORE* (CARUB_v10021901mg), *AlyrLORE* (gi297837335), and *AhalLORE* (Araha.6790s0007) were cloned from cDNA prepared from the respective plant species as described in 8.1.13. If necessary, enzyme recognition sites were mutated *via* a Golden Gate-based approach or site-directed mutagenesis (section 8.1.5, section 8.1.8). All genes were cloned into the vectors pGGIn-221C, pGGIn-224C, and pGGIn-225C (Supplementary Table 1). A kinase dead version of LORE (LORE-Km) was generated by mutating the putative ATP-binding site from lysine at position 516 to alanine in the catalytic domain (Ranf *et al.*, 2015). As SD-RLKs expression other than *At*LORE was lethal for *E. coli*, the sequence of the first intron of *AtLORE* was introduced to *AtSD1-23* and *AtSD1-28* using Golden Gate assembly and indicated by the letter i (e.g. SD1-23i). The intron was amplified from a genomic fragment of *AtLORE*. All primers are listed in Table 1.

Table 1 Summary of all primers used to amplify *LORE* (SD1-29), *AtLORE* ortho- and paralogs. Primers to introduce the first intron to *SD-RLKs* or to mutate enzyme recognition sites in the sequences are listed. Golden Gate enzyme recognition sites are depicted in bold and the fusion site is underlined (**START** AATG, **STOP** TAGT). The AGI locus identifier is listed for the genes from *A. thaliana*, the Phytozome identifier is listed for *A. halleri*, and the GenBank identifier is listed for *C. rubella* and *A. lyrata*.

organism	primer name	sequence 5' to 3'	gene identifier	reference
C. rubella	CARUB29-START	**tgaagactt**AATGGGTATGGTTTTATTTGC	CARUB_v10021901mg	this study
	CARUB-STOPm	**tgaagactt**ACTAGCGTCCTTGGATCATAGATTG		
	CARUB29-_EspF	**tgaagactc**CGCCTGGGGAGTTCACAC		
	CARUB29_EspR	**tgaagactt**GGCGACGGATCACTGTAAC		
A. thaliana	SD129-START	**tcgtctct**AATGGGTATGGTTTTATTTGCTTGC	At1g61380	Dr. S. Ranf
	SD129-STOP	**tcgtctct**ACTACCTTCCTTGGATCATAGATTCTG		
	SD129-EspMut-F	**tcgtctct**GTtAGACGTACAAAATTATCTTGCC		
	SD129-EspMut-R	**tcgtctcc**TaACACACCCACTTGTCCAG		
	SD129-K516A_F	**tgaagactt**TgcaCGCCTTGCTAGTAGTTCC		this study
	SD129-K516A_R	**tgaagactt**TgcaACACCTATTTCCTTCCCATC		
	129intron-F	**tttgaagactt**GGGTAAGGATAAAATACATTTCTTCC		
	129intron-R	**tttgaagacga**AGCTGAGATATTCACCAG		

Table 1 (continued)

organism	primer name	sequence 5' to 3'	gene identifier	reference
A. thaliana	SD123_START	**tgaagactt**AATGTACAAACTTC CACAAAG	At1g61390	
	SD123_START	**tgaagactt**AATGTACAAACTTC CACAAAG	At1g61390	Dr. S. Ranf
	SD123-STOP	**tgaagactt**ACTAACGCCCTTGA ATCAC		
	SD123-BpiM_R	**tgaagacga**gGACTGAGGCAGC ATAGTATTACC		
	SD123-BpiM_F	**tgaagacca**GTCCTCTGTGATGT ATGATATTCC		
	SD123-EspM_R	**tgaagactc**TGACACACCCACTT GTCCAATTC		
	SD123-EspM_F	**tgaagacgt**GTCAGACGTACACA ATTATC		
	SD123-BsaM_R	**tgaagacca**GATCTCGGTGAATT ACCC		
	SD123-BsaM_F	**tgaagacga**GATCTGAAGGTCA GCAAC		
	SD123intron_F	**tttgaagactc**AGCTTCTTCAGTC CTAATAATTC		
	SD123intron_R	**tttgaagactt**ACCCTAGCTCATA AACTCC		
A. thaliana	SD128-START	**tcgtctct**AATGGATCTGAAGGA GAACTC	At1g11280	this study
	SD128-STOP	**tcgtctct**ACTATCGCCCATATAT CTCAGTTTG		
	SD128-Bm2_as	CATTGGCCAGACGATAGAAcA CGTCTACACCTTTTCTTG		

Table 1 (continued)

organism	primer name	sequence 5' to 3'	gene identifier	reference
	SD128-Bm2_s	CAAGGAAAAGGTGTAGACGT gTTCTATCGTCTGGCCAATG		
	SD128-Bm1_as2	CACTTATTAGATATGGAAGGc CTTCTGGTTGACCAAACAAC		
	SD128-Bm1_s2	GTTGTTTGGTCAACCAGAAGg CCTTCCATATCTAATAAGTG		
	SD128intron-F	**tgaagactt**AGCTTCTTCAGTCC TAACAACTCTC		this study
	SD128intron-R	**tgaagactt**ACCCTAACTCATAA AATCCACCAG		
A. lyrata	CARUB29-START	**tgaagactt**AATGGGTATGGTTT TATTTGC	XM_021034387/ LOC9322615	this study
	CARUB-STOPm	**tgaagactt**ACTAGCGTCCTTGG ATCATAGATTG		
A. halleri	Arha-START	**ttgaagactt**AATGGGTATGGTTT TATTTGC	Araha.6790s0007	this study
	Arha-STOP	**ttgaagactt**ACTATCTTCCTTGA ATCATAG		

8.1.10 Cloning of domain swaps of *LORE* and its orthologs and paralogs

For investigation of LORE domain functionality, domain swaps of LORE with AlyrLORE, SD1-23, and SD1-28 were generated. All used primers, templates, and detailed fusion sites are listed in Table 2. Domain swaps (DS) of the complete extracellular domain (DS-LLEP), the complete extracellular domain plus transmembrane domain (DS-LLEPT), the complete intracellular domain (DS-JKD), the complete intracellular domain plus transmembrane domain (DS-TJKD), and parts of the extracellular domain (DS-LL and DS-EP) were cloned. Golden Gate fusion sites were defined for each domain according to sequence similarity and predicted domains (section 4.1, Table 2, and Supplementary Figure 11). The molecular cloning approach for the domain swap pGGEntL-EP21_DSAlyr-LLEP is described exemplarily. The ectodomain of *AlyrLORE* (LLEP) with the fusion sites START and N was amplified as described in section 8.1.4. Accordingly, the intracellular and transmembrane domain of

LORE (TJKD) and the pGGEntL-EP21 vector backbone were amplified using the fusion sites N (tTCA) and START (aATG) (Figure 35).

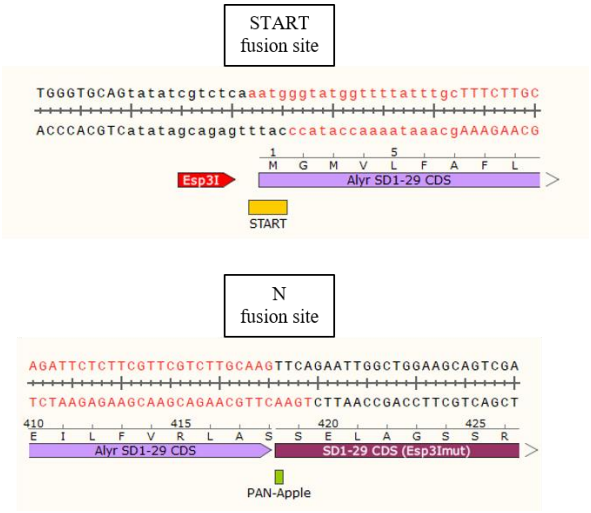

Figure 35 Example of the cloning approach to clone domain swaps of LORE (SD1-29) and its para- and orthologs. Part of the fragment amplified of *AlyrLORE* (LLEP) is shown in red carrying the fusion sites **START** AATG/CATT and **N** TTCA/TGAA. The plasmid and the fragment of *LORE* carry the complementary fusion site **START** AATG/CATT and **N** TTCA/TGAA which were defined according to domain border predictions and sequence similarity of SD-RLKs (Supplementary Figure 11)

Both PCR products (50 ng each) were mixed and a BpiI restriction and ligation was performed (section 8.1.8). Plasmids were verified by restriction digestion and sequencing (section 8.1.7). All domain swaps were shuffled to pGGIn-221C, pGGIn-224C, and pGGIn-225C and afterwards into pGGPlantXL or pGGPXB (Supplementary Table 1, Supplementary Table 2). To ensure correct localization, the signal peptide of *AtLORE* was used for all chimeric receptor variants.

Table 2 Primer sequences for cloning of domain swaps of *LORE* (SD1-29) with *AlyrLORE*, *SD1-23*, and *SD1-28*. The Golden Gate fusion site of the primer is underlined (**START** AATG, **STOP** TAGT, **A** TATA, **C** TTGG, **N** TTCA, **P** CACC). The enzyme recognition site is highlighted in bold. All domain swaps were shuffled to pGGIn-221C, pGGIn-224C, and pGGIn-225C and into pGGPlantXL or pGGPXB (Supplementary Table 1, Supplementary Table2). An alignment with the detailed fusion sites can be found in Supplementary Figure 11. An i indicates the introduction of the first intron of *AtLORE* (section 8.1.9).

amplified fragment	primer name	sequence 5' to 3'	fusion site	reference
SD1-29-TJKD-backbone	DS-START-EP21-R	**tgaagaccc**CATTTGAGACGATATACTGC	START N	

Table 2 (continued)

amplified fragment	primer name	sequence 5' to 3'	fusion site	reference
	SD129-DSN-F	**tgaagacag**TTCAGAATTGGCTGGAAG		
SD1-29-JKD-backbone	DS-START-EP21-R	**tgaagaccc**CATTTGAGACGATATACTGC	START P	
	SD129-DSP-F	**tgaagacgc**CACCAATAACTTCAGTCC		
SD1-29-LLEPT-backbone	DS-STOP-EP21-F	**tgaagacgg**TAGTAGAGACGTCCGC	P STOP	
	SD129-DSN-R	**tgaagactc**TGAACTTGCAAGACGAATG		
SD1-29-LLEP-backbone	DS-STOP-EP21-F	**tgaagacgg**TAGTAGAGACGTCCGC	N STOP	
	SD129-DSP-R	**tgaagactt**GGTGGCAGTTCGTATTG		
SD1-29-EPTJKD-backbone	SD129_DSA_R	**tttgaagactt**TATAGCTGCATAGCCACAAG	A C	
	SD129_DSC_F	**tttgaagacaa**TTGGAAGCTTCACTTGTC		
SD1-29-LLTJKD-backbone	SD129_DSC_R	**tttgaagactt**CCAATTATTTCCATCATCCC	C N	
	SD129-DSN-F	**tgaagacag**TTCAGAATTGGCTGGAAG		
DSAlyr-LLEP	CARUB29-START	**tgaagactt**AATGGGTATGGTTTTATTTGC	START N	this study
	ALYR129-DSN-R	**tgaagactc**TGAACTTGCAAGACGAAC		
DSAlyr-LLEPT	CARUB29-START	**tgaagactt**AATGGGTATGGTTTTATTTGC	START P	this study
	ALYR129-DSP-R	**tgaagactt**GGTGGCAGTTCGTATG		
DSAlyr-JKD	SD129-DSP-F	**tgaagacgc**CACCAATAACTTCAGTCC	P STOP	this study, Tina Illig

Table 2 (continued)

amplified fragment	primer name	sequence 5' to 3'	fusion site	reference
	CARUB-STOPm	**tgaagactt**ACTAGCGTCCTTGGATCATAGATTG		
DSAlyr-TJKD	ALYR129-DSN-F	**tgaagacag**TTCAGAATTGGCTGGAAG	N STOP	this study, Tina Illig
	CARUB-STOPm	**tgaagactt**ACTAGCGTCCTTGGATCATAGATTG		
DSAlyr-LL	ALYR129_DSA_F	**tttgaagacgc**TATAAACACATCAAGTCc	A C	this study, Sonja Eibel
	ALYR129_DSC_R	**ttgaagactt**CCAATTTTTTCCATCATCCC		
DSAlyr-EP	ALYR129_DSC_F	**tttgaagacaa**TTGGAAGCTTCACTTGTC	C N	this study, Sonja Eibel
	ALYR129-DSN-R	**tgaagactc**TGAACTTGCAAGACGAAC		
DS123-LLEPi	SD123_START	**tgaagactt**AATGTACAAACTTCCACAAAG	START N	this study
	SD123-DSN-R	**tgaagactc**TGAACTTGCAAGCCGAAG		
DS123-LLEPTi	SD123_START	**tgaagactt**AATGTACAAACTTCCACAAAG	START P	this study
	SD123-DSP-R	**tgaagactt**GGTGGCAGTACGTATAG		
DS123-JKD	SD123-DSP-F	**tgaagacgc**CACCAATAACTTCAGTTC	P STOP	this study, Tina Illig
	SD123-STOP	**tgaagactt**ACTAACGCCCTTGAATCAC		
DS123-TJKD	SD123-DSN-F	**tgaagacag**TTCAGAATTGGCTGGTAG	N STOP	this study, Tina Illig
	SD123-STOP	**tgaagactt**ACTAACGCCCTTGAATCAC		
DS123-LLi	SD123-DSA-F	**ttgaagacga**TATAAACACATCAAGTCC	A C	this study

Table 2 (continued)

amplified fragment	primer name	sequence 5' to 3'	fusion site	reference
	SD123-DSC-R	**ttgaagactt**CCAACTTTTTCCATCATTC		
DS123-EP	SD123_DSC_F	**ttgaagacag**TTGGAAGCTTCACTTTG	C N	this study, Sonja Eibel
	SD123-DSN-R	**tgaagactc**TGAACTTGCAAGCCGAAG		
DS128-LLEPi	SD128-DSN-R-BpiI	**tgaagactt**TGAACTTGCAAGACGAATG	START N	this study
	SD128-START-BpiI	**tgaagactt**AATGGATCTGAAGGAGAACTC		
DS128-LLEPTi	SD128-DSP-R-BpiI	**tgaagactt**GGTgGCAGCTCGTATGGTATTC	START P	this study
	SD128-START-BpiI	**tgaagactt**AATGGATCTGAAGGAGAACTC		
DS128-JKD	SD128-DSP-F	**tcgtctct**CACCAATAACTTCAATGTCTC	P STOP	this study, Tina Illig
	SD128-STOP	**tcgtctct**ACTATCGCCCATATATCTCAGTTTG		
DS128-TJKD	SD128-DSN-F	**tcgtctcgt**TCAGAACTGGCTGGAAG	N STOP	this study, Tina Illig
	SD128-STOP	**tcgtctct**ACTATCGCCCATATATCTCAGTTTG		
DS128-LL	SD128_DSA_F	**tttgaagactt**TATAACTATTTCAAGTCCTTTGAC	A C	this study
	SD128_DSC_R	**tttgaagactt**CCAACCTGTCCCATTGTACCG		
DS128-EP	SD128_DSC_F	**tttgaagactt**TTGGGTTCTGGACTTTATCAC	C N	this study
	SD128-DSN-R-BpiI	**tgaagactt**TGAACTTGCAAGACGAATG		

8.1.11 Cloning of *LORE*, *SD1-23*, *SD1-28*, and *AlyrLORE* truncations

For investigation of LORE homodimerization, truncated *LORE* variants were cloned. Soluble and membrane-associated extracellular domains (dTJKD and dJKD) as well as kinase domains (dLLEPT, dLLEP) were cloned. For reasons of an improved reading flow, LORE-dTJKD will be named in the main text as eLORE, LORE-dJKD is equivalent to tLORE. LORE-dLLEPT will be named kLORE and LORE-dLLEP/LORE-Km-dLLEP is equivalent to iLORE/iLORE-Km. A schematic illustration of the truncations can be found in section 4.2.2, Figure 7. Moreover, truncations of the extracellular domain of *SD1-23*, *SD1-28*, and *AlyrLORE* were cloned and labeled in accordance with the LORE truncations. eSD123, eSD128, and eAlyrLORE are equivalent to SD1-23-dTJKD, SD1-28-dTJKD, and AlyrLORE-dTJKD, respectively. Apoplastic mCherry was cloned as a negative control. All variants were amplified as described in section 8.1.4. The primers and the respective fusion sites are listed in Table 3. The PCR products were ligated into the pGGEntL-EP21 vector *via* BpiI restriction and ligation as described in section 8.1.8. All truncation variants were shuffled into pGGIn-221C and pGGIn-225C and further in the binary pGGPXB vector. iLORE/LORE-dLLEP was shuffled into pGGIn-226C instead of pGGIn-221C. The signal peptide of *AtLORE* was used for all truncations.

Table 3 Primers used to clone soluble and transmembrane bound extracellular domains of *LORE* (*SD1-29*) and its para- and orthologs. The Golden Gate fusion site is underlined (**START** AATG, **STOP** TAGT, **N** TTCA, **P** CACC), the enzyme recognition site is highlighted in bold. All variants were shuffled into pGGIn-221C and pGGIn-225C and subsequently cloned into the pGGPXB-vector.

construct name	primer name	sequence 5 to 3'	fusion site	reference
SD129-dLLEP	SD129-TM-F	**tgaagactt**AGCTGGAAGCAGTCGAAGG	N STOP	this study
	SD129-SP-R	**tgaagactt**AGCTGCATAGCCACAAG		
SD129-dTJKD	SD129-START-Bpi	**tgaagactt**AATGGGTATGGTTTTATTTGCTTGC	START N	this study, Tina Illig
	SD129-EC-R	**tgaagactt**ACTAGCTTCCAGCCAATTCTG		
SD129-dJKD	SD129-START-Bpi	**tgaagactt**AATGGGTATGGTTTTATTTGCTTGC	START P	this study, Tina Illig
	SD129-EC-TM-R	**tgaagactt**ACTAATTTTGTTTCGCTCTGTATC		

Table 3 (continued)

construct name	primer name	sequence 5 to 3'	fusion site	reference
SD123-dTJKDi	SD123_START	**tgaagactt**AATGTACAAACTTCCACAAAG	START N	this study
	SD123-EC-R	**tgaagactt**ACTAGCTACCAGCCAATTCTG		
SD123-dJKDi	SD123_START	**tgaagactt**AATGTACAAACTTCCACAAAG	START P	this study
	SD123-EC-TM-R	**tgaagactt**ACTAATTTTGTTTTGTTCTGTATCT		
SD128-dTJKDi	SD128-START-BpiI	**tgaagactt**AATGGATCTGAAGGAGAACTC	START N	this study
	SD128-EC-R	**tgaagactt**ACTAGCTTCCAGCCAGTTCTG		
SD128-dJKDi	SD128-START-BpiI	**tgaagactt**AATGGATCTGAAGGAGAACTC	START P	this study
	SD128-EC-TM-R	**tgaagactt**ACTAATTTTGTTTTGCTCTGTATCT		
nHA-SD129-dTJKD	SD129-START-Bpi	**tgaagactt**AATGGGTATGGTTTTATTTGCTTGC	START N	this study
	SD129-EC-R	**tgaagactt**ACTTACTAGCTTCCAGCCAATTCTG		
nHA-SD129-dJKD	SD129-START-Bpi	**tgaagactt**AATGGGTATGGTTTTATTTGCTTGC	START P	this study
	SD129-EC-TM-R	**tgaagactt**ACTAATTTTGTTTCGCTCTGTATC		
Alyr-dTJKD	CARUB29-START	**tgaagactt**AATGGGTATGGTTTTATTTGC	START N	this study
	SD129-EC-R	**tgaagactt**ACTAGCTTCCAGCCAATTCTG		

Table 3 (continued)

construct name	primer name	sequence 5 to 3'	fusion site	reference
nHA-SD129-dTJKD	SD129-START-Bpi	**tgaagactt**AATGGGTATGGTTTTATTTGCTTGC	START N	this study
	SD129-EC-R	**tgaagactt**ACTTACTAGCTTCCAGCCAATTCTG		
Alyr-dJKD	CARUB29-START	**tgaagactt**AATGGGTATGGTTTTATTTGC	START P	this study
	SD129-EC-TM-R	**tgaagactt**ACTAATTTTGTTTCGCTCTGTATC		
apoplastic mCherry	apomCh_F	**tttcgtctct**AATGGTGAGCAAGGGCGAGG		this study
	apomCh_R	**tttcgtctct**CATTGCATAGCCACAAGTTGG		

8.1.12 RNA isolation

Plant RNA was extracted using the Trizol reagent. First, plant material was ground and 1 mL of Trizol reagent (38% phenol, 0.8 M guanidine thiocyanate, 0.4 M ammonium thiocyanate, 0.1 M sodium acetate pH 5.0, 5% glycerol) was added. Tubes were inverted and centrifuged (1 min, 4°C, 14.000 g) to pellet cell debris. The soluble fraction was transferred into fresh tubes and 200 µL trichloromethane was added. Tubes were inverted and incubated for 5 min, RT, followed by a centrifugation step (15 min, 4°C, 14.000 g). The aqueous phase was transferred into new tubes and 500 µL of isopropyl alcohol was added to achieve RNA precipitation. The mixture was incubated for 10 min, RT and centrifuged (15 min, 4°C, 14.000 g). The supernatant was discarded and the pellet was washed with 1 mL 75% ethanol. The ethanol was removed and the pellet was dried. The RNA pellet was dissolved in 50 to 100 µL Millipore water depending on the amount of used plant material. RNA quality was checked by gel electrophoresis using a 2% agarose gel (section 8.1.6).

8.1.13 cDNA synthesis

RNA was transcribed into complementary DNA (cDNA) using a reverse transcriptase. First, RNA was treated for 30 min at 37°C with DNaseI to eliminate genomic DNA impurities (1 U DNaseI, DNaseI buffer (10x), 40 U Ribolock (all Thermo Fisher Scientific, Waltham, USA) and 1 to 2 µg of

RNA were mixed in 10 µL). 1 µL 50 mM EDTA was added and incubated for 10 min at 70°C to inactivate DNaseI. The RNA was placed on ice. 200 U RevertAid Reverse Transcriptase (Thermo Fisher Scientific, Waltham, USA), 20U Ribolock, 2 µL 10 mM dNTPs, 5xRT buffer, and 1 µL 10 µM Oligo(dT)$_{18}$ primer were added with a final volume of 20 µL. The mixture was incubated for 5 min at 37°C, 60 min at 42°C, and 15 min at 72°C. The cDNA was diluted 1:10 with fresh millipore water and stored at -20°C.

8.1.14 Plant material

All plant species and mutant plant lines used in this study are listed in Table 4.

Table 4 Plant lines and plant species used in this study. Listed are all wild type and mutant plant lines from *A. thaliana* as well as their NASC (Nottingham Arabidopsis Stock Centre) identifier. All other plant lines were provided as indicated in the reference column or the IPK identifier (Leibniz-Institut für Pflanzengenetik und Kulturpflanzenforschung).

plant line	reference	NASC/IPK identifier
A. thaliana Col-0^{Aeq}	provided by Dr. S. Ranf (TU München)	
A. thaliana Col-0	provided by Dr. S. Ranf (TU München)	
lore-1	Ranf *et al.*, 2015	
pub22/23/24	Trujillo *et al.*, 2008	*pub22* (SALK_072621) *pub23* (SALK_133841) *pub24* (SALK_041046)
mpk3-1	Ranf *et al.*, 2011, Wang *et al.*, 2007	SALK_151594
Capsella rubella	*	N22697
Arabidopsis lyrata ssp. *lyrata*	*	N22696
Arabidopsis halleri	provided by Prof. Falter-Braun, Helmholtz Zentrum München	
Brassica juncea (L.) ssp. *juncea* var. *juncea*	*	CR 2898
Brassica napus ssp. *napus* var. *napus*	*	CR 3182

Table 4 (continued)

plant line	reference	NASC/IPK identifier
Brassica nigra ssp. *hispida* var. *rigida* Sinskaya	*	CR 2744
Brassica rapa L. ssp. *chinensis*	*	BRA 1322
Brassica oleracea	*	N29002
Cardamine hirsuta	*	
Eruca sativa mill	*	ERU 119
Lepidium sativum L. ssp.*sativum* var. *sativum*	*	LEP 4
Raphanus sativus L. convar. *sativus*	*	RA 22
Thellungiella halophila	*	N22504
Sinapis arvensis L. var. *arvensis*	*	CR 515
Thlaspi arvense L	*	THLA 2
Nicotiana benthamiana	provided by Dr. Pröls; TU München	
Nicotiana tabacum	provided by Dr. Pröls; TU München	
Glycine max Williams 82	provided by Prof. Conrath/Sebastian Beyer; RWTH Aachen	
Hordeum vulgare Golden Promise	provided by Prof. Hückelhoven; TU München	
Oryza sativa japonica Nipponbare	provided by Prof. Schaffrath; RWTH Aachen	
Fragariaxmagna Maria de Bois	provided by Prof. Schwab; TU München	
Populus trichocarpa	provided by Prof. Grill/Michael Papacek; TU München	

Table 4 (continued)

plant line	reference	NASC/IPK identifier
Solanum lycopersicum Heinz 1706	provided by Prof. Poppenberger/Tanja Ibrom; TU München	

* material kindly provided by Prof. Quint; MLU Halle-Wittenberg

8.1.15 Plant growth conditions and seed sterilization

Arabidopsis thaliana and all other Brassicaceae plants used for experiments were grown on soil (Typ ED73, Einheitserde und Humuswerke, Sinntal-Jossa, Germany) mixed with vermiculite (ratio 4:1) under short day conditions (8 h light, 16 h darkness, 21°C, and 60% relative humidity, light flux 120 µM). Before, *A. thaliana* seeds were stratified for at least 48 h at 4°C in darkness. Arabidopsis plants were transferred to long day conditions (16 h light, 8 h darkness, 24°C, and 60% humidity, light flux 160 µM) for flower induction and seed set. *N. benthamiana* used for transient transformation experiments was grown under long day conditions. All other plant species (see Table 4) were grown under short day conditions. *A. thaliana* seedlings were grown in liquid culture according to Ranf *et al.* (2012). Seeds were transferred into 24-well plates, surface-sterilized and MS liquid medium was added (section 9). After 48 h stratification at 4°C, plates were moved to long-day conditions. Experiments were performed with 10 to 14-days-old seedlings. Arabidopsis seeds were surface-sterilized in 24-well plates for 4 h with chlorine gas as described in Ranf *et al.* (2012).

8.1.16 Generation of stable transgenic plant lines

Stable transgenic Arabidopsis lines were generated using the floral dip method (Logemann *et al.*, 2006). *A. tumefaciens* GV3101 was transformed with the binary vector pGGPlantXL (section 8.1.2, Table 5). Flowering *lore*-1 plants were dipped into a suspension containing agrobacteria of an optical density OD_{600} of 2.0, 0.5% sucrose, and 0.03% of the surfactant Silwet-77 (Kurt Obermeier GmbH, Bad Berleburg, Germany). Inflorescences were evenly covered with the suspension. Dipped plants were grown under long day conditions and mature seeds were harvested. Glufosinate ammonium spray selection identified positively transformed plants.

Table 5 List of stable transgenic Arabidopsis lines complementing or overexpressing *LORE* with or without epitope tag in *lore*-1 mutant background generated by floral dip transformation.

Plant line	ID	genetic background	transformed construct	vector backbone	reference
OE-NT1	8.4_C8_D8	*lore*-1(Ranf *et al.*, 2015)	p35S::LORE	pGGPlant-XL	Dr. S. Ranf
OE-NT2	2.1-2#4_A3	*lore*-1	p35S::LORE	pGGPlant-XL	Dr. S. Ranf
OE-NT3	3.1-5#D5_D9	*lore*-1	p35S::LORE	pGGPlant-XL	Dr. S. Ranf
OE-HA1	51-1_H8x5	*lore*-1	p35S::LORE-HA	pGGPlant-XL	this study
OE-HA2	51-8-A12_1	*lore*-1	p35S::LORE-HA	pGGPlant-XL	this study
OE-HA3	51-5	*lore*-1	p35S::LORE-HA	pGGPlant-XL	this study
CL 1	CL-F12	*lore*-1	pLORE::LORE	pGGPlant-XL	Dr. S. Ranf
CL 2	CL-E9	*lore*-1	pLORE::LORE	pGGPlant-XL	Dr. S. Ranf
CL-GFP1	14-15_7E	*lore*-1	pLORE::LORE-GFP	pGGPlant-XL	this study
CL-GFP2	14-17_8E	*lore*-1	pLORE::LORE-GFP	pGGPlant-XL	this study
CL-GFP3	14-2	*lore*-1	pLORE::LORE-GFP	pGGPlantXL	this study
OE-GFP1	17-7-H1_H5	*lore*-1	p35S::LORE-GFP	pGGPlant-XL	this study
OE-GFP2	17-2-B1_A9	*lore*-1	p35S::LORE-GFP	pGGPlant-XL	this study
OE-GFP3	17-5-H1_H8	*lore*-1	p35S::LORE-GFP	pGGPlant-XL	this study

8.1.17 Transient transformation of *N. benthamiana*

For transient transformation, gain-of-function experiments and generation of apoplastic wash fluids (AWF), 6 to 8-weeks-old *N. benthamiana* plants were used. Over-night cultures of *A. tumefaciens* GV3101 grown in induction medium (47 mL AB-medium (4.1 g/L MES (2-(*N*-morpholino)ethanesulfonic acid), 10.6 g/L glucose, pH 5.5), 0.5 mL AB-buffers (60 g/L K_2HPO_4, 20 g/L NaH_2PO_4) and 2.5 mL AB-salts (20 g/L NH_4Cl, 6 g/L $MgSO_4$-7xH_2O, 3 g/L KCl, 0.2 g/L $CaCl_2$, 50 mg/L $FeSO_4$-7xH_2O)) supplemented with 100 µM acetosyringone, 30 µg/mL gentamycin, and 50 µg/mL kanamycin at 28°C, 200 rpm. The bacterial cultures were harvested (2500 g, 2 min), washed twice with infiltration medium and resuspended in infiltration medium (10 mM $MgSO_4$, 10 mM MES pH 5.5, 150 µM acetosyringone). The optical density was adjusted to an absorbance of 0.5 at OD_{600}. For AWFs and transient transformation, agrobacteria with an OD_{600} 0.5 were equally

mixed with p19 silencing suppressor (kindly provided by Prof. Döhlemann, University of Cologne) and infiltrated into leaves. For gain-of-function experiments, bacterial cultures were diluted in infiltration medium to a final OD_{600} of 0.025 and mixed with an equal amount of p19 silencing suppressor. For competition gain-of-function assays, truncated receptor variants were added in a ratio of 3:1 to active LORE. Leaf discs, for analysis of accumulation of ROS (section 8.1.19), were taken 36 h after transformation and examined after 6 h. Apoplastic wash fluids were harvested between 3 to 5 days after transformation (section 8.1.26). For CoIP experiments, samples were harvested 48 h after transformation (section 8.1.28).

8.1.18 Elicitors used to study immune responses

Lipopolysaccharide preparations used in this study were kindly provided by Dr. Gisch (Leibniz-Zentrum, Borstel, Germany) (Ranf *et al.*, 2015). *Escherichia coli* O111:B4 LPS was purchased from Enzo Life Sciences (New York, USA). LPS from *Pseudomonas aeruginosa* (*Pa* H4), *Pseudomonas syringae* pv. *tomato* DC3000 (*Pst* DC3000), *Xanthomonas campestris* pv. *malvacearum* (*Xcm* #2, *Xcm* #4), and *Escherichia coli* (*Ec* B4) was used in concentrations of 10 to 25 µg/mL. Throughout this work, 3-hydroxydecanoic acid (3-HDA) was identified as the immunogenic epitope in LPS preparations (section 3.9). 3-HDA was purchased from Matreya LLC (State College, USA) and used in final concentrations of 1 µM to 10 µM. The peptidal elicitors flg22 (QRLSTGSRINSAKDDAAGLQIA), elf18 (ac-SKEKFERTKPHVNVGTIG), and *Fusarium oxysporum* nlp20 (AIMYAWYWPKDQPADGNLVSGHR) were kindly provided by Dr. Lee (IPB Halle) and synthesized with an Abimed EPS221 system (Abimed, Langenfeld, Germany). Chitin from shrimps (Sigma-Aldrich, St. Louis, USA) ground to fine powder was mixed with water. The soluble fraction was used for experiments.

8.1.19 Measurement of reactive oxygen species

ROS production after treatment with various elicitors (section 8.1.18) was analyzed in leaf discs (4 mm diameter) of 6-weeks-old plants according to Ranf *et al.* (2015). Leaf discs were floated over night on water. The water was replaced by a HRP-mix (2 µg/mL horseradish peroxidase, 10 µM L-012 (WAKO Chemicals GmbH, Neuss, Germany)) shortly before the measurement. After 10 min background measurement, elicitors or water or MeOH as control treatments, were added. Accumulation of ROS was observed for 45 to 360 min using a microplate reader (Infinite F200 PRO, Tecan, Grödig, Austria or Luminoskan Ascent 2.1, Thermo Fisher Scientific, Waltham, USA). For the investigation of the source of the ROS burst, 10 min background ROS level was measured, 3-HDA or MeOH as control were added. After 30 min was the measurement stopped and water, 100U catalase, or 100U catalase in combination with 100U super oxide dismutase were added to the leaf discs and the measurement was continued. The obtained data were normalized to the average ROS accumulation

of 5 min of the background measurement. The control treatment was subtracted. Control and elicitor treatments for each genotype were performed on the same plate.

8.1.20 Measurement of cytosolic calcium elevations

Plant lines expressing cytosolic apoaequorin (section 8.1.14 and Table 5) were grown for 9 to 10 days in liquid MS medium (section 9.1.2). Single seedlings were transferred into 96-well plates and incubated over night in 10 µM coelenterazine-h in water (P.J.K GmbH, Kleinblittersdorf, Germany). Luminescence counts of seedlings after treatment with an elicitor were quantified using a microplate reader (Luminoskan Ascent 2.1, Thermo Fisher Scientific Waltham, USA). To determine the remaining level of aequorin in each seedling, 150 µL 2 M $CaCl_2$ with 20% ethanol was added. As described in Ranf *et al.* (2012), cytosolic calcium concentrations ($[Ca^{2+}]_{cyt}$) were calculated by division of luminescence counts (L) per second with the sum of the remaining luminescence counts of a single seedling (L/L_{max})

8.1.21 MAP kinase activation

Activation of MAPK was analyzed in 10-days-old seedlings grown in MS liquid medium (section 9.1.2). Old medium was substituted by fresh medium 24 h prior to the performance of the experiment. 30 min before elicitation, medium was removed. Seedlings were treated with 10 µM 3-HDA, 50 µg/mL LPS *Pa* H4, or 500 nm flg22 diluted in MS liquid medium. Plant material was harvested at 0, 2, 4, 10, 20, and 60 min or 0, 10, 30, 60, 90, and 120 min after elicitation and frozen in liquid nitrogen. The plant material was ground using the TissueLyzerII (Qiagen, Hilden, Germany) for 1 min 30 f/s and frozen in liquid nitrogen. This step was repeated once. 200 µL of 2x kinase extraction buffer (50 mM Tris-HCl, pH 7.5, 100 mM NaCl, 20 mM EGTA, 30 mM glycerophosphate, 30 mM 4-*p*-nitrophenylphosphate, 20 mM $MgCl_2$, 4 mM NaF, 4 mM Na_3VO_4, 4 mM Na_2MoO_4, 1% (v/v) protease inhibitor cocktail P9599 (Sigma-Aldrich, St. Louis, USA), for protein extraction, was added. The samples were ground again for 3 min 30 f/s with the TissueLyzerII (Qiagen, Hilden, Germany) at RT. Samples were transferred into low bind tubes after centrifugation (20 min, 4°C, 18.000 g). The protein concentration was determined using the Bradford assay (Bio-Rad, Hercules, USA). 50 µg of total protein was separated by SDS-PAGE and analyzed *via* immunoblot as described in section 8.1.31. Phosphorylated MPKs were detected using the 1:1000 diluted α-p44/42-MAPK (T202/Y204) antibody (9101S, Cell signaling Technology, Danvers, USA) and the secondary 1:50000 anti-rabbit (A9169) antibody (Sigma-Aldrich, St. Louis, USA) (Table 8). The SuperSignal® West Femto Maximum Sensitivity Substrate (Pierce, Rockford, USA) was used for detection.

8.1.22 Induction of early defense genes

10-days-old seedlings, grown in 24-well plates in liquid MS medium (section 9.1.2) under long-day conditions, were treated for 4 h with 5 µM 3-HDA or MeOH as control. The plant material was harvested and frozen in liquid nitrogen. RNA of the treated plant material was isolated as described in section 8.1.12 and transcribed into cDNA as described in section 8.1.13. The induction of early defense genes was analyzed *via* qRT-PCR (section 8.1.24).

8.1.23 Induction of ethylene production

ET (ethylene) production of various plant lines was measured in response to 1 µM nlp20, 10 µM 3-HDA, or MeOH as control (section 8.1.18). Leaf discs were harvested and floated over night on water. Three leaf discs of 8-weeks old plants per genotype and treatment were transferred to 20 mM MES, pH 5.4 in glass reaction tubes. The leaf discs were treated with elicitor or control treatment for 4 h and incubated while shaking at RT. The amount of ET in 1 mL air was analyzed by gas chromatography (Varian 3300, Agilent Technologies Inc., Santa Clara, USA).

8.1.24 Quantitative real time polymerase chain reaction

Plants material was treated as described in section 8.1.22. Total RNA was isolated and transcribed into cDNA as described in sections 8.1.12 and 8.1.13. Quantitative real-time PCR (qRT-PCR) was performed on AriaMx (Agilent Technologies Inc., Santa Clara, USA) using the Maxima SYBR Green/ROX qPCR Master Mix (Thermo Fisher Scientific, Waltham, USA). qRT-PCR reactions were set up according to manufacturer's guidelines with 1 µL cDNA in a total volume of 10 µL. Samples were cycled 40 times (95°C 0:05 s; 60°C 0:20 s; 72°C 0:20 s). Amplification specificity was analyzed by non-template controls and dissociation curves of the used primer. Data analysis was done with the AriaMx software version 1.3. The expression levels were normalized to the housekeeping gene expression of ubiquitin (*AtUBQ5*). The fold change was calculated relatively to Col-0^{Aeq} treated with MeOH (calibrator) using the ΔΔCt method (Livak *et al.*, 2001).

Table 6 List of primers used for quantitative real time PCR.

primer name	sequence 5' to 3'	gene	reference
UBQ5-F	CCAAGCCGAAGAAGATCAA	*AtUBQ5*	Weis *et al.*, 2013
UBQ5-R	ACTCCTTCCTCAAACGCTGA	At3g62250	
qFRK1-F	TGCAGCGCAAGGACTAGAG	*AtFRK1*	He *et al.*, 2006
qFRK1-R	ATCTTCGCTTGGAGCTTCTC	At2g19190	

Table 6 (continued)

primer name	sequence 5' to 3'	gene	reference
qNHL10-F	TTCCTGTCCGTAACCCAAAC	*AtNHL10*	Boudsocq *et al.*, 2010
qNHL10-R	CCCTCGTAGTAGGCATGAGC	At2g35980	
after_SAIL857E06-F	AGCGGAAAGAGAATTTCACG	*AtLORE*	Ranf *et al.*, 2015
after_SAIL857E06-R	ACTTCGAATGCTTGGCATGT	At1g63180	

8.1.25 Seedling growth inhibition assay

Seedling growth inhibition assays were performed with surface-sterilized seeds (section 8.1.15) which were transferred on ATS plates (section 9.1.2) supplemented with 10 µM 3-HDA or MeOH as control. 10 to 12 seeds of wild-type and 10 to 12 seeds of OE lines or *lore*-1 were transferred with a sterile toothpick in one line on the upper third of square ATS plates (section 9.1.2). The seeds were stratified at 4°C for 48 h and grown under long day conditions in a vertical position. Root length and fresh weight of seedlings was analyzed after 8 days. The relative root length upon treatment was calculated relative to wild type treated with MeOH.

8.1.26 Apoplastic wash fluids

Apoplastic wash fluids (AWFs) were produced in *N. benthamiana* leaves transiently transformed as described in 8.1.17. To harvest AWFs, leaves were cut above the leaf stem and rinsed with distilled water. Leaves were vacuum-infiltrated (PDS-1000; Bio-Rad, Hercules, USA) with 1xTris-buffered saline (10x TBS-buffer 60.6 g/L Tris base, 87.6 g/L NaCL, pH 7.6) until the leaf was soaked evenly with liquid. For extraction of AWFs, the surface of the leaf was dried with a paper towel. The leaf was wrapped around a blue tip, put into the barrel of a syringe and the complete set up was transferred into a 50 mL falcon tube. AWFs were collected by centrifugation for 5 min, 4°C at 500 g. For further analysis, aliquots of the AWFs were frozen in liquid nitrogen and stored at -80°C.

8.1.27 Bacterial infection assays

Pseudomonas syringae pv. tomato DC3000 and *Pseudomonas syringae* pv. tomato DC3000 COR^- were used for bacterial infection assays in *Arabidopsis thaliana* (Melotto *et al.*, 2006, Katagiri *et al.*, 2002, Table 7). The bacterial infection assays were modified from Katagiri *et al.* (2002). Spray inoculation: *Pseudomonas* was grown over night at 26°C on King's B medium plates (section 9.1.1). Plates were rinsed with 3 mL Millipore water to collect bacterial colonies. The optical density was

adjusted to OD_{600} 0.2 in 10 mM $MgCl_2$ and 0.03% Silwet-77 (Kurt Obermeier GmbH, Bad Berleburg). 8-weeks-old plants were evenly sprayed with the bacterial suspension. Three plants per genotype and treatment were used for each experiment. Five of the sprayed leaves per plant were marked with a permanent marker for easier identification of the sprayed leaves at day 3. Samples were harvested after 4 h (day 0) and on day 3 post infection. Two of the marked leaves of each plant were cut off and surface-sterilized by rinsing the leaves in 70% ethanol for 15 s and subsequently in Millipore water for 15 s. Three technical replicates, consisting each of 9 leaf discs (4 mm diameter) transferred to 100 µL 10 mM $MgCl_2$, were prepared. Leaf discs were ground for 3 min and 30 f/s in a TissueLyzerII (Qiagen, Hilden, Germany). Dilution series in 1:10 steps were prepared in 96-well plates starting from the undiluted sample. Therefore, 100 µL sample was transferred to the 96-well plates and 20 µL of which were subsequently mixed with 180 µL Millipore water. A dilution series, with 3 dilution steps (to 10^{-3}) on day 0 and 7 dilution steps on day 3 (to 10^{-7}), was spotted on LSLB plates (section 9.1.1) supplemented with 75 µg/mL rifampicin (section 9.1.3) and incubated at 26°C over night. Colonies were counted and the colony forming units (cfu) per cm^2 leaf area were calculated.

Infiltration inoculation: The optical density of *Pseudomonas* for infiltration assays was adjusted to OD_{600} 0.002. Infiltrated leaves (five per plant) were marked with a permanent marker. Otherwise, the experiment was set up as described for the spray inoculation assays.

Pre-spray inoculation: Plants were evenly sprayed with 10 µM 3-HDA or MeOH supplemented with 0.01% Silwet-77 (Kurt Obermeier GmbH, Bad Berleburg). 2 h later, plants were surface-inoculated with *Pto* DC3000 as described for the spray inoculation assays. Samples were harvested 4 h upon infection as described for the spray inoculation assays.

Table 7 *Pseudomonas* strains used in this study.

Bacterial strain		reference
Pseudomonas syringae pathovar tomato DC3000	*Pto* DC3000	Prof. Jens Boch, Universität Hannover
Pseudomonas syringae pathovar tomato DC3000 COR$^-$	*Pto* DC3118 *Pto* DC3000 COR^{--}	Prof. Sheng Yang He, MSU, Michigan

8.1.28 Immunoprecipitation and co-immunoprecipitation

N. benthamiana leaves were transiently transformed as described in section 8.1.17. For co-immunoprecipitation experiments (CoIP), agrobacteria carrying plasmids coding for genes of interest were mixed in the ratio 1:1 and infiltrated in *N. benthamiana* leaves. Plant material (60 to 70 leaf discs per CoIP) was harvested 48 h after transient transformation, frozen in liquid nitrogen, and stored

at -80°C. Prior to protein extraction, plant material was ground for 1 min and 30 f/s in a TissueLyzerII (Qiagen, Hilden, Germany) and subsequently frozen in liquid nitrogen. This step was repeated twice. Total protein was extracted by addition of 6 µL extraction buffer per harvested leaf disc. The tobacco protein extraction buffer consisted of a premix (150 mM Tris-HCl, pH 7.5, 150 mM NaCl, 10% glycerol, 1% Nonidet-P40, 10 mM EDTA, 1 mM Na_2MoO_4, 1 mM NaF) and freshly added components (1 mM DTT, 1% (w/v) polyvinylpyrrolidon (PVPP), 1% (v/v) protease inhibitor cocktail P9599 (Sigma-Aldrich, St. Louis, USA)). Tubes were incubated at 4°C rotating for 20 to 30 min to achieve membrane solubilization. The supernatant was transferred into low bind tubes after centrifugation (4°C, 20 min, 18000 g). Depending on the experiment, HA-Trap magnetic beads (88836, Thermo Fisher Scientific, Waltham, USA), GFP-Trap_MA (magnetic beads, ChromoTek, Munich, Germany) or GFP-Trap_A (agarose beads, ChromoTek, Munich, Germany) were added to the protein extracts and incubated for 1 to 2 h at 4°C, rotating. Protein traps were prepared prior to addition to the protein extracts by rinsing the beads with washing buffer (150 mM Tris-HCL pH 7.5, 150 mM NaCl, 0.5% Nonidet-P40) which was repeated three times. After incubation, CoIP mixes were washed three times with washing buffer. After the last wash, the supernatant was removed and 20 µL 1xSDS-sample buffer was added. 20 µL input sample of each CoIP was saved and 5 µL 5xSDS-sample buffer (60 mM Tris-HCL pH 6.8, 2% SDS, 10% glycerol, 5% β-mercaptoethanol, 0.01% bromophenolblue) was added. All samples were incubated for 10 min at 95°C and analyzed by SDS-PAGE and immunoblot (section 8.1.31). The same procedure was used for immunoprecipitation experiments (IP) of stable transgenic *A. thaliana* lines. Leaf discs of mature plants or seedlings grown in liquid MS medium were used depending on the experiment as indicated in the results section. The extraction buffer consisted of a premix (150 mM Tris-HCl, pH 7.5, 150 mM NaCl, 10% glycerol, 1% Nonidet-P40, 10 mM EDTA, 1 mM Na_2MoO_4, 1 mM Na_3VO_4, 1 mM NaF) and freshly added components (1 mM DTT, 1% (v/v) protease inhibitor cocktail P9599 (Sigma-Aldrich, St. Louis, USA)).

8.1.29 Protein extraction of Arabidopsis seedlings and leaf discs

For the extraction of total protein of Arabidopsis seedlings or leaf discs of mature plants, material was harvested and frozen in liquid nitrogen. Prior to protein extraction, plant material was ground for 1 min and 30 f/s in a TissueLyzerII (Qiagen, Hilden, Germany) and subsequently frozen in liquid nitrogen. 6 µL extraction buffer per leaf disc was added. In case of seedlings, the material weight was scaled and 10 µL extraction buffer per 1 mg material weight was added. The extraction buffer consisted of a premix (150 mM Tris-HCl, pH 7.5, 150 mM NaCl, 10% glycerol, 1% Nonidet-P40, 10 mM EDTA, 1 mM Na_2MoO_4, 1 mM Na_3VO_4, 1 mM NaF) and freshly added components (1 mM DTT, 1% (v/v) protease inhibitor cocktail P9599 (Sigma-Aldrich, St. Louis, USA)). The tubes were incubated for 30 min at 4°C, rotating. The supernatant was transferred into low bind tubes after centrifugation (4°C, 30 min, 18000 g). The protein concentration was determined using the Bradford assay (Bio-Rad,

Hercules, USA). 50 µg of total protein was separated by SDS-PAGE and analyzed *via* immunoblots as described in section 8.1.31.

8.1.30 Pull-down experiments

Apoplastic wash fluids were generated as described in section 8.1.26. For immunoprecipitation (IP) experiments, AWFs were mixed in the ratio 1:1 and incubated 30 min rotating at 4°C. 20 µL of input samples were saved and mixed with SDS-sample buffer. HA trap (Thermo Fisher Scientific, Waltham, USA) was prepared as described in section 8.1.28 and added to the AWFs mixture. After 1 to 2 h incubation rotating at 4°C, IP mixes were washed three times with washing buffer (section 8.1.28). The supernatant was removed and 20 µL 1xSDS-sample buffer was added. All samples were incubated for 10 min at 95°C and analyzed with SDS-PAGE and immunoblot (section 8.1.31).

8.1.31 SDS-polyacrylamide gel electrophoresis and immunoblot analysis

Proteins were separated by SDS-polyacrylamide gel electrophoresis (SDS-PAGE, Laemmli (1970). Acrylamide gels with 5% stacking gel (680 µL/mL dH_2O, 170 µL/mL 30% acrylamide mix, 130 µL/mL 1 M Tris pH 6.8, 10 µL/mL 10% SDS, 10 µL/mL 10% ammonium persulfate, 1 µL/mL TEMED (*N*, *N*, *N´*, *N´* tetramethylethylenediamine)) and 10% resolving gel (380 µL/mL dH_2O, 340 µL/mL 30% acrylamide mix, 260 µL/mL 1.5 M Tris pH 8.8, 10 µL/mL 10%SDS, 10 µL/mL 10% ammonium persulfate, 0.4 µL/mL TEMED) of 1 mm thickness were used. Gel electrophoresis was performed at 60 V to 100 V in 1x Laemmli running buffer (10 g/L Tris base, 14.4 g/L glycine, and 0.1 g/L SDS, pH 8.3) until adequate protein separation was achieved using the Mini Protean III Cell system (Bio-Rad, Hercules, USA). The PageRuler Plus Prestained Protein Ladder (Thermo Fisher Scientific, Waltham, USA) was used as a ladder. For immunoblot analysis, proteins were transferred onto a 0.2 µm Protran™ nitrocellulose membrane (GE healthcare, Chicago, USA) using 1x transfer buffer (3.03 g/L Tris base, 14.4 g/L glycine, 20% methanol, and 0.05% SDS) and a semi dry transfer cell (Bio-Rad, Hercules, USA) at 1 mA/cm^2 for 1 h. Subsequently, free binding sites were blocked with protein free blocking solution T20 (Pierce, Rockford, USA; Tris buffered saline pH 7.4, 0.04% (v/v) Tween20) for 1 h, RT, or at 4°C over night. For detection of proteins, the appropriate antibody was applied as indicated in Table 8. Membranes were incubated rolling for 1 h at RT, or at 4°C over night with the primary antibody. Then, membranes were washed three times for 10 min with 1xTBS-T buffer (6.06 g/L Tris base, 8.76 g/L NaCl, pH 6.7, 0.05% Tween20) and incubated with the secondary antibody rolling for 1 h at RT followed by three washing steps. Chemiluminescence was detected with the CCD camera system Fusion-SL4 (Vilber Lourmat, Marne la Valée, France) with the FusionCapt Advance Solo 4 software. Low abundant proteins were detected with SuperSignal® West Femto Maximum Sensitivity Substrate (Pierce, Rockford, USA) and highly expressed proteins with

SuperSignal®West Dura Extended Duration Substrate (Pierce, Rockford, USA). Total protein was stained by amido black protein stain (1 g/L amido black, 250 mL/L isopropyl, 100 mL/L acetic acid).

8.1.32 Membrane stripping

Nitrocellulose membranes were stripped to remove bound antibodies. Therefore, membranes were incubated shaking for 30 min at 50°C with stripping buffer (2% SDS, 62.5 mM Tris-HCl pH 6.7, 100 mM β-mercaptoethanol). The membranes were washed three times and free binding sites were blocked with protein free blocking solution T20 (Pierce, Rockford, USA) for 1 h at RT.

Table 8 Name and dilution of antibodies used in this study. Primary antibodies were diluted in protein free blocking solution T20 (Pierce, Rockford, USA). Secondary antibodies were diluted in 1xTBS 0.05% Tween20. Primary antibodies were incubated for 1 h at RT or over night at 4°C, secondary antibodies were incubated for 1 h at RT.

primary antibody	dilution	secondary antibody
anti-GFP 3H9 (ChromoTek, Munich, Germany)	1:1000	1:20000 anti-rat A9542 (Sigma-Aldrich, St. Louis, USA)
anti-Red 5F8 (ChromoTek, Munich, Germany)	1:2000	1:20000 anti-rat A9542 (Sigma-Aldrich, St. Louis, USA)
anti-HA-HRP 3F10 (Sigma-Aldrich, St. Louis, USA)	1:2000	no secondary antibody required
α-p44/42-MAPK (T202/Y204) (Cell signaling, Danvers, USA)	1:1000	1:50000 anti-rabbit A9169 (Sigma-Aldrich, St. Louis, USA)
c-Myc 9E10 (Santa Cruz, Dallas, USA)	1:500	1:5000 anti-mouse sc-2031 (Santa Cruz, Dallas, USA)

8.1.33 Bimolecular fluorescence complementation assay

To analyze protein-protein interaction *in planta*, bimolecular fluorescence complementation assays (BiFC) were carried out in transiently transformed *N. benthamiana* leaves. Cytosolic SPYCE served as negative control. Protein-protein interaction was visually evaluated with confocal scanning microscopy (section 8.1.34). Fluorescence intensity of 24 leaf discs per sample was measured (excitation 485 nm, emission 535 nm) for 5 min with a plate-reader luminometer (Luminoskan Ascent 2.1, Thermo Fisher Scientific Waltham, USA). Protein expression in 24 leaf discs was analyzed with

immunoblot analysis (section 8.1.31). The Golden Gate BiFC vectors are based on the vector system published by Walter *et al.* (2004) and are listed in Table 9.

Table 9 List of constructs used for bimolecular-fluorescence complementation assays. pGGIn-228C represents SPYNE (n-terminal part of YFP; based on pSPYNE(R)173-35S) and pGGIn-229C represents SPYCE (c-terminal part of YFP, based on pSPYCE(M)-35S) (Walter *et al.*, 2004). pGGIn-220_cytSPYCE represents the cytosolic C-terminal part of YFP used as a negative control.

construct	abbreviation	reference
pGGIn-228C_LORE-Km	LORE-Km-N	this study, Sonja Eibel
pGGIn-229C_LORE-Km	LORE-Km-C	this study, Sonja Eibel
pGGIn-229C_LORE-dLLEP	iLORE-C	this study, Sonja Eibel
pGGIn-229C_LORE-dJKD	tLORE-C	this study, Sonja Eibel
pGGIn-220_cytSPYCE	cyt. C	this study, Sonja Eibel

8.1.34 Confocal laser scanning microscopy

Microscopic evaluation of fluorophore-tagged proteins was done with a Leica TCS SP5 (Leica Microsystems, Mannheim, Germany) confocal microscope. Pictures were processed using the Leica Application Suite Advanced fluorescence software (LAS AF version 2.5.1.6757). Excitation and emission wavelength used for different fluorophores are summarized in Table 10.

Table 10 Fluorophores and their excitation wavelength and emission spectra used in this study for microscopic evaluation.

fluorophore	excitation in nm	emission spectrum in nm
eGFP	488	500 - 535
mCherry	561	570 - 610
YFP	514	525 - 550

8.1.35 Thermal imaging

Thermal imaging was performed to analyze changes in the leaf temperature of several plant lines in response to various treatments and hence stomatal closure. Therefore, 2-weeks-old plants were separated into single pots. Seven days later, the soil was covered with parafilm to obtain an even

background for imaging. Four weeks later, plants were analyzed and sprayed with 10 µM 3-HDA or *Pto* DC3000 with an OD of 0.2 supplemented with 0.01% Silwet-77 (Kurt Obermeier GmbH, Bad Berleburg). MeOH or water supplemented with 0.01% Silwet-77 was sprayed as control treatment, respectively. Pictures were taken with a thermal camera (InfraTec, Dresden, Germany) before treatment and 2h, in case of bacterial treatment 3h, after spraying. Six plants of each genotype were grown on one tray, three were sprayed with the elicitor or bacteria, three with the control treatment. The leaf area temperature of up to eight leaves of each plant was analyzed with the IRBIS3 software using the thermograms (InfraTec, Dresden, Germany). The average leaf temperature overall plants was calculated. The Δ leaf temperature before treatment was calculated by subtraction of the average wild-type leaf temperature. For example, Δ leaf temperature before treatment of *lore*-1 was calculated by subtraction of the average wild type leaf temperature. The Δ leaf temperature due to treatment was calculated by subtraction of the average leaf temperature of the respective genotype with the control treatment of the respective genotype for the specific time point (Table 11).

Table 11 Summary of the equations used for calculation of changes in leaf temperature

Δ leaf temperature	**equation**
before treatment	Δ leaf temperature before treatment = average leaf temperature genotype – average leaf temperature wild type
after treatment	Δ leaf temperature before treatment = average leaf temperature genotype treated – average leaf temperature genotype control treated

8.1.36 Software used in this study

All software and online databanks used for this study are summarized in Table 12.

Table 12 List of software and online accessible databases as well as prediciton tools used within this study.

name	**URL**	**purpose**	**reference**
Clustal Omega	https://www.ebi.ac.uk/Tools/msa/clustalo/	multiple sequence alignments	Sievers *et al.*, 2011
Genevestigator	https://genevestigator.com/gv/index.jsp	reference gene expression database	Hruz *et al.*, 2008

Table 12 (continued)

name	URL	purpose	reference
GenBank	http://www.ncbi.nlm.nih.gov	nucleotide sequence database	Lipman *et al*., 2012
GraphPad Prism6	https://www.graphpad.com/	figure design and statistical analysis	GraphPad Software, La Jolla, USA
IRBIS3		analysis of thermal images	InfraTec, Dresden, Germany
Jalview	https://www.jalview.org	edit multiple sequence alignments	Waterhouse *et al.*, 2009
MEGA X		phylogenetic analysis	Kumar *et al.*, 2018
PyMOL (TM)		molecular 3D visualization of proteins	DeLano Scientific LLC, San Francisco, USA
Phytozome 12	https://phytozome.jgi.doe.gov/pz/portal	plant genomic resource	The Regents of the University of California
SnapGene	https://www.graphpad.com	molecular cloning, primer design	GSL Biotech LLC, Chicago, USA
TAIR10	http://www.arabidopsis.org	sequences and protein information	Phoenix Bioinformatics Corporation
UbPred	http://www.ubpred.org/	prediction of ubiquitination sites	Radivojac *et al.*, 2010
UniProt	http://www.uniprot.org/	protein domain predictions	The UniProt Consortium , 2017
WebLogo	http://weblogo.berkeley.edu/logo.cgi	generation of sequence logo	Crooks *et al.*, 2004
14-3-3-pred	https://www.compbio.dundee.ac.uk/1433pred/	prediction of 14-3-3 binding sites	Madeira *et al.*, 2015

9 Media

9.1.1 Medium used for bacterial cultivation

All media used in this study for the cultivation of *E. coli*, *A. tumefaciens*, and *P. syringae* are listed within this section. Medium used for the cultivation of *A. thaliana* seedlings is also described in this section. Application details are mentioned in section 8.1.

Luria-Bertani medium (LB medium), for the cultivation of *E. coli* and *A. tumefaciens*, consists of 10 g/L peptone, 5 g/L yeast extract, 10 g/L NaCl. The pH value was adjusted to pH 7.0 with 1 M KOH. For LB plates, 20g/L agar was added before autoclaving. LB plates were supplemented with appropriate antibiotics after autoclaving. Low Salt Luria-Bertani medium (LSLB medium), for the cultivation of *Pseudomonas* bacteria, consists of 10 g/L peptone, 5 g/L yeast extract, and 5 g/L NaCl. Before autoclaving, the pH value was adjusted to pH 7.0 with 1 M KOH and 20 g/L agar was added for LSLB plates. LSLB plates were supplemented with 75 µg/mL rifampicin. King's B medium (KB medium) for the cultivation of *Pseudomonas* on plates consists of 20 g/L peptone, 1.5 g/L $MgSO_4$-$7xH_2O$, 1.5 g/L K_2HPO_4, and 15 g glycerol. The pH value was adjusted to pH 7.0 with HCl and 20 g/L agar was added before autoclaving. Terrific Broth medium (TB medium) was used for the cultivation of *E. coli* used for plasmid amplification (section 8.1.3). TB medium consists of 12 g/L tryptone, 24 g/L yeast extract, and 4 mL/L glycerol. 100 mL/L K_2HPO_4 pH 7.5 was added after autoclaving.

9.1.2 Medium used for cultivation of Arabidopsis

Murashige & Skoog medium (MS medium) was used for the cultivation of Arabidopsis seedlings in 24-well plates. MS medium consists of 2.2 g/L MS (Duchefa Biochemie, MS including modified vitamins), 2.5 g/L sucrose, and 0.195 g/L MES buffer. The pH value was adjusted to pH 5.7 with 1 M KOH and for MS plates 5 g/L agar gel (Sigma-Aldrich, St. Louis, USA) was added before autoclaving. Arabidopsis seedlings were cultivated on Arabidopsis thaliana solution (ATS medium) for seedling growth inhibition assays (section 8.1.25). ATS medium consists of 5 mL/L 1 M KNO_3, 2.5 mL/L 1 M K_2HPO_4, 2 mL/L 1 M $MgSO_4$, 2 mL/L 1 M $Ca(NO_3)_2$, 2.5 mL/L 20 mM Fe-EDTA, 1 mL/L micronutrients (70 mM H_3BO_3, 14 mM $MnCl_2$, 0.5 mM $CuSO_4$, 1 mM $ZnSO_4$, 0.2 mM Na_2MoO_4, 10 mM NaCl, 0.01 mM $CoCl_2$), and 5 g/L sucrose. 5 g/L agar gel (Sigma-Aldrich, St. Louis, USA) was added before autoclaving.

9.1.3 Antibiotics and other supplements

The concentrations of antibiotics and other supplements for media used in this study are listed in Table 13.

Table 13 Summary of concentrations used for antibiotics and other supplements.

antibiotics and other supplements	concentrations
ampicillin	250 µg/mL
gentamycin	30 µg/mL
kanamycin	50 µg/mL
streptomycin	50 µg/mL
rifampicin	75 µg/mL for LSLB plates 10 µg/mL for LB plates
X-Gal (5-Bromo-4-Chloro-3-Indolyl β-D-Galactopyranoside)	30 µg/mL
IPTG (Isopropyl-β-D-thiogalactopyranosid)	0.05 mM

10 Bibliography

Ade, J., DeYoung, B. J., Golstein, C. & Innes, R. W. (2007) Indirect activation of a plant nucleotide binding site–leucine-rich repeat protein by a bacterial protease *Proceedings of the National Academy of Sciences* 104, 2531-2536.

Albert, I., Böhm, H., Albert, M., Feiler, C. E., Imkampe, J., Wallmeroth, N., Brancato, C., Raaymakers, T. M., Oome, S., Zhang, H., Krol, E., Grefen, C., Gust, A. A., Chai, J., Hedrich, R., Van den Ackerveken, G. & Nürnberger, T. (2015) An RLP23–SOBIR1–BAK1 complex mediates NLP-triggered immunity *Nature Plants* 1, 15140.

Albert, M., Jehle, A. K., Fürst, U., Chinchilla, D., Boller, T. & Felix, G. (2013) A two-hybrid-receptor assay demonstrates heteromer formation as switch-on for plant immune receptors *Plant Physiology* 163, 1504-1509.

Albert, M., Jehle, A. K., Mueller, K., Eisele, C., Lipschis, M. & Felix, G. (2010) Arabidopsis thaliana pattern recognition receptors for bacterial elongation factor Tu and flagellin can be combined to form functional chimeric receptors *Journal of Biological Chemistry* 285, 19035-19042.

Alexander, C. & Rietschel, E. T. (2001) Bacterial lipopolysaccharides and innate immunity *Journal of Endotoxin Research* 7, 167-202.

Ali, G. S., Prasad, K. V. S. K., Day, I. & Reddy, A. S. N. (2007) Ligand-dependent reduction in the membrane mobility of FLAGELLIN SENSITIVE2, an Arabidopsis receptor-like kinase *Plant and Cell Physiology* 48, 1601-1611.

Asai, T., Tena, G., Plotnikova, J., Willmann, M. R., Chiu, W.-L., Gomez-Gomez, L., Boller, T., Ausubel, F. M. & Sheen, J. (2002) MAP kinase signalling cascade in Arabidopsis innate immunity *Nature* 415, 977.

Azevedo, C., Santos-Rosa, M. J. & Shirasu, K. (2001) The U-box protein family in plants *Trends in Plant Science* 6, 354-358.

Balagué, C., Gouget, A., Bouchez, O., Souriac, C., Haget, N., Boutet-Mercey, S., Govers, F., Roby, D. & Canut, H. (2017) The Arabidopsis thaliana lectin receptor kinase LecRK-I.9 is required for full resistance to Pseudomonas syringae and affects jasmonate signalling *Molecular Plant Pathology* 18, 937-948.

Bardin, M., Ajouz, S., Comby, M., Lopez-Ferber, M., Graillot, B., Siegwart, M. & Nicot, P. C. (2015) Is the efficacy of biological control against plant diseases likely to be more durable than that of chemical pesticides? *Frontiers in Plant Science* 6.

Bardoel, B. W., van der Ent, S., Pel, M. J. C., Tommassen, J., Pieterse, C. M. J., van Kessel, K. P. M. & van Strijp, J. A. G. (2011) Pseudomonas evades immune recognition of flagellin in both mammals and plants *PLoS Pathogens* 7, e1002206.

Barrett, S. C. H. (2002) The evolution of plant sexual diversity *Nature Reviews Genetics* 3, 274.

Beattie, G. A. & Lindow, S. E. (1995) The secret life of foliar bacterial pathogens on leaves *Annual Review of Phytopathology* 33, 145-172.

Beck, M., Wyrsch, I., Strutt, J., Wimalasekera, R., Webb, A., Boller, T. & Robatzek, S. (2014) Expression patterns of FLAGELLIN SENSING 2 map to bacterial entry sites in plant shoots and roots *Journal of Experimental Botany* 65, 6487-6498.

Beck, M., Zhou, J., Faulkner, C., MacLean, D. & Robatzek, S. (2012) Spatio-temporal cellular dynamics of the Arabidopsis flagellin receptor reveal activation status-dependent endosomal sorting *Plant Cell* 24, 4205-4219.

Bellande, K., Bono, J.-J., Savelli, B., Jamet, E. & Canut, H. (2017) Plant lectins and lectin receptor-like kinases: How do they sense the outside? *International Journal of Molecular Sciences* 18, 1164.

Bender, C. L. (1999) Chlorosis-inducing phytotoxins produced by Pseudomonas syringae *European Journal of Plant Pathology* 105, 1-12.

Bender, C. L., Alarcón-Chaidez, F. & Gross, D. C. (1999) Pseudomonas syringae phytotoxins: mode of action, regulation, and biosynthesis by peptide and polyketide synthetases *Microbiology and Molecular Biology Reviews* 63, 266-292.

Bi, G., Liebrand, T. W. H., Bye, R. R., Postma, J., van der Burgh, A. M., Robatzek, S., Xu, X. & Joosten, M. H. A. J. (2016) SOBIR1 requires the GxxxG dimerization motif in its transmembrane domain to form constitutive complexes with receptor-like proteins *Molecular Plant Pathology* 17, 96-107.

Bleckmann, A., Weidtkamp-Peters, S., Seidel, C. A. M. & Simon, R. (2010) Stem cell signaling in Arabidopsis requires CRN to localize CLV2 to the plasma membrane *Plant Physiology* 152, 166-176.

Boggs, N. A., Dwyer, K. G., Nasrallah, M. E. & Nasrallah, J. B. (2009) In vivo detection of residues required for ligand-selective activation of the S-Locus Receptor in Arabidopsis *Current Biology* 19, 786-791.

Böhm, H., Albert, I., Oome, S., Raaymakers, T. M., Van den Ackerveken, G. & Nürnberger, T. (2014) A conserved peptide pattern from a widespread microbial virulence factor triggers pattern-induced immunity in Arabidopsis *PLoS Pathogens* 10, e1004491.

Boller, T. & Felix, G. (2009) A renaissance of elicitors: Perception of microbe-associated molecular patterns and danger signals by pattern-recognition receptors *Annual Review of Plant Biology* 60, 379-406.

Boudsocq, M., Willmann, M. R., McCormack, M., Lee, H., Shan, L., He, P., Bush, J., Cheng, S. H. & Sheen, J. (2010) Differential innate immune signalling via Ca(2+) sensor protein kinases *Nature* 464, 418-422.

Boureau, T., Routtu, J., Roine, E., Taira, S. & Romantschuk, M. (2002) Localization of hrpA-induced Pseudomonas syringae pv. tomato DC3000 in infected tomato leaves *Molecular Plant Pathology* 3, 451-460.

Boutrot, F., Segonzac, C., Chang, K. N., Qiao, H., Ecker, J. R., Zipfel, C. & Rathjen, J. P. (2010) Direct transcriptional control of the Arabidopsis immune receptor FLS2 by the ethylene-dependent transcription factors EIN3 and EIL1 *Proceedings of the National Academy of Sciences* 107, 14502-14507.

Boutrot, F. & Zipfel, C. (2017) Function, discovery, and exploitation of plant pattern recognition receptors for broad-spectrum disease resistance *Annual Review of Phytopathology* 55, 257-286.

Bouwmeester, K., de Sain, M., Weide, R., Gouget, A., Klamer, S., Canut, H. & Govers, F. (2011) The Lectin Receptor Kinase LecRK-I.9 Is a Novel Phytophthora Resistance Component and a Potential Host Target for a RXLR Effector *PLoS Pathogens* 7, e1001327.

Bouwmeester, K. & Govers, F. (2009) Arabidopsis L-type lectin receptor kinases: phylogeny, classification, and expression profiles *Journal of Experimental Botany* 60, 4383-4396.

Bouwmeester, K., Han, M., Blanco-Portales, R., Song, W., Weide, R., Guo, L.-Y., van der Vossen, E. A. G. & Govers, F. (2014) The Arabidopsis lectin receptor kinase LecRK-I.9 enhances resistance to Phytophthora infestans in Solanaceous plants *Plant Biotechnology Journal* 12, 10-16.

Bower, M. S., Matias, D. D., Fernandes-Carvalho, E., Mazzurco, M., Gu, T., Rothstein, S. J. & Goring, D. R. (1996) Two members of the thioredoxin-h family interact with the kinase domain of a Brassica S locus receptor kinase *Plant Cell* 8, 1641-1650.

Brooks, D. M., Bender, C. L. & Kunkel, B. N. (2005) The Pseudomonas syringae phytotoxin coronatine promotes virulence by overcoming salicylic acid-dependent defences in Arabidopsis thaliana *Molecular Plant Pathology* 6, 629-639.

Brooks, D. M., Hernández-Guzmán, G., Kloek, A. P., Alarcón-Chaidez, F., Sreedharan, A., Rangaswamy, V., Peñaloza-Vázquez, A., Bender, C. L. & Kunkel, B. N. (2004) Identification and characterization of a well-defined series of coronatine biosynthetic mutants of Pseudomonas syringae pv. tomato DC3000 *Molecular Plant-Microbe Interactions* 17, 162-174.

Brutus, A., Sicilia, F., Macone, A., Cervone, F. & Lorenzo, G. (2010) A domain swap approach reveals a role of the plant wall-associated kinase 1 (WAK1) as a receptor of oligogalacturonides *Proceedings of the National Academy of Sciences* 107, 9452-9457.

Bücherl, C. A., Jarsch, I. K., Schudoma, C., Segonzac, C., Mbengue, M., Robatzek, S., MacLean, D., Ott, T. & Zipfel, C. (2017) Plant immune and growth receptors share common signalling components but localise to distinct plasma membrane nanodomains *eLife* 6, e25114.

Cabrillac, D., Cock, J. M., Dumas, C. & Gaude, T. (2001) The S-locus receptor kinase is inhibited by thioredoxins and activated by pollen coat proteins *Nature* 410, 220-223.

Cao, Y., Liang, Y., Tanaka, K., Nguyen, C. T., Jedrzejczak, R. P., Joachimiak, A. & Stacey, G. (2014) The kinase LYK5 is a major chitin receptor in Arabidopsis and forms a chitin-induced complex with related kinase CERK1 *eLife* 3, e03766.

Chen, D., Cao, Y., Li, H., Kim, D., Ahsan, N., Thelen, J. & Stacey, G. (2017) Extracellular ATP elicits DORN1-mediated RBOHD phosphorylation to regulate stomatal aperture *Nature Communications* 8, 2265.

Chen, L.-J., Wuriyanghan, H., Zhang, Y.-Q., Duan, K.-X., Chen, H.-W., Li, Q.-T., Lu, X., He, S.-J., Ma, B., Zhang, W.-K., Lin, Q., Chen, S.-Y. & Zhang, J.-S. (2013) An S-Domain receptor-like kinase, OsSIK2, confers abiotic stress tolerance and delays dark-induced leaf senescence in rice *Plant Physiology* 163, 1752-1765.

Chen, X., Chern, M., Canlas, P. E., Jiang, C., Ruan, D., Cao, P. & Ronald, P. C. (2010) A conserved threonine residue in the juxtamembrane domain of the XA21 pattern recognition receptor is critical for kinase autophosphorylation and XA21-mediated immunity *Journal of Biological Chemistry* 285, 10454-10463.

Chen, X., Shang, J., Chen, D., Lei, C., Zou, Y., Zhai, W., Liu, G., Xu, J., Ling, Z., Cao, G., Ma, B., Wang, Y., Zhao, X., Li, S. & Zhu, L. (2006) A B-lectin receptor kinase gene conferring rice blast resistance *The Plant Journal* 46, 794-804.

Chen, X., Zuo, S., Schwessinger, B., Chern, M., Canlas, P. E., Ruan, D., Zhou, X., Wang, J., Daudi, A., Petzold, C. J., Heazlewood, J. L. & Ronald, P. C. (2014) An XA21-associated kinase (OsSERK2) regulates immunity mediated by the XA21 and XA3 immune receptors *Molecular Plant* 7, 874-892.

Cheng, S.-H., Willmann, M. R., Chen, H.-C. & Sheen, J. (2002) Calcium signaling through protein kinases. The Arabidopsis calcium-dependent protein kinase gene family *Plant Physiology* 129, 469-485.

Chinchilla, D., Bauer, Z., Regenass, M., Boller, T. & Felix, G. (2006) The Arabidopsis receptor Kinase FLS2 binds flg22 and determines the specificity of flagellin perception *Plant Cell* 18, 465-476.

Chinchilla, D., Zipfel, C., Robatzek, S., Kemmerling, B., Nurnberger, T., Jones, J. D. G., Felix, G. & Boller, T. (2007) A flagellin-induced complex of the receptor FLS2 and BAK1 initiates plant defence *Nature* 448, 497-500.

Chitrakar, R. & Melotto, M. (2010) Assessing stomatal response to live bacterial cells using whole leaf imaging *Journal of Visualized Experiments*, 2185.

Choi, J., Tanaka, K., Cao, Y., Qi, Y., Qiu, J., Liang, Y., Lee, S. Y. & Stacey, G. (2014) Identification of a plant receptor for extracellular ATP *Science* 343, 290-294.

Chung, E.-H., da Cunha, L., Wu, A.-J., Gao, Z., Cherkis, K., Afzal, A. J., Mackey, D. & Dangl, J. L. (2011) Specific threonine phosphorylation of a host target by two unrelated Type III effectors activates a host innate immune receptor in plants *Cell Host & Microbe* 9, 125-136.

Couto, D. & Zipfel, C. (2016) Regulation of pattern recognition receptor signalling in plants *Nature Reviews Immunology* 16, 537.

Crooks, G. E., Hon, G., Chandonia, J. M. & Brenner, S. E. (2004) WebLogo: a sequence logo generator *Genome Research* 14, 1188-1190.

Cui, H., Qiu, J., Zhou, Y., Bhandari, D. D., Zhao, C., Bautor, J. & Parker, J. E. (2018) Antagonism of transcription factor MYC2 by EDS1/PAD4 complexes bolsters salicylic acid defense in Arabidopsis effector-triggered immunity *Molecular Plant* 11, 1053-1066.

Cui, H., Tsuda, K. & Parker, J. E. (2015) Effector-triggered immunity: From pathogen perception to robust defense *Annual Review of Plant Biology* 66, 487-511.

Cunnac, S., Chakravarthy, S., Kvitko, B. H., Russell, A. B., Martin, G. B. & Collmer, A. (2011) Genetic disassembly and combinatorial reassembly identify a minimal functional repertoire of type III effectors in Pseudomonas syringae *Proceedings of the National Academy of Sciences* 108, 2975-2980.

Dangl, J. L., Horvath, D. M. & Staskawicz, B. J. (2013) Pivoting the plant immune system from dissection to deployment *Science* 341, 746-751.

Dardick, C., Schwessinger, B. & Ronald, P. (2012) Non-arginine-aspartate (non-RD) kinases are associated with innate immune receptors that recognize conserved microbial signatures *Current Opinion in Plant Biology* 15, 358-366.

De Lorenzo, G., Brutus, A., Savatin, D. V., Sicilia, F. & Cervone, F. (2011) Engineering plant resistance by constructing chimeric receptors that recognize damage-associated molecular patterns (DAMPs) *FEBS Letters* 585, 1521-1528.

Desaki, Y., Kouzai, Y., Ninomiya, Y., Iwase, R., Shimizu, Y., Seko, K., Molinaro, A., Minami, E., Shibuya, N., Kaku, H. & Nishizawa, Y. (2018) OsCERK1 plays a crucial role in the lipopolysaccharide-induced immune response of rice *New Phytologist* 217, 1042-1049.

Desaki, Y., Miya, A., Venkatesh, B., Tsuyumu, S., Yamane, H., Kaku, H., Minami, E. & Shibuya, N. (2006) Bacterial lipopolysaccharides induce defense responses associated with programmed cell death in rice cells *Plant and Cell Physiology* 47, 1530-1540.

Desikan, R., Horák, J., Chaban, C., Mira-Rodado, V., Witthöft, J., Elgass, K., Grefen, C., Cheung, M.-K., Meixner, A. J., Hooley, R., Neill, S. J., Hancock, J. T. & Harter, K. (2008) The histidine kinase AHK5 integrates endogenous and environmental signals in Arabidopsis guard cells *PLoS ONE* 3, e2491.

Doehlemann, G. & Hemetsberger, C. (2013) Apoplastic immunity and its suppression by filamentous plant pathogens *New Phytologist* 198, 1001-1016.

Domínguez-Ferreras, A., Kiss-Papp, M., Jehle, A. K., Felix, G. & Chinchilla, D. (2015) An overdose of the Arabidopsis coreceptor BRASSINOSTEROID INSENSITIVE1-ASSOCIATED RECEPTOR KINASE1 or its ectodomain causes autoimmunity in a SUPPRESSOR OF BIR1-1-dependent manner *Plant Physiology* 168, 1106-1121.

Dörmann, P., Gopalan, S., Yang He, S. & Benning, C. (2000) A gene family in Arabidopsis thaliana with sequence similarity to NDR1 and HIN1 *Plant Physiology and Biochemistry* 38, 789-796.

Dubiella, U., Seybold, H., Durian, G., Komander, E., Lassig, R., Witte, C.-P., Schulze, W. X. & Romeis, T. (2013) Calcium-dependent protein kinase/NADPH oxidase activation circuit is required for rapid defense signal propagation *Proceedings of the National Academy of Sciences* 110, 8744-8749.

Fan, J., Bai, P., Ning, Y., Wang, J., Shi, X., Xiong, Y., Zhang, K., He, F., Zhang, C., Wang, R., Meng, X., Zhou, J., Wang, M., Shirsekar, G., Park, C. H., Bellizzi, M., Liu, W., Jeon, J.-S., Xia, Y., Shan, L. & Wang, G.-L. (2018) The monocot-specific receptor-like kinase SDS2 controls cell death and immunity in rice *Cell Host & Microbe* 23, 496-510.

Felix, G., Duran, J. D., Volko, S. & Boller, T. (1999) Plants have a sensitive perception system for the most conserved domain of bacterial flagellin *The Plant Journal* 18, 265-276.

Feys, B., Benedetti, C. E., Penfold, C. N. & Turner, J. G. (1994) Arabidopsis mutants selected for resistance to the phytotoxin coronatine are male sterile, insensitive to methyl jasmonate, and resistant to a bacterial pathogen *Plant Cell* 6, 751-759.

Flor, H. H. (1971) Current status of the gene-for-gene concept *Annual Review of Phytopathology* 9, 275-296.

Fradin, E. F., Zhang, Z., Rovenich, H., Song, Y., Liebrand, T. W., Masini, L., van den Berg, G. C., Joosten, M. H. & Thomma, B. P. (2014) Functional analysis of the tomato immune receptor Ve1 through domain swaps with its non-functional homolog Ve2 *PLoS ONE* 9, e88208.

Freeman, B. C. & Beattie, G. A. (2008) An overview of plant defenses against pathogens and herbivores *The Plant Health Instructor*.

Fritz-Laylin, L. K., Krishnamurthy, N., Tör, M., Sjölander, K. V. & Jones, J. D. G. (2005) Phylogenomic analysis of the receptor-like proteins of rice and Arabidopsis *Plant Physiology* 138, 611-623.

Furlan, G., Nakagami, H., Eschen-Lippold, L., Jiang, X., Majovsky, P., Kowarschik, K., Hoehenwarter, W., Lee, J. & Trujillo, M. (2017) Changes in PUB22 ubiquitination modes triggered by MITOGEN-ACTIVATED PROTEIN KINASE3 dampen the immune response *Plant Cell* 29, 726-745.

Gao, M., Wang, X., Wang, D., Xu, F., Ding, X., Zhang, Z., Bi, D., Cheng, Y. T., Chen, S., Li, X. & Zhang, Y. (2009) Regulation of cell death and innate immunity by two receptor-like kinases in Arabidopsis *Cell Host & Microbe* 6, 34-44.

Georgieva, M. V., Yahya, G., Codó, L., Ortiz, R., Teixidó, L., Claros, J., Jara, R., Jara, M., Iborra, A., Gelpí, J. L., Gallego, C., Orozco, M. & Aldea, M. (2015) Inntags: small self-structured epitopes for innocuous protein tagging *Nature Methods* 12, 955.

Gerber, I. B., Zeidler, D., Durner, J. & Dubery, I. A. (2004) Early perception responses of Nicotiana tabacum cells in response to lipopolysaccharides from Burkholderia cepacia *Planta* 218, 647-657.

Gimenez-Ibanez, S., Hann, D. R., Ntoukakis, V., Petutschnig, E., Lipka, V. & Rathjen, J. P. (2009) AvrPtoB targets the LysM receptor kinase CERK1 to promote bacterial virulence on plants *Current Biology* 19, 423-429.

Giranton, J. L., Dumas, C., Cock, J. M. & Gaude, T. (2000) The integral membrane S-locus receptor kinase of Brassica has serine/threonine kinase activity in a membranous environment and spontaneously forms oligomers in planta *Proceedings of the National Academy of Sciences* 97, 3759-3764.

Glazebrook, J. (2005) Contrasting mechanisms of defense against biotrophic and necrotrophic pathogens *Annual Review of Phytopathology* 43, 205-227.

Glazebrook, J. & Ausubel, F. M. (1994) Isolation of phytoalexin-deficient mutants of Arabidopsis thaliana and characterization of their interactions with bacterial pathogens *Proceedings of the National Academy of Sciences* 91, 8955-8959.

Göhre, V., Spallek, T., Haweker, H., Mersmann, S., Mentzel, T., Boller, T., de Torres, M., Mansfield, J. W. & Robatzek, S. (2008) Plant pattern-recognition receptor FLS2 is directed for degradation by the bacterial ubiquitin ligase AvrPtoB *Current Biology* 18, 1824-1832.

Gomez-Gomez, L. & Boller, T. (2000) FLS2: an LRR receptor-like kinase involved in the perception of the bacterial elicitor flagellin in Arabidopsis *Molecular Cell* 5, 1003-1011.

Gómez-Gómez, L., Felix, G. & Boller, T. (1999) A single locus determines sensitivity to bacterial flagellin in Arabidopsis thaliana *The Plant Journal* 18, 277-284.

Grant, J. J. & Loake, G. J. (2000) Role of reactive oxygen intermediates and cognate redox Signaling in disease resistance *Plant Physiology* 124, 21-29.

Gu, T., Mazzurco, M., Sulaman, W., Matias, D. D. & Goring, D. R. (1998) Binding of an arm repeat protein to the kinase domain of the S-locus receptor kinase *Proceedings of the National Academy of Sciences* 95, 382-387.

Guan, R., Su, J., Meng, X., Li, S., Liu, Y., Xu, J. & Zhang, S. (2015) Multilayered regulation of ethylene induction plays a positive role in Arabidopsis resistance against Pseudomonas syringae *Plant Physiology* 169, 299-312.

Guo, M., Kim, P., Li, G., Elowsky, Christian G. & Alfano, James R. (2016) A bacterial effector co-opts calmodulin to target the plant microtubule network *Cell Host & Microbe* 19, 67-78.

Gust, A. A., Biswas, R., Lenz, H. D., Rauhut, T., Ranf, S., Kemmerling, B., Götz, F., Glawischnig, E., Lee, J., Felix, G. & Nürnberger, T. (2007) Bacteria-derived peptidoglycans constitute pathogen-associated molecular patterns triggering innate immunity in Arabidopsis *Journal of Biological Chemistry* 282, 32338-32348.

Guzel Deger, A., Scherzer, S., Nuhkat, M., Kedzierska, J., Kollist, H., Brosché, M., Unyayar, S., Boudsocq, M., Hedrich, R. & Roelfsema, M. R. G. (2015) Guard cell SLAC1-type anion channels mediate flagellin-induced stomatal closure *New Phytologist* 208, 162-173.

Halkier, B. A. & Gershenzon, J. (2006) Biology and Biochemistry of glucosinolates *Annual Review of Plant Biology* 57, 303-333.

Halter, T., Imkampe, J., Mazzotta, S., Wierzba, M., Postel, S., Bücherl, C., Kiefer, C., Stahl, M., Chinchilla, D., Wang, X., Nürnberger, T., Zipfel, C., Clouse, S., Borst, Jan W., Boeren, S., de Vries, Sacco C., Tax, F. & Kemmerling, B. (2014) The leucine-rich repeat receptor kinase BIR2 is a negative regulator of BAK1 in plant immunity *Current Biology* 24, 134-143.

Hayafune, M., Berisio, R., Marchetti, R., Silipo, A., Kayama, M., Desaki, Y., Arima, S., Squeglia, F., Ruggiero, A., Tokuyasu, K., Molinaro, A., Kaku, H. & Shibuya, N. (2014) Chitin-induced activation of immune signaling by the rice receptor CEBiP relies on a unique sandwich-type dimerization *Proceedings of the National Academy of Sciences* 111, 404-413.

He, P., Shan, L., Lin, N. C., Martin, G. B., Kemmerling, B., Nurnberger, T. & Sheen, J. (2006) Specific bacterial suppressors of MAMP signaling upstream of MAPKKK in Arabidopsis innate immunity *Cell* 125, 563-575.

He, Z., Wang, Z.-Y., Li, J., Zhu, Q., Lamb, C., Ronald, P. & Chory, J. (2000) Perception of brassinosteroids by the extracellular domain of the receptor kinase BRI1 *Science* 288, 2360-2363.

Heese, A., Hann, D. R., Gimenez-Ibanez, S., Jones, A. M. E., He, K., Li, J., Schroeder, J. I., Peck, S. C. & Rathjen, J. P. (2007) The receptor-like kinase SERK3/BAK1 is a central regulator of innate immunity in plants *Proceedings of the National Academy of Sciences* 104, 12217-12222.

Helft, L., Thompson, M. & Bent, A. F. (2016) Directed evolution of FLS2 towards novel flagellin peptide recognition *PLoS ONE* 11, e0157155.

Hirano, S. S. & Upper, C. D. (2000) Bacteria in the leaf ecosystem with emphasis on Pseudomonas syringae - a pathogen, ice nucleus, and epiphyte *Microbiology and Molecular Biology Reviews* 64, 624-653.

Hodgkin, T., Lyon, G. D. & Dickinson, H. G. (1988) Recognition in flowering plants: A comparison of the Brassica self-incompatibility system and plant pathogen interactions *New Phytologist* 110, 557-569.

Holton, N., Nekrasov, V., Ronald, P. C. & Zipfel, C. (2015) The phylogenetically-related pattern recognition receptors EFR and XA21 recruit similar immune signaling components in monocots and dicots *PLoS Pathogens* 11, e1004602.

Hothorn, M., Belkhadir, Y., Dreux, M., Dabi, T., Noel, J. P., Wilson, I. A. & Chory, J. (2011) Structural basis of steroid hormone perception by the receptor kinase BRI1 *Nature* 474, 467.

Hruz, T., Laule, O., Szabo, G., Wessendorp, F., Bleuler, S., Oertle, L., Widmayer, P., Gruissem, W. & Zimmermann, P. (2008) Genevestigator v3: a reference expression database for the meta-analysis of transcriptomes *Advances in Bioinformatics* 2008, 420747-420747.

Hückelhoven, R. (2007) Cell wall–associated mechanisms of disease resistance and susceptibility *Annual Review of Phytopathology* 45, 101-127.

Hugouvieux, V., Barber, C. E. & Daniels, M. J. (1998) Entry of Xanthomonas campestris pv. campestris into hydathodes of Arabidopsis thaliana leaves: A system for studying early infection events in bacterial pathogenesis *Molecular Plant-Microbe Interactions* 11, 537-543.

Huot, B., Yao, J., Montgomery, B. L. & He, S. Y. (2014) Growth–defense tradeoffs in plants: A balancing act to optimize fitness *Molecular Plant* 7, 1267-1287.

Hurst, C. H., Turnbull, D., Myles, S. M., Leslie, K., Keinath, N. F. & Hemsley, P. A. (2018) Variable effects of C-terminal fusions on FLS2 function: Not all epitope tags are created equal *Plant Physiology* 177, 522-531.

Ichinose, Y., Shimizu, R., Ikeda, Y., Taguchi, F., Marutani, M., Mukaihara, T., Inagaki, Y., Toyoda, K. & Shiraishi, T. (2003) Need for flagella for complete virulence of Pseudomonas syringae pv. tabaci: genetic analysis with flagella-defective mutants ΔfliC and ΔfliD in host tobacco plants *Journal of General Plant Pathology* 69, 244-249.

Ivanov, R., Fobis-Loisy, I. & Gaude, T. (2010) When no means no: guide to Brassicaceae self-incompatibility *Trends in Plant Science* 15, 387-394.

Iwano, M., Ito, K., Fujii, S., Kakita, M., Asano-Shimosato, H., Igarashi, M., Kaothien-Nakayama, P., Entani, T., Kanatani, A., Takehisa, M., Tanaka, M., Komatsu, K., Shiba, H., Nagai, T., Miyawaki, A., Isogai, A. & Takayama, S. (2015) Calcium signalling mediates self-incompatibility response in the Brassicaceae *Nature Plants* 1, 15128.

Jaggard, K. W., Qi, A. & Ober, E. S. (2010) Possible changes to arable crop yields by 2050 *Philosophical Transactions of the Royal Society B: Biological Sciences* 365, 2835-2851.

Jarsch, I. K., Konrad, S. S. A., Stratil, T. F., Urbanus, S. L., Szymanski, W., Braun, P., Braun, K.-H. & Ott, T. (2014) Plasma membranes are subcompartmentalized into a plethora of coexisting and diverse microdomains in Arabidopsis and Nicotiana benthamiana *The Plant Cell Online* 26, 1698-1711.

Johnson, L. N., Noble, M. E. M. & Owen, D. J. (1996) Active and inactive protein kinases: Structural basis for regulation *Cell* 85, 149-158.

Jones, J. D. G. & Dangl, J. L. (2006) The plant immune system *Nature* 444, 323-329.

Kachroo, A., Schopfer, C. R., Nasrallah, M. E. & Nasrallah, J. B. (2001) Allele-specific receptor-ligand interactions in Brassica self-incompatibility *Science* 293, 1824-1826.

Kadota, Y., Sklenar, J., Derbyshire, P., Stransfeld, L., Asai, S., Ntoukakis, V., Jones, Jonathan D., Shirasu, K., Menke, F., Jones, A. & Zipfel, C. (2014) Direct regulation of the NADPH oxidase RBOHD by the PRR-associated kinase BIK1 during plant immunity *Molecular Cell* 54, 43-55.

Katagiri, F., Thilmony, R. & He, S. Y. (2002) The Arabidopsis thaliana-Pseudomonas syringae interaction *Arabidopsis Book* 1, e0039.

Kemp, B. P. & Doughty, J. (2007) S cysteine-rich (SCR) binding domain analysis of the Brassica self-incompatibility S-locus receptor kinase *New Phytologist* 175, 619-629.

Kim, S. Y., Shang, Y., Joo, S. H., Kim, S. K. & Nam, K. H. (2017) Overexpression of BAK1 causes salicylic acid accumulation and deregulation of cell death control genes *Biochemical and Biophysical Research Communications* 484, 781-786.

Kimura, S., Waszczak, C., Hunter, K. & Wrzaczek, M. (2017) Bound by fate: The role of reactive oxygen species in receptor-like kinase signaling *Plant Cell* 29, 638-654.

Kouzai, Y., Kaku, H., Shibuya, N., Minami, E. & Nishizawa, Y. (2013) Expression of the chimeric receptor between the chitin elicitor receptor CEBiP and the receptor-like protein kinase Pi-d2 leads to enhanced responses to the chitin elicitor and disease resistance against Magnaporthe oryzae in rice *Plant molecular biology* 35, 287-295.

Krupa, A., Preethi, G. & Srinivasan, N. (2004) Structural modes of stabilization of permissive phosphorylation sites in protein kinases: Distinct strategies in Ser/Thr and Tyr kinases *Journal of Molecular Biology* 339, 1025-1039.

Kudla, J. & Bock, R. (2016) Lighting the way to protein-protein interactions: Recommendations on best practices for bimolecular fluorescence complementation analyses *Plant Cell* 28, 1002-1008.

Kumar, S., Stecher, G., Li, M., Knyaz, C. & Tamura, K. (2018) MEGA X: Molecular evolutionary genetics analysis across computing platforms *Molecular Biology and Evolution* 35, 1547-1549.

Kunze, G., Zipfel, C., Robatzek, S., Niehaus, K., Boller, T. & Felix, G. (2004) The N terminus of bacterial elongation factor Tu elicits innate immunity in Arabidopsis plants *Plant Cell* 16, 3496-3507.

Kutschera, A., Dawid, C., Gisch, N., Schmid, C., Raasch, L., Gerster, T., Schäffer, M., Smakowska-Luzan, E., Belkhadir, Y., Vlot, A. C., Chandler, C. E., Schellenberger, R., Schwudke, D., Ernst, R. K., Dorey, S., Hückelhoven, R., Hofman, T. & Ranf, S. (2019) Bacterial medium-chain 3-hydroxy fatty acid metabolites trigger immunity in Arabidopsis plants *unpublished*.

Kwak, J. M., Mori, I. C., Pei, Z. M., Leonhardt, N., Torres, M. A., Dangl, J. L., Bloom, R. E., Bodde, S., Jones, J. D. G. & Schroeder, J. I. (2003) NADPH oxidase AtrbohD and AtrbohF genes function in ROS-dependent ABA signaling in Arabidopsis *The EMBO Journal* 22, 2623-2633.

Lacombe, S., Rougon-Cardoso, A., Sherwood, E., Peeters, N., Dahlbeck, D., van Esse, H. P., Smoker, M., Rallapalli, G., Thomma, B. P., Staskawicz, B., Jones, J. D. & Zipfel, C. (2010) Interfamily transfer of a plant pattern-recognition receptor confers broad-spectrum bacterial resistance *Nature Biotechnology* 28, 365-369.

Laemmli, U. K. (1970) Cleavage of structural proteins during the assembly of the head of bacteriophage T4 *Nature* 227, 680-685.

Laluk, K., Luo, H., Chai, M., Dhawan, R., Lai, Z. & Mengiste, T. (2011) Biochemical and genetic requirements for function of the immune response regulator BOTRYTIS-INDUCED KINASE1 in plant growth, ethylene signaling, and PAMP-triggered immunity in Arabidopsis *Plant Cell* 23, 2831-2849.

Lamb, C. & Dixon, R. A. (1997) The oxidative burst in plant disease resistance *Annual Review of Plant Physiology and Plant Molecular Biology* 48, 251-275.

Leben, C. & Daft, G. C. (1971) Bacterial blight of soybeans: Epidemiology of blight outbreaks. *Phytopathology* 62, 57-62.

Lee, D., Bourdais, G., Yu, G., Robatzek, S. & Coaker, G. (2015) Phosphorylation of the plant immune regulator RPM1-INTERACTING PROTEIN4 enhances plant plasma membrane H+-ATPase activity and inhibits flagellin-triggered immune responses in Arabidopsis *Plant Cell* 27, 2042-2056.

Lee, S., Choi, H., Suh, S., Doo, I. S., Oh, K. Y., Choi, E. J., Schroeder Taylor, A. T., Low, P. S. & Lee, Y. (1999) Oligogalacturonic acid and chitosan reduce stomatal aperture by inducing the evolution of reactive oxygen species from guard cells of tomato and Commelina communis *Plant Physiology* 121, 147-152.

Lemmon, M. A. & Schlessinger, J. (2010) Cell signaling by receptor tyrosine kinases *Cell* 141, 1117-1134.

Li, J., Wen, J., Lease, K. A., Doke, J. T., Tax, F. E. & Walker, J. C. (2002) BAK1, an Arabidopsis LRR receptor-like protein kinase, interacts with BRI1 and modulates brassinosteroid signaling *Cell* 110, 213-222.

Li, L., Li, M., Yu, L., Zhou, Z., Liang, X., Liu, Z., Cai, G., Gao, L., Zhang, X., Wang, Y., Chen, S. & Zhou, J.-M. (2014) The FLS2-associated kinase BIK1 directly phosphorylates the NADPH oxidase RbohD to control plant immunity *Cell Host & Microbe* 15, 329-338.

Liao, D., Cao, Y., Sun, X., Espinoza, C., Nguyen, C. T., Liang, Y. & Stacey, G. (2017) Arabidopsis E3 ubiquitin ligase PLANT U-BOX13 (PUB13) regulates chitin receptor LYSIN MOTIF RECEPTOR KINASE5 (LYK5) protein abundance *New Phytologist* 214, 1646-1656.

Liebrand, T. W., van den Burg, H. A. & Joosten, M. H. (2014) Two for all: receptor-associated kinases SOBIR1 and BAK1 *Trends in Plant Science* 19, 123-132.

Liebrand, T. W. H., van den Berg, G. C. M., Zhang, Z., Smit, P., Cordewener, J. H. G., America, A. H. P., Sklenar, J., Jones, A. M. E., Tameling, W. I. L., Robatzek, S., Thomma, B. P. H. J. & Joosten, M. H. A. J. (2013) Receptor-like kinase SOBIR1/EVR interacts with receptor-like proteins in plant immunity against fungal infection *Proceedings of the National Academy of Sciences* 110, 10010-10015.

Liese, A. & Romeis, T. (2013) Biochemical regulation of in vivo function of plant calcium-dependent protein kinases (CDPK) *Biochimica et Biophysica Acta (BBA) - Molecular Cell Research* 1833, 1582-1589.

Lin, Z.-J. D., Liebrand, T. W. H., Yadeta, K. A. & Coaker, G. (2015) PBL13 is a serine/threonine protein kinase that negatively regulates Arabidopsis immune responses *Plant Physiology* 169, 2950-2962.

Lindow, S. E. & Brandl, M. T. (2003) Microbiology of the phyllosphere *Applied and Environmental Microbiology* 69, 1875-1883.

Lipman, D. J., Benson, D. A., Karsch-Mizrachi, I., Ostell, J., Clark, K., Cavanaugh, M. & Sayers, E. W. (2012) GenBank *Nucleic Acids Research* 41, D36-D42

Liu, J., Elmore, J. M., Fuglsang, A. T., Palmgren, M. G., Staskawicz, B. J. & Coaker, G. (2009) RIN4 functions with plasma membrane H+-ATPases to regulate stomatal apertures during pathogen attack *PLoS Biology* 7, e1000139.

Liu, J., Liu, B., Chen, S., Gong, B.-Q., Chen, L., Zhou, Q., Xiong, F., Wang, M., Feng, D., Li, J.-F., Wang, H.-B. & Wang, J. (2018) A tyrosine phosphorylation cycle regulates fungal activation of a plant receptor Ser/Thr kinase *Cell Host & Microbe* 23, 241-253.

Liu, T., Liu, Z., Song, C., Hu, Y., Han, Z., She, J., Fan, F., Wang, J., Jin, C., Chang, J., Zhou, J.-M. & Chai, J. (2012) Chitin-induced dimerization activates a plant immune receptor *Science* 336, 1160-1164.

Liu, Y., Wu, H., Chen, H., Liu, Y., He, J., Kang, H., Sun, Z., Pan, G., Wang, Q., Hu, J., Zhou, F., Zhou, K., Zheng, X., Ren, Y., Chen, L., Wang, Y., Zhao, Z., Lin, Q., Wu, F., Zhang, X., Guo, X., Cheng, X., Jiang, L., Wu, C., Wang, H. & Wan, J. (2014) A gene cluster encoding lectin receptor kinases confers broad-spectrum and durable insect resistance in rice *Nature Biotechnology* 33, 301.

Liu, Y. & Zhang, S. (2004) Phosphorylation of 1-Aminocyclopropane-1-Carboxylic Acid Synthase by MPK6, a stress-responsive Mitogen-Activated Protein Kinase, induces ethylene biosynthesis in Arabidopsis *Plant Cell* 16, 3386-3399.

Livak, K. J. & Schmittgen, T. D. (2001) Analysis of relative gene expression data using real-time quantitative PCR and the $2^{-\Delta\Delta CT}$ method *Methods* 25, 402-408.

Logemann, E., Birkenbihl, R. P., Ülker, B. & Somssich, I. E. (2006) An improved method for preparing Agrobacterium cells that simplifies the Arabidopsis transformation protocol *Plant Methods* 2, 1-5.

Lozano-Duran, R., Bourdais, G., He, S. Y. & Robatzek, S. (2014) The bacterial effector HopM1 suppresses PAMP-triggered oxidative burst and stomatal immunity *New Phytologist* 202, 259-269.

Lozano-Durán, R., Macho, A. P., Boutrot, F., Segonzac, C., Somssich, I. E. & Zipfel, C. (2013) The transcriptional regulator BZR1 mediates trade-off between plant innate immunity and growth *eLife* 2, e00983.

Lozano-Durán, R. & Robatzek, S. (2015) 14-3-3 proteins in plant-pathogen interactions *Molecular Plant-Microbe Interactions* 28, 511-518.

Lu, D., Lin, W., Gao, X., Wu, S., Cheng, C., Avila, J., Heese, A., Devarenne, T. P., He, P. & Shan, L. (2011) Direct ubiquitination of pattern recognition receptor FLS2 attenuates plant innate immunity *Science* 332, 1439-1442.

Lu, D., Wu, S., Gao, X., Zhang, Y., Shan, L. & He, P. (2010) A receptor-like cytoplasmic kinase, BIK1, associates with a flagellin receptor complex to initiate plant innate immunity *Proceedings of the National Academy of Sciences* 107, 496-501.

Lu, F., Wang, H., Wang, S., Jiang, W., Shan, C., Li, B., Yang, J., Zhang, S. & Sun, W. (2015) Enhancement of innate immune system in monocot rice by transferring the dicotyledonous elongation factor Tu receptor EFR *Journal of Integrative Plant Biology* 57, 641-652.

Ma, R., Han, Z., Hu, Z., Lin, G., Gong, X., Zhang, H., Nasrallah, J. B. & Chai, J. (2016) Structural basis for specific self-incompatibility response in Brassica *Cell Research* 26, 1320.

Macho, A. P., Schwessinger, B., Ntoukakis, V., Brutus, A., Segonzac, C., Roy, S., Kadota, Y., Oh, M. H., Sklenar, J., Derbyshire, P., Lozano-Duran, R., Malinovsky, F. G., Monaghan, J., Menke, F. L., Huber, S. C., He, S. Y. & Zipfel, C. (2014) A bacterial tyrosine phosphatase inhibits plant pattern recognition receptor activation *Science* 343, 1509-1512.

Mackey, D., Holt, B. F., III, Wiig, A. & Dangl, J. L. (2002) RIN4 interacts with Pseudomonas syringae Type III Effector molecules and is required for RPM1-mediated resistance in Arabidopsis *Cell* 108, 743-754.

Madeira, F., Tinti, M., Murugesan, G., Berrett, E., Stafford, M., Toth, R., Cole, C., MacKintosh, C. & Barton, G. J. (2015) 14-3-3-Pred: improved methods to predict 14-3-3-binding phosphopeptides *Bioinformatics* 31, 2276-2283.

Mahmud, Z. A., Jenkins, L., Ulven, T., Labéguère, F., Gosmini, R., De Vos, S., Hudson, B. D., Tikhonova, I. G. & Milligan, G. (2017) Three classes of ligands each bind to distinct sites on the orphan G protein-coupled receptor GPR84 *Scientific Reports* 7, 17953.

Mansfield, J., Genin, S., Magori, S., Citovsky, V., Sriariyanum, M., Ronald, P., Dow, M. A. X., Verdier, V., Beer, S. V., Machado, M. A., Toth, I. A. N., Salmond, G. & Foster, G. D. (2012) Top 10 plant pathogenic bacteria in molecular plant pathology *Molecular Plant Pathology* 13, 614-629.

Mansvelt, E. L. & Hattingh, M. J. (1989) Scanning electron microscopy of invasion of apple leaves and blossoms by Pseudomonas syringae pv. syringae *Applied and Environmental Microbiology* 55, 533-538.

Melotto, M., Underwood, W., Koczan, J., Nomura, K. & He, S. Y. (2006) Plant stomata function in innate immunity against bacterial invasion *Cell* 126, 969-980.

Meng, X. & Zhang, S. (2013) MAPK cascades in plant disease resistance signaling *Annual Review of Phytopathology* 51, 245-266.

Merlot, S., Leonhardt, N., Fenzi, F., Valon, C., Costa, M., Piette, L., Vavasseur, A., Genty, B., Boivin, K., Müller, A., Giraudat, J. & Leung, J. (2007) Constitutive activation of a plasma membrane H+ ATPase prevents abscisic acid-mediated stomatal closure *The EMBO Journal* 26, 3216-3226.

Mew, T. W., Alvarez, A. M., Leach, J. E. & Swings, J. (1993) Focus on bacterial blight of rice *Plant Disease* 77, 5-12.

Miller, S. I., Ernst, R. K. & Bader, M. W. (2005) LPS, TLR4 and infectious disease diversity *Nature Reviews Microbiology* 3, 36.

Mittal, S. & Davis, K. R. (1995) Role of the phytotoxin coronatine in the infection of Arabidopsis thaliana by Pseudomonas syringae pv. tomato *Molecular Plant-Microbe Interactions* 8, 165-171.

Miya, A., Albert, P., Shinya, T., Desaki, Y., Ichimura, K., Shirasu, K., Narusaka, Y., Kawakami, N., Kaku, H. & Shibuya, N. (2007) CERK1, a LysM receptor kinase, is essential for chitin elicitor signaling in Arabidopsis *Proceedings of the National Academy of Sciences* 104, 19613-19618.

Monaghan, J., Matschi, S., Shorinola, O., Rovenich, H., Matei, A., Segonzac, C., Malinovsky, F. G., Rathjen, J. P., MacLean, D., Romeis, T. & Zipfel, C. (2014) The calcium-dependent protein kinase CPK28 buffers plant immunity and regulates BIK1 turnover *Cell Host & Microbe* 16, 605-615.

Monier, J.-M. & Lindow, S. E. (2004) Frequency, size, and localization of bacterial aggregates on bean leaf surfaces *Applied and Environmental Microbiology* 70, 346-355.

Montillet, J.-L., Leonhardt, N., Mondy, S., Tranchimand, S., Rumeau, D., Boudsocq, M., Garcia, A. V., Douki, T., Bigeard, J., Laurière, C., Chevalier, A., Castresana, C. & Hirt, H. (2013) An abscisic acid-independent oxylipin pathway controls stomatal closure and immune defense in Arabidopsis *PLoS Biology* 11, e1001513.

Mueller, K., Bittel, P., Chinchilla, D., Jehle, A. K., Albert, M., Boller, T. & Felix, G. (2012) Chimeric FLS2 receptors reveal the basis for differential flagellin perception in Arabidopsis and Tomato *Plant Cell* 24, 2213-2224.

Murase, K., Shiba, H., Iwano, M., Che, F.-S., Watanabe, M., Isogai, A. & Takayama, S. (2004) A membrane-anchored protein kinase involved in Brassica self-incompatibility signaling *Science* 303, 1516-1519.

Mustilli, A. C., Merlot, S., Vavasseur, A., Fenzi, F. & Giraudat, J. (2002) Arabidopsis OST1 protein kinase mediates the regulation of stomatal aperture by abscisic acid and acts upstream of reactive oxygen species production *Plant Cell* 14, 3089-3099.

Naithani, S., Chookajorn, T., Ripoll, D. R. & Nasrallah, J. B. (2007) Structural modules for receptor dimerization in the S-locus receptor kinase extracellular domain *Proceedings of the National Academy of Sciences* 104, 12211-12216.

Nasrallah, J. B. (1997) Evolution of the Brassica self-incompatibility locus: A look into S-locus gene polymorphisms *Proceedings of the National Academy of Sciences* 94, 9516.

Navarro, L., Zipfel, C., Rowland, O., Keller, I., Robatzek, S., Boller, T. & Jones, J. D. (2004) The transcriptional innate immune response to flg22. Interplay and overlap with Avr gene-dependent defense responses and bacterial pathogenesis *Plant Physiology* 135, 1113-1128.

Nekrasov, V., Li, J., Batoux, M., Roux, M., Chu, Z.-H., Lacombe, S., Rougon, A., Bittel, P., Kiss-Papp, M., Chinchilla, D., van Esse, H. P., Jorda, L., Schwessinger, B., Nicaise, V., Thomma, B. P. H. J., Molina, A., Jones, J. D. G. & Zipfel, C. (2009) Control of the pattern-recognition receptor EFR by an ER protein complex in plant immunity *The EMBO Journal* 28, 3428-3438.

Newman, M.-A., Von Roepenack, E., Daniels, M. & Dow, M. (2000) Lipopolysaccharides and plant responses to phytopathogenic bacteria *Molecular Plant Pathology* 1, 25-31.

Newman, M. A., Daniels, M. J. & Dow, J. M. (1995) Lipopolysaccharide from Xanthomonas campestris induces defense-related gene expression in Brassica campestris *Molecular Plant-Microbe Interactions* 8, 778-780.

Nikaido, Y., Koyama, Y., Yoshikawa, Y., Furuya, T. & Takeda, S. (2015) Mutation analysis and molecular modeling for the investigation of ligand-binding modes of GPR84 *The Journal of Biochemistry* 157, 311-320.

Nolen, B., Taylor, S. & Ghosh, G. (2004) Regulation of protein kinases *Molecular Cell* 15, 661-675.

Ntoukakis, V., Schwessinger, B., Segonzac, C. & Zipfel, C. (2011) Cautionary notes on the use of C-terminal BAK1 fusion proteins for functional studies *Plant Cell* 23, 3871-3878.

Oerke, E. C. (2006) Crop losses to pests *The Journal of Agricultural Science* 144, 31-43.

Ogasawara, Y., Kaya, H., Hiraoka, G., Yumoto, F., Kimura, S., Kadota, Y., Hishinuma, H., Senzaki, E., Yamagoe, S., Nagata, K., Nara, M., Suzuki, K., Tanokura, M. & Kuchitsu, K. (2008) Synergistic activation of the Arabidopsis NADPH Oxidase AtRBOHD by Ca2+ and phosphorylation *Journal of Biological Chemistry* 283, 8885-8892.

Ogawa, M., Shinohara, H., Sakagami, Y. & Matsubayashi, Y. (2008) Arabidopsis CLV3 Peptide Directly Binds CLV1 Ectodomain *Science* 319, 294-294.

Oh, M.-H., Clouse, S. & Huber, S. (2012) Tyrosine phosphorylation of the BRI1 receptor kinase occurs via a post-translational modification and is activated by the juxtamembrane domain *Frontiers in Plant Science* 8, 175.

Oku, H. *Plant pathogenesis and disease control*. (Lewis Publishers, 1994).

Panchal, S., Chitrakar, R., Thompson, B. K., Obulareddy, N., Roy, D., Hambright, W. S. & Melotto, M. (2016) Regulation of stomatal defense by air relative humidity *Plant Physiology* 172, 2021-2032.

Passardi, F., Penel, C. & Dunand, C. (2004) Performing the paradoxical: how plant peroxidases modify the cell wall *Trends in Plant Science* 9, 534-540.

Pel, M. J. C., van Dijken, A. J. H., Bardoel, B. W., Seidl, M. F., van der Ent, S., van Strijp, J. A. G. & Pieterse, C. M. J. (2014) Pseudomonas syringae evades host immunity by degrading flagellin monomers with alkaline protease AprA *Molecular Plant-Microbe Interactions* 27, 603-610.

Peng, Y., van Wersch, R. & Zhang, Y. (2017) Convergent and divergent signaling in PAMP-triggered immunity and effector-triggered immunity *Molecular Plant-Microbe Interactions* 31, 403-409.

Perraki, A., DeFalco, T. A., Derbyshire, P., Avila, J., Séré, D., Sklenar, J., Qi, X., Stransfeld, L., Schwessinger, B., Kadota, Y., Macho, A. P., Jiang, S., Couto, D., Torii, K. U., Menke, F. L. H. & Zipfel, C. (2018) Phosphocode-dependent functional dichotomy of a common co-receptor in plant signalling *Nature* 561, 248-252.

Petutschnig, E. K., Jones, A. M. E., Serazetdinova, L., Lipka, U. & Lipka, V. (2010) The lysin motif receptor-like kinase (LysM-RLK) CERK1 is a major chitin-binding protein in Arabidopsis thaliana and subject to Chitin-induced phosphorylation *Journal of Biological Chemistry* 285, 28902-28911.

Pietraszewska-Bogiel, A., Lefebvre, B., Koini, M. A., Klaus-Heisen, D., Takken, F. L. W., Geurts, R., Cullimore, J. V. & Gadella, T. W. J. (2013) Interaction of Medicago truncatula lysin motif receptor-like kinases, NFP and LYK3, produced in Nicotiana benthamiana induces defence-like responses *PLoS ONE* 8, e65055.

Poltorak, A., He, X., Smirnova, I., Liu, M.-Y., Huffel, C. V., Du, X., Birdwell, D., Alejos, E., Silva, M., Galanos, C., Freudenberg, M., Ricciardi-Castagnoli, P., Layton, B. & Beutler, B. (1998) Defective LPS signaling in C3H/HeJ and C57BL/10ScCr mice: mutations in Tlr4 gene *Science* 282, 2085-2088.

Radivojac, P., Vacic, V., Haynes, C., Cocklin, R. R., Mohan, A., Heyen, J. W., Goebl, M. G. & Iakoucheva, L. M. (2010) Identification, analysis, and prediction of protein ubiquitination sites *Proteins: Structure, Function, and Bioinformatics* 78, 365-380.

Ramos, L. J. & Volin, R. B. (1987) Role of stomatal opening and frequency on infection of Lycopersicum spp. by Xanthomonas campestris pv. vesicatoria *Phytopathology* 77, 1311-1317.

Ranf, S., Eschen-Lippold, L., Frohlich, K., Westphal, L., Scheel, D. & Lee, J. (2014) Microbe-associated molecular pattern-induced calcium signaling requires the receptor-like cytoplasmic kinases, PBL1 and BIK1 *BMC Plant Biology* 14, 374.

Ranf, S., Eschen-Lippold, L., Pecher, P., Lee, J. & Scheel, D. (2011) Interplay between calcium signalling and early signalling elements during defence responses to microbe- or damage-associated molecular patterns *The Plant Journal* 68, 100-113.

Ranf, S., Gisch, N., Schäffer, M., Illig, T., Westphal, L., Knirel, Y. A., Sánchez-Carballo, P. M., Zähringer, U., Hückelhoven, R., Lee, J. & Scheel, D. (2015) A lectin S-domain receptor kinase mediates lipopolysaccharide sensing in Arabidopsis thaliana *Nature Immunology* 16, 426-433.

Ranf, S., Grimmer, J., Pöschl, Y., Pecher, P., Chinchilla, D., Scheel, D. & Lee, J. (2012) Defense-related calcium signaling mutants uncovered via a quantitative high-throughput screen in Arabidopsis thaliana *Molecular Plant* 5, 115-130.

Rapicavoli, J., Ingel, B., Blanco-Ulate, B., Cantu, D. & Roper, C. (2018) Xylella fastidiosa: an examination of a re-emerging plant pathogen *Molecular Plant Pathology* 19, 786-800.

Ray, D. K., Mueller, N. D., West, P. C. & Foley, J. A. (2013) Yield trends are insufficient to double global crop production by 2050 *PLoS ONE* 8, e66428.

Robatzek, S., Bittel, P., Chinchilla, D., Köchner, P., Felix, G., Shiu, S.-H. & Boller, T. (2007) Molecular identification and characterization of the tomato flagellin receptor LeFLS2, an orthologue of Arabidopsis FLS2 exhibiting characteristically different perception specificities *Plant Molecular Biology* 64, 539-547.

Robatzek, S., Chinchilla, D. & Boller, T. (2006) Ligand-induced endocytosis of the pattern recognition receptor FLS2 in Arabidopsis *Genes & Development* 20, 537-542.

Roine, E., Wei, W., Yuan, J., Nurmiaho-Lassila, E.-L., Kalkkinen, N., Romantschuk, M. & He, S. Y. (1997) Hrp pilus: An hrp-dependent bacterial surface appendage produced by Pseudomonas syringae pv. tomato DC3000 *Proceedings of the National Academy of Sciences* 94, 3459-3464.

Ross, A. F. (1961) Systemic acquired resistance induced by localized virus infections in plants *Virology* 14, 340-358.

Roux, M., Schwessinger, B., Albrecht, C., Chinchilla, D., Jones, A., Holton, N., Malinovsky, F. G., Tör, M., de Vries, S. & Zipfel, C. (2011) The Arabidopsis leucine-rich repeat receptor–like kinases BAK1/SERK3 and BKK1/SERK4 are required for innate immunity to hemibiotrophic and biotrophic pathogens *The Plant Cell Online* 23, 2440-2455.

Sachs, T. *Pattern formation in plant tissues*. (Cambridge University Press, 1991).

Saijo, Y., Tintor, N., Lu, X., Rauf, P., Pajerowska-Mukhtar, K., Häweker, H., Dong, X., Robatzek, S. & Schulze-Lefert, P. (2009) Receptor quality control in the endoplasmic reticulum for plant innate immunity *The EMBO Journal* 28, 3439-3449.

Samuel, M. A., Chong, Y. T., Haasen, K. E., Aldea-Brydges, M. G., Stone, S. L. & Goring, D. R. (2009) Cellular pathways regulating responses to compatible and self-incompatible pollen in Brassica and Arabidopsis stigmas intersect at Exo70A1, a putative component of the exocyst complex *The Plant Cell Online* 21, 2655-2671.

Samuel, M. A., Mudgil, Y., Salt, J. N., Delmas, F., Ramachandran, S., Chilelli, A. & Goring, D. R. (2008) Interactions between the S-domain receptor kinases and AtPUB-ARM E3 ubiquitin ligases suggest a conserved signaling pathway in Arabidopsis *Plant Physiology* 147, 2084-2095.

Sanabria, N., Goring, D., Nurnberger, T. & Dubery, I. (2008) Self/nonself perception and recognition mechanisms in plants: a comparison of self-incompatibility and innate immunity *New Phytologist* 178, 503-514.

Santiago, J., Henzler, C. & Hothorn, M. (2013) Molecular mechanism for plant steroid receptor activation by somatic embryogenesis co-receptor kinases *Science* 341, 889-892.

Sato, K., Nishio, T., Kimura, R., Kusaba, M., Suzuki, T., Hatakeyama, K., Ockendon, D. J. & Satta, Y. (2002) Coevolution of the S-Locus Genes SRK, SLG and SP11/SCR in Brassica oleracea and B. rapa *Genetics* 162, 931-940.

Sawinski, K., Mersmann, S., Robatzek, S. & Böhmer, M. (2013) Guarding the green: Pathways to stomatal immunity *Molecular Plant-Microbe Interactions* 26, 626-632.

Scherzer, S., Maierhofer, T., Al-Rasheid, K. A. S., Geiger, D. & Hedrich, R. (2012) Multiple calcium-dependent kinases modulate ABA-activated guard cell anion channels *Molecular Plant* 5, 1409-1412.

Schopfer, C. R., Nasrallah, M. E. & Nasrallah, J. B. (1999) The male determinant of self-incompatibility in Brassica *Science* 286, 1697-1700.

Schreiber, L. (2010) Transport barriers made of cutin, suberin and associated waxes *Trends in Plant Science* 15, 546-553.

Schulze, B., Mentzel, T., Jehle, A. K., Mueller, K., Beeler, S., Boller, T., Felix, G. & Chinchilla, D. (2010) Rapid heteromerization and phosphorylation of ligand-activated plant transmembrane receptors and their associated kinase BAK1 *Journal of Biological Chemistry* 285, 9444-9451.

Schwessinger, B., Bahar, O., Thomas, N., Holton, N., Nekrasov, V., Ruan, D., Canlas, P. E., Daudi, A., Petzold, C. J., Singan, V. R., Kuo, R., Chovatia, M., Daum, C., Heazlewood, J. L., Zipfel, C. & Ronald, P. C. (2015) Transgenic expression of the dicotyledonous pattern recognition receptor EFR in rice leads to ligand-dependent activation of defense responses *PLoS Pathogens* 11, e1004809.

Schwessinger, B., Roux, M., Kadota, Y., Ntoukakis, V., Sklenar, J., Jones, A. & Zipfel, C. (2011) Phosphorylation-dependent differential regulation of plant growth, cell death, and innate immunity by the regulatory receptor-like kinase BAK1 *PLOS Genetics* 7, e1002046.

Seck, P. A., Diagne, A., Mohanty, S. & Wopereis, M. C. S. (2012) Crops that feed the world 7: Rice *Food Security* 4, 7-24.

Seybold, H., Trempel, F., Ranf, S., Scheel, D., Romeis, T. & Lee, J. (2014) Ca2+ signalling in plant immune response: from pattern recognition receptors to Ca2+ decoding mechanisms *New Phytologist* 204, 782-790.

Shang-Guan, K., Wang, M., Myint Phyu Sin Htwe, N., Li, P., Li, Y., Qi, F., Zhang, D., Cao, M., Kim, C., Weng, H., Cen, H., Black, I. M., Azadi, P., Carlson, R. W., Stacey, G. & Liang, Y. (2018) Lipopolysaccharides trigger two successive bursts of reactive oxygen species at distinct cellular locations *Plant Physiology* 176, 2543–2556.

She, J., Han, Z., Kim, T.-W., Wang, J., Cheng, W., Chang, J., Shi, S., Wang, J., Yang, M., Wang, Z.-Y. & Chai, J. (2011) Structural insight into brassinosteroid perception by BRI1 *Nature* 474, 472.

Shimazu, R., Akashi, S., Ogata, H., Nagai, Y., Fukudome, K., Miyake, K. & Kimoto, M. (1999) MD-2, a molecule that confers lipopolysaccharide responsiveness on Toll-like Receptor 4 *The Journal of Experimental Medicine* 189, 1777-1782.

Shimizu, T., Nakano, T., Takamizawa, D., Desaki, Y., Ishii-Minami, N., Nishizawa, Y., Minami, E., Okada, K., Yamane, H., Kaku, H. & Shibuya, N. (2010) Two LysM receptor molecules,

CEBiP and OsCERK1, cooperatively regulate chitin elicitor signaling in rice *The Plant Journal* 64, 204-214.

Shimosato, H., Yokota, N., Shiba, H., Iwano, M., Entani, T., Che, F.-S., Watanabe, M., Isogai, A. & Takayama, S. (2007) Characterization of the SP11/SCR high-affinity binding site involved in self/nonself recognition in Brassica self-incompatibility *Plant Cell* 19, 107-117.

Shinya, T., Yamaguchi, K., Desaki, Y., Yamada, K., Narisawa, T., Kobayashi, Y., Maeda, K., Suzuki, M., Tanimoto, T., Takeda, J., Nakashima, M., Funama, R., Narusaka, M., Narusaka, Y., Kaku, H., Kawasaki, T. & Shibuya, N. (2014) Selective regulation of the chitin-induced defense response by the Arabidopsis receptor-like cytoplasmic kinase PBL27 *The Plant Journal* 79, 56-66.

Shirsekar, G. S., Vega-Sanchez, M. E., Bordeos, A., Baraoidan, M., Swisshelm, A., Fan, J., Park, C. H., Leung, H. & Wang, G.-L. (2014) Identification and characterization of suppressor mutants of spl11-mediated cell death in rice *Molecular Plant-Microbe Interactions* 27, 528-536.

Shiu, S.-H. & Bleecker, A. B. (2001a) Receptor-like kinases from Arabidopsis form a monophyletic gene family related to animal receptor kinases *Proceedings of the National Academy of Sciences* 98, 10763-10768.

Shiu, S. H. & Bleecker, A. B. (2003) Expansion of the receptor-like kinase/Pelle gene family and receptor-like proteins in Arabidopsis *Plant Physiology* 132, 530-543.

Shiu, S. H. & Bleecker, A. B. (2001b) Plant receptor-like kinase gene family: Diversity, function, and signaling *Science Signaling* 2001, re22.

Shiu, S. H., Karlowski, W. M., Pan, R., Tzeng, Y. H., Mayer, K. F. & Li, W. H. (2004) Comparative analysis of the receptor-like kinase family in Arabidopsis and rice *Plant Cell* 16, 1220-1234.

Sievers, F., Wilm, A., Dineen, D., Gibson, T. J., Karplus, K., Li, W., Lopez, R., McWilliam, H., Remmert, M., Söding, J., Thompson, J. D. & Higgins, D. G. (2011) Fast, scalable generation of high-quality protein multiple sequence alignments using Clustal Omega *Molecular Systems Biology* 7, 539.

Sirichandra, C., Gu, D., Hu, H.-C., Davanture, M., Lee, S., Djaoui, M., Valot, B., Zivy, M., Leung, J., Merlot, S. & Kwak, J. M. (2009) Phosphorylation of the Arabidopsis AtrbohF NADPH oxidase by OST1 protein kinase *FEBS Letters* 583, 2982-2986.

Smakowska-Luzan, E., Mott, G. A., Parys, K., Stegmann, M., Howton, T. C., Layeghifard, M., Neuhold, J., Lehner, A., Kong, J., Grünwald, K., Weinberger, N., Satbhai, S. B., Mayer, D., Busch, W., Madalinski, M., Stolt-Bergner, P., Provart, N. J., Mukhtar, M. S., Zipfel, C., Desveaux, D., Guttman, D. S. & Belkhadir, Y. (2018) An extracellular network of Arabidopsis leucine-rich repeat receptor kinases *Nature* 553, 342.

Smith, J. M., Salamango, D. J., Leslie, M. E., Collins, C. A. & Heese, A. (2014) Sensitivity to flg22 is modulated by ligand-induced degradation and de novo synthesis of the endogenous flagellin-receptor FLAGELLIN-SENSING2 *Plant Physiology* 164, 440-454.

Somssich, M., Ma, Q., Weidtkamp-Peters, S., Stahl, Y., Felekyan, S., Bleckmann, A., Seidel, C. A. M. & Simon, R. (2015) Real-time dynamics of peptide ligand–dependent receptor complex formation in planta *Science Signaling* 8, ra76.

Song, W.-Y., Wang, G.-L., Chen, L.-L., Kim, H.-S., Pi, L.-Y., Holsten, T., Gardner, J., Wang, B., Zhai, W.-X., Zhu, L.-H., Fauquet, C. & Ronald, P. (1995) A receptor kinase-like protein encoded by the rice disease resistance gene, Xa21 *Science* 270, 1804-1806.

Song, W., Han, Z., Wang, J., Lin, G. & Chai, J. (2017) Structural insights into ligand recognition and activation of plant receptor kinases *Current Opinion in Structural Biology* 43, 18-27.

Spoel, S. H. & Dong, X. (2012) How do plants achieve immunity? Defence without specialized immune cells *Nature Reviews Immunology* 12, 89.

Stadler, C., Rexhepaj, E., Singan, V. R., Murphy, R. F., Pepperkok, R., Uhlén, M., Simpson, J. C. & Lundberg, E. (2013) Immunofluorescence and fluorescent-protein tagging show high correlation for protein localization in mammalian cells *Nature Methods* 10, 315.

Stegmann, M., Anderson, R. G., Ichimura, K., Pecenkova, T., Reuter, P., Žárský, V., McDowell, J. M., Shirasu, K. & Trujillo, M. (2012) The ubiquitin ligase PUB22 targets a subunit of the exocyst complex required for PAMP-triggered responses in Arabidopsis *Plant Cell* 24, 4703-4716.

Stein, J. C., Howlett, B., Boyes, D. C., Nasrallah, M. E. & Nasrallah, J. B. (1991) Molecular cloning of a putative receptor protein kinase gene encoded at the self-incompatibility locus of Brassica oleracea *Proceedings of the National Academy of Sciences* 88, 8816-8820.

Stone, S. L., Anderson, E. M., Mullen, R. T. & Goring, D. R. (2003) ARC1 is an E3 ubiquitin ligase and promotes the ubiquitination of proteins during the rejection of self-incompatible Brassica pollen *Plant Cell* 15, 885-898.

Su, J., Zhang, M., Zhang, L., Sun, T., Liu, Y., Lukowitz, W., Xu, J. & Zhang, S. (2017) Regulation of stomatal immunity by interdependent functions of a pathogen-responsive MPK3/MPK6 cascade and abscisic acid *Plant Cell* 29, 526-542.

Sun, W., Cao, Y., Jansen Labby, K., Bittel, P., Boller, T. & Bent, A. F. (2012) Probing the Arabidopsis flagellin receptor: FLS2-FLS2 association and the contributions of specific domains to signaling function *Plant Cell* 24, 1096-1113.

Sun, Y., Han, Z., Tang, J., Hu, Z., Chai, C., Zhou, B. & Chai, J. (2013a) Structure reveals that BAK1 as a co-receptor recognizes the BRI1-bound brassinolide *Cell Research* 23, 1326.

Sun, Y., Li, L., Macho, A. P., Han, Z., Hu, Z., Zipfel, C., Zhou, J.-M. & Chai, J. (2013b) Structural Basis for flg22-Induced Activation of the Arabidopsis FLS2-BAK1 Immune Complex *Science* 342, 624-628.

Suzuki, M., Shibuya, M., Shimada, H., Motoyama, N., Nakashima, M., Takahashi, S., Suto, K., Yoshida, I., Matsui, S., Tsujimoto, N., Ohnishi, M., Ishibashi, Y., Fujimoto, Z., Desaki, Y., Kaku, H., Kito, K. & Shibuya, N. (2016) Autophosphorylation of specific threonine and tyrosine residues in Arabidopsis CERK1 is essential for the activation of chitin-Induced immune signaling *Plant and Cell Physiology* 57, 2312-2322.

Suzuki, M., Watanabe, T., Yoshida, I., Kaku, H. & Shibuya, N. (2018) Autophosphorylation site Y428 is essential for the in vivo activation of CERK1 *Plant Signaling & Behavior* 13, e1435228.

Taguchi, F., Takeuchi, K., Katoh, E., Murata, K., Suzuki, T., Marutani, M., Kawasaki, T., Eguchi, M., Katoh, S., Kaku, H., Yasuda, C., Inagaki, Y., Toyoda, K., Shiraishi, T. & Ichinose, Y. (2006) Identification of glycosylation genes and glycosylated amino acids of flagellin in Pseudomonas syringae pv. tabaci *Cellular Microbiology* 8, 923-938.

Takai, R., Isogai, A., Takayama, S. & Che, F.-S. (2008) Analysis of flagellin perception mediated by flg22 receptor OsFLS2 in rice *Molecular Plant-Microbe Interactions* 21, 1635-1642.

Takasaki, T., Hatakeyama, K., Suzuki, G., Watanabe, M., Isogai, A. & Hinata, K. (2000) The S receptor kinase determines self-incompatibility in Brassica stigma *Nature* 403, 913-916.

Tanaka, K., Choi, J., Cao, Y. & Stacey, G. (2014) Extracellular ATP acts as a damage-associated molecular pattern (DAMP) signal in plants *Frontiers in Plant Science* 5, 446.

Tans-Kersten, J., Huang, H. & Allen, C. (2001) Ralstonia solanacearum needs motility for invasive virulence on tomato *Journal of Bacteriology* 183, 3597-3605.

Tantikanjana, T., Rizvi, N., Nasrallah, M. E. & Nasrallah, J. B. (2009) A dual role for the S-Locus Receptor Kinase in self-incompatibility and pistil development revealed by an Arabidopsis rdr6 mutation *Plant Cell* 21, 2642-2654.

The UniProt Consortium. in *Nucleic Acids Research* Vol. 45 D158-D169 (2017).

Thines, B., Katsir, L., Melotto, M., Niu, Y., Mandaokar, A., Liu, G., Nomura, K., He, S. Y., Howe, G. A. & Browse, J. (2007) JAZ repressor proteins are targets of the SCF(COI1) complex during jasmonate signalling *Nature* 448, 661-665.

Tian, D., Traw, M. B., Chen, J. Q., Kreitman, M. & Bergelson, J. (2003) Fitness costs of R-gene-mediated resistance in Arabidopsis thaliana *Nature* 423, 74.

Tian, Y., Fan, M., Qin, Z., Lv, H., Wang, M., Zhang, Z., Zhou, W., Zhao, N., Li, X., Han, C., Ding, Z., Wang, W., Wang, Z.-Y. & Bai, M.-Y. (2018) Hydrogen peroxide positively regulates brassinosteroid signaling through oxidation of the BRASSINAZOLE-RESISTANT1 transcription factor *Nature Communications* 9, 1063.

Torres, M. A. (2010) ROS in biotic interactions *Physiologia Plantarum* 138, 414-429.

Torres, M. A., Jones, J. D. G. & Dangl, J. L. (2005) Pathogen-induced, NADPH oxidase–derived reactive oxygen intermediates suppress spread of cell death in Arabidopsis thaliana *Nature Genetics* 37, 1130.

Toum, L., Torres, P. S., Gallego, S. M., Benavídes, M. P., Vojnov, A. A. & Gudesblat, G. E. (2016) Coronatine inhibits stomatal closure through guard cell-specific inhibition of NADPH oxidase-dependent ROS production *Frontiers in Plant Science* 7, 1851.

Trujillo, M. (2017) News from the PUB: plant U-box type E3 ubiquitin ligases *Journal of Experimental Botany* 69, 371–384.

Trujillo, M., Ichimura, K., Casais, C. & Shirasu, K. (2008) Negative regulation of PAMP-triggered immunity by an E3 ubiquitin ligase triplet in Arabidopsis *Current Biology* 18, 1396-1401.

Tsuda, K. & Katagiri, F. (2010) Comparing signaling mechanisms engaged in pattern-triggered and effector-triggered immunity *Current Opinion in Plant Biology* 13, 459-465.

Vaid, N., Pandey, P. & Tuteja, N. (2012) Genome-wide analysis of lectin receptor-like kinase family from Arabidopsis and rice *Plant Molecular Biology* 80, 365-388.

Van Damme, Els J M., Nakamura-Tsuruta, S., Smith, David F., Ongenaert, M., Winter, Harry C., Rougé, P., Goldstein, Irwin J., Mo, H., Kominami, J., Culerrier, R., Barre, A., Hirabayashi, J. & Peumans, Willy J. (2007) Phylogenetic and specificity studies of two-domain GNA-related lectins: generation of multispecificity through domain duplication and divergent evolution *Biochemical Journal* 404, 51-61.

Waadt, R. & Kudla, J. (2008) In planta visualization of protein interactions using Bimolecular Fluorescence Complementation (BiFC) *Cold Spring Harbor Protocol* 3, pdb.prot4995.

Walter, M., Chaban, C., Schütze, K., Batistic, O., Weckermann, K., Näke, C., Blazevic, D., Grefen, C., Schumacher, K., Oecking, C., Harter, K. & Kudla, J. (2004) Visualization of protein interactions in living plant cells using bimolecular fluorescence complementation *The Plant Journal* 40, 428-438.

Wan, J., Tanaka, K., Zhang, X.-C., Son, G. H., Brechenmacher, L., Nguyen, T. H. N. & Stacey, G. (2012) LYK4, a lysin motif receptor-like kinase, is important for chitin signaling and plant innate immunity in Arabidopsis *Plant Physiology* 160, 396-406.

Wan, J., Zhang, X.-C., Neece, D., Ramonell, K. M., Clough, S., Kim, S.-y., Stacey, M. G. & Stacey, G. (2008) A LysM receptor-like kinase plays a critical role in chitin signaling and fungal resistance in Arabidopsis *Plant Cell* 20, 471-481.

Wang, H., Ngwenyama, N., Liu, Y., Walker, J. C. & Zhang, S. (2007) Stomatal development and patterning are regulated by environmentally responsive mitogen-activated protein kinases in Arabidopsis *Plant Cell* 19, 63-73.

Wang, J., Grubb, L. E., Wang, J., Liang, X., Li, L., Gao, C., Ma, M., Feng, F., Li, M., Li, L., Zhang, X., Yu, F., Xie, Q., Chen, S., Zipfel, C., Monaghan, J. & Zhou, J.-M. (2018) A regulatory module controlling homeostasis of a plant immune kinase *Molecular Cell* 69, 493-504.e496.

Wang, J., Qu, B., Dou, S., Li, L., Yin, D., Pang, Z., Zhou, Z., Tian, M., Liu, G., Xie, Q., Tang, D., Chen, X. & Zhu, L. (2015) The E3 ligase OsPUB15 interacts with the receptor-like kinase PID2 and regulates plant cell death and innate immunity *BMC Plant Biology* 15, 49.

Warwick, S. I. in *Genetics and genomics of the Brassicaceae* (eds R. Schmidt & I. Bancroft) Ch. 2, 34-65 (2011).

Waterhouse, A. M., Procter, J. B., Martin, D. M. A., Clamp, M. & Barton, G. J. (2009) Jalview Version 2—a multiple sequence alignment editor and analysis workbench *Bioinformatics* 25, 1189-1191.

Weber, E., Engler, C., Gruetzner, R., Werner, S. & Marillonnet, S. (2011) A modular cloning system for standardized assembly of multigene constructs *PLoS ONE* 6, e16765.

Wei, H.-L. & Collmer, A. (2017) Defining essential processes in plant pathogenesis with Pseudomonas syringae pv. tomato DC3000 disarmed polymutants and a subset of key type III effectors *Molecular Plant Pathology* 19, 1779-1794.

Weis, C., Hückelhoven, R. & Eichmann, R. (2013) LIFEGUARD proteins support plant colonization by biotrophic powdery mildew fungi *Journal of Experimental Botany* 64, 3855-3867.

Whalen, M. C., Innes, R. W., Bent, A. F. & Staskawicz, B. J. (1991) Identification of Pseudomonas syringae pathogens of Arabidopsis and a bacterial locus determining avirulence on both Arabidopsis and soybean *Plant Cell* 3, 49-59.

Whitfield, C. & Trent, M. S. (2014) Biosynthesis and export of bacterial lipopolysaccharides *Annual Review of Biochemistry* 83, 99-128.

Wildermuth, M. C., Dewdney, J., Wu, G. & Ausubel, F. M. (2001) Isochorismate synthase is required to synthesize salicylic acid for plant defence *Nature* 414, 562.

Williams, P. H. (1980) Black rot: A continuing threat to world crucifers *Plant Disease* 64, 736-742.

Willmann, R., Lajunen, H. M., Erbs, G., Newman, M. A., Kolb, D. & Tsuda, K. (2011) Arabidopsis lysin-motif proteins LYM1 LYM3 CERK1 mediate bacterial peptidoglycan sensing and immunity to bacterial infection *Proceedings of the National Academy of Sciences* 108, 19824-19829.

Wilson, M., Hirano, S. S. & Lindow, S. E. (1999) Location and survival of leaf-associated bacteria in relation to pathogenicity and potential for growth within the leaf *Applied and Environmental Microbiology* 65, 1435-1443.

Wright, S., Ramos, R., Tobias, P., Ulevitch, R. & Mathison, J. (1990) CD14, a receptor for complexes of lipopolysaccharide (LPS) and LPS binding protein *Science* 249, 1431-1433.

Wulff, B. B., Thomas, C. M., Smoker, M., Grant, M. & Jones, J. D. (2001) Domain swapping and gene shuffling identify sequences required for induction of an Avr-dependent hypersensitive response by the tomato Cf-4 and Cf-9 proteins *Plant Cell* 13, 255-272.

Xin, X.-F. & He, S. Y. (2013) Pseudomonas syringae pv. tomato DC3000: A model pathogen for probing disease susceptibility and hormone signaling in plants *Annual Review of Phytopathology* 51, 473-498.

Xin, X.-F., Nomura, K., Aung, K., Velásquez, A. C., Yao, J., Boutrot, F., Chang, J. H., Zipfel, C. & He, S. Y. (2016) Bacteria establish an aqueous living space in plants crucial for virulence *Nature* 539, 524.

Xing, S., Li, M. & Liu, P. (2013) Evolution of S-domain receptor-like kinases in land plants and origination of S-locus receptor kinases in Brassicaceae *BMC Evolutionary Biology* 13, 69.

Yamada, K., Saijo, Y., Nakagami, H. & Takano, Y. (2016a) Regulation of sugar transporter activity for antibacterial defense in Arabidopsis *Science* 354, 1427-1430.

Yamada, K., Yamaguchi, K., Shirakawa, T., Nakagami, H., Mine, A., Ishikawa, K., Fujiwara, M., Narusaka, M., Narusaka, Y., Ichimura, K., Kobayashi, Y., Matsui, H., Nomura, Y., Nomoto, M., Tada, Y., Fukao, Y., Fukamizo, T., Tsuda, K., Shirasu, K., Shibuya, N. & Kawasaki, T. (2016b) The Arabidopsis CERK1-associated kinase PBL27 connects chitin perception to MAPK activation *The EMBO Journal* 35, 2468-2483.

Yamaguchi, K., Mezaki, H., Fujiwara, M., Hara, Y. & Kawasaki, T. (2017) Arabidopsis ubiquitin ligase PUB12 interacts with and negatively regulates Chitin Elicitor Receptor Kinase 1 (CERK1) *PLoS ONE* 12, e0188886.

Yan, J., Zhang, C., Gu, M., Bai, Z., Zhang, W., Qi, T., Cheng, Z., Peng, W., Luo, H., Nan, F., Wang, Z. & Xie, D. (2009) The Arabidopsis CORONATINE INSENSITIVE1 protein is a jasmonate receptor *Plant Cell* 21, 2220-2236.

Yan, L., Ma, Y., Liu, D., Wei, X., Sun, Y., Chen, X., Zhao, H., Zhou, J., Wang, Z., Shui, W. & Lou, Z. (2012) Structural basis for the impact of phosphorylation on the activation of plant receptor-like kinase BAK1 *Cell Research* 22, 1304.

Yao, J. & Allen, C. (2006) Chemotaxis is required for virulence and competitive fitness of the bacterial wilt pathogen Ralstonia solanacearum *Journal of Bacteriology* 188, 3697-3708.

Ye, W. & Murata, Y. (2016) Microbe associated molecular pattern signaling in guard cells *Frontiers in Plant Science* 7, 583.

Yeh, Y.-H., Chang, Y.-H., Huang, P.-Y., Huang, J.-B. & Zimmerli, L. (2015) Enhanced Arabidopsis pattern-triggered immunity by overexpression of cysteine-rich receptor-like kinases *Frontiers in Plant Science* 6.

Yekondi, S., Liang, F.-C., Okuma, E., Radziejwoski, A., Mai, H.-W., Swain, S., Singh, P., Gauthier, M., Chien, H.-C., Murata, Y. & Zimmerli, L. (2017) Nonredundant functions of Arabidopsis LecRK-V.2 and LecRK-VII.1 in controlling stomatal immunity and jasmonate-mediated stomatal closure *New Phytologist* 218, 253-268.

Yu, X., Feng, B., He, P. & Shan, L. (2017) From chaos to harmony: Responses and signaling upon microbial pattern recognition *Annual Review of Phytopathology* 55, 109-137.

Yu, X., Lund, S. P., Scott, R. A., Greenwald, J. W., Records, A. H., Nettleton, D., Lindow, S. E., Gross, D. C. & Beattie, G. A. (2013) Transcriptional responses of Pseudomonas syringae to growth in epiphytic versus apoplastic leaf sites *Proceedings of the National Academy of Sciences* 110, 425-434.

Yuliar, Nion, Y. A. & Toyota, K. (2015) Recent trends in control methods for bacterial wilt diseases caused by Ralstonia solanacearum *Microbes and Environments* 30, 1-11.

Zacharias, D. A., Violin, J. D., Newton, A. C. & Tsien, R. Y. (2002) Partitioning of lipid-modified monomeric GFPs into membrane microdomains of live cells *Science* 296, 913-916.

Zeng, L.-R., Qu, S., Bordeos, A., Yang, C., Baraoidan, M., Yan, H., Xie, Q., Nahm, B. H., Leung, H. & Wang, G.-L. (2004) Spotted leaf11, a negative regulator of plant cell death and defense, encodes a U-Box/armadillo repeat protein endowed with E3 Ubiquitin ligase activity *Plant Cell* 16, 2795-2808.

Zeng, W. & He, S. Y. (2010) A prominent role of the flagellin receptor FLAGELLIN-SENSING2 in mediating stomatal response to Pseudomonas syringae pv tomato DC3000 in Arabidopsis *Plant Physiology* 153, 1188-1198.

Zhang, D., Tian, C., Yin, K., Wang, W. & Qiu, J.-L. (2018) Post-invasive bacterial resistance conferred by open stomata in rice *Molecular Plant-Microbe Interactions*.

Zhang, J., Li, W., Xiang, T., Liu, Z., Laluk, K., Ding, X., Zou, Y., Gao, M., Zhang, X., Chen, S., Mengiste, T., Zhang, Y. & Zhou, J.-M. (2010) Receptor-like cytoplasmic kinases integrate signaling from multiple plant immune receptors and are targeted by a Pseudomonas syringae effector *Cell Host & Microbe* 7, 290-301.

Zhang, J., Shao, F., Li, Y., Cui, H., Chen, L., Li, H., Zou, Y., Long, C., Lan, L., Chai, J., Chen, S., Tang, X. & Zhou, J.-M. (2007) A Pseudomonas syringae effector inactivates MAPKs to suppress PAMP-induced immunity in plants *Cell Host & Microbe* 1, 175-185.

Zheng, X.-y., Spivey, Natalie W., Zeng, W., Liu, P.-P., Fu, Zheng Q., Klessig, Daniel F., He, Sheng Y. & Dong, X. (2012) Coronatine Promotes Pseudomonas syringae Virulence in Plants by Activating a Signaling Cascade that Inhibits Salicylic Acid Accumulation *Cell Host & Microbe* 11, 587-596.

Zhou, J., Liu, D., Wang, P., Ma, X., Lin, W., Chen, S., Mishev, K., Lu, D., Kumar, R., Vanhoutte, I., Meng, X., He, P., Russinova, E. & Shan, L. (2018) Regulation of Arabidopsis brassinosteroid receptor BRI1 endocytosis and degradation by plant U-box PUB12/PUB13-mediated ubiquitination *Proceedings of the National Academy of Sciences* 115, 1906-1915.

Zielonka, J., Lambeth, J. D. & Kalyanaraman, B. (2013) On the use of L-012, a luminol-based chemiluminescent probe, for detecting superoxide and identifying inhibitors of NADPH oxidase: A re-evaluation *Free Radical Biology & Medicine* 65, 1310-1314.

Zipfel, C., Kunze, G., Chinchilla, D., Caniard, A., Jones, J. D., Boller, T. & Felix, G. (2006) Perception of the bacterial PAMP EF-Tu by the receptor EFR restricts Agrobacterium-mediated transformation *Cell* 125, 749-760.

Zipfel, C., Robatzek, S., Navarro, L., Oakeley, E. J., Jones, J. D. G., Felix, G. & Boller, T. (2004) Bacterial disease resistance in Arabidopsis through flagellin perception *Nature* 428, 764-767.

Zou, X., Qin, Z., Zhang, C., Liu, B., Liu, J., Zhang, C., Lin, C., Li, H. & Zhao, T. (2015) Over-expression of an S-domain receptor-like kinase extracellular domain improves panicle architecture and grain yield in rice *Journal of Experimental Botany* 66, 7197-7209.

Zoulias, N., Harrison, E. L., Casson, S. A. & Gray, J. E. (2018) Molecular control of stomatal development *Biochemical Journal* 475, 441-454.

Zurbriggen, M. D., Carrillo, N. & Hajirezaei, M.-R. (2010) ROS signaling in the hypersensitive response: When, where and what for? *Plant Signaling & Behavior* 5, 393-396.

Zurbriggen, M. D., Carrillo, N., Tognetti, V. B., Melzer, M., Peisker, M., Hause, B. & Hajirezaei, M. R. (2009) Chloroplast-generated reactive oxygen species play a major role in localized cell death during the non-host interaction between tobacco and Xanthomonas campestris pv. vesicatoria *The Plant Journal* 60, 962-973.

Züst, T., Rasmann, S. & Agrawal, A. A. (2015) Growth–defense tradeoffs for two major anti-herbivore traits of the common milkweed Asclepias syriaca *Oikos* 124, 1404-1415.

11 Supplementary Information

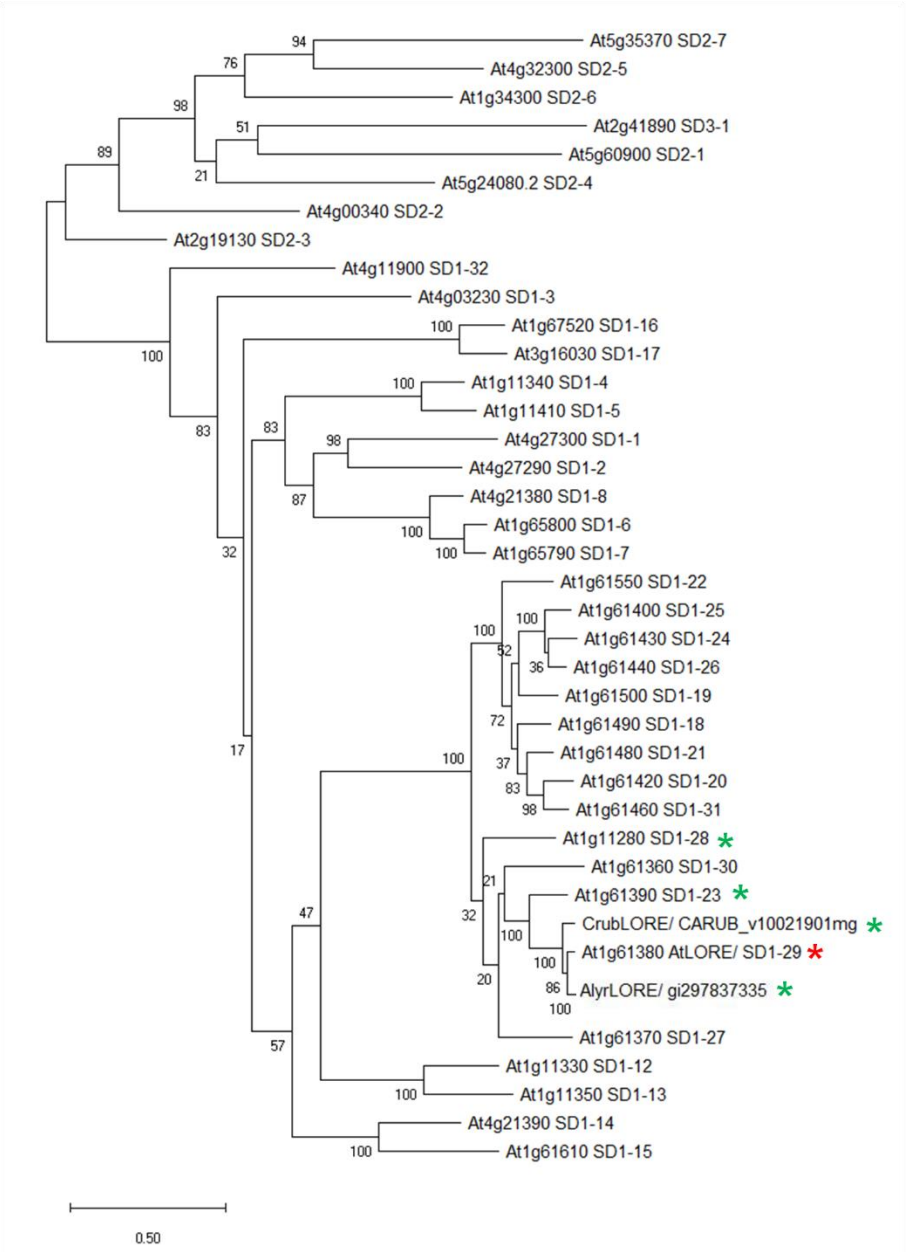

Supplementary Figure 1 Phylogenetic analysis of Arabidopsis SD-RLKs and close *At*LORE orthologs. Amino acid sequences were aligned using ClustalW (Sievers *et al.*, 2011). The phylogenetic tree was generated using the Maximum Likelihood method conducted in MEGA X (Kumar *et al.*, 2018). The phylogeny was investigated using the bootstrap method with 500 replications. The branch lengths indicate the number of substitutions per site (scale 0.5). The analysis comprised 40 amino acid sequences. Arabidopsis SD-RLKs sequences were obtained from TAIR10, CrubLORE and AlyrLORE sequences were obtained from Phyotzome12 (Table 12). *At*LORE is highlighted with a red asterisk, the paralogs and putative orthologs used in this study with a green asterisk.

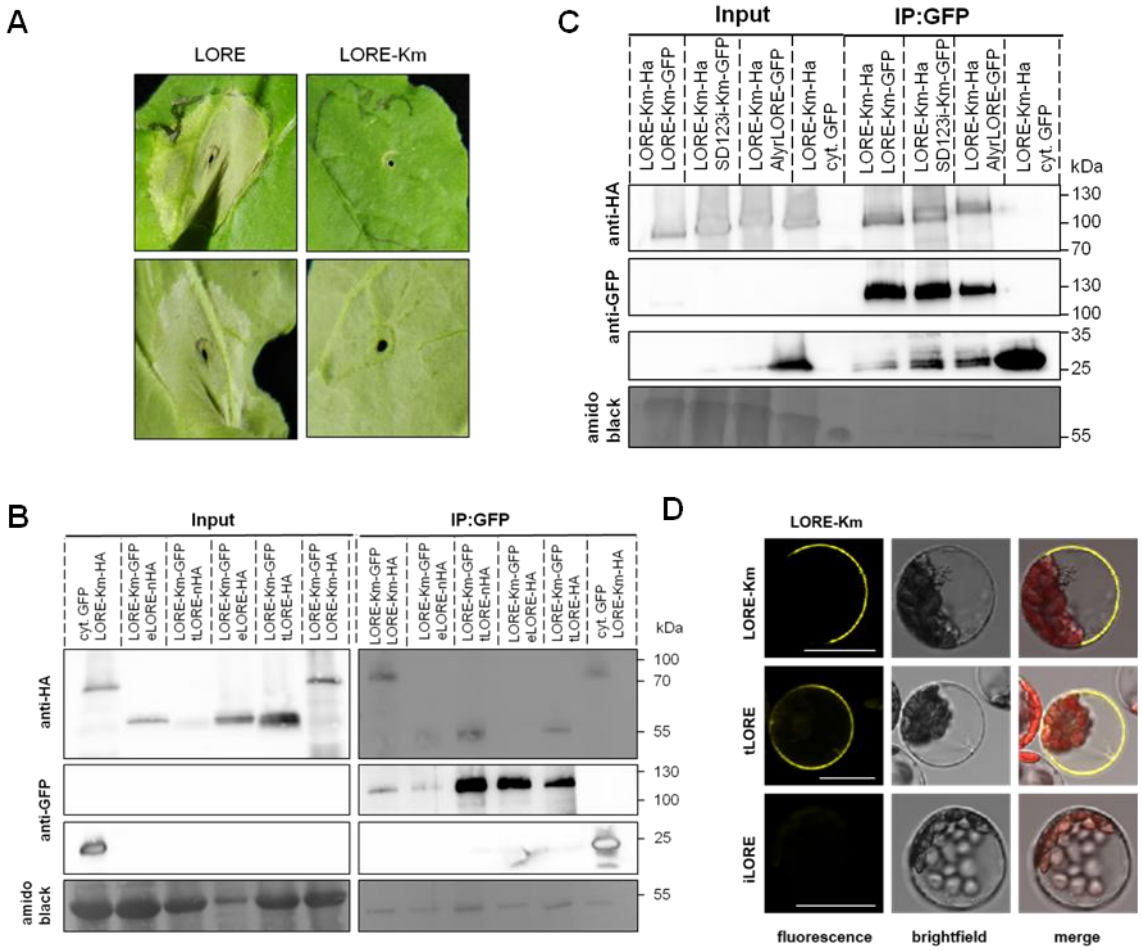

Supplementary Figure 2 Homo- and heterodimerization of LORE. A) *N. benthamiana* leaves were transiently transformed with LORE-GFP and LORE-Km-GFP. Pictures were taken 6 dpi showing the cell death phenotype induced by LORE in *N. benthamiana*. B) Immunoblot analysis of CoIP experiments of transiently transformed *N. benthamiana*. LORE-Km-GFP (~130 kDa) was co-transformed with LORE-Km-HA (~100 kDa), tLORE-nHA (~70 kDa), eLORE-nHA (~65 kDa), tLORE-HA (~70 kDa), eLORE-HA (~65 kDa). Cytosolic GFP (~30 kDa, cyt. GFP) was co-transformed with LORE-Km-HA. Interacting proteins were immunoprecipitated with a GFP trap (IP: GFP). Experiment was repeated once. C) Immunoblot analysis of CoIP experiments of heterodimerization of LORE-Km-HA (~100 kDa), LORE-Km-GFP (~130 kDa), AlyrLORE-GFP (~130 kDa), SD1-23-GFP (~130 kDa), and cytosolic GFP (~30 kDa) in transiently transformed *N. benthamiana*. The experiment was repeated once. Amido black staining shows equal protein loading. (B, C). SuperSignal®West Dura Extended Duration Substrate (Pierce, Rockford, USA) was used for detection (B, C). D) Microscopic evaluation of BiFC assay in *Arabidopsis* protoplasts after 48 h. LORE-Km-N was co-transformed with iLORE-C or tLORE-C. Representative pictures are depicted.

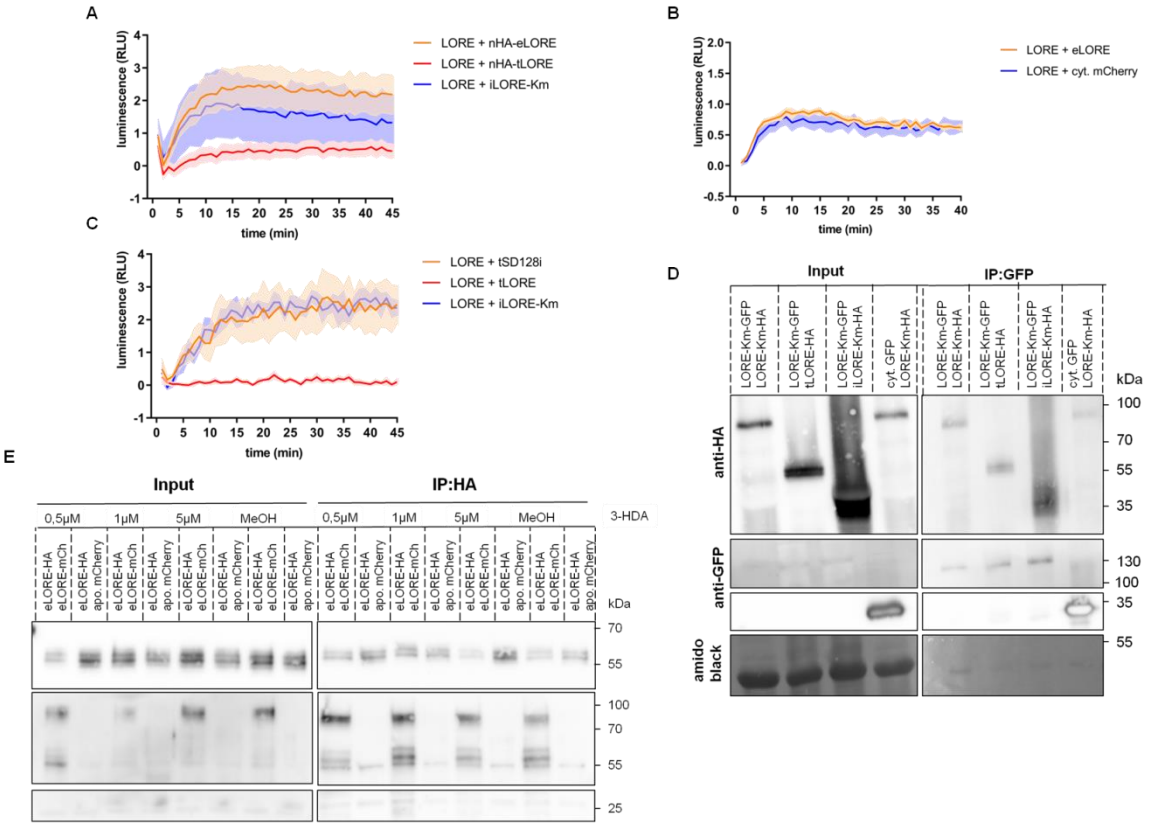

Supplementary Figure 3 eLORE and tSD128i do not exert a dominant-negative effect on LORE activity and 3-HDA has no influence on eLORE homodimerization. A) Competitive ROS accumulation in transiently co-transformed *N. benthamiana* leaves transformed with LORE-GFP and nHA-eLORE, nHA-tLORE, or iLORE-Km, respectively. B) Competitive ROS accumulation in transiently co-transformed *N. benthamiana* leaves transformed with LORE-GFP and eLORE, or cytosolic mCherry, respectively. C) Competitive ROS accumulation in transiently co-transformed *N. benthamiana* leaves transformed with LORE-GFP and tSD128i, tLORE, or iLORE-Km, respectively. Leaf discs were treated with 5 µM 3-HDA and values represent the mean ± SEM (each n = 8) (A, B, C). The experiments were repeated twice (A, B, C). D) CoIP experiment using a GFP trap fitting to competition gain-of-function assay described in section 4.2.3. LORE-Km-GFP (~130 kDa) was co-transformed with LORE-Km-HA (~100 kDa), tLORE-HA (~70 kDa), and iLORE-Km-HA (~40 kDa). Cytosolic GFP (~30 kDa) was co-transformed with LORE-Km-HA. Amido black shows equal protein loading. E) Pull-down experiments of apoplastic wash fluids containing eLORE-HA (~65 kDa), eLORE-mCherry (~90 kDa), or apoplastic mCherry (~30 kDa) supplemented with 0.5, 1, 5 µM 3-HDA, or MeOH. Multiple bands detected on the immunoblot can be degradation products or differential or partial glycosylated ectodomains. The experiment was repeated twice. SuperSignal® West Femto Maximum Sensitivity Substrate (Pierce, Rockford, USA) was used for detection (D, E).

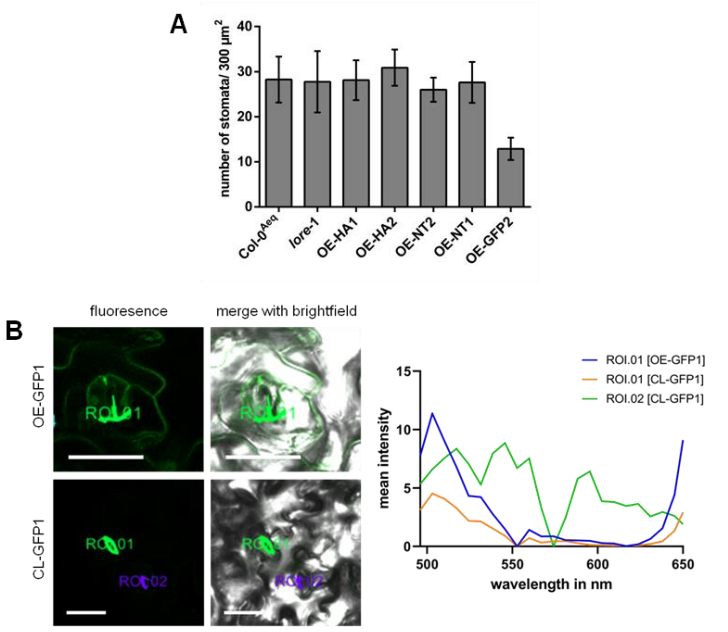

Supplementary Figure 4 Stomata phenotype of OE-GFP and lambda scan of CL-GFP1 and OE-GFP1. A) The number of normally developed stomata of Col-0^{Aeq}, *lore*-1, OE-HA1, OE-HA2, OE-NT1, OE-NT2, and OE-GFP1 per 300 µM^2 leaf area were counted. Therefore, stomata of two leaf discs of two leaves of two individual 8-weeks-old plants were counted under the light microscope. Depicted is the mean ± SEM of n = 4 leaf discs. B) Leaf discs of CL-GFP1 and OE-GFP1 were microscoped and a lambda scan (490 nm–650 nm) showing the detected emission from the excited signal. OE-GFP1 (ROI.01 [OE-GFP1] (Region of interest), blue) shows a clear emission maximum at 510 nm which indicates fluorescence derived from GFP. ROI.01[CL-GFP1] (orange) shows likewise a emission maximum at 510 nm. ROI.02[CL-GFP1] (green) shows a different emission spectrum.

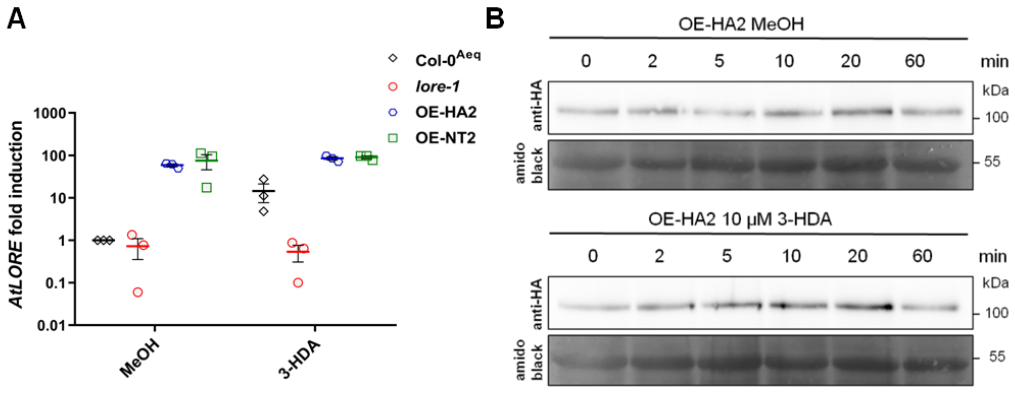

Supplementary Figure 5 *AtLORE* and LORE-HA regulation in response to 3-HDA. A) Relative quantitative expression analysis of *AtLORE* in Col-0^{Aeq}, *lore*-1, OE-HA2, and OE-NT2 10-days-old seedlings treated for 4 h with MeOH or 5 µM 3-HDA. Expression levels were normalized to *AtUBQ5*. Fold change induction was calculated relatively to Col-0^{Aeq} treated with MeOH. Single data are presented in a dot blot with the mean ± SEM of three biological replicates. B) Immunoblot analysis of OE-HA2 10-days-old seedlings treated with MeOH or 10 µM 3-HDA for 0, 2, 5, 10, 20, or 60 min. 50 µg of total protein extracts were loaded. LORE-HA is detected around 100 kDa. Amido black staining shows equal loading.

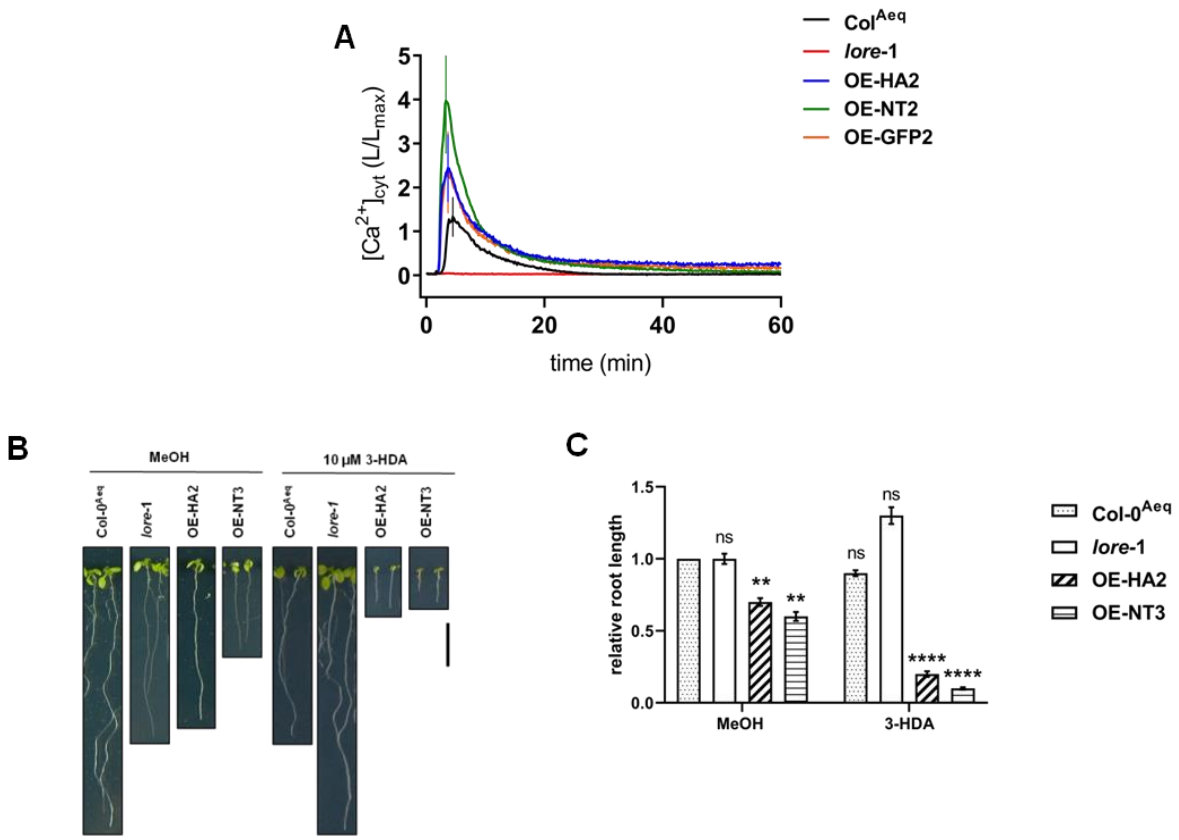

Supplementary Figure 6 Overexpression lines show enhanced immune outputs compared to wild type. A) $[Ca^{2+}]_{cyt}$ elevation of Col-0^{Aeq} (n = 12), *lore*-1 (n = 12), OE-HA2 (n = 24), OE-GFP2 (n = 24), and OE-NT2 (n = 24) in response to 1 µM 3-HDA measured in 10-days-old seedlings for 60 min. Depicted is the mean ± SD at the maximum of one experiment. Measurements were repeated four times with similar results. B) Picture of Col-0^{Aeq}, *lore*-1, OE-HA2, and OE-NT3 8-days-old seedlings grown on ATS medium supplemented with 10 µM 3-HDA or MeOH as control under long day conditions in a vertical position. Scale bar 2 cm. C) Analysis of root growth inhibition of Col-0^{Aeq}, *lore*-1, OE-HA2, and OE-NT3 in response to 10 µM 3-HDA or MeOH. Depicted is the relative root length compared to Col-0^{Aeq} treated with MeOH (mean ± SEM, pooled data of two independent experiments with each n ≥ 22 seedlings of each genotype per treatment). Data were analyzed with a two-way ANOVA and Dunnett's multiple comparison post test in comparison to Col-0^{Aeq} treated with MeOH. Asterisks indicate significant differences (** $P < 0.01$, **** $P < 0.0001$).

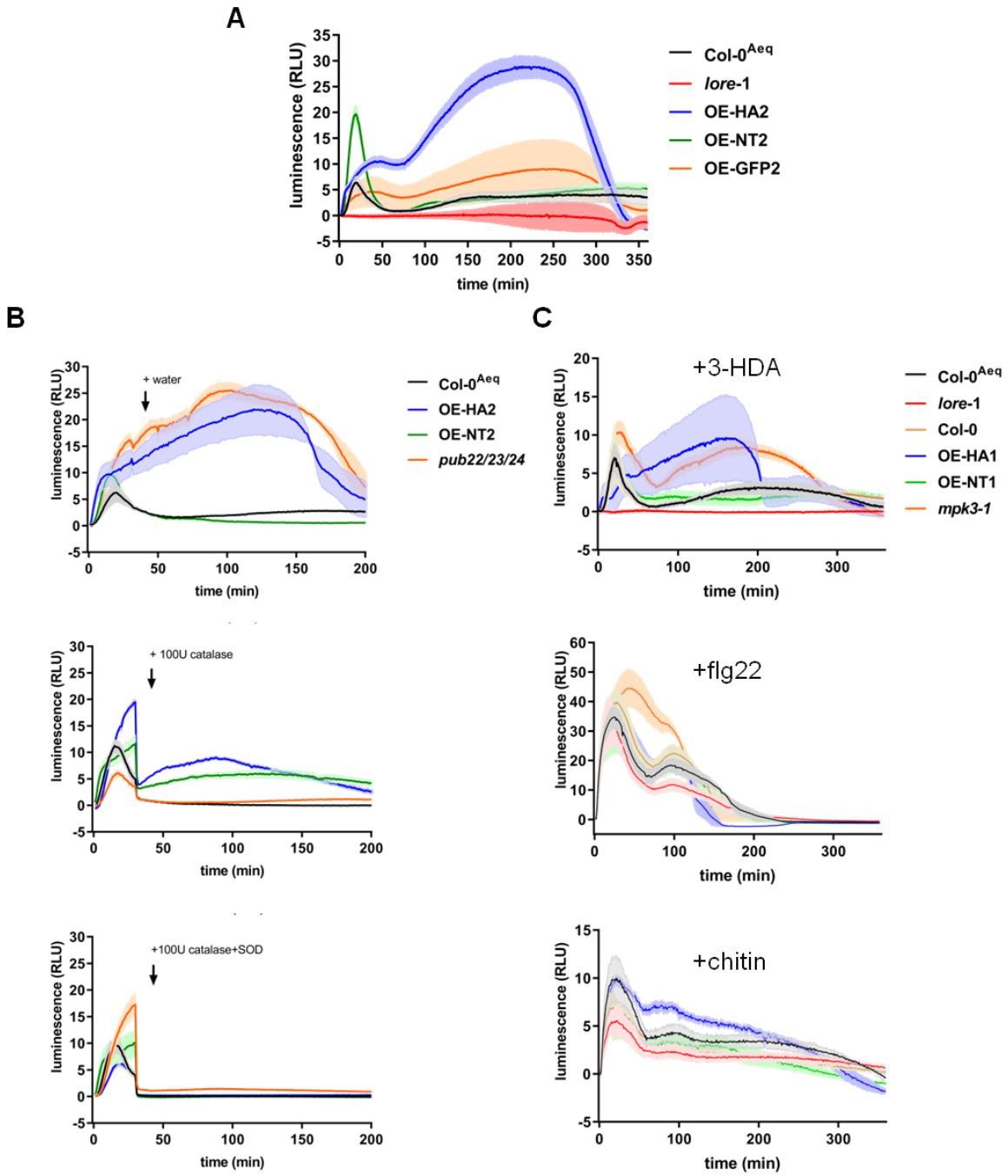

Supplementary Figure 7 Measurement of ROS production in overexpression lines. ROS accumulation was measured in leaf discs of 6-weeks-old-plants. Depicted is the mean ± SEM of one representative experiment as relative light units (RLU) (A, B, C). A) Measurement of Col-0^{Aeq}, *lore*-1 and OE-HA2, OE-NT2, and OE-GFP2 (both growth phenotype) in response to 1 µM 3-HDA (each n = 16). The measurement was repeated four times. B) Measurement of Col-0^{Aeq}, OE-HA2, OE-NT2, and *pub22/23/24* in response to 1 µM 3-HDA. After 30 min 100U catalase, 100U catalase and 100U superoxide dismutase (SOD) or water as control were added (each n = 8). This measurement was repeated three times C) Measurement of Col-0^{Aeq}, *lore*-1, OE-HA1, OE-NT1, Col-0, and *mpk3-1* in response to 1 µM 3-HDA, 100 nM flg22, or 50 µg/mL chitin. The measurement was repeated two times.

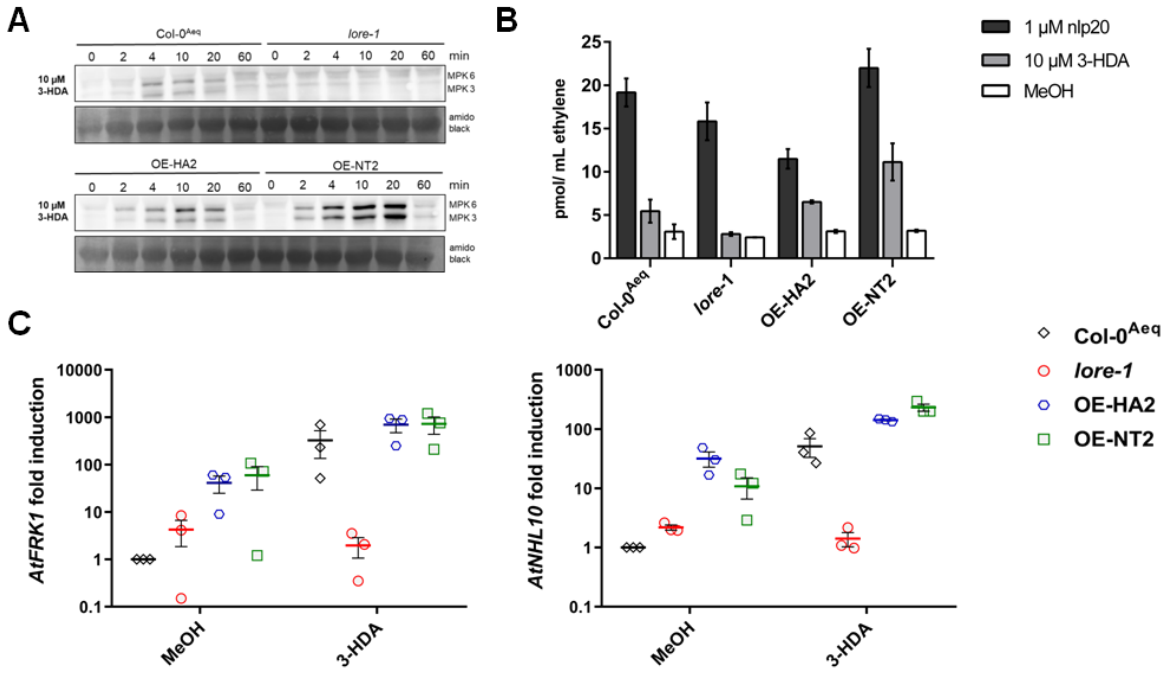

Supplementary Figure 8 MAPK activation, ethylene production, and defense gene expression are elevated in overexpression lines compared to wild type. A) Col-0^{Aeq}, *lore*-1, OE-HA2, and OE-NT2 10-days-old seedlings were treated with 10 µM 3-HDA for 0, 2, 3, 10, 20, or 60 min. Phosphorylated *At*MPK6 and *At*MPK3 were detected in 50 µg total protein extract. Amido black staining shows equal protein loading. This experiment was repeated two times with similar results. B) Ethylene production in leaf discs of 8-weeks-old Col-0^{Aeq}, *lore*-1, OE-HA2, and OE-NT2 in response to 1 µM *Fo*nlp20, 10 µM 3-HDA, or MeOH as control (n = 3). This experiment was repeated twice with similar results. C) Relative quantitative expression of PTI marker genes *AtFRK1* (left) and *AtNHL10* (right) in 10-days-old seedlings of Col-0^{Aeq}, *lore*-1, OE-HA2, and OE-NT2 treated for 4 h with MeOH or 5 µM 3-HDA. Expression levels were normalized to *AtUBQ5*. Fold change induction was calculated relatively to Col-0^{Aeq} treated with MeOH. Single data are presented in a dot blot with the mean ± SEM of three biological replicates.

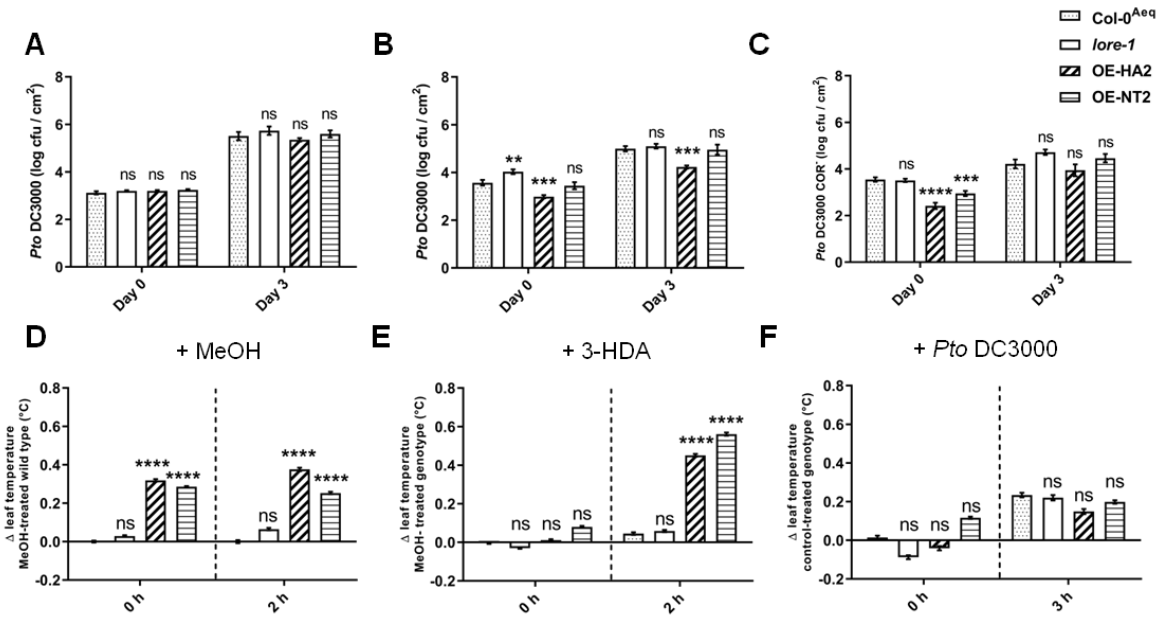

Supplementary Figure 9 OE-HA is more resistant to spray inoculation and overexpression lines show differential stomatal regulation. Bacterial infection assays were performed with 8-weeks-old plants. Bacterial titers were assessed on day 0 (4 h) and on day 3 post infection (A, B, C). Data represent the colony forming units (cfu) per cm^2 leaf area and are depicted as the mean ± SEM (A, B, C). A) *Pto* DC3000 was syringe-infiltrated into the leaf apoplastic space of Col-0^{Aeq}, *lore*-1, OE-HA2, and OE-NT2 (n = 12; pooled data of four independent experiments). B) Surface-inoculation of Col-0^{Aeq}, *lore-1*, OE-HA2, and OE-NT2 with *Pto* DC3000 (n = 9, pooled data of three independent experiments). C) Surface-inoculation of Col-0^{Aeq}, *lore-1*, OE-HA2, and OE-NT2 with *Pto* DC3000 COR^- (n = 12, pooled data of four independent experiments). Data were analyzed with a one-way ANOVA and Dunnett's multiple comparison post test comparing each genotype to Col-0^{Aeq}. Day 0 and day 3 were analyzed separately. Asterisks indicate significant differences (** $P < 0.01$, *** $P < 0.001$, **** $P < 0.0001$, ns = not significant) (A, B, C). 7-weeks-old plants grown under 60% relative humidity were used for thermal imaging (D, E, F). D) Calculation of the leaf temperature change (Δ leaf temperature) of OE-HA2, OE-NT2, and *lore*-1 compared to Col-0^{Aeq} treated with MeOH. E) Calculation of the Δ leaf temperature in response to 3-HDA of OE-HA2, OE-NT2, *lore*-1, and Col-0^{Aeq} compared to the leaf temperature of the respective MeOH-treated genotype. F) Calculation of the Δ leaf temperature in response to *Pto* DC3000 (OD 0.2) spray inoculation of OE-HA2, OE-NT2, *lore*-1, and Col-0^{Aeq} compared to the leaf temperature of the respective control-treated genotype. Data represent the mean ± SEM of two independent experiments (n ≥ 49 leaves per genotype, treatment and time point) (D, E, F). Data of each time point were analyzed with a one-way ANOVA and Tukey's multiple comparison post test in relation to the wild-type control (D, E, and F at 0 h), or to the control-treated genotype (D and E at 2 h, F at 3 h). Asterisks indicate significant differences (**** $P < 0.0001$, ns = not significant) (D, E, F). A third experiment with similar results was performed. Because of minor changes in the experimental setup, data were not included into the calculation.

Supplementary Figure 10 Predicted ubiquitination sites of *At*LORE. Predicted lysine residues as potential ubiquitination sites of *At*LORE are color-coded in grey. The prediction was performed using UbPred (Radivojac *et al.*, 2010, accessed October 08, 2018). Lysine 769 is located in the domain of unknown function 3430 at the very C terminus of *At*LORE.

Supplementary Table 1 List of Golden Gate vectors used in this study. The vector backbones have a letter code representing the enzymes used for ligation (in) and restriction (out) of the vector. The numerical code determines in pGGEntL the enzyme order. 1 represents the enzyme used to insert the gene of interest and 2 represent the enzyme used to cut it out. The numerical code of pGGIns determines the promoter, terminator and C- or N-terminal epitope tag.

vector name	resistance	enzymes in/out	function
pGGEntL_EP21	ampicillin	BpiI/Esp3I	Golden Gate entry vector
pGGInAE-220C	streptomycin	Esp3I/AarI	35S promoter, 35S Terminator, no tag
pGGInAE-221C	streptomycin	Esp3I/AarI	35S promoter, 35S Terminator, 1xHA tag
pGGInALE-221C	streptomycin	Esp3I/LguI/AarI	35S promoter, 35S Terminator, 1xHA tag
pGGInAE-224C	streptomycin	Esp3I/AarI	35S promoter, 35S Terminator, eGFP tag
pGGInALE-224C	streptomycin	Esp3I/LguI/AarI	35S promoter, 35S Terminator, eGFP tag
pGGInAE-225C	streptomycin	Esp3I/AarI	35S promoter, 35S Terminator, mCherry tag
pGGInALE-225C	streptomycin	Esp3I/LguI/AarI	35S promoter, 35S Terminator, mCherry tag
pGGInAE-226C	streptomycin	Esp3I/AarI	35S promoter, 35S Terminator, 3xHA tag
pGGInALE-226C	streptomycin	Esp3I/LguI/AarI	35S promoter, 35S Terminator, 3xHA tag
pGGInAE-228C	streptomycin	Esp3I/AarI	35S promoter, 35S Terminator, SPYCE tag
pGGInAE-229C	streptomycin	Esp3I/AarI	35S promoter, 35S Terminator, SPYNE tag
pGGInAE-314C	streptomycin	Esp3I/AarI	pLORE, NOS-terminator, eGFP tag

Supplementary Table 1 (continued)

vector name	resistance	enzymes in/out	function
pGGPlantXL	kanamycin	AarI (not suitable for restriction-ligation)	binary vector for expression *in planta* and in bacteria
pGGPXB	kanamycin	AarI	binary vector for expression *in planta* and in bacteria

Supplementary Table 2 List of all plasmids generated and used in this study. Genes of interest were cloned into the Golden Gate entry vector pGGEntL and then further shuffled into various intermediate pGGIn-vectors as indicated in the table. All pGGIn-plasmids were further shuffled to the binary pGGPXB-vector (Supplementary Table 1). SD1-29 is equivalent to LORE.

plasmid name	insert	shuffled into pGGIn
pGGEntL-EP21_SD129	CDS SD1-29	pGGIn-220, 221C, 224C, 225C, 314C
pGGEntL-EP21_SD129-Km	CDS SD1-29 K516A	pGGIn-221C, 224C, 225C, 228C, 229C
pGGEntL-EP21_SD123i	CDS SD1-23 plus first intron of LORE	pGGIn-224C, 225C
pGGEntL-EP21_SD128i	CDS SD1-28 plus first intron of LORE	pGGIn-224C, 225C
pGGEntL-EP21_AlyrLORE	CDS AlyrLORE	pGGIn-224C, 225C
pGGEntL-EP21_AhalLORE	CDS AhalLORE	pGGIn-224C, 225C
pGGEntL-EP21_CrubLORE	CDS CrubLORE	pGGIn-224C, 225C
pGGEntL-EP21_DSAlyr-LLEPT	CDS of LORE plus CDS of LLEPT of AlyrLORE	pGGIn-221C, 224C, 225C
pGGEntL-EP21_DSAlyr-JKD	CDS of LORE plus CDS of JKD of AlyrLORE	pGGIn-221C, 224C, 225C
pGGEntL-EP21_DSAlyr-LL	CDS of LORE plus CDS of LL of AlyrLORE	pGGIn-221C, 224C, 225C
pGGEntL-EP21_DSAlyr-EP	CDS of LORE plus CDS of EP of AlyrLORE	pGGIn-221C, 224C, 225C
pGGEntL-EP21_DS123-LLEPTi	CDS of LORE plus CDS of LLEPT of SD123i	pGGIn-221C, 224C, 225C
pGGEntL-EP21_DS123-JKD	CDS of LORE plus CDS of JKD of SD123i	pGGIn-221C, 224C, 225C
pGGEntL-EP21_DS123-LLi	CDS of LORE plus CDS of LL of SD123i	pGGIn-221C, 224C, 225C

Supplementary Table 2 (continued)

plasmid name	insert	shuffeled into pGGIn
pGGEntL-EP21_DS123-EP	CDS of LORE plus CDS of EP of SD123i	pGGIn-221C, 224C, 225C
pGGEntL-EP21_DS128-LLEPTi	CDS of LORE plus CDS of LLEPT of SD128i	pGGIn-221C, 224C, 225C
pGGEntL-EP21_DS128-JKD	CDS of LORE plus CDS of JKD of SD128i	pGGIn-221C, 224C, 225C
pGGEntL-EP21_DS128-LLi	CDS of LORE plus CDS of LL of SD128i	pGGIn-221C, 224C, 225C
pGGEntL-EP21_DS128-EP	CDS of LORE plus CDS of EP of SD128i	pGGIn-221C, 224C, 225C
	truncations	
pGGEntL-EP21_SD129-dJKD	CDS of tLORE	pGGIn-221C, 224C, 225C, 229C
pGGEntL-EP21_SD129-dTJKD	CDS of eLORE	pGGIn-221C, 225C
pGGEntL-EP21_SD129-dLLEP	CDS of iLORE	pGGIn-221C, 224C, 225C, 229C
pGGEntL-EP21_SD129-dLLEPT	CDS of kLORE	pGGIn-221C, 225C
pGGEntL-EP21_SD129-dJKD-nHA	CDS of tLORE	pGGIn-220
pGGEntL-EP21_SD129-dTJKD-nHA	CDS of eLORE	pGGIn-220
pGGEntL-EP21_AlyrLORE-dTJKD	CDS of eAlyrLORE	pGGIn-221C, 225C
pGGEntL-EP21_SD123i-dTJKD	CDS of eSD123i plus first LORE intron	pGGIn-221C, 225C
pGGEntL-EP21_SD128i-dTJKD	CDS of eSD128i plus first LORE intron	pGGIn-221C, 225C

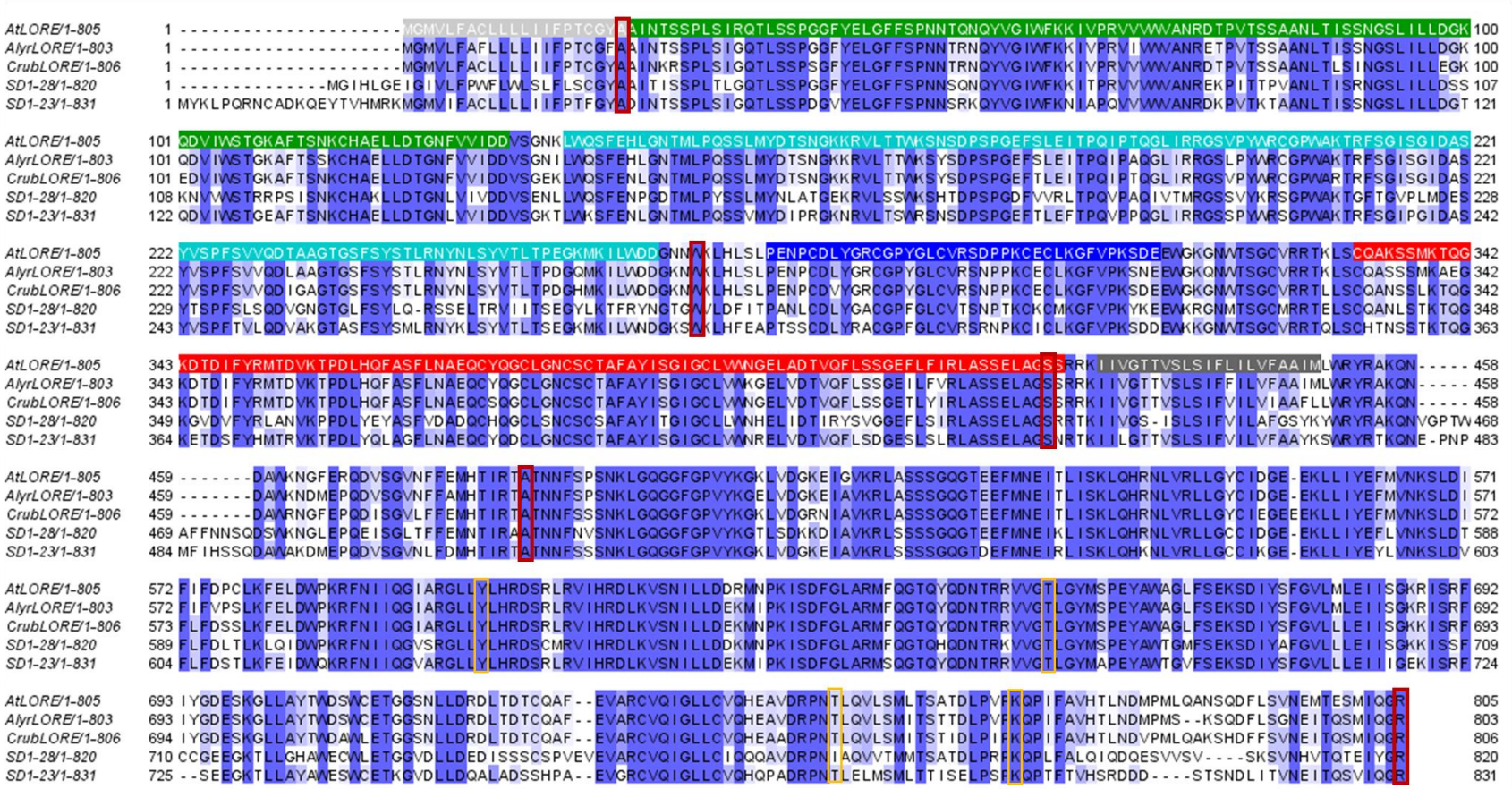

Supplementary Figure 11 Multiple amino acid sequence alignment of S-domain receptor-like kinases used for domain swaps with LORE. ClustalW alignment modified with Jalview (2.9.0b2). The sequences (*At*LORE, AlyrLORE, CrubLORE, *At*SD1-23, *At*SD1-28) are colored according to their percentage identity (residues which are congruent with the consensus sequence of the column are colored in blue). The predicted *At*LORE domains according to Naithani *et al.*, 2007 are highlighted as follows: signal peptide (light grey), lectin-like domain 1(green), lectin-like domain 2 (turqoise), EGF-like (blue), PAN-domain (red), and transmembrane domain (grey). The defined fusion sites are highlighted with red boxes in order of appearance **START** (alanine; A), **C** (tryptophane; W), **N** (serine; S), **P** (alanine; A), and **STOP** (arginine; R). The conserved residues in the kinase domain of RLKs Thr653 and Tyr600 as well as the putative 14-3-3 regulation site Thr752 and the potential ubiquitylation site Lys769 are highlighted with an orange box.

12 Danksagung

Ich möchte mich herzlich bei Dr. Stefanie Ranf für die Überlassung des interessanten Themas und die Betreuung meiner Arbeit bedanken. Vielen Dank für das entgegengebrachte Vertrauen und die vielen Möglichkeiten unsere Arbeit zu gestalten und zu präsentieren.

Ebenso möchte ich mich bei Prof. Dr. Ralph Hückelhoven bedanken, dass er meine Arbeit mitbetreut und durch seinen wissenschaftlichen Input bereichert hat. Außerdem vielen Dank für die freundliche Aufnahme am Lehrstuhl.

Prof. Dr. Brigitte Poppenberger danke ich herzlich für die Übernahme des Prüfungsvorsitzes.

Prof. Dr. Kay Schneitz möchte ich recht herzlich für die Übernahme der Rolle des Zweitprüfers danken.

Desweiteren möchte ich mich bei allen gegenwärtigen und ehemaligen Mitarbeitern des Lehrstuhls für Phytopathologie für ihre Unterstützung, die Hilfsbereitschaft und die angenehme Arbeitsatmosphäre bedanken. Besonders danke ich allen Doktorand/-innen sowie Johanna Hofer für die vielen schönen Mittagspausen, die gemeinsamen Stammtische und das gemeinsame Bouldern. Besonderer Dank gilt meinen Kollegen der AG LORE Alexander Kutschera und Lars Raasch sowie Christopher McCollum für die gemeinsamen Jahre. Vielen Dank für Eure Unterstützung im Labor, die wissenschaftlichen sowie privaten Diskussionen und unsere gemeinsamen Ausflüge in die Berge. Darüberhinaus möchte ich mich bei Tina Illig, Sonja Eibel, Yvonne Bigott, Anna Kossek, Nadine Pöller und Sabine Eschrig bedanken, die durch die Bearbeitung von Teilprojekten im Rahmen von Laborpraktika, Master- und Bachelorarbeiten meine Arbeit vorangebracht haben. Außerdem möchte ich mich auch bei Jule Kriegel, Johanna Hofer und unseren HiWis für die großartige technische Unterstützung bedanken.

Bei Dr. Zhenyu Yang vom Lehrstuhl der Botanik bedanke ich mich für die Unterstützung bei der Etabilierung des *thermal imaging* sowie für die gemeinsame Diskussion der Daten.

Ich bedanke mich bei Lars Raasch, Alexander Coleman, Christopher McCollum, Alexander Kutschera und Sebastian Schäffer für das Korrekturlesen der ganzen bzw. Teile dieser Arbeit.

Ein besonders großer Dank geht an meine Familie und Sebastian für die Unterstützung, ihr Vertrauen in mich und die vielen schönen gemeinsamen Erlebnisse.